Aus dem *Institut für Schlaganfall und Demenzforschung, Ludwig-Maximilians-Universität München*

Dissertation

zum Erwerb des Doctor of Philosophy (Ph.D.) an der

Medizinischen Fakultät der

Ludwig-Maximilians-Universität zu München

The pericyte response to ischemic stroke

vorgelegt von

Joshua James Shrouder

aus

Southport, England

Jahr 2021

Mit Genehmigung der Medizinischen Fakultät der

Ludwig-Maximilians-Universität zu München

First supervisor *Prof. Dr. med Nikolaus Plesnila*

Second supervisor *Prof .Dr. Leda Dimou*

Third supervisor *Dr. Christoff Haffner*

Dean: Prof. Dr. med. Thomas Guderman

Datum der Verteidigung: 12th October 2021

Table of content

Abstract

Pericytes are a previously understudied, but crucial cell type of the vessel wall. In the brain, pericytes are part of the neurovascular unit and are involved in the control and regulation of cerebral blood flow, formation and maintenance of the blood-brain-barrier, and initiating evolutionarily conserved inflammatory and wound healing responses in the context of injury and disease. Previous research suggests that pericytes are particularly susceptible to cerebral ischemia, dying almost immediately after reduction of blood flow and constricting the microcirculation thereby causing 'no-reflow' after ischemic stroke. If true, this would preclude any therapy to ameliorate stroke outcome. These previous studies, however, lacked *in vivo* evidence, required deeper, more dynamic experimentation and pivotally, left many questions unanswered. Therefore, we used transgenic mice where pericytes express enhanced green fluorescent protein (EGFP) under the control of the platelet derived growth factor receptor β promoter (PDGFRb), in tandem with 2-photon microscopy, laser speckle imaging, histological and transcriptomic analyses, to assess in detail the pericyte response to stroke.

Firstly, we demonstrate a novel damaged pericyte phenotype, where half of all pericyte sub-types incur damage in the form of blebs during stroke *in vivo*, which persists acutely after reperfusion as a loss of cellular membrane integrity. 24 hours after stroke, we show that pericyte death occurs acutely, with a 25% loss in pericyte density in the ischemic territory, and 30% of remaining pericytes staining $TUNEL^{+}$. Critically, this leaves half the pericyte population alive in the sub-acute phase (Day 3-7). Here, we demonstrate that pericyte survival is region dependent within the infarct core where neurons are eradicated. Despite this, we further show that pericytes respond to local reductions in population density by entering the cell cycle, increasing vessel coverage and upregulating transcriptional profiles associated with the cell cycle, extracellular matrix deposition, and blood vessel morphogenesis.

Functionally, we demonstrate during a transient one-hour filament middle cerebral artery occlusion, pericytes ubiquitously constrict the microvasculature in a spectrum of severity. 87% of pericytes constrict their associated capillary by 25% on average in a sub-type and depth dependent manner. Specifically, thin-strand pericytes constrict more than junctional or mesh pericytes and along with all other sub-types, continue to constrict their associated capillary after reperfusion. The consequences of pericyte constriction materialize in the form of entrapped non-flowing vascular elements, where during stroke, we show that one third of pericytes are associated with non-flowing vascular elements (capillary stalls), and this association persists acutely post-reperfusion. In doing so, we causally implicate acute pericyte dysfunction in the 'no-reflow' phenomenon after stroke. Importantly, 24 hours post-stroke, we no longer detect significant amounts of entrapped vascular elements at pericyte locations, and concomitantly find that all cortical pericyte sub-type populations have dilated their associated capillaries to pre-stroke levels, implying functional impairment of pericytes, not immediate pericyte death, causes constriction of the microvasculature in the ischemic cortex. Strikingly, in the sub-acute phase, we identify a previously unreported second phase of pericyte constriction, where thin-strand and junctional pericytes reconstrict their associated capillaries to a degree previously predicted by the severity of pericyte constriction during stroke. Finally, we demonstrate using laser speckle imaging that bi-phasic microvascular pericyte constriction post-stroke correlates with and contributes to large-scale reductions of blood flow within the ischemic cortex.

Taken together, our research demonstrates that pericytes are more resistant to cerebral ischemia than previously believed and are causally implicated in the "no-reflow" phenomenon after ischemic stroke. Thus, pericytes may be functionally impaired by stroke in the ischemic cortex far earlier than they die, suggesting they represent a potential target for stroke therapy acutely after reperfusion of the occluded artery.

List of figures

List of tables

List of abbreviations

ECM – Extracellular matrix

NVU – Neurovascular unit

BBB – Blood brain barrier

CNS - Central Nervous system

CADASIL – Cerebral autosomal dominant arteriopathy with subcortical infarcts and leukoencephalopathy

CARASIL - Cerebral autosomal recessive arteriopathy with subcortical infarcts and leukoencephalopathy

ATP – Adenosine tri-phosphate

NMDA - N-methyl-d-aspartate

Nnos - Neuronal nitric oxide synthase

ROS – Reactive oxygen spcies

MCA – Middle cerebral artery

CBF – Cerebral blood flow

CSD – Cortical spreading depolarization

tPA – Tissue plasminogen activator

MRI – Magnetic resonance imaging

PET – Positron emission tomography

K^+ - Potassium ions

EMT – Epithelial-mesenchymal transition

VSMCs – Vascular smooth muscle cells

PDGFRb – Platelet derived growth factor receptor beta

PDGF – Platelet derived growth factor

SH2 – Src homology domain 2

Mrna – Messenger ribonucleic acid

Ras – Rat sarcoma, a small G-protein

MAPK – Microtubule associated protein kinase

PI3K – Phosphoinositide 3-Kinase

PLC-γ – Phosphoinositide phospholipase C gamma

Grb2 – Growth factor receptor bound protein 2

Sos1 – Son of sevenless homolog 1, a guanine nucleotide exchange factor (GEF)

SHP-2 – Src homolog domain containing non-transmembrane protein tyrosine phosphatase

Cbl - E3 ubiquitin-protein ligase

Tie-2 – TEK tyrosine kinase 2

TGFβ – Transforming growth factor beta

Alk1 – Activin receptor-like kinase 1

Alk5 - Activin receptor-like kinase 5

Smad2/3 – meaning small worm phenotype and MAD family (mothers against decapentaplegic, Drosophila genes)

Notch – Notch 1 homolog

1. Introduction

1.1 The neurovascular unit

The microvasculature structure in the brain is highly specialized and conserved across many species. Pial and cortical penetrating arteries consist of an endothelial layer, which run across the surface and dive into the brain, the basal lamina made from extracellular matrix (ECM), myointimal layers of smooth muscles cells encased in ECM, and adventitia originating from the leptomeninges. Within the cortex, an extension of the subarachnoid space forms the Virschow-Robin space, surrounding cortical penetrating arterioles until reaching the capillary bed where it disappears into the glia limitans formed by astrocytic end-feet - a space which has recently been shown to clear solutes from the brain during sleep and is now known as the glymphatic system (del Zoppo and Mabuchi, 2003, Iliff et al., 2012). Further, along the vascular arbor as the vessels continue to branch and decrease in lumen diameter, the glia limitans fuses with the basement membrane at the capillary level, encasing mural cells called pericytes between two layers of ECM on the abluminal side of the vessel. These pericytes cover approximately 37% of the endothelium via the extension of cytoplasmic protrusions called processes. Parenchymal resident astrocytes reach out via end-feet and contact pericytes and blood vessels, covering almost the entire endothelium (Mathiisen et al., 2010). As the capillaries transition to venules, perivascular fibroblasts are found encased within the basement membrane and are found in increasing frequency on ascending venules which rise back toward the cortical surface. Together, pericytes, astrocytes, and endothelial cells form the blood-brain barrier (BBB) which is a unique, highly polarized, selective barrier that is necessary to maintain central nervous system homeostasis and provide trophic support to neurons, enabling unhindered, coordinated neuronal signaling across the brain. In combination with peri-capillary microglia, oligodendrocytes and neurons, these cells make up the Neurovascular unit (NVU).

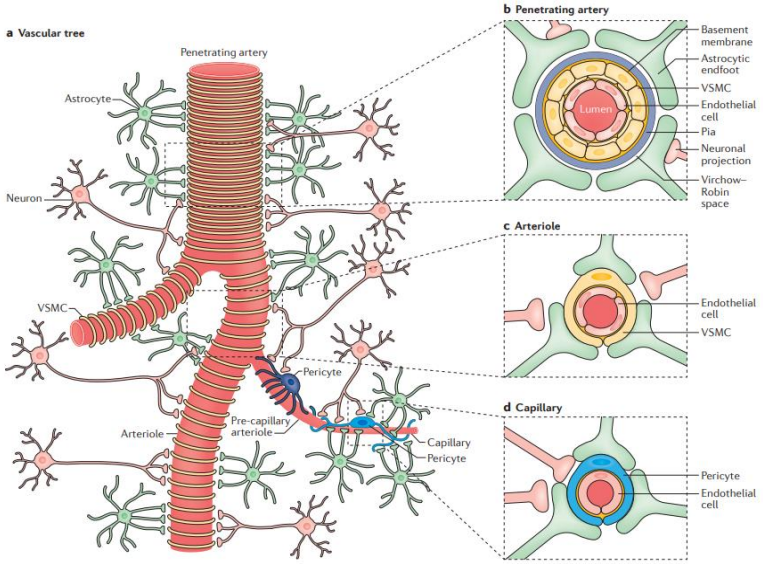

Fig. 1. Brain vascular architecture and vascular unit components.

a) Depiction of a penetrating artery, branching off into arterioles, contacted on all sides by astrocytic end-feet, forming the glia limitans and Virschow-Robin space. **b)** Cross-sectional view of cellular components involved in penetrating artery construction. **c)** Cross-sectional view of arteriole construction. **d)** Cross-sectional view of capillary construction, adapted with permission from (Kisler et al., 2017a)

1.2 Ischemic stroke: an overview

Ischemic stroke is an acute-onset disease representing 87% of all strokes and is caused by the sudden obstruction of blood flow to a portion of the central nervous system (CNS) (Lloyd-Jones et al., 2010). Typically, this obstruction is caused by formation of a thrombus in a large artery (a coagulation of clotted blood components) or an embolus (parts of a plaque, thrombi, air bubble or fat tissue) in brain, spinal cord or retina and results in limited perfusion of downstream tissue causing permanent damage to tissues at risk. To date, ischemic stroke is responsible for 5% of all disability-adjusted life years and accounts for 10% of all death worldwide (second leading cause of death); with the majority of this burden showing a heavy skew toward low and middle-income countries (Naghavi et al., 2017).

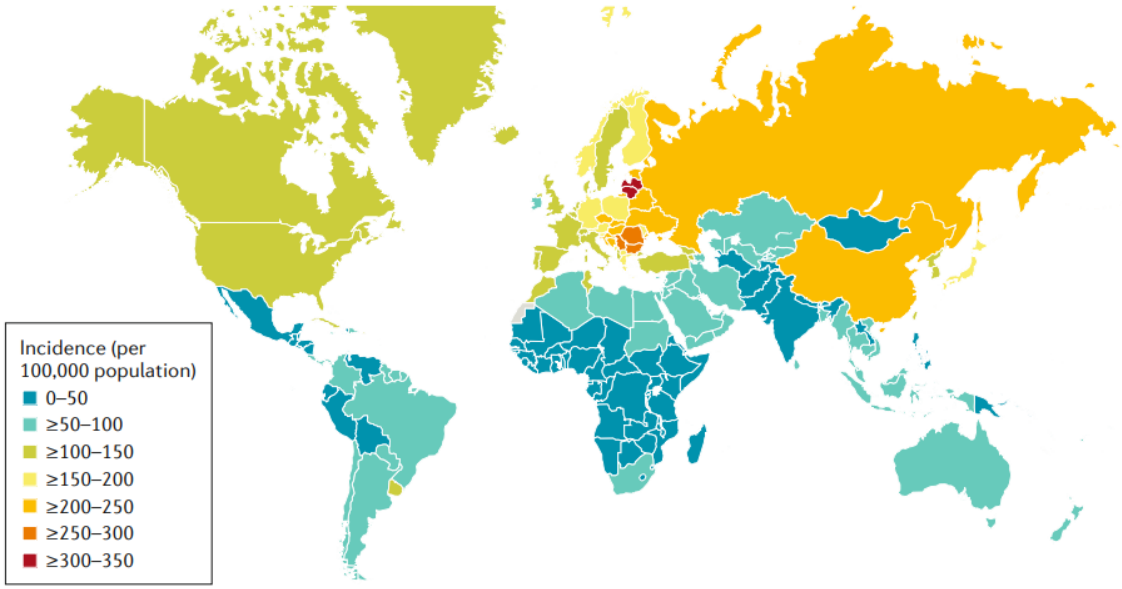

Fig. 2. Epidemiology of ischemic stroke.

Global distribution of ischemic stroke incidence by country, Data from (Naghavi et al., 2017), adapted with permission from (Campbell et al., 2019).

As a disease, the prevalence and incidence of ischemic stroke is modestly increasing with a large increase in the likelihood of stroke in adults between 20-64 years of age (Feigin et al., 2015). Recently, it's estimated that 1 in 4 adults will experience an ischemic stroke in their lifetime and this high frequency contributes to approximately 80 million stroke survivors worldwide (Krishnamurthi et al., 2015, Campbell et al., 2019). Interestingly, the stroke based incidence-mortality ratio and disability-adjusted life years vary according to country income, with a significant decrease occurring in high-income countries, while in middle and low-income countries these metrics remained unchanged between 1990 - 2010 (Naghavi et al., 2017). The reasons for this asymmetry are many fold and likely the result of differences in national health care prevention, life expectancy and age demographic biases.

Collectively, modifiable risk factors (lifestyle and situation dependent criteria) such as hypertension, lack of high-level activity, smoking, cardiac associated issues, diet, alcohol consumption, waist to hip ratio, depression and psychosocial stress account for up to 91.5% of stroke risk among populations worldwide (O'Donnell et al., 2010). In addition to these factors, several other

risk factors also account for low levels of stroke risk such as sleep apnea and environmental pollution which are likely to increase in frequency in the future due to global population growth.

Although most ischemic stroke cases occur sporadically, there are a number of risk factors that contribute to the likelihood of stroke occurrence (Bevan et al., 2012). Statistically speaking, stroke is more common in men than in women and occurs heritably with a probability of 37.9% because of monogenic diseases such as CADASIL and CARASIL (dominant and recessive forms of cerebral autosomal arteriopathy with subcortical infarcts and leukoencephalopathy, respectively) (Feigin et al., 2015, Bevan et al., 2012).

1.2.1 Cellular pathophysiology of stroke

Specifically, although neurons make up only 2% of the body mass in humans, they require 20% of the body's O_2 and 25% of all the glucose metabolized by the body. This is due to the high energetic cost required to maintain resting membrane potential, reorganizing synaptic connections and initiating action potentials (Bordone et al., 2019). Consequently, after the occlusion of an upstream vessel the brain tissue requires more energy than it is supplied with; resulting in rapid depletion of limited energy providing perivascular glycogen stores normally found in astrocytes in the adult brain, and triggering further *dramatic* effects on downstream tissue - in particular on neuroglial health and function (Alarcon-Martinez et al., 2019) .

A lack of glucose and O_2 availability in neurons initiates an ischemic cascade beginning with the disruption of their transmembrane gradient (maintained by an adenosine tri-phosphate-dependent Na^+/K^+ exchange pump). This has several downstream effects; initially this impairs neuronal signaling by depolarizing the neuron (anoxic depolarization) and triggers the release of neurotransmitters at pre-synaptic terminals. These neurotransmitters are not cleared from the synaptic cleft under conditions of ischemia (which itself is an ATP dependent process) leading to increasing concentrations of extracellular glutamate (Obrenovitch et al., 1993). Secondarily, N-methyl-d-aspartate (NMDA) receptors normally blocked by magnesium ions under physiological conditions are opened by magnesium removal, which in turn alters conductance of these channels, triggering calcium influx and the release of internal calcium stores inside neurons (Nowak et al., 1984). Thirdly, a rise in intracellular calcium activates neuronal nitric oxide synthase (nNOS) which generates reactive oxygen species (ROS) that can injure mitochondria triggering cytochrome c release and initiating apoptosis. Alternatively, ROS can also trigger necrosis, necroptosis and autophagy in neurons and glia in a paracrine manner (Mayer and Miller, 1990, Love, 1999). In addition to the lethal effects on neurons and other cells (oligodendrocytes, microglia, pericytes), excessive glutamate release in the extracellular space triggers astrocyte swelling and osmotic overload and can result in enlargement of astrocyte end-feet; compressing vessels further and exacerbating an already insufficient blood supply (Vella et al., 2015). Furthermore, swelling of astrocytes indirectly reduces the volume of extracellular space, raising extracellular glutamate to excitotoxic levels and resulting in lethal cellular damage (Choi and Rothman, 1990). Taken together, the loss of energy supply within a CNS highly dependent on ATP delineates the onset of an irreversible cascade of damage in areas perfused by solitary vessels with little access to proximal collaterals, ultimately leading to tissue necrosis within minutes. The extent of brain damage caused by these processes is widely understood to be a function of the severity of the occlusion and time (Bevan et al., 2012). However, many areas of the gray matter are perfused by collateral flow, which can extend the survival time of distinct regions of the gray matter to several hours.

1.2.2 The ischemic core and ischemic penumbra

The metabolic starvation of tissue downstream of the clot can cause irreversible cell death in minutes (the ischemic core). Despite this, collaterals (minor vessels that can expand to perfuse brain regions normally supplied by the blocked vessels) and vascular redundancy within the ischemic brain afford other at risk tissue with a time-window in which cells become electrically inactive, effectively hibernating within a hypoperfused, oligaemic non-functional tissue termed the ischemic penumbra. Crucial experiments performed in the 1970's attribute many of the acute onset clinical deficits seen in patients to the ischemic penumbra which importantly, is brain tissue which can still be saved (Astrup et al., 1981). Rapid reperfusion of the ischemic penumbra can restore function to at risk tissue and this finding prompted the impetus for research focused on reperfusion therapies, which are the most effective stroke therapies to date and transform the lives of many stroke survivors (TheNationalInstituteofNeurologicalDisordersandStrokert-PAStrokeStudyGroup, 1995, StrokeUnitTrialistsCollaboration, 1997).

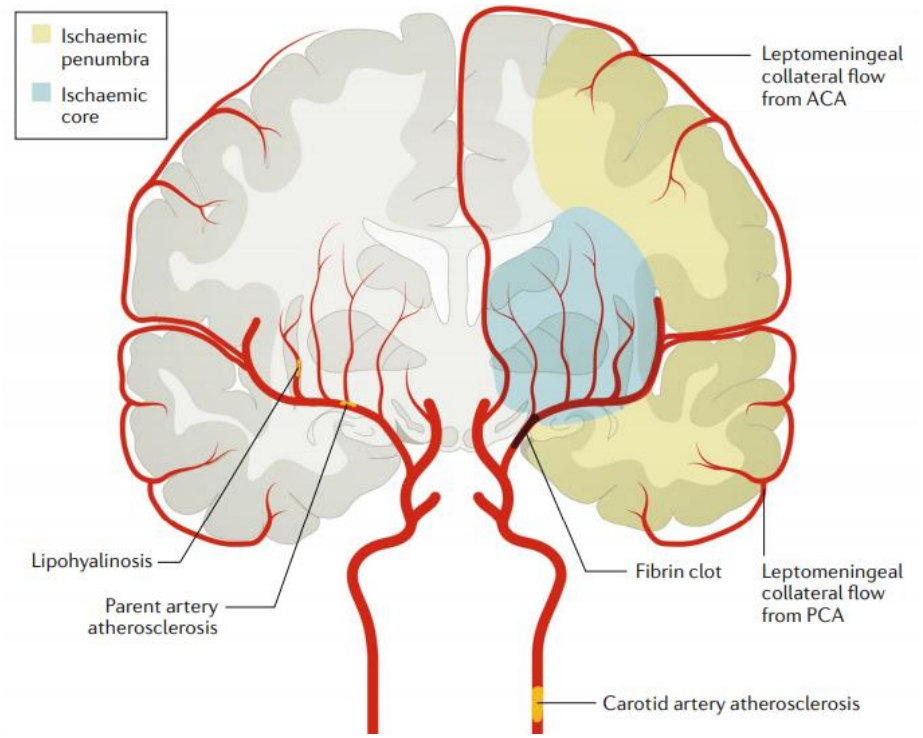

Fig. 3. The ischemic core and penumbra.

The ischemic core in the image above (pale blue color) represents where lenticulostriate 'end arteries' enter the brain and perfuse the striatum and basal ganglia with blood, but have no proximal collaterals or anastomoses. The ischemic penumbra (pale yellow) represents the area of 'at-risk' but salvageable tissue perfused by the distal MCA. Here, damaged tissue can potentially receive blood flow from the posterior communicating (PCA) or anterior communicating arteries (ACA) through the opening of leptomeningeal collateral flow, adapted with permission from (Campbell et al., 2019).

1.2.3 Transition from penumbra to core infarction

The ischemic penumbra represents the parenchymal cells hypoperfused by blood that reside in an inactive metabolically challenged but salvageable state. Critical research in animal models, which vary the duration of ischemia, has expanded our understanding of penumbra to core infarct transition. Specifically, 2 hours of transient ischemia in rats produces the same size of infarcted tissue as a permanent 24-hour middle cerebral artery occlusion, indicating that 2 hours of occlusion causes irreversible cell death in the region of the brain perfused by the middle cerebral artery. Shortening the duration of ischemia to 90 minutes reveals evidence of a penumbra, and an occlusion time of 60 minutes further expands this penumbra. By calculating the ratio of at risk, to dead tissue, researchers could demonstrate that the average speed of infarct expansion in a 300 g rat is close to 3.3 mg/minute after MCA occlusion (Eschenfelder et al., 2008, Liu et al., 2010). Understanding what contributes to infarct expansion is crucial to determining how to save the at risk tissue. Extent of cerebral blood-flow (CBF) dominates this picture, specifically, when CBF is reduced to 55 ml/100g/min protein synthesis is inhibited, glycolysis takes over the role of glucose metabolism when CBF reaches 35 ml/100g/min. Neurotransmitter disturbances occur at a CBF of 20 ml/100g/min and ATP depletion and anoxic depolarization form at CBF values below 15 ml/100g/min. Each of these thresholds, define differential mechanisms and rates of cell death in the ischemic penumbra, which typically is reported to have a CBF of 15-25 ml/100g/min (Hossmann, 1994) (Murphy et al., 2006). These reported viability thresholds reflect a topological gradient of ischemia in which the tissue is prone to spontaneously occurring peri-infarct depolarizations, which form and propagate through neurons and glia in the form of a wave at a rate of 3-5 mm/min after brain ion homeostasis is compromised (Lauritzen et al., 2011).

These waves share similar properties to cortical spreading depolarizations (CSD), which are associated with the aura phase of migraine, but in the context of ischemia, the number and duration of these self-propagating waves in penumbral tissue correlates strongly with the expansion of the infarct over time (Mies et al., 1993, Dijkhuizen et al., 1999). The mechanism underpinning this correlation is thought to relate to an imbalance between the metabolic workload required to restore cell membrane ion gradients after depolarization events and concomitant depletion of the tissue glucose pool. Importantly in this time, peri-infarct depolarizations trigger a brief period of dilation in arterioles, which leads to a short burst of hyperperfusion, followed by a sustainted hypoperfusion as a result of inverse neurovascular coupling, which reduces oxygen and glucose delivery by 20-30% and is believed to exacerbate tissue damage and further delay restoration of cell membrane ion gradients (Hossmann, 2006). In addition, controversially it has been described that peri-infarct depolarizations alter the volume of the paravascular space through constriction of arterioles, forcing cerebral spinal fluid (CSF) into the brain parenchyma which exacerbates edema formation and further worsens ischemic damage (Mestre et al., 2020). Moreover, CSD propagation in the penumbra has also been shown to contribute to the breakdown of the blood-brain-barrier through the activation of matrix metallo proteinases (Gursoy-Ozdemir et al., 2004).

Crucially, the aforementioned deleterious processes negatively impact penumbral tissue survival and highlight that if conditions are not changed by an increase in collateral flow or therapeutic intervention, penumbral tissue will also succumb within hours to sustained levels of oligemia, extracellular excitotoxic compound build up, cell swelling and consistent waves of energy dependent depolarization (Campbell et al., 2019). This facet of stroke pathology led to coining of the term ‘time is brain’ by neurologist Camilo Gomez, which accurately depicts the need for an effective acute stroke therapy and highlights that overtime, penumbral ‘salvageable’ tissue will transition to core necrotic tissue if the perfusion is not reestablished.

The growth function of an ischemic stroke has been estimated to occur as a function of three criteria: 1. The interval from onset to completion of a typical ischemic stroke 2. The volume of the brain compromised by the stroke and 3. The total number of neural circuit elements of interest. Using these functions, researchers estimate that during a large vessel supratentorial ischemic stroke, a patient can expect to lose 1.9 million neurons, 14 billion synapses and 12 kilometers of myelinated fibers per minute. Cumulatively this equates to the brain aging 3.6 years each hour during stroke and highlights the need for acute treatment (Saver Jeffrey, 2006). However, despite the severity of stroke, using MRI diffusion-perfusion mismatch and PET imaging, evidence of a persisting penumbra can be shown in half of the patients with a large vessel ischemic stroke for as long as 8-12 hours (Darby et al., 1999, Baron, 1999, Markus et al., 2004).

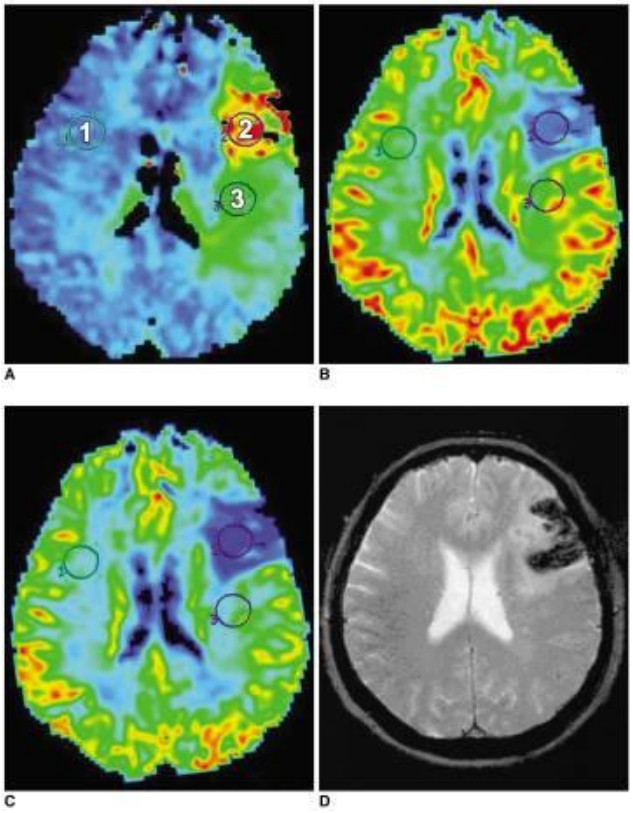

Fig. 4. Magnetic resonance perfusion maps of a 72 year old stroke patient 3 hours after system onset.

A) Shows the mean transit time map, which is regarded as the most sensitive map for perfusion abnormalities while the other maps, such as the cerebral blood volume map **B)** and the cerebral blood flow map **C)**, provide ancillary information. Area 1 represents normal perfusion state and it has no risk of infarction. Area 2 shows a marked extension of the mean transit time with the concomitant decrease of both the cerebral blood volume and cerebral blood flow. This area typically has no chance to survive from infarction and eventually showed hemorrhagic infarction. **D)** Area 3 of moderately prolonged mean transit time shows a slightly increased cerebral blood volume value to maintain the cerebral blood flow. This area often has a benign course and it is salvageable via recanalization treatment, ie. Represents the penumbra, adapted with permission from (Lee et al., 2005).

1.2.4 Acute therapeutic intervention for ischemic stroke

To date, the only drug supported by level 1 evidence (a systematic review of clinical randomized controlled trials) is recanalization of the ischemic territory by intravenous (i.v) injection of alteplase within 4.5 hours of symptom onset. Mechanistically, alteplase causes thrombolysis and achieves recanalization of the major artery occluded and has remained the gold standard in acute stroke therapy since 1996. With a number needed to treat of 7.7, alteplase is a recombinant serine protease that catalyzes the breakdown of plasminogen to plasmin and serves to enzymatically lyse the blood clot; working on both large artery occlusions and lacunar infarcts. Drugs designed to lyse clots are grouped into a class called tissue plasminogen activators (tPA) and have been found to increase the survival in patients suffering from ischemic stroke in a recent meta-analysis consisting of 12 independent clinical trials (Wardlaw et al., 2012). The same Meta analyses also suggests that tPA may be beneficial in patients for as long as 6 hours post stroke citing trials which display improved functional outcome in these stroke patients (Wardlaw et al., 2003a, Wardlaw et al., 2003b). These beneficial treatment effects are also present when mechanically removing the occluding clot using catheter angiography within 6 hours, and in patients which have been screened and selected using brain imaging for as long as 24 hours post-stroke (Albers et al., 2018). However, despite these promising advancements, not more than 20% of stroke patients are eligible to be given such treatment; explaining the need for further stroke therapies which can be administered to a higher percentage of stroke patients (Stroke (2017).

Compounding these major issues in stroke research, after removal of a large artery occlusion, many deleterious secondary consequences of ischemic stroke continue to play out, negatively affecting cell survival post-reperfusion of the occluded vessel. Although decades of research and enormous economical investment has been funneled into stroke therapies, there is no single drug approved by the FDA (Food and drug administration) acting on brain cells to ameliorate stroke outcome (Dirnagl and Macleod, 2009). Furthermore, while reperfusion therapies have shown great promise in clinical trials, crucially, they do not address the key emergent pathological sequelae of ischemic stroke that occur through distinct mechanisms at the level of the microcirculation and push penumbral at risk tissue toward death.

1.3 The ‘no-reflow’ phenomenon

1.3.1 A historical perspective on the no-reflow phenomenon

The no-reflow phenomenon relates to observations that under conditions of ischemia, restoration of patency or reperfusion of the large artery does not adequately restore perfusion to the microvasculature downstream. The microvasculature denoted here refers to vessels under 100 µm in size within the brain parenchyma, including capillaries and their afferent connections and their relationship to the no-reflow phenomenon was first described in the brain in the 1960s in canine and rabbit models (Ames et al., 1968). When experiencing ischemia for 2½ minutes, reperfusion appeared to restore normal flow to brain tissue in rabbits. However, when prolonging the duration of ischemia, researchers noticed that despite successful reopening of the artery, normal blood flow in the brain flow was impaired (Majno et al., 1967, Rezkalla Shereif and Kloner Robert, 2002). This phenomenon occurs in several organs including the brain, skin, heart and kidney and hints at differences in susceptibility of capillaries, arterioles and venules when compared to large vessels following ischemia (Summers and Jamison, 1971, Chait et al., 1978, Allen et al., 1995, Niccoli et al., 2009, O'Farrell and Attwell, 2014). After no-reflow was initially described across multiple organs, further investigations highlighted that no-reflow is not instantaneous, but instead appears to be a process, increasing in severity over time in proportion to the duration of ischemia (Ambrosio et al., 1989).

1.3.2 Pathophysiological hallmarks of the no-reflow phenomenon

Currently, understanding of the pathophysiology of the no-reflow phenomenon remains imcomplete. Despite enjoying a brief period of research interest in the 1960’s, several concerns that no-reflow may be an experimental artifact were raised (de la Torre et al., 1992, Tsuchidate et al., 1997, Li et al., 1998) and then subsequently revised (Hallenbeck et al., 1986, Garcia et al., 1994, del Zoppo and Mabuchi, 2003, Hossmann, 2006, Liu et al., 2002) leading to a lag time in understanding no-reflow pathophysiology. It is now well accepted to occur following transient ischemia and appears to be multi-factorial in nature.

Reports of no-reflow in the brain have been shown to occur after only 5-10 minutes of ischemia, when compared against studies of no-reflow in the heart (where no-reflow did not occur until ischemia lasted 30 minutes)(Ames et al., 1968). Furthermore, incomplete reperfusion is a common feature among stroke survivors that undergo intra-arterial recanalization of the major clot occlusion (Arsava et al., 2018). These findings indicate that the brain may be particularly susceptible to short bouts of ischemia and that removal of the large vessel occlusion should not be the sole focus of therapies aimed at ameliorating stroke outcome.

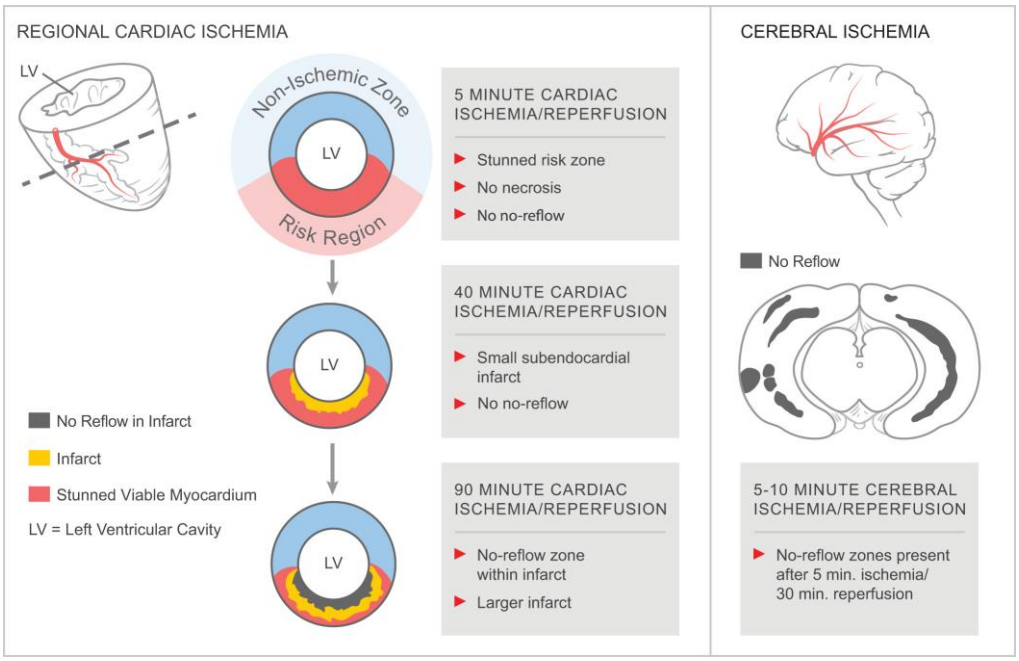

Fig. 5. No-reflow in the heart and brain.

Adapted with permission from (Rezkalla Shereif and Kloner Robert, 2002).

The early reports on no-reflow demonstrated that elements of the blood become entrapped within the microcirculation and result in a mottled appearance, whereby regions of non-perfused tissue were interspersed with regions of perfused tissue (Ames et al., 1968). It is now understood that plasma flow can often persist despite entrapment of cellular elements like erythrocytes, leukocytes and platelets, which has important implications for oxygen circulation and for perfusion imaging in human patients suffering from the sequelae of stroke (Yemisci et al., 2009). At the ultrastructural level, early reports of swollen pericytes and vascular glia (astrocytic endfeet swelling) and bleb formation suggest that the microvasculature is acutely affected in a visible way (Chiang et al., 1968). Furthermore, while pericytes are implicated in the no-reflow phenomenon, neutrophil infiltration and stoppage of these cells in capillaries and post-capillary venules have also been reported as deleterious factors in relation to the no reflow phenomenon (Yemisci et al., 2009, El Amki et al., 2020). Moreover, the spreading depolarization caused by ischemic events elevates the level of extracellular K^+ ions, resulting in spasmic cycles of hyperemia and hypoperfusion which have been shown to contribute to secondary damage during reflow (Wade et al., 1975). Mechanistically, this dramatic alteration of ion flux in the post-ischemic brain also triggers endothelial and astrocyte swelling within an hour of reperfusion (Garcia et al., 1994). Importantly, these processes precede the maxima of neuron cell death, which occurs between 12-24 hours; suggesting therapies targeted at reducing cytotoxic edema which work in animal models may successfully translate to humans (Karibe et al., 1995). These swelling events are followed by an upregulation of endothelial immune receptors, which home leukocytes to the site of ischemic injury and increase blood-brain barrier permeability further, contributing to swelling within the interstitial space, ultimately playing a role in closing off capillaries and exacerbating no-reflow (Mohamed Mokhtarudin and Payne, 2015).

2. Pericytes

Though initially described by C.J Eberth in 1871, the discovery of these contractile mural cells surrounding the endothelium at the capillary level is commonly attributed to Charles-Marie Benjamin Rouget (Eberth, 1871, Rouget, 1873). In the 1920's Robert Zimmerman further characterized these cells, initially calling them Rouget cells, then later creating the name 'pericytes' to infer their perivascular location around the endothelium. Although pericytes were described as contractile, a series of research articles and reviews in the 1950's questioned the true contractility of these cells (Sims, 1986), which is a debate that only recently has been settled with the advent of optogenetic stimulation (Berthiaume et al., 2018b, Nelson et al., 2020). These same reviews however, also generated the accepted definition of a mature pericyte as a 'cell embedded within the vascular basement membrane', which remains useful to this day.

Because of their location, researching pericytes in their mature state is challenging. Some of the initial concerns regarding contractility arose due to experimental challenges, particularly concerning the heterogeneity of the cell population and their identity at large and continued until very recently (Hill et al., 2015). Today, we understand their precise location, morphology and a large part of their role within the neurovascular unit, despite the absence of a true pericyte marker commonly available for all other cell types that make up the NVU.

2.1 Pericyte Ontogeny

Pericytes belong to the family of mural cells (encased within a basement membrane, vSMCs, pericytes, and fibroblasts) and have a wide range of developmental origins, ranging from neural crest, secondary heart field, somites, and splanchnic mesoderm in the case of pericytes lining the aorta. A slew of lineage tracing studies have helped to elucidate many of these heterogeneous developmental origins (reviewed by (Majesky et al., 2011), however it is clear that in the CNS and thymus, the majority of pericytes are neural crest derived, with the exception of cerebral dorsal midline pericytes which arise early on in development from a sub-set of macrophages (Bergwerff et al., 1998, Korn et al., 2002, Heglind et al., 2005, Yamamoto et al., 2017).

Vascular mural cells in other organs have also been mapped. Gut, liver and lung pericytes arise from the mesothelium, a single layer squamous epithelium lining coelomic cavities and its organs (Wilm et al., 2005, Que et al., 2008, Asahina et al., 2011). In this instance, epicardial mesothelium gives rise to coronary vSMCs and pericytes. These findings suggest a common origin of pericytes in coelomic organs of the body, where pericytes undergo epithelial-to-mesenchymal transition (EMT). This is a process under which mural cells delaminate and migrate to these organs to produce mesenchymal components such as fibroblasts, vSMCs and pericytes. Such studies highlight that pericyte and fibroblast origin is closely intertwined and so it logically follows that these cells may respond in a similar fashion under pathological conditions (Fabris and Strazzabosco, 2011, Schrimpf and Duffield, 2011).

Despite the heterogeneous origin of pericytes in the body, endothelial cells which form the inner vessel wall, and mural cells which coat the endothelial cell tube share a number of preserved signalling pathways in most organs of the body that enable the precise control of blood flow, remove waste metabolites and protect the organ from harm.

2.2 Signalling pathways involved in pericyte recruitment & maturation

2.2.1 PDGFB/PDGFRb signaling

Platelet derived growth factor receptor beta (PDGFRb) is one of the most validated mural cell markers in pericyte research and is expressed by pericytes, smooth muscle cells and fibroblasts at high levels. Specifically, PDGFRb is a tyrosine kinase located on the plasma membrane of pericytes and when in contact with its ligand PDGFB, the PDGFRb receptor dimerizes and auto-phosphorylates the cytoplasmic tyrosine residues and binds SH2 domain containing proteins which initiate an array of signal transduction pathways which stimulate, proliferation, migration, negative regulation of apoptosis and recruitment of pericytes.

During the development of angiogenic sprouts, PDGFB serves as a chemotactic attractant for pericytes. Upon secretion, PDGFB binds to heparin sulfate proteoglycans on the cell surface, or within the extracellular matrix through its C-terminal retention motif: limiting the range of this paracrine interaction between PDGFB and its receptor on mural cells. This close receptor/ligand interaction has been shown to be pivotal for pericyte maturation on the vessel wall and knocking out of the retention motif on PDGFB in mice results in a loss of pericyte investment in the microvessel wall (Hirschi et al., 1999, Abramsson et al., 2003). In this way, the PDGFB/PDGFRb signalling axis functions as a crucial (knocking out either results in perinatal lethality via vascular leakage) paracrine-signaling loop between the endothelium and pericytes (Levéen et al., 1994, Bjarnegård et al., 2004).

During vascular development PDGFB/PDGFRb signalling is not uniform. Instead, an arteriole-venuous gradient can be observed corresponding to the thickness of the mural cell coat within the CNS vasculature and the tip of angiogenic sprouts show high levels of PDGFB expression and mRNA production; quickly recruiting pericytes to the tip of the developing vascular lumen (Lindblom et al., 2003). However, this signalling axis is not only important during development, but throughout the lifetime of the organism. Research indicates that constitutive activation of the PDGFRb receptor promotes proliferation of mural cells (including pericytes) and inhibits differentiation in mural cells (Olson and Soriano, 2011).

A mature pericyte engaged in the adult brain has a number of activated pathways triggered by PDGFB/PDGFRb signalling, specifically: Ras, MAPK, PI3K and PLC-γ. First, after binding of the SH2 domain on Grb2 to PDGFRb complexes with Sos1 through SH3 domains. This triggers activation of Ras, which leads to downstream activation of Raf-1 and the MAPK cascade. This MAPK signalling activates gene transcription that function to stimulate cell growth and differentiation and migration and represents one of the key downstream effectors induced by the paracrine signalling of PDGFB/PDGFRb between endothelial cells and pericytes (Seger and Krebs, 1995). In addition, the PI3K family of enzymes are activated by PDGFRb signaling in pericytes, which serve to promote actin reorganization, direct cell movements and inhibit apoptosis. Importantly, PDGFRb has been shown to interact with integrins, localizing the receptor to sites of focal adhesions where several signalling pathways initiate and crosstalk (Clark and Brugge, 1995).

As PDGFB/PDGFRb signalling constitutes a master regulator of gene expression and cell function in pericytes, the balance of ligand/receptor quantity and downstream effector function must be carefully regulated. This is achieved by ligand occupancy of the PDGFRb receptor. Receptors

bound to PDGFB are promoted toward dephosphorylation by binding of SHP-2 tyrosine phosphatases, which dephosphorylate the PDGFb receptor and its substrates and promote endocytotic receptor internalization. Internalised PDGFRbs are degraded in lysosomal compartments by c-Cbl and receptor ubiquitination, limiting the duration of PDGFRb signalling (Andrae et al., 2008).

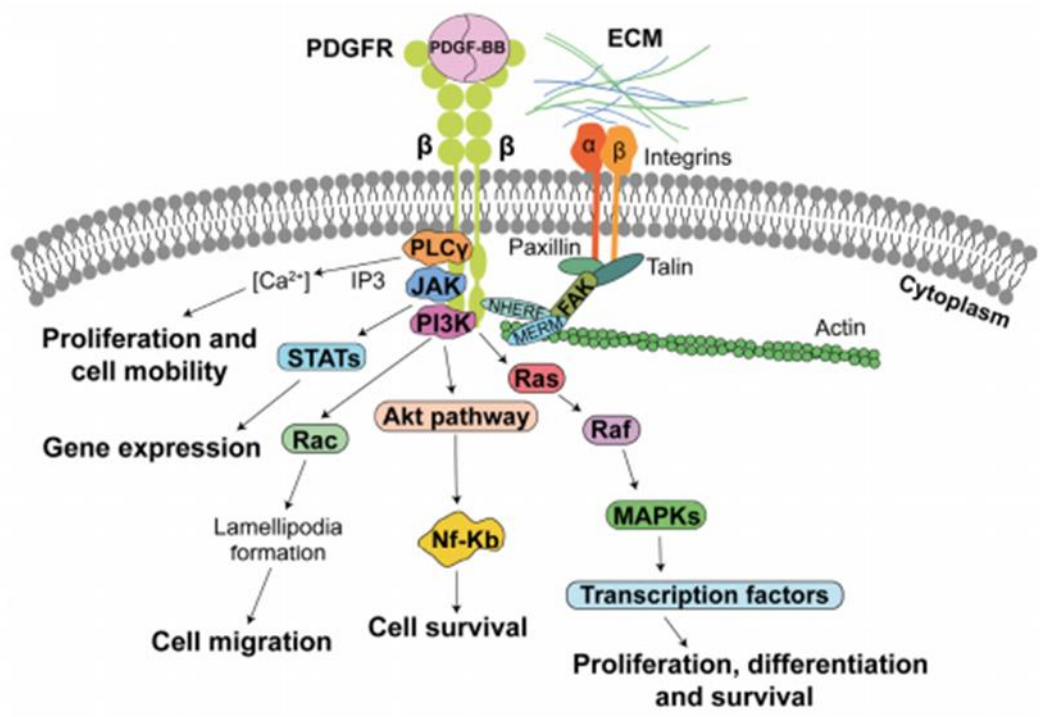

Fig. 6. Downstream signalling pathways activated by PDGF-BB mediated activation of the PDGFRb receptor.

Adapted with permission from (Evrova and Buschmann, 2017).

2.2.2 Angiopoietin-1/Tie-2 signaling axis

Pericytes express angiopoietin-1 (Ang-1) while its receptor Tie-2 is expressed on endothelial cells. This interaction can be thought of as how pericytes aid endothelial maturation; while the aforementioned PDGFB/PDGFRb interaction initiated by endothelial cells matures pericytes respectively. The interaction of Ang-1/Tie-2 serves to reduce vascular leakage and regulate endothelial stability and several studies involving Ang1 or tie2 deficient mice highlight the importance of these signalling molecules (Thurston et al., 1999). Deficiency of either molecule results in cardiovascular defects and closer analysis of the vasculature identified a lack of mural cells. Mutations associated with the TIE2 gene result in venuous malformation resulting from the loss of the venuous mural cell population (Patan, 1998). Interestingly, pericyte recruitment to the endothelium can occur independently of the Ang1/Tie2 signalling axis (Jeansson et al., 2011, Jones et al., 2001); however, competitive over expression of the Tie2 antagonist Ang2 appears to mediate pericyte loss (Hammes et al., 2004).

One of the most interesting aspects of this signalling cascade arises from vascular studies on the overexpression of Ang1. In this scenario, researchers found that the Ang1 contributes to emergent vascular complexity; noting that vessels were remodelled into a highly branched, higher-order hierarchical structure (Thurston et al., 2005, Uemura et al., 2002). Though many aspects of the Ang1/Tie2 pathway remain to be elucidated, it appears clear that pericyte Ang1 interacts with

endothelial Tie2 to stabilize the vasculature and promote its quiescence, maturing the endothelium and preventing additional branching once vessels are formed (Armulik et al., 2011).

2.2.3 TGFβ signalling

To date, understanding of TGFβ and its receptor and their role in relation to pericyte function remain incomplete because both endothelial cells and pericytes express both the ligand and its receptor; making knock-out studies challenging. Endothelial cells and pericytes express TGFβ and as a signalling axis it is believed to induce mural/endothelial cell differentiation and proliferation. Since the signalling is interdependent between the two cell types, elucidating the relative contribution to each cell type is challenging, but the identification of two TGFβ receptors Activin receptor-like kinase 1 and 5 have helped to elucidate some of the TGFβ function. Alk1 and Alk5 are expressed on both cell types but interestingly; appear to confer opposite cellular effects. Alk5 leads to phosphorylation of Smad2/3, promoting mitotic and migratory quiescence and differentiation into a smooth muscle cell subtype of mural cell; where Alk1 phosphorylates Smad1/5 which functions to oppose SMC differentiation and promotes cell proliferation and migration (Goumans et al., 2002). These pathways hint at Alk5 being involved in vessel maturation at the arterial side of the vasculature during the transition to a fully formed vasculature, whereas Alk1 expression may dominate during early development.

2.2.4 Notch signalling

Notch signalling is a crucial cell-cell communication pathway conserved from *Drosphila melanogaster* to humans. Currently, there are four different notch receptors known (Notch1, 2, 3, 4) and five different ligands (Jagged1, 2 and Delta like-1, 2 and 3). Notch receptors are transmembrane proteins expressed in a wide variety of cell types and regulate cell fate determination, proliferation and survival of neighbouring cells through lateral inhibition. Notch3 is highly expressed in pericytes and smooth muscle cells of the mural cell lineage and disruption of notch3 signalling results in enlarged vessels due to lack of pericytes (Que et al., 2008). Accordingly, patients suffering from CADASIL syndrome, which is associated with notch 3 mutation also present vessels lacking pericytes (Louvi et al., 2006). Taken together, these results demonstrate that Notch3 is necessary for fully functioning arteries and pericyte involvement. Interestingly, the study of Notch3 signalling in relation to pericytes were some of the first studies which indicate that pericyte presence on the capillary endothelium may serve to *limit* capillary lumen diameter (Hellström et al., 2001).

2.2.5 Ephrin signalling

While many of the aforementioned pathways confer mural cell investment across the entire vascular endothelium (arteriole-capillary-venule), pericytes remain unique cells at the capillary level and have recently been shown to be regulated by another class of tyrosine kinases called Ephrin receptors. Ephrin B2, the ligand for EphB receptor has been shown to be required for normal association with small diameter blood vessels. In this work, the authors show that mutant mice deficient for Ephrin B2 display perinatal lethality, vascular defects in a variety of organs and abnormal migration of smooth muscle cells to lymphatic capillaries. In addition, the authors point out that extracellular matrix deposition and the interactions occurring at this level are also negatively affected. Interestingly, the authors also note vSMCs are rounded, rather than banded suggesting that the spreading and correct orientation of these cells is also Ephrin B2 dependent. Moreover, the authors also note that pericytes were frequently observed to bridge two capillaries; making

only loose contact with endothelial cells (ECs), stretching away from vessels and appearing rounded. Morphologically, high-Eph2-EphB signalling denotes a defined cytoskeletal structure, whereas low Eph2-EphB signalling denotes a certain level of mural cell motility and plasticity (Foo et al., 2006). In summary, Ephrin signalling in mural cells and pericytes is starting to shed light on the unique shape and appearance of mural cells at the microvessel level.

2.3 Pericyte morphology & motility

Mural cells in relation to their function, display a remarkable range of unique morphologies depending on their location within the vasculature. Arteries and arterioles are coated by vSMCS, which are short, ring-shaped, and densely packed. In stark contrast, pericytes, which cover capillaries intermittently, have protruding ovoid cell bodies with long thin processes that run longitudinally along capillaries; making inter-digitated 'peg and socket' connections directly with ECs.

It appears obvious at first glance that these cells are arranged in a meshwork along the vasculature, suggestive of a network. Nevertheless, it remains unclear how this network is formed or regulated at the biochemical level, but recent work has shed light on the motility of pericytes. It has recently been shown that pericyte soma do not move in the adult brain. However, through targeted deletion of pericytes using laser ablation, it is now understood that under basal conditions their longitudinal processes extend and retract in a 'pull-push' territorial exchange, extending and retracting respectively from the cell soma over days to weeks (Cudmore et al., 2017, Berthiaume et al., 2018a). This appears to occur in an attempt for each process to cover the entire endothelium, with proximal pericytes invading the territory of the pericyte ablated.

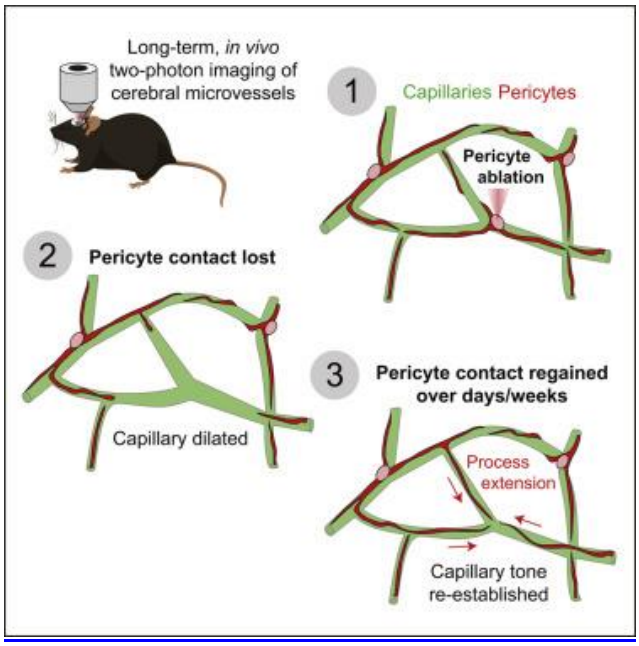

Fig. 7. Dynamic territorial coverage of pericyte processes in response to laser ablation.

Ablation of pericytes triggers movement of pericyte processes, in between basal tone of the capillary is lost at the site the pericyte was ablated till neighbouring pericyte processes extend over the ablated pericyte territory and reestablish basal capillary tone, adapted with permission from (Berthiaume et al., 2018a).

According to recent exquisite research by Roger Grant from the lab of Andy Shih, a number of morphologically different pericyte sub-types can be found within the microvasculature and can be distinguished based on the degree of coverage over the endothelium and cell length (Grant, 2019). Here, the authors describe that pericytes after the smooth muscle actin terminus (a contractile element present up until the pre-capillary arteriole-arteriole transition) can be distinguished into ensheathing pericytes, mesh pericytes and thin-strand pericytes. Ensheathing pericytes cover most of the endothelium and are found on large capillaries ~9 µm in diameter, while mesh pericytes cover around 70% of the endothelium and are found on vessels approximately 6.3 µm in diameter. Thin-strand pericytes are present on higher order capillaries around 4.9 µm in diameter, cover approximately 51% of the endothelium and are the longest cell type at an average of over 150 µm when including their processes. Briefly, pericyte vessel coverage decreases as branch order increases, but the distance between each pericyte grows with thin-strand pericytes extending their processes to reach to the territory of the neighboring pericyte up to 75 µm away.

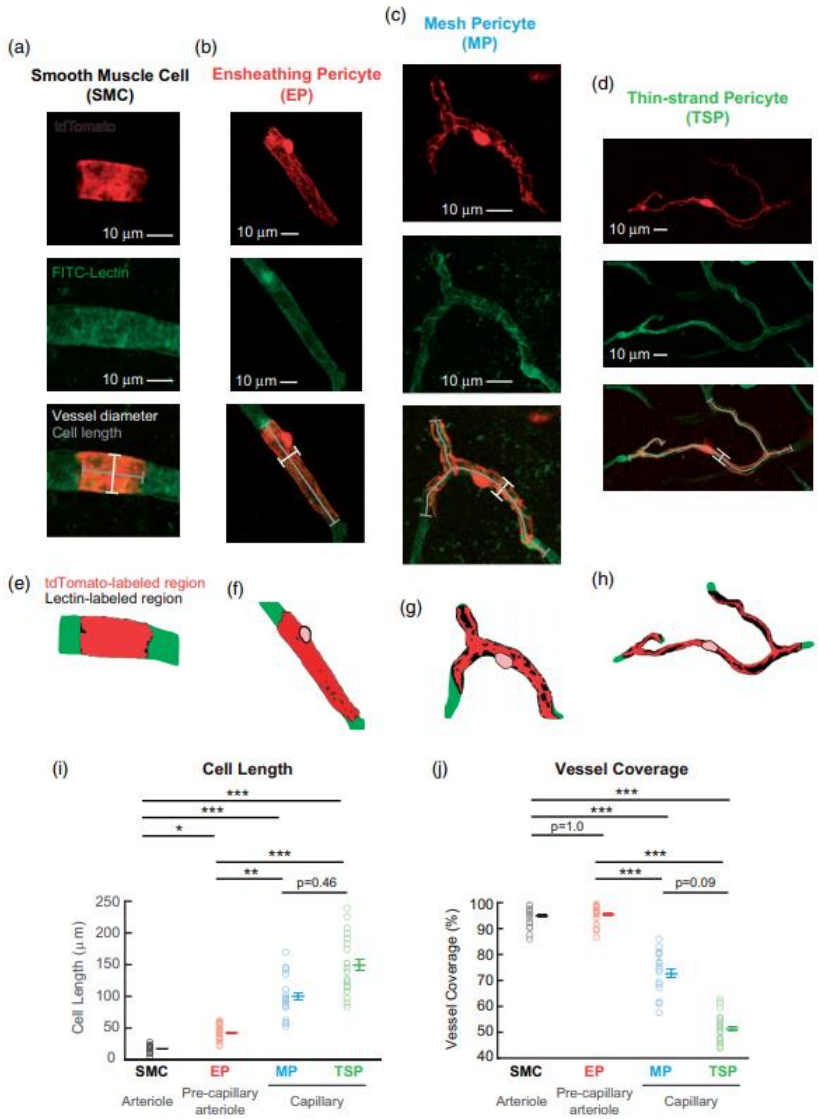

Fig. 8. Mural cell types exhibit varying cell length and degree of coverage.

A, B, C, D) varying mural cell types labelled using a PDGFRbCre mouse expressing Tdtomato. **E, F, G, H**) Morphological schematic of different pericyte sub-type appearance. **I)** Average cell length of each reported mural cell type. **J**) Average vessel coverage in percentage of each mural cell sub-type, adapted with permission from (Grant et al., 2019)

2.4 Pericyte function in the healthy brain

Among all organs, pericytes within the CNS are found in most abundance, with an endothelial: pericyte ratio of 1:1-3:1 (Sims, 1986, Mathiisen et al., 2010). Other organs, which have notably high pericyte abundance, are the testis and retina and appear to reflect the endothelial barrier properties of the CNS and the complexity of the vascular plexus in which they reside (Díaz-Flores et al., 2009).

2.4.1 Pericytes and the blood-brain barrier

One of the unique aspects of the CNS is that it is preferentially protected from passive transport of cells and metabolites across the vessel wall into the parenchyma in favour of specific, targeted active transport via tailored receptors. This 'tightness', or heavily regulated aspect of the vasculature is called the blood-brain barrier and is crucial for physiological NVU function (Sagare et al., 2013). Vascular permeability must be regulated in a bespoke way by each component of the NVU and an increase in vascular permeability can lead to the development of serious pathological conditions such as sepsis, allergic reactions, autoimmune diseases and viral infection. The double-edged sword of blood-brain barrier is that it creates a scenario in which the brain is immune privileged, which in turn increases the importance of a functional BBB to CNS function. In 1885 Paul Ehrlich noted that many vital dyes did not stain the brain and spinal cord, but the existence of the BBB as a system was first reported in 1898 – 1900, when intravenous injection of cholic acids or sodium ferrocyanide had no pharmacological effects on the CNS, when compared against intraventricular application of the same substances (Kraus, 1898, Lewandowsky, 1900). Since this early research, the BBB is now recognised as a multicomponent system, with many regulatory elements that work in synchrony to achieve a tightly regulated specific non-permissive transport system (Abbott et al., 2010).

Many of these recent advances in the study of the BBB have noted that pericytes play a pivotal role in the establishment and maintenance of the BBB, with CNS pericytes harbouring specialised functions and marker expression when compared against other organs (Armulik et al., 2010, Bell et al., 2010, Daneman et al., 2010). The way in which pericytes regulate the BBB is many fold, with the first reports coming from *in vitro* assays of pericyte-endothelial culture indicating that the presence of pericytes increases the trans endothelial electronic resistance (TEER)(Hayashi et al., 2004, Al Ahmad et al., 2009). Though many of these studies helped elucidate that endothelial cells may form tighter junctions with one another in the presence of pericytes when compared against other cells such as astrocytes, conflicting reports made a definitive conclusion on the matter problematic (Zozulya et al., 2008).

The understanding of BBB formation and regulation pivotally advanced forward when developmental and vascular labs performed experiments on PDGFRb deficient mice independently, both coming to the same conclusions, that pericytes decrease endothelial cell permeability and the extent of pericyte loss correlated directly with the amount of vessel permeability (Daneman et al., 2010, Armulik et al., 2010). Interestingly, both studies noticed that loss of pericytes did not alter the general profile related to the endothelial cell signature. Despite this, several altered genes in endothelial cells were found using microarray assays such as: vegfa, ang2 and ang1, suggesting that these genes play a crucial role in BBB maintenance and that the presence of pericytes aids in tailoring the endothelial transcriptomic profile toward a mature BBB. Moreover, the same studies identified that loss of pericytes stimulates endothelial cells to upregulate transcytosis pathways that do not discriminate molecule size, and induces the presence of astrocytic end foot defects.

Taken together, pericytes exert several independent, partially understood pathways in a paracrine manner on NVU cells in direct contact to create a functioning BBB.

2.4.2 Pericyte influence on capillary blood flow

In order to sustain neuronal function, neurovascular coupling (NVC) must effectively couple supply to demand through the increase of blood flow to the region of neuronal firing, this process is known as 'functional hyperaemia' and underlies the signal generated from blood oxygen level dependent (BOLD) imaging when patients undergo an MRI. Specifically, blood is shunted to regions of high neuronal activity, which requires coordination of the neurovascular unit at multiple hierarchical levels from artery to capillary.

Previously, this blood flow increase at the capillary level was attributed to large vessels upstream such as arteries and arterioles, which are coated with large numbers of vSMCs that constrict and relax to regulate blood flow. Interestingly, the same molecules which dilate and constrict arterioles such as arachidonic acid derivatives and neurotransmitters were shown to work on pericytes cultured on rubber membranes (Shepro and Morel, 1993), and in a series of research, these neurotransmitters were shown to alter the intracellular Ca^{2+} in pericytes; suggesting that intracellular Ca^{2+} may alter pericyte cytoskeleton formation (Puro, 2007). Later, in excellent work from Claire peppiatt and colleagues, pericytes were shown to regulate the CNS capillary diameter in a bidirectional manner (Peppiatt et al., 2006). However, data explaining how blood flow increases could be attributable to pericytes in the stimulated brain *in vivo* was still missing. Subsequent *in vivo* research applying thromboxane, which constricted pericytes, highlighted that pericytes were contractile, but in the very same paper, authors suggested that in relation to neurovascular coupling, pericytes passively dilated due to the effect of cortical spreading depolarizations on upstream arterioles. The authors go on to state that they believe CSDs should be a sufficiently short term stimuli to recruit a pericyte response temporally independently from upstream arterioles, but failed to demonstrate pericyte involvement in the hyperemic response as a result (Fernández-Klett et al., 2010). Recent research has clarified this experimental issue.

In 2014, Catherine Hall and colleagues demonstrated that pericytes increase blood flow *in vivo* in response to whisker stimulation, and further highlighted that pericytes dilated *before* arterioles; suggesting the presence of a retrograde signal, initiated at the capillary level and back propagating upstream prior to arteriole dilation (Hall et al., 2014). Not only was this research groundbreaking as it marked the true transition from NVC experimentation on brain slices to the living animal, but also in the same paper, the authors attempted to decipher many of the signalling pathways through which pericytes could dilate or constrict in exquisite detail. In this work, they reveal how prostaglandin E_2 mediates pericyte dilation, but requires suppression of 20-HETE (a vasoconstricting metabolite) by nitric oxide release in order to successfully relax pericytes and expand capillary lumen diameter.

With the discovery that pericytes can alter capillary diameter, work began on exactly which contractile elements could mediate this pericyte induced capillary dilation. Using flash freezing tissue preparation and actin stabilisation methods, Alarcon-Martinez and colleagues could show that pericytes express contractile proteins normally associated with vSMCs (Alarcon-Martinez et al., 2018), though interestingly, not all pericytes require these canonical contractile elements to dilate/constrict the capillary (Hartmann et al., 2018).

How these capillary level dilations are coordinated to produce the 100 µm-400 µm spatial size corresponding to the area matching neuronal interactions seen with fMRI BOLD imaging

remained an intruguing question for pericyte researchers. In 2019, using retinal explants, the pericyte connectome was revealed using dye injections into single pericytes, and revealed that each pericyte could communicate locally with each other, both along the same capillary network and across capillary networks; explaining the spatial blood flow increase noted after BOLD imaging at the capillary level. These pericytes were then demonstrated to be capable of signalling to one another through intracellular Ca^{2+} waves in a connected fashion via gap junctions (Connexins) (Hamilton et al., 2010, Alarcon-Martinez et al., 2018, Kovacs-Oller et al., 2019).

The question of how pericytes preferentially direct blood flow responses to one capillary network or another was also recently deciphered last year, when research showed that pericytes direct local blood flow at capillary level junctions (Gonzales et al., 2020). To date, understanding of whether potassium or Ca^{2+} transients mediate the change in cytoskeleton required to constrict or dilate vessels, remains unclear.

Since initial contradictory articles suggesting that pericytes may be incapable of initiating functional hyperemia based blood-flow increases at the capillary level (Hill et al., 2015), the understanding of pericyte function in relation to blood flow control has *staggeringly* increased over the last decade and is no longer in question. Moreover, recently, two independent labs have used channel rhodopsin expression in capillary pericytes to demonstratively prove *in vivo* that pericytes can indeed control capillary diameter in response to optogenetic stimulation. In summary, recent research *overwhelmingly* suggests that pericytes *do* exert a substantial but slow influence on capillary diameter, though the temporal aspects of this dilation in relation to previous research require further clarification and remain highly disputed (Hartmann et al., 2021).

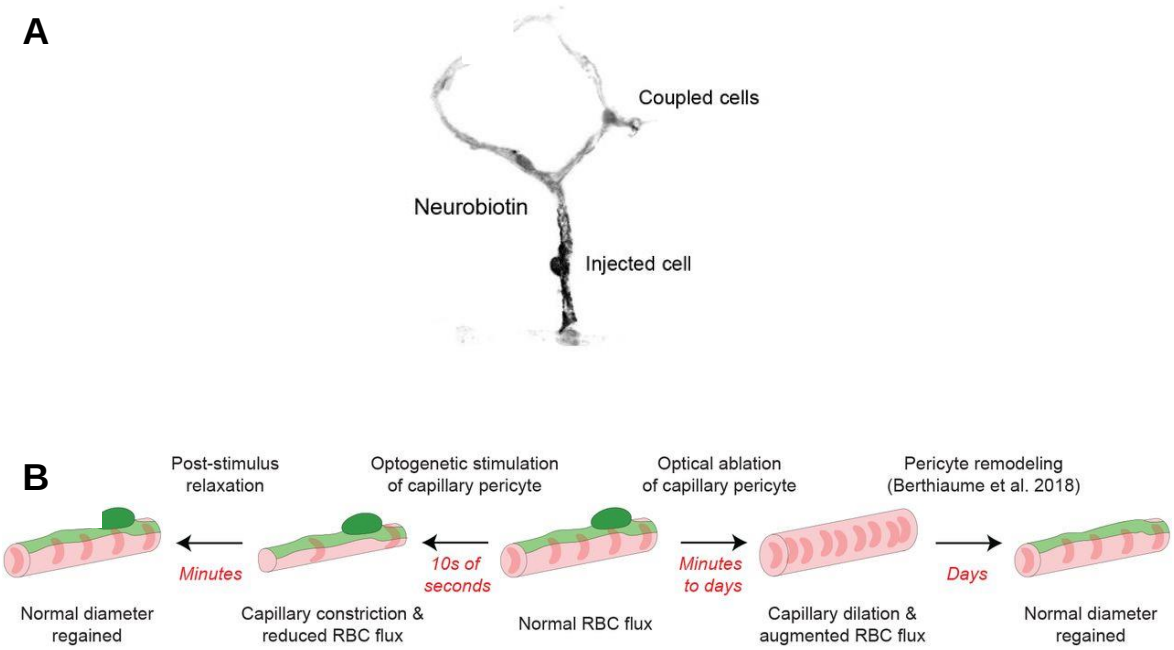

Fig. 9. Recent advancements in pericyte research.

A) A pericyte on a retinal capillary injected with biotin connects to neighbouring pericytes, proving that interpericyte channels exist and establishing the notion of a pericyte connectome. **B)** Pericyte response to channel rhodopsin stimulation contracts slowly over 10s of seconds, ablation of pericytes leads to capillary dilation and augmented RBC flux until pericyte processes grow over the bare capillary, re-establishing a basal constrictive tone and normal diameter is regained, adapted with permission from (Kovacs-Oller et al., 2019, Hartmann et al., 2021)

2.5 Pericyte dysfunction in disease

2.5.1 CADASIL

CADASIL is the single most common cause of stroke and dementia (Chabriat et al., 1995, Dichgans et al., 1998, Chabriat et al., 2009). Caused by mutation of Notch 3 which encodes for a surface receptor on smooth muscle cells and pericytes, the mutated form of Notch 3 accumulates in blood vessels of CADASIL patients and CADASIL mice. As a result, arteries become fibrotic, reducing blood flow and this ultimately results in white matter lesions, thinning of the cortex and dementia (Joutel et al., 1996). CADASIL cellular pathogenesis was originally noted in smooth muscle cells, which were reported to sustain damage and die due to the accumulation of mutant Notch3 extra cellular domain aggregates (Joutel et al., 2010). However, in mouse brains, SMC viability appeared to be unaffected, which suggested another origin of CADASIL pathogenesis (Joutel et al., 2010). Subsequently, recent work from our lab has shown that a source of CADASIL pathogenesis actually occurs in pericytes. With increasing age, mutated notch 3 aggregated around periytes causing detachment of astrocytic end-feet, leakage of plasma proteins and reduction in adherens junctions on endothelial cells (required for BBB maintenance), ultimately resulting in microvascular dysfunction at the capillary level (Ghosh et al., 2015).

2.5.2 Alzheimer's disease (AD)

Alzheimer's disease results from the pathological production of Amyloid β (Aβ) oligomers, downstream protein tau dysfunction and triggers neuronal damage through loss of synapses, synaptic plasticity and eventually cell loss that results in severe cognitive impairment. Surprisingly, though most Alzheimer's research focuses on neuronal pathology, the first biomarker of the disease is actually reduced cerebral blood flow; implicating a profound microvascular dysfunction in the progression of the disease (Iturria-Medina et al., 2016, de la Torre and Mussivand, 1993). This has triggered a wave of recent research that implicates pericytes in Alzheimer's disease progression (Nortley et al., 2019, Montagne et al., 2020, Miners et al., 2018, Kisler et al., 2017b). As part of this wave of scientific progress, researchers uncovered that Amyloid β oligomers constrict human capillaries in Alzheimer's disease through signalling to pericytes. Specifically, they demonstrate using mouse models and fixed brain slices from human patients that capillaries were specifically constricted at pericyte location. when applying Aβ oligomers to live human brain slices they could demonstrate that pericytes constricted capillaries through a mechanism involving reactive oxygen species (ROS) through NOX4 (reduced nicotinamide adenine dinucleotide phosphate oxidase 4) which stimulated release of Endothelin-1 acting on ET_A receptors to evoke pericyte contraction (Nortley et al., 2019). Moreover, this pericyte contraction in the context of Alzheimer's disease appears to reduce blood flow in the brain by half without involvement of arterioles and venules. Ultimately, this accumulation of Aβ in pericytes results in cell death (Hamilton et al., 2010).

2.5.3 Traumatic brain injury

Traumatic brain injury (TBI) accounts for 30% of injury-related death in the United States and is defined as a brain lesion caused by either direct or indirect external mechanical impact. A direct TBI could come from penetration of a projectile like a bullet or blunt object, or in the indirect case, explosions that trigger a blast wave, shaking and disrupting the normal function of the brain. Traumatic brain injury can be separated into mild (concussion) moderate and severe cases (presence of bleeding).

In 2000 Paula Dore-Duffy's lab demonstrated that pericytes were capable of migrating away from the vessel wall after traumatic brain injury (Dore-Duffy et al., 2000). Interestingly, contrasting with other diseases where pericytes remain on the vessel (Alzheimer's, stroke, subarachnoid haemorrhage) 40% of the pericytes are reported to migrate away from the vessel in the site proximal to TBI within the first hour. These data represent some of the first investigations of pericytes after traumatic brain injury and research carried out since has helped elucidate that pericytes respond to TBI in a biphasic fashion. In 2015, researchers identified that pericytes respond to TBI in two separate stages, after the initial impact, rapid pericyte loss is observed within the first 12 hours and is subsequently followed by reactive pericytosis on day 5 (Zehendner et al., 2015). The authors report stark changes in peri-contusional pericyte morphology, noting an amoeboid shape, which did not imply they were in close vascular contact. Furthermore, the authors report that pericytes were $Ki67^{+}$ (a marker for cell cycle entry), suggesting an active cell response at the infarct edge. These findings mirror the study of many acute on-set pathologies such as the pericyte response to ischemic stroke, which is discussed in detail below.

2.6 Pericyte response to stroke

2.6.1 Acute phase

Pericytes are reported to constrict during stroke, entrap erythrocytes and fail to restore flow due to oxidative-nitrative stress after reperfusion (Yemisci et al., 2009). This contraction is likely the result of a failure to expel Ca^{2+} ions from the cell leading to an intracellular Ca^{2+} increase, which compromises the initial arrangement of the pericyte cytoskeleton, which may be responsible for regulating basal capillary tone. Under conditions of chemical ischemia seen in brain slices, this constriction maximally occurs within 30 minutes, constricting blood vessels by up to 80% which occurs concomitantly with a loss of selective membrane transport indicated by positive propidium iodide staining (PI); a membrane impermeable dye under physiological conditions. In these models, 90 mins of ischemia in the rat was sufficient to kill approximately 70% of pericytes, which then constricted vessels and produced long-lasting constriction of the microvascular bed despite reoxygenation (Hall et al., 2014).

Mechanistically, this pericyte death was mediated in part by glutamate excitotoxicity but in contrast to earlier work, was unaffected by scavenging free radicals (Yemisci et al., 2009, Deguchi et al., 2014). Together, this had led pericyte biologists to the theory that under conditions of ischemia, 'pericytes first constrict and then die in rigor' (Hall et al., 2014). These findings are partially, but not fully supported by compelling new *in vivo* findings that demonstrate that pericytes in the retina constrict maximally after 30 minutes of ligation of the ophthalmic vessels upstream (Alarcon-Martinez et al., 2020). However, according to the authors, maximal constriction of pericytes was not 80%, but 30% *in vivo* - a radically different result from brain slice experimentation

reported earlier (Hall et al., 2014). In stark contrast to this work, using transgenic mouse models and *in vivo* 2-photon microscopy, other researchers could show optogenetic, whisker stimulation and spreading depolarisation (which occurs acutely during stroke) induced change in blood flow occurred at sites where microvessels were covered in SMCs, but not at the capillary level where pericytes are found (Hill et al., 2015). Moreover, using a transient model of middle cerebral artery occlusion, these authors could show that hypoperfusion was caused upstream of pericytes, in SMC covered vessels. Taken together, this research implies that pericytes are *not* responsible for reducing brain perfusion in pathological contexts.

In addition, pericytes have also been shown to acutely induce the breakdown of the BBB by rapidly releasing MMP9 after occlusion of the upstream vessel using *in vivo* 2-photon microscopy. In this study, the authors report that plasma leakage at the pericyte cell body was three times higher than along pericyte processes after cessation of upstream flow (Underly et al., 2017). These findings strongly implicate pericyte induced BBB breakdown in the damaging sequelae, which occur from plasma leakage into parenchyma - a facet of stroke known to increase tissue damage (Haley and Lawrence, 2017, Brouns et al., 2011). Interestingly, circulating PDGFRb release into the blood stream is a biomarker of stroke negatively associated with stroke outcome, which may hint at early loss of pericytes (Brouns et al., 2011).

Taken together, though there is an extreme paucity of longitudinal *in vivo* research on pericytes in the context of stroke, the findings that *do* exist so far are contradictory. Overall, they appear to suggest that unlike endothelial cells, pericytes cluster with neurons into an extremely sensitive cell type which die after prolonged exposure to ischemic conditions, entrapping erythrocytes and increasing microvascular resistance, further harming neurons. In this way pericytes are currently thought of as a cell type deleterious to neuronal survival, contributing from ischemic penumbra to ischemic core transition as they constrict and die, starving the brain parenchyma from the O_2, glucose and other metabolites necessary for cells to survive.

2.6.2 Sub-acute phase

Following the first hours of ischemic stroke, the aforementioned reports would suggest that pericytes within the infarct core are dead and remain constricted on the vessel until they are removed by microglia (Hall et al., 2014, Fernández-Klett et al., 2013). In the days following stroke, pericytes have been reported to upregulate expression of NOX4 in the peri-infarct region, an enzyme that produces ROS and leads to downstream production of MMP9, further exacerbating ischemic damage on days 1 - 4 post stroke (Vallet et al., 2005, Nishimura et al., 2016).

In addition, interesting data suggest that pericytes have a multi-potent capacity following stroke and may acquire a microglial phenotype in the sub-acute phase. This phenotype switch appears to happen within 7 days and occurs concomitantly with proliferation of pericytes, activation and migration from the vessel wall into the brain parenchyma (Özen et al., 2014). Pericytes which leave the vessel wall in this way may be multipotent, and following stroke have been shown to express the activated marker Regulator of G protein coupled signalling 5 (RGS5), an amoeboid morphology and galectin-3 - a marker canonically associated with macrophages/microglia (Özen et al., 2014, Sakuma et al., 2016). Though RGS5 is a marker of activated pericytes, the researchers subsequently showed that genetic knockdown of RGS5 in pericytes leads to neurovascular protection (Özen et al., 2018). This research implies that the activation of pericytes and subsequent migration away from the vessel wall may be detrimental, though the current mechanisms through which this damage is mediated is unknown. Contrastingly, research using a transcription factor called Tbx18 to lineage trace populations of pericytes has shown that pericytes do not

behave in a stem cell like fashion in vivo, questioning their multipotent capacities in both physiological and pathological contexts (Guimarães-Camboa et al., 2017).

2.6.3 Chronic phase

To date, little is known about how pericytes contribute to long-term recovery processes in the brain in the weeks post stroke. After the acute damage of stroke has concluded, a glial scar begins to form from glial fibrillary acid protein$^+$ astroglia in the peri-infarct area composed of chondroitin sulfate proteoglycans such as neurocan and phosphocan along with the generation and secretion of large amounts of extracellular matrix proteins like laminin and Collagen IV. This functions to separate healthy tissue from compromised tissue and is crucial to the wound resolution process, which limits inflammation and further neuron damage.

Recently, using lineage tracing experiments labelling glutamate aspartate transporter GLAST$^+$ pericytes, which represent about 10% of all pericyte cells within the CNS vasculature, researchers could show that pericytes are also involved in fibrotic scar formation and that this a highly evolutionarily conserved mechanism. In this work, researchers demonstrate that after spinal cord injury, traumatic brain injury, stroke, brain tumor formation and a mouse model of multiple sclerosis called experimental autoimmune encephalomyelitis (EAE), the same cellular origin of fibrotic scar tissue could be traced back to what they term type A pericytes. In contrast to the work mentioned previously (Özen et al., 2014) and in other models of CNS trauma, this study could show that nearly all Type A (scar forming) pericytes remained associated with the vasculature and drastically increased in number on Day 5 post stroke. As opposed to the contralateral hemisphere, where Type A$^+$ pericytes represented 10% of all pericytes, the type A$^+$ scar forming pericytes represented between 40 - 60% of the PDGFRb$^+$ pericytes in the infarct core.

Subsequently, it was shown that the lesion gradually condensed over time and the number of cells declined. Interestingly, when the lesion was large enough to affect both cortex and striatum, the investigation showed that cortico-striatal infarcts displaced a large number of PDGFRb$^+$ stromal cells from the vessel wall; suggesting differential percyte responses based on gray matter location (Dias et al., 2020)

To what extent this pericyte formed scar limits the brains ability to recover is currently unknown. On the one hand, scar tissue is necessary to separate the injured brain from the healthy brain, on the other hand, scar formation, originated from Type A pericytes, has been shown to inhibit axon regrowth in the context of spinal cord injury (Dias et al., 2018).

2.7 Project aim

In the last 15 years, pericytes, a previously neglected but vital component of the brain, have been implicated in a wide range of pathologies which affect the most crucial of NVU components, and often in a deleterious manner. While a consensus on pericyte involvement in BBB maintenance, contribution to Alzheimer's disease progression, spinal cord injury and many other pathological disorders has been reached, no such consensus can be applied to stroke. In part because stroke is a complex, multiphasic, acute onset disease. As previously mentioned, a wide range of contrasting and conflicting reports regarding pericyte contractility, dysfunction and eventual cell fate muddy the water of pericyte research. One key reason for this relates to the identification of these cells, which to date, have no true validated and exclusive marker. Consequently, our understanding of pericyte cell fate after ischemic stroke is incomplete.

During stroke pathology, identification of on-going deleterious processes related to pericytes *in vivo* is experimentally challenging, and requires the use of complex experimental methods and modalities. These difficulties were highlighted in a letter in response to the first intravital imaging of pericytes during ischemia-reperfusion injury (Yemisci et al., 2009) in 2010 (Vates et al., 2010). In this correspondence, the author's state that while the experimental evidence provided is compelling, it is currently incomplete (Yemisci et al., 2009). They go on to state that dynamic evidence of pericyte contractility during stroke is missing, stating that the data on entrapment of red blood cells (RBCs) is not visually convincing. Furthermore, they highlight the issues with extrapolating from *ex vivo* data to explain *in vivo* findings by raising concerns about the artifacts associated with tissue fixation. They also state that cells reported as pericytes by the publication may not indeed be pericytes, citing inconsistencies in the author's own reporting on the morphology of these cells. Ultimately, although this paper was a large step forward in pericyte research, and was the first to implicate pericytes in the post stroke 'no-reflow phenomenon' in a convincing manner, they fall short of providing definitive proof.

In the 10 years since, our understanding of pericytes, their array of morphologies, criteria for identification and knowledge of their physiological function has expanded exponentially (Zhang et al., 2020), yet dynamic longitudinal imaging of single pericytes as they experience stroke pathology has still not been achieved.

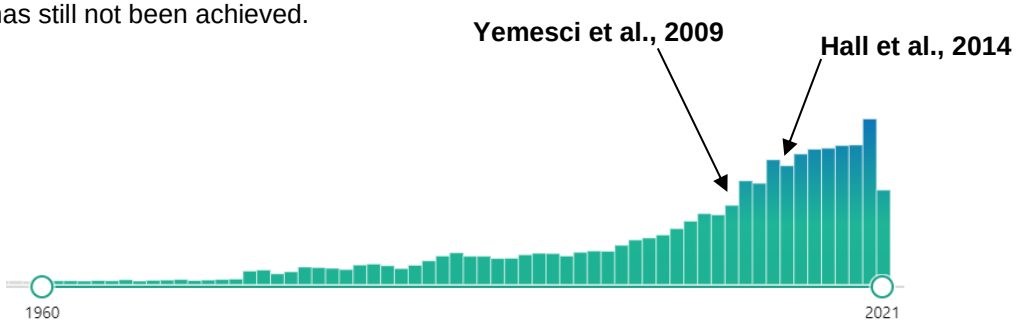

Fig. 10. Pericyte publications since 1960-2021. (source: pubmed)

Therefore, the aim with this project was to use complimentary imaging modalities (*ex vivo* and *in vivo*) to characterise and map pericyte cell fate at both the population and single cell level, to understand how these cells are damaged by stroke, if as a population they die or survive and what functions surviving pericytes may possess. In tandem, the project aimed to unravel the influence of pericyte contractility on vessel diameter by imaging single pericytes *in vivo* over the course of a week in the oedematous stroked brain; with a view to definitively answer whether pericytes are responsible for the long-lasting reduction in blood flow which occurs after stroke.

3. Materials

3.1 Mice

Throughout the project either C57BL/6NJ, NG2DsRed, PDGFRbEGFP or NG2dsRedxPDGFRbEGFP mice were used to conduct the investigation. C57BL/6NJ mice are a sub-line of C57BL/6J mice separated in 1951 and distinguished by 5 single nucleotide polymorphisms (SNP's). Widely used in the field of stroke research, the C57BL/6N strain produces large, homogenously distributed infarcts that do not differ between sexes; making them an ideal test bed for monitoring the sequelae of ischemic stroke (Zhao et al., 2019). PDGFRbEGFP mice were bred for six consecutive generations until the KO retention motif was eradicated from the mouse line to enable dual reporting of pericytes with NG2dsRed and EGFP.

Table 1: Mice

Name	Description	Provider
C57BL6/NJ	(#005304) A National institute of health subline of C57BL6/J mice separated from C57BL6/J mouse line by 5 unique single nucleotide polymorphisms.	Jackson Laboratory, Bar Harbor, ME, USA
(Cspg4-DsRed.T1)1Akik-NG2dsRed	Transgenic insertion consisting of 208kb C57BL/6J mouse bacterial artificial chromosome. This BAC contained the Cspg4 gene, modified by the insertion of an optimised red fluorescent protein variant (DsRed) sequence. This mouseline allows visualisation of DsRed in NG2 expressing cells.	Available in-house
PDGF-Rß$^{tm3.1Cbet}$ (PDGFb$^{ret/ret}$-EGFP)	In knock-out variants of these animals the stop codon inserted into exon 6 remains intact and precludes translation of the retention motif (ret) which is required for investment of pericytes in the microvessel wall. (Lindblom et al., 2003). However, the retention motif was bred out of animals for use in the current thesis and wild-type mice present no defects. Expression of EGFP in this mouse line is controlled by the PDGFRb promoter.	Available in-house

3.1.1 Antibodies

Table 2: Antibodies

Name	Description	Provider
anti-mouse PDGFRb	(AF1042), Polyclonal Goat IgG	R&D Systems, Inc. Biotechne GmbH, Minneapolis, MN
anti-mouse Collagen IV	(ab19808)	Abcam, Cambridge, United Kingdom
anti-mouse Ki67	(D3-B5)	Cell Signaling Frankfurt am Main Germany
anti-mouse Aqp4	(AB2216)	Merck,Millipore, Darmstadt, Germany
anti-NeuN	(ab177487)	Abcam Cambridge, United Kingdom
anti-Iba1	(019-19741)	Wako, Saitama, Japan

3.1.2 PCR Primers for genotyping and RT-PCR

Table 3: PCR primers for genotyping

Name	Nucleotide sequence	Provider
Pdgfrb (31796) F	GTGGAAGCAGAGAGGAGAG-CATTTG	Metabion, Planegg, Bavaria, Deutschland
GS eGFP R3	GGTCGGGGTAGCGGCTGAA	Metabion, Planegg, Bavaria, Deutschland
NG2dsRed (IMR8699) F	TTCCTTCGCCTTACAAGTCC	Metabion, Planegg, Bavaria, Deutschland
NG2dsRed (IMR8700) R	GAGCCGTACTGGAACTGG	Metabion, Planegg, Bavaria, Deutschland
RetWT F	CATGCTGCCTTGTAATCCGT	Metabion, Planegg, Bavaria, Deutschland
RetWT R	CGGCGGATTCTCACCGT	Metabion, Planegg, Bavaria, Deutschland
RetRet F	CTCGGGTGACCATTCGGTAA	Metabion, Planegg, Bavaria, Deutschland
RetRet R	TCTAAGTCACAGCGAGGGAG	Metabion, Planegg, Bavaria, Deutschland

Table 4: PCR primers for RT-PCR

Name	Nucleotide sequence	Provider
GAPDH F	ATTGTCAGCAATGGATCCTG	Metabion, Planegg, Bavaria, Deutschland
GAPDH R	ATGGACTGTGGTCATGAGCC	Metabion, Planegg, Bavaria, Deutschland
eGFP F	ACGTAAACGGCCACAAGTTC	Metabion, Planegg, Bavaria, Deutschland
eGFP R	AAGTCGTGCTGCTTCATGTG	Metabion, Planegg, Bavaria, Deutschland
Pdgfrb F	AGGACAACCGTACCTTGGGT	Metabion, Planegg, Bavaria, Deutschland
Pdgfrb R	CAGTTCTGACACGTACCGGG	Metabion, Planegg, Bavaria, Deutschland
NG2 F	AATGAGGACCTGCTACACGG	Metabion, Planegg, Bavaria, Deutschland
NG2 R	CATCTGTAGTCAACAGCCGC	Metabion, Planegg, Bavaria, Deutschland
RGS5 F	ATGTGTAAGGGACTGGCAGC	Metabion, Planegg, Bavaria, Deutschland
RGS5 R	ATACTTGATTAGCTCCTTAT	Metabion, Planegg, Bavaria, Deutschland
DsRed F	GGCACCTTCATCTACCACG	Metabion, Planegg, Bavaria, Deutschland
DsRed R	CTTGTGGATCTCGCCCTTC	Metabion, Planegg, Bavaria, Deutschland

3.1.3 Enzymes

Table 5: Enzymes

Name	Product number	Provider
Collagenase/Dispase®	11097113001	Sigma-Aldrich Chemie GmbH, Munich, Germany
DNAase1	10104159001	Roche Diagnostics, Mannheim, Germany

3.1.4 Commercial Kits

Table 6: Commercial kits

Name	Application	Provider
ApopTag® Red In Situ Apotosis Detection kit	(S7165) Detection of fragmented DNA in dead cells via nick-end labeling	Merck,Millipore, Darmstadt, Germany
Click-iT ™ Plus EdU Cell proliferation kit for imaging AlexaFluor™647 dye	(C10640) Detection of EdU positive cells via click-iT ™ chemistry	Thermo Fisher Scientific, Waltham, MA, USA

3.1.5 Chemicals

Table 7: Chemicals

Name	Description	Provider
Agarose, universal DNA grade	(443666A) molecular biology grade	VWR Life Science, Germany
Actinomycin D	(11805017) gene expression inhibiter; antibiotic	Thermofisher Scientific, Waltham, MA, USA
BSA Bovine serum Albumin	(A3912-500g) Heat shock fraction pH 5.2	Sigma-Aldrich Chemie GmbH, Munich, Germany
DAPI	(62248)4′,6-diamidino-2-phenylindole; nuclei labelling	Thermofisher Scientifc, Waltham, MA, USA
EdU(5-ethynyl-2'-deoxyuridine)	(A10044) Injection labelling of DNA incorporation for cell proliferation	Thermofisher Scientific, Waltham, MA, USA
FBS (Fetal Bovine Serum)	(F2442) Fetal bovine serum	Merck Millipore Darmstadt, Germany
Gelatin from cold water fish skin	(G7041) Fish-skin gelatin	Sigma-Aldrich Chemie GmbH, Munich, Germany
Triton ™ X-100	(8X100-500mL) laboratory grade	Sigma-Aldrich Chemie GmbH, Munich, Germany
Tween 20®	Polysorbate, Polyoxyethylene-20-sorbitan monolaurate	CarlRoth Karlsruhe, Germany

3.1.6 Buffers, solutions and media

Table 8: Buffers, solutions and media

Name	Description	Application
1X PBS- 0.3% Triton X-100	Triton X-100 diluted in PBS	Tissue permeabilization
Primary Antibody buffer	1%BSA, 0.1% Fish-skin gelatin, 0.1% Triton X-100, 0.05% Tween 20 in 1XPBS pH7.258	Blocking and permeabilization of vibratome fixed brain tissue
4% Agarose in 1XPBS	Agarose in powder form diluted into PBS	For creation of brain moulds for subsequent cutting at the vibratome
Nuclease-free water	Water free of impurity	Genotyping
10X Blocking buffer	2%BSA, 2%FCS, 0.2% Fish-skin gelatin diluted down in 1XPBS	Immunofluorescence staining during the secondary antibody step
4% PFA in 1XPBS	Diluted down from 37% PFA stock in PBS	For fixation of cells, fresh-frozen brain slices and isolated vessels
1XPBS	Diluted down from 10x PBS buffer stock at pH7.4 Di-Sodiumhydrogen phosphate-Dihydrate 148.0g;Potassiumhydrogenphosphate 23.0g, SodiumChloride 900g in 10 litres of water	Foundation of antibody buffers to Immunofluorescence staining an tissue collection
Everbrite Mounting medium™	Anti-fade mounting medium used	Preservation of Cyanine spectrum dyes within brain sections
Nail Polish	Various providers and types	Sealant of microscope slides and coverslips
Tris-sodium citrate buffer	(10Mm tris-sodium citrate dehydrate, 2.94g, 0.05% Tween 20, 0.5Ml) in 1000ml of distilled water adjusted to pH6.0 with sodium hydroxide	For heat-mediated antigen retrieval of difficult to reach epitopes

3.1.7 Consumable equipment

Table 9: Consumable equipment

Name	Application	Provider
6,12,24 Multi-well Tissue culture plates (353046, 3513, 3526)	Storage and staining of vibratome cut brain sections	FALCON®, NY, USA

15, 50ml Falcon tubes (352097, 352070)	Master-mix preparation, Brain storage.	FALCON®, NY, USA
Costar stripette® 2ml, 5ml, 10ml (4486, 4487, 4488)	Pipettes for use with the pipette boy	Corning, Corning incorporated, New York, USA
KIMTECH precision wipes	Cleaning of microscope slides, objectives and general use	Kimberly-Clark® Texas, USA
Parafilm	Sealing of falcon tubes	Bemis™, Curwood, USA
Feather Disposable scalpel	Cutting of brain tissue, of parafilm-	Feather Safety Razor CO., LTD, Osaka, Japan
0.5ml,1.5ml,2ml,5ml Eppendorf tubes® (121.023, 120.094,120.086, 110.401)	Storage of solutions	Eppendorf® Hamburg, Germany

3.1.8 Hardware and equipment

Table 9: Hardware and equipment

Name	Description	Provider
Axio Observer.Z1	Fluorescence microscope	Carl Zeiss AG, Oberkochen, Germany
Vortex UZUSIO VTX-3000L	Vortex	Lab unlimited, Dublin, Ireland
-20ºc Freezer. LGex 3410 Mediline	Lab freezer	Liebherr, Berlin, Germany
Fridge-Freezer combi, KG36VVW30	Lab fridge freezer	Siemens, Munich, Germany
pH-meter S201, Seven compact	pH-meter	Mettler Toledo, Gießen, Germany
NeoMag® Magnetic stirrer D-6011	Magnetic stirring device	Neolab, Heidelberg, Germany
Pippette helper, pipetboy	Pipette helper	Integra, ZIzers, Switzerland
Real-time PCR-System	Light Cycler 480 II	Roche, Penzberg, Germany
Microwave	Microwave	Siemens, Munich, Germany
Heraeus Pico 17	Micro-centrifuge	Thermofisher Scientific, Waltham, MA, USA
Vortex	Vortex-Genie 2	Scientific industries, New York, USA
PCR machine	PeqStar 2x	Peqlab (Avantor), Pennsylvania, USA
Agarose-gel chamber (40-0708)	Small agarose gel chamber	Peqlab (Avantor), Pennsylvania, USA

Agarose gel chamber (40-1214)	Large agarose gel chamber	Peqlab (Avantor), Pennsylvania, USA
Electrophoresis device	peq Power 300	Peqlab (Avantor), Pennsylvania, USA
Thermomixer	Thermomixer pro	CellMedia GmBH, Leipzig, Germany
Mini-centrifuge	Mini centrifuge for PCR	Sprout, Heathrow scientific, Illinois, USA
IKA Rocker 3D Digital	Multi-platform plate shaker	IKA®-Werke GmbH & Co.KG, Staufen, Germany
Multi Bio 3D	Programmable mini-shaker	Biosan, Riga, Latvia
Centrifuge	5810R centrifuge for FACS	Eppendorf, Hamburg, Germany
Spectrophotometer ND-1000	Spectrophotometer for RNA measurement	Thermofisher Scientific, Waltham, MA, USA
Agilent Bioanalyser 2100	Bioanalyser for RNA integrity	Peqlab (Avantor), Pennsylvania, USA
Vortex V1-Plus	(144200B)	Kisker Biotech GmbH, Steinfurt, Germany
Centifuge 5417R	Centrifuge for Westernblot	Eppendorf, Hamburg, Germany
Axioimager M2	Histology microscope	Carl Zeiss AG, Oberkochen, Germany
BioRad C1000 Touch	Thermocycler	Bio-Rad, Feldkirchen, Germany
BioRad iMark	Microplate reader	Bio-Rad, Feldkirchen, Germany
Stereo Discovery V8	Leica Dissection microscope	Lecia Microsystems, Wetzlar, Germany
Leica VT1200S	Leica Vibratome	Lecia Microsystems, Wetzlar, Germany
CryoStar NX70	Cryostat for cutting fresh-frozen/fixed tissue	Thermofisher Scientific, Waltham, MA, USA
LSM 7MP	Twin scanner multi-photon microscope	Carl Zeiss AG, Oberkochen, Germany
Cell sorter (SH800S)	Cell sorter for FACS experiments	Sony Biotechnology, San Jose, USA
Stereo microscope	Leica M80 surgery microscope	Lecia Microsystems, Wetzlar, Germany
Periflux system 5000	Laser Doppler Flowmetry measurement device	Perimed, Las Vegas, USA
Pericam PSI	Laser Speckle Imaging device	Perimed, Las Vegas, USA

OxyDig	O_2 measurement device for surgery	Drägerwerk, Prittwiching, Germany
Digiflow	Device for measurement of flow	Drägerwerk, Prittwiching, Germany
O2 sensor	Measures O2 concentration within tubing	Drägerwerk, Prittwiching, Germany
Isoflurane funnel-fill vaporizer	(34-1040SV) Storage and distribution of isoflurane for surgery	Harvard Apparatus, Massachusetts, USA
Powerlab 16/35	Integration of multiple different surgical monitoring devices	AD Instruments, Sydney, Australia
Mediheat ™	Heating cabinet for mice post-surgery	Pecoservices, Brough, United Kingdom
Capnograph Type 340	Measurement of CO_2 outflow from mouse	Hugo Sachs Elektronik GmbH, March, Germany
FHC Temperature controller	Feedback controlled temperature controller	FHC, Bowdoin, USA
Weighing scales	Scales for measurement of Mouse weight	OHAUS, Nänikon, Switzerland
X-Cite series 120Q	120 Lumen Fluorscence lamp for 2-photon imaging	Excelitas technologies ®, Wiesbaden, Germany
Newport stabilizer S-2000 series	Vibration isolating table for 2-photon microscopy	Newport Corportation ®, California, USA
Chameleon Ultra	Modelocked Ti:Sapphire Laser	Coherent®, California, USA
Filter Sets (BiG)	A range of filter sets for 2-photon microscopy imaging	Carl Zeiss AG, Oberkochen, Germany
KL2500 LED light source	LED based light-source for Lecia surgical stereo microscopes	Lecia Microsystems, Wetzlar, Germany
Objective W "Plan-Apochromat" 20x/1,0 DIC M27 70mm objective	Objective lens used for 2-photon imaging experiments	Carl Zeiss AG, Oberkochen, Germany
Pipettes P2,P10,P20,P200,P1000	A range of Gilson pipettes (F167380)	Gilson, Wisconsin, USA
Zeiss LSM 800	Inverted Confocal Microscope	Carl Zeiss AG, Oberkochen, Germany
Zeiss 7MP	2-Photon microscope	Carl Zeiss AG, Oberkochen, Germany

3.1.9 Software

Table 10: Software

Name	Application	Provider
Microsoft Office	Complete suite for word-processing, presentations and data tabulation	Microscoft Corporation, WA, USA
Graphpad 8.4.3	Data processing/graphical figure creation	Prism, San Diego, USA
Imaris®	3D reconstruction of cells and vessels	Bitplane, Zürich, Switzerland
Zen Black/Blue	Image processing and data acquisition	Carl Zeiss AG, Oberkochen, Germany
Pimsoft	Laser speckle data gathering and analysis	Perimed, Las Vegas, USA
FlowJo v10	FACS data processing	FlowJo LLC, Vancouver, BC, Canada
Matlab	Script processing of Laser speckle data	Mathworks,Massachusetts, USA
FIJI (Fiji is just image J)	Image presentation and analysis	Open-source, collaborative, global
Abodbe Illustrator	Figure creation	Adobe, California, USA
Adobe Photoshop	Figure creation and image representation	Adobe, California, USA
Sony SH800s	Cell sorting and data analysis software	Sony Biotechnology, California, USA

3.1.10 Drugs (Analgesics, Anaesthetics and post-operative care)

Table 11: Drugs

Name	Description	Provider
Buprenorphrine	Temgesic 0.3mg/ml	Schering-Plough
Carprofen: Rimadyl	50mg/ml analgesic	Zoetis
Medetomidine	1mg/ml (100mg/kg per injection)	Dorbene vet
Midazolam	5mg/5ml	B.Braun
Fentanyl	0.5mg/10ml	Piramal
Isoflurane	Iso vet 1000mg/g	Dechra, Northwich, United Kingdom

Bepanthen	Antiseptic cream	Bayervital GmbH, Leverkeusen, Germany

3.1.11 Surgery tools and consumables

Table 12: Surgery tools and consumables

Name	Description	Provider
FMCAo sutures	Filament for insertion into MCAO to induce stroke	Doccol®,MA, USA
Micro serrefines	(18055-04) arterial cross clamp	Fine scientific tools, California, USA
Micro-serrefine clamp	(18057-14) clamp applying forceps	Fine scientific tools, California, USA
Dumont forceps	(11253-20) Micro-blunted tips	Fine scientific tools, California, USA
45º Dumont forceps	(11253-25) Micro-blunted tips	Fine scientific tools, California, USA
Dumont #5CO forceps	A rough coated tip on one side and smooth on the other for dura removal	Fine scientific tools, California, USA
Extra fine Bonn scissors	(14084-08)	Fine scientific tools, California, USA
Needle holders with suture cutters	(12002-12)	Fine scientific tools, California, USA
Dissecting scissors	(14393)	World precision instruments, Friedberg, Germany
Spring scissors	(15000-08) scissors for cutting common carotid artery	Fine scientific tools, California, USA
Straight microtip	(MTB500-02240) laser Doppler fibre	Perimed, Las Vegas, USA
Silk braided sutures	(10C103000)	Pearsalls limited, London, United Kingdom
Drechseln Maxi cure glue	(BSI-112) Cyanoacrylate for Doppler attachment	Drechseln, Weiden, Germany
Glue accelerator	(BSI-151) Insta-set™ accelerator	Drechseln, Weiden, Germany
3M Durapore surgical tape	(1538-0)	3M, Minnesota, USA
Sodium Chloride	(14NM32)	Fresenius kabi GmbH, Bad Homburg, Germany
Aquad ad injectabilia	(2822633)	Berlin Chemie, Berlin, Germany

Gazin® swabs	(18504) Gauze	Lohmann & Rauscher, Neuwied, Germany
Ti-Cron sutures	(5CD30586)	Covidien (Medtronic), Dublin, Ireland
Insulin syringe	(V-100) BD Safety glide	BD, Heidelberg, Germany
Surflo® Winged infusion set	(SV*S25NL30) Butterfly perfusion syring tip	Terumo Europe, Leuven, Belgium
Braun Syringes	Syringes for IP injection;subcutaneous injection	Braun, Kronberg, Germany

4. Methods

4.1 Animal surgery & behavior testing

4.1.1 Transient filament middle cerebral artery occlusion

30 minutes prior to surgery mice were weighed and injected with 0.1 mg/kg buprenorphine subcutaneously (s.c). Mice were anaesthetized using 4% isoflurane in air (1 l/min) in an induction chamber and placed in prone position on a heating pad set to 37°C, a rectal probe was inserted into the mice for feedback controlled heat regulation. Anesthesia was maintained with isoflurane (1.8 - 2%) in 50% O_2 in air using a facemask. Bepanthen was applied to protect the eyes from dryness and paw reflex was checked with forceps prior to starting surgery. Ointment was applied to the head of the mouse, where a small incision was made on the left side of the head (between eye and ear) and the skull was exposed. A sharp scalpel was used to detach the temporal muscle from the skull and create a pouch between muscle and bone. The laser Doppler probe was placed onto the dry exposed left parietal skull over the middle cerebral artery territory (MCA) and fixed using cyanoacrylate glue (1 drop) and glue accelerator. Care was taken to achieve laser Doppler flow values of above 200 arbitrary units (AU) and the mouse was flipped face up and fixed in the supine position using surgical tape. A longitudinal incision was made along the middle of the neck using scissors and the common carotid artery (CCA), external carotid artery (ECA) and internal (ICA) were isolated and exposed. During this process, care was taken to avoid touching or harming the vagal nerve running beneath the CCA. The left CCA and ECA were ligated and an additional loose knot was made around the CCA. A small surgical clamp was then applied to the ICA and a small incision in the CCA between ligation and loose knot was made using micro scissors. Subsequently, the occlusion filament was inserted into the incision, the loose knot was tightened around the filament and the surgical clamp on the ICA was removed. The filament was advanced along the ICA to the base of the circle of Willis until it obstructed the MCA; where an immediate reduction of cerebral blood flow (>80%) was achieved. The knot securing the filament was then fixed to ensure the filament was held in place and the neck incision was carefully closed using 2-3 single sutures. The mice were then placed in recovery chambers set to 32°C prior to beginning surgery. After 55 minutes of occlusion anesthesia was re-induced, the neck incision was reopened and at precisely 60 minutes of ischemia, the filament was removed from the exposed CCA without bleeding by tightening the knot immediately after withdrawing the filament. 1 ml of saline and 100 µl of Carprofen (4 mg/kg) was injected s.c prior to termination of anesthesia. Mice were then placed in a recovery chamber at 32°C for 2 hours.

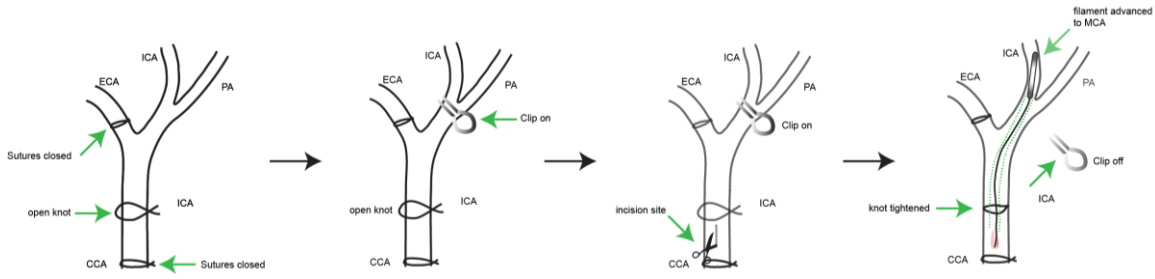

Fig. 11. Schematic detailing the sequential steps involved in transient filament middle cerebral artery occlusion.

4.1.2 Neuroscore

Mice subjected to surgery were observed following surgery and assessed for various neurological deficits, behavioral condition and core physiological parameters collectively named as the Neuroscore; which permits evaluation of each animal and determines termination end-points based on humane criteria. An example of the scoresheet is found in the supplementary information Chapter 8.

4.1.3 Experimental stroke scale (ESS)

In addition to the neuroscore performed on each animal after stroke, the experimental stroke scale (used in prior publications (Lourbopoulos et al., 2017)) was used as an evaluation to determine focal and general components relating to mouse condition. Focal deficits (fESS) comprise evaluation of specific neurological deficits relating to brain related behavior such as: body symmetry, gait, climbing, circling behavior, fore and hind-limb symmetry, compulsory circling, whisker response, forelimb placing, posture and beam balance. This focal component is scored out of 42 points to mimic the scoring system used by the National institute of health stroke scale with a higher score indicating more severe impairment. The general component of the experimental stroke scale (gESS) relates to the systemic behavior of the mouse and is scored out of 16 points based on separate criteria such as condition of the hair, ears and eyes, spontaneous activity and anxiety behavior. A complete score sheet is found in the supplementary information in chapter 8.

4.1.4 Perfusion of mice

Mice were injected with a triple dose of MMF (medetomidine 0.036 mg, midazolam 0.375 mg, fentanyl 0.0039 mg for a 25 g mouse) intra-peritoneally and assessed for reflex action by applying forceps to the hindpaws. Once under anesthesia, an incision along the midline from lower stomach to thorax was made to expose the internal organs. Using a surgical clamp, the xyphoid was lifted and positioned above the mouse exposing the diaphragm. Using surgical scissors, the diaphragm and rib cage was cut allowing it to be folded back, the surgical clamp holding the xyphoid was moved further back to expose the pulsating heart. The left ventricle of the heart was penetrated with a butterfly needle and the three-way switch of the perfusion pump was moved to the open position to allow ice-cold PBS to perfuse at a perfusion pressure of between 100-120 mmHg through the mouse vasculature. Immediately after, the returning vena cava was severed to bloodlet the mouse and PBS perfusion was performed for 5 mins. After the outflow of the mouse turns from blood red to clear and the liver turned gray, the perfusion was switched to ice cold 4% PFA to fix the mouse for 5mins. Following this, the brain of the mouse was extracted by severing the head and cleaning away the skin and muscle from the back of the neck and making three angular cuts at the base of the skull; followed by a scissor tip insertion to the bregma of the skull and opening of the scissors. This exposes the brain by splitting the skull down the middle, then, using a small spatula the brain is removed from the skull and placed into a 5 ml Eppendorf tube filled with 4% PFA and placed at 4˚C overnight where it was switched to PBS for further storage until the brain was needed for downstream applications.

4.1.5 Post-operative care

A previously described post-operative care regimen was modified to maximize and preserve the survival of animals with large cortical infarcts following fMCAo surgery (Lourbopoulos et al., 2017). Briefly, animals were immediately placed in a heating chameber at 32˚C after surgery for 2 hours before being placed in their home cages. Pellet food (12.8 KJ/g of metabolizable energy;ssniff-Spezialdiäten GmbH, Soest, Germany) was scattered on the floor of the home cage to allow mice to easily reach nourishment. In addition, in the evening after surgery and each morning following the initial stroke surgery, petri-dishes filled with a powdered form of the aforementioned pellet food were mixed with water into a paste at a 1:3 ratio. Mice were sub-cutaneously injected with 10% Glucose mixed with saline at a 1:1 ratio and administed 50µl of carprofen in the morning and evening to act as pain relief. To supplement dehydration occurring in mice after stroke, petri-dishes filled with water were laid on the ground of the cage at the same time points, this procedure was performed for each mouse until they regained their bodyweight.

4.2 Animal experimentation, tissue processing and image analysis

4.2.1 Fresh frozen analysis of pericyte death, coverage and proliferation bodies

Twenty male C57BL/6J mice aged between 6 - 12 weeks old were subjected to either fMCAo and sacrificed on day 1 or day 3, after sham surgery or in naïve conditions in a randomized, blinded manner with five mice per group. At the end of the experiment, mice were anaesthetized with 5% isoflurane prior to cervical dislocation; brains were removed and immediately fresh-frozen in dry ice prior to serial sectioning in 20 µm sections at the cryostat. Microscope slides containing fresh-frozen brain slices were rehydrated for 15 mins in PBS at room temperature. Subsequently, brain slices were fixed for 10 mins in 4% paraformaldehyde in PBS and washed in PBS 3 times. Slices were then blocked and permeabilized in 2% BSA, 2% FCS, 0.2% fish-skin gelatin in 1XPBS and 0.03% Triton x-100 for 1 hour at room temperature. After blocking and permeabilization, slices were sealed with a hydrophobic pen; creating a well in which to incubate the primary antibody buffer mix consisting of gtPDGFRb (1:100), rbCollagen IV (1:250) and diluted in 2% BSA, 2% FCS, 0.2% fish-skin gelatin in 1XPBS overnight at 4˚C on a horizontal shaker. The next day brain sections were washed 3x with 1XPBS in a coplin jar and incubated with donkey anti-goat Alexa fluor® 488 (1:1000) and donkey anti-rabbit Alexafluor® 647 (1:300) secondary antibodies in 2% BSA, 2% FCS, 0.2% fish-skin gelatin in 1XPBS overnight at room temperature in a humidified chamber. Sections were then washed in a coplin jar 3x with 1XPBS and samples were then subjected to ApopTag® Red In Situ Apoptosis Detection kit staining (Terminal deoxynucleotidyl transferase dUTP nick end labelling, TUNEL staining) following manufacturers guidelines. During the secondary incubation of the dioxygenin conjugate antibody which binds to the nick end label on fragmented DNA strands, sections were incubated with DAPI in PBS at a concentration of 1:1000 for 2 hours at 37°C. Finally, brain slices were washed 3x in 1XPBS in a coplin jar and mounted with aqueous mounting medium.

Five images per region of interest were stereotactically acquired: 3x striatum, 2x cortex (infarct core, peri-infarct tissue and contralateral side) in two brain slices per animal at a bregma consistent with where the MCA territory feeds the striatum and the cortex. For analysis, the number

of PDGFRb$^+$ cells present on microvessels in each region was measured along with the number of TUNEL$^+$ cells. Then, the number of TUNEL$^+$ cells that were PDGFRb$^+$ and encased within the collagen IV basement membrane were totaled to give the percentage of pericyte cell death at each time-point in each region. Total pericyte number was generated from the total cell number of PDGFRb$^+$ cells within the collagen IV$^+$ basement membrane at the level of the microcirculation.

Finally, PDGFRb (green) and Collagen IV (far-red) channels were thresh-holded to generate PDGFRb$^+$ masks and Collagen IV$^+$ masks. The percentage of image covered by the collagen IV mask was used to quantify vessel density per region while dividing the PDGFRb mask over the collagen IV mask was used to generate pericyte coverage per image/region/condition/mouse.

4.2.2 Analysis of pericyte damage in stroked PDGFRbEGFP$^+$ mice 90 mins post-reperfusion

Four male PDGFRbEGFP mice aged between 6 - 20 weeks underwent fMCAo surgery and were transcardially perfused with saline and 4% PFA as previously described in section 4.1.4. The fixed brains were embedded in 4% agarose and serially sliced into 100 µm thick sections at the vibratome, collected into 12 well plates and stored at 4°C in PBS prior to immunostaining. Immunostaining was carried out as follows: 3 100 µm brain sections containing the MCA territory were incubated in a primary antibody buffer solution (1% BSA, 0.1% fish-skin gelatin, 0.1% Triton X-100, 0.05% Tween 20 in 1XPBS) which blocks and permeabilizes fixed vibratome tissue with 1:100 dilutions of rabbit anti-collagen IV and goat anti-Aquaporin IV and incubated for several days on a rotary shaker at 4°C. Sections were then thoroughly washed in 1XPBS 3x for 30 minutes on a rotary shaker at medium speed to remove traces of unbound primary antibody buffer. Sections were incubated with a secondary antibody buffer mix (in 2% BSA, 2% FCS, 0.2% fish-skin gelatin in 1XPBS) containing donkey anti-rabbit AlexaFluor® 594 and donkey anti-goat AlexaFluor® 647 (1:300) for two days at 4°C on a rotary shaker until even Collagen IV staining was observed. Sections were then washed 3X thoroughly to remove unbound secondary antibodies and during the last washing step DAPI was added to the PBS at a concentration of 1:1000 for 30 minutes. Washing using 1XPBS was repeated 3X for 30 minutes prior to mounting on glass coverslips with EverBrite™ mounting medium.

For imaging, observation of damaged pericytes within the infarct territory was first assessed and pre-defined criteria for damaged pericytes were established. Given that pericytes are ensheathed within the collagen IV$^+$ basement membrane under physiological conditions, damaged pericytes were assessed as pericytes with EGFP$^+$ extrusions from the cell that reach beyond the basement membrane. Then, using high-resolution confocal imaging with the 100x oil objective, approximately 30 pericytes/mouse in the infarct core region and contralateral hemisphere were imaged for downstream analysis. Pericytes were separated by sub-type definition: Thin-strand, Mesh, Junctional and re-constructed using IMARIS® software. 3D z-stacks of pericytes were subjected to a surface creation pipeline in which the DAPI$^+$ nuclei within EGFP$^+$ pericytes formed a mask in which to measure EGFP mean fluorescence intensity in damaged and non-damaged pericytes. The surface creation of DAPI$^+$ nuclei allowed measurement of nucleus volume, sphericity and generated unique pericyte identification tags, damaged and healthy pericytes were compared against contralateral hemisphere pericytes after a randomized selection using the aforementioned pericyte ID's by a research colleague. In total, 61 thin-strand pericytes and 40 junctional pericytes were compared for final analyses. Criteria for damaged/healthy pericytes is shown below.

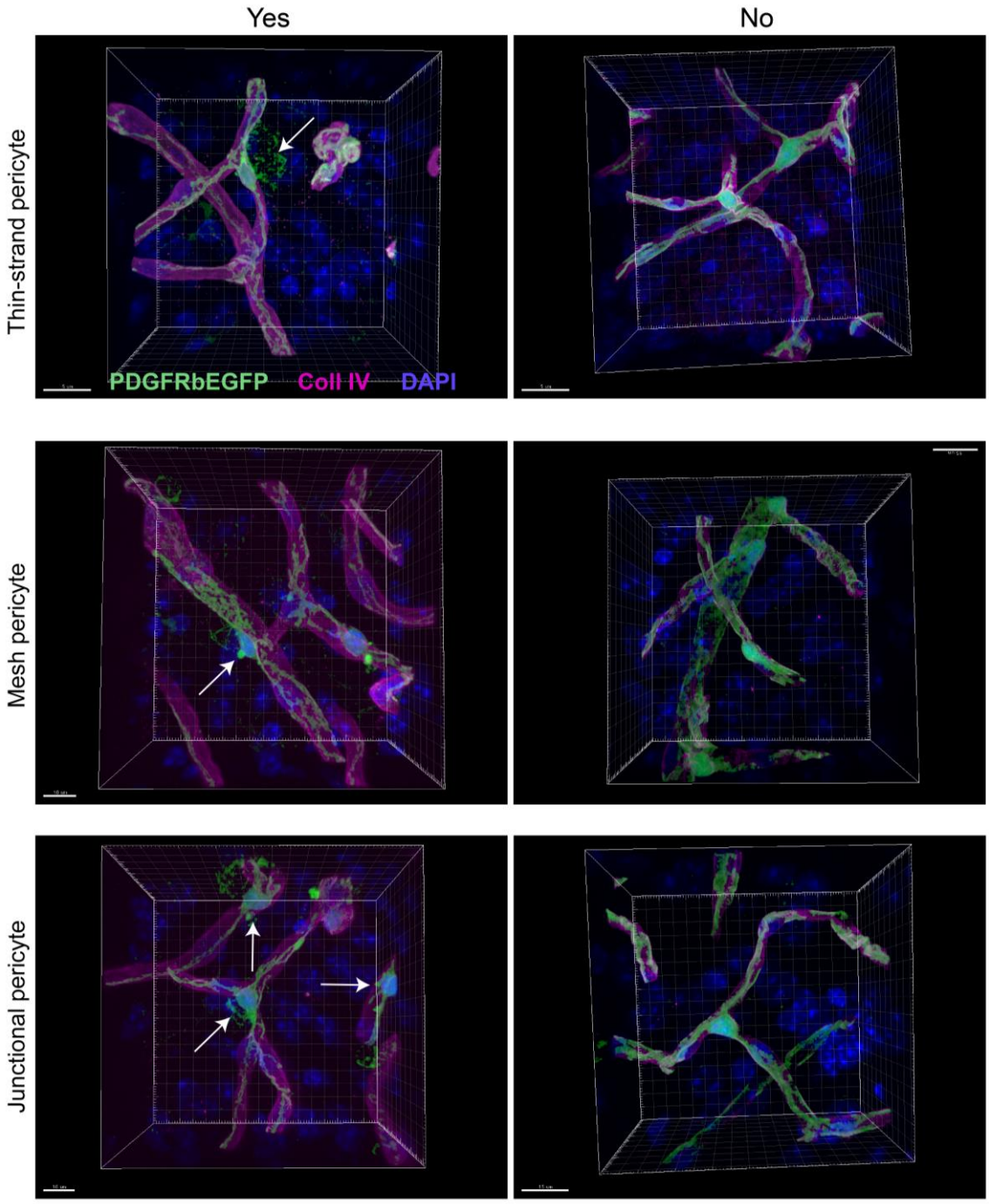

Fig. 12. Damage assessment criteria for EGFP+ pericytes.

Pericytes under physiological conditions are encased within a bi-layer of the basement membrane, a component of which is Collagen IV (magenta). Here, Collagen IV staining was used to differentiate two distinct pericyte phenotypes, those, which are damaged, and those that are intact. Pericytes which we termed damaged have extracellular accumulations of EGFP extending beyond the collagen IV staining (magenta) and points of this extracellular accumulation are shown with the white arrows indicated (left). Intact pericytes however, are completely encased within two layers of collagen IV and display no signs of extracellular EGFP emanating from beyond the basement membrane (right). *Scale bars, 10 µm.*

4.2.3 Bregma dependent analysis of pericyte survival 3 Days post-stroke

Four male 6-12 week old PDGFRbEGFP^{+} mice, subjected to a one-hour transient fMCAO with large cortical strokes were sacrificed on day three post-stroke, brains were removed and fixed with 4% PFA and serially sectioned into 100 µm thick sections at the vibratome. Three brain sections per mouse ranging from the posterior MCA territory (bregma -0.9/-1.2 mm), MCA territory (bregma 0/0.1 mm) to anterior cortex (bregma +2.5/2.71 mm) were then subjected to immunostaining. First, sections were incubated with primary antibody buffer (1% BSA, 0.1% fish-skin gelatin, 0.1% Triton X-100, and 0.05% Tween 20 in 1XPBS) with 1:200 rabbit anti-NeuN (ab177487) for 2 days on a rotary shaker at 4°C. Sections were thoroughly washed 3x in 1XPBS to remove unbound primary antibody and incubated with a secondary antibody mix consisting of 2% BSA, 2% FCS, 0.2% fish-skin gelatin in 1XPBS and 1:300 donkey anti-rabbit AlexaFluor® 647 on a rotary shaker at 4°C for 2 days. Sections were then washed twice for 1 hour in 1XPBS to remove unbound secondaries and during the third washing step, DAPI was added to the PBS wash at a concentration of 1:1000 and left for 1 hour on a rotary shaker at room temperature. Sections were then washed 3X in 1XPBS before mounting with Everbrite™ mounting medium.

Sections were then taken to the confocal microscope and imaged in high quality (1024x1024) by using a 5X air objective tile-scan method involving creating a bounding grid around the edges of the brain tissue until the tiles created cover the whole brain slice. This process was repeated across all mice using the same laser settings across all bregma positions. For analysis of pericyte population surivival, images were imported into IMARIS® and the PDGFRbEGFP channel and NeuN channel were separated. Using the NeuN$^{+/-}$ signal within the tissue three areas were traced: infarct core, ipsilateral hemisphere and contralateral hemisphere. By tracing around the separate regions, infarct volume, ipsilateral hemisphere volume and contralateral volume could be calculated and converted to mm^2. Furthermore, by using each distinct region the PDGFRbEGFP was masked in respect to infarct core, ipsilateral hemisphere and contralateral hemisphere. Then, the PDGFRbEGFP channel was subjected to surface creation based on a minimum feature size of 8 µm which highlighted all mural cell soma in the brain tissue. This procedure immediately allows calculation of the mural cell number in each distinct region: infarct core, ipsilateral hemisphere and contralateral hemisphere. Finally, spots were deleted based on their vascular location (arteries, veins) or doublets; leaving capillary level cell soma that were PDGFRbEGFP^{+} which shared a morphology with pericytes and thus were termed as such. Finally, the number of pericytes per mm^2 in each region was normalized to the number in the contralateral hemisphere/mm^2 to allow a fair calculation of pericyte density reduction in relation to the contralateral hemisphere per mouse.

4.2.4 Cell cycle entry analysis Day 3 post-stroke

Four male 6-12 week old PDGFRbEGFP^{+} mice, subjected to a one-hour transient fMCAo with large cortical strokes were sacrificed on Day 3 post-stroke, brains were removed and fixed with 4% PFA and serially sectioned into 100 µm thick sections at the vibratome. Two brain sections per mouse at a bregma where the MCA enters the brain were chosen for further immunostaining. Briefly, sections were incubated with primary antibody buffer (1% BSA, 0.1% fish-skin gelatin, 0.1% Triton X-100, and 0.05% Tween 20 in 1XPBS) with 1:200 rabbit anti-Ki67 (Cell Signaling clone D3B5) for 2 days on a rotary shaker at 4°C. Sections were thoroughly washed 3X in 1XPBS to remove unbound primary antibody and incubated with a secondary antibody mix consisting of 2% BSA, 2% FCS, 0.2% fish-skin gelatin in 1XPBS and 1:300 donkey anti-rabbit AlexaFluor® 647 on a rotary shaker at 4°C for 2 days. For imaging, three regions of interest were chosen in the

striatum and cortex in the infarct core, the peri-infarct region and contralateral regions per mouse. The pericyte density was assessed by counting the number of PDGFRbEGFP$^+$ cells at the capillary level. The number of Ki67$^+$ cells were then counted to generate the number of proliferating cells and finally the number of Ki67$^+$ pericytes was counted. Pericyte density was normalized and represented as a percentage of the contralateral side and the number of Ki67$^+$ pericytes was represented as a percentage of that normalized population density.

4.2.5 5-Ethynyl-2'-deoxyuridine (EdU) administration and staining Day 3 post-stroke

Four PDGFRbEGFP$^+$ male mice aged between 6-12 weeks old were subjected to one-hour transient fMCAo. 24 hours post stroke, each animal was injected intra-peritoneally every 8 hours with 80 mg/kg (2 mg EdU/injection) EdU dissolved in *aqua ad injectabilia* (Chemie, Berlin) until sacrifice at 72 hours. Mice were injected with MMF as previously described (methods section 4.1.4) and transcardially perfused with ice cold 1XPBS for 5 mins, followed by 4% PFA for 5 mins and brains were stored in 4% PFA at 4°C for 24 hours before exchange to 1XPBS. 100 µm thick sections of the brain were cut at the vibratome and serially collected and 3 brain sections corresponding to the posterior MCA territory, the MCA territory and anterior cortex (as previously described) were used for further processing. Brain sections were stained in a free-floating manner with Click-iT ™ Plus EdU Cell proliferation kit following manufacturer's instructions and during the last washing step DAPI was added at 1:1000 before three more washes in 1XPBS. Once sections were thoroughly washed, Everbrite™ mounting medium was applied to a coverslip and folded over the microscope slide containing the brain sections and sealed with ethanol free nail varnish to prepare slides for imaging. Using the 40X oil objective at the confocal, three images per brain section/mouse per region were stereotactically acquired (3x Infarct core striatum, 3x Infarct core cortex, 3x Peri-infarct striatum, 3x Peri-infarct cortex, 3x Contralateral striatum, 3x Contralateral cortex). For image analysis total number of pericytes, EdU$^+$ cells and DAPI$^+$ cells were counted per region of interest. The number of pericytes and DAPI$^+$ nuclei positive for EdU were totaled to give a percentage of cells per region that incorporated EdU into their DNA (during S-phase of the mitotic cycle) and percentage of EdU$^+$ pericytes. Finally, the number of total pericytes per ROI was normalized to the contralateral pericyte number to display pericyte density in relation to the contralateral hemisphere and the total number of EdU$^+$ pericytes were displayed as a percentage of the remaining pericyte density within each region (infarct core/periinfarct striatum, cortex).

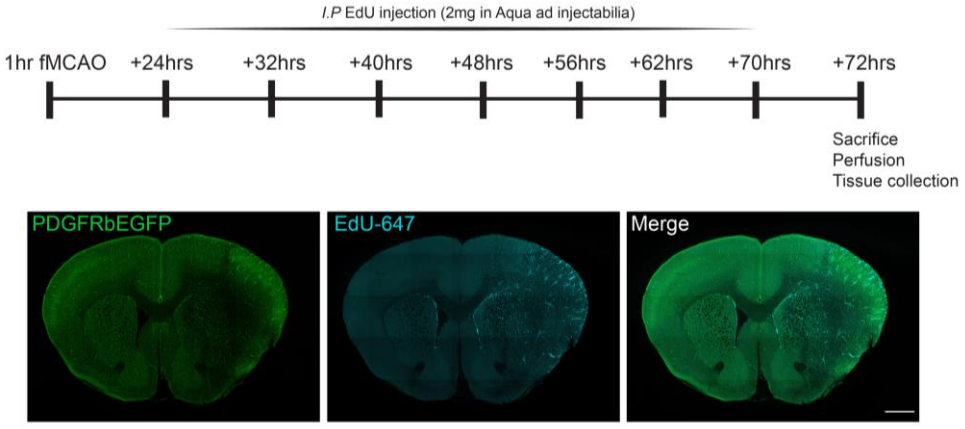

Fig. 13. EdU uptake in the ischemic brain (day 3 post-stroke).

4.2.6 Bulk RNAseq analysis pipeline

Methodology for bulk sequencing library preparation was performed as described in a prior publication (Safaiyan et al., 2021). Briefly, pools of 50 DsRed/EGFP$^+$ cells isolated from the brains of day 3 stroke or sham animals were sorted into 96 well plates, already filled with 4 µL lysis buffer containing 0.05% Triton X-100 (Sigma) and, ERCC (External RNA Controls Consortium) RNA spike-in Mix (Ambion, Life Technologies) (1:24000000 dilution), 2.5 µM oligo-dT, 2.5 mM dNTP and 2 U/µL of recombinant RNase inhibitor (Clontech) then spun down and frozen at -80°C.

4.2.7 Library preparation for Smart-seq2

The 96-well plates containing the sorted pools were first thawed and then incubated for 3 min at 72°C and thereafter immediately placed on ice. To perform reverse transcription (RT), we added to each well a mix of 0.59 µL H2O, 0.5 µL SMARTScribe™ Reverse Transcriptase (Clontech), 2 µL 5x First Strand buffer, 0.25 µL Recombinant RNase Inhibitor (Clontech), 2 µL Betaine (5 M Sigma), 0.5 µL DTT (100 mM), 0.06 µL MgCl2 (1 M Sigma), 0.1 µL Template-switching oligos (TSO) (100 µM AAGCAGTGGTATCAACGCAGAGTACrGrG+G). Next, RT reaction mixes were incubated at 42°C for 90 min followed by 70°C for 5 min and 10 cycles of 50°C 2 min, 42°C 2 min; finally ending with 70°C for 5 min for enzyme inactivation. Pre-amplification of cDNA was performed by adding 12.5 µL KAPA HiFi Hotstart 2x (KAPA Biosystems), 2.138 µL H2O, 0.25 µL ISPCR primers (10 µM, 5′ AAGCAGTGGTATCAACGCAGAGT-3), 0.1125 µL Lambda Exonuclease under the following conditions: 37°C for 30 min, 95°C for 3 min, 19 cycles of (98°C for 20 sec, 67°C for 15 sec, 72°C for 4 min), and a final extension at 72°C for 5 min. Libraries were then cleaned using AMPure bead (Beckman-Coulter) cleanup at a 0.7:1 ratio of beads to PCR product. Library was assessed by Bio-analyzer (Agilent 2100), using the High Sensitivity DNA analysis kit, and also fluorometrically using Qubit's DNA HS assay kits and a Qubit 4.0 Fluorometer (Invitrogen, LifeTechnologies) to measure the concentrations. Samples were normalized to 160 pg/µL. Sequencing libraries were constructed by using an in-house produced Tn5 transposase (Picelli et al., 2014). Libraries were barcoded with the Illumina Nextera XT (FC-131-1096, Illumina) and pooled, then underwent three rounds of AMPure bead (Beckman-Coulter) cleanup at a 0.8:1 ratio of beads to library. Libraries were sequenced 2x100 reads base pairs (bp) paired-end on Illumina HiSeq4000.

4.2.8 Processing and analyses of Smart-seq2 data

BCL files were demultiplexed with the bcl2fastq software from Illumina. After quality-control with FastQC, reads were aligned using rnaSTAR (Dobin et al., 2013) to the GRCm38 (mm10) genome with ERCC synthetic RNA added. Read counts were collected using the parameter "quantMode GeneCounts" of rnaSTAR and using the unstranded values. From that point, Seurat R v.3.1.2 package was used (Stuart et al., 2019). Low-quality samples were filtered out from the dataset based on a threshold for the number of genes detected (min 1000 unique genes/pool), percentage of mitochondrial genes (max 0.75%), percentage of ERCCs (2.5% max) and number of reads (between 200k to 2M). 189 pools passed the quality-control. Gene expressions were log normalized using the NormalizeData function of Seurat with a scale factor of 100,000. Dataset were scaled and percentage of ERCCs and plate batches were regressed using ScaleData function. The top 2000 most variable genes were considered for the PCA. PC1 explained 4.4% and PC2 explained 1.8% of the variance. The pericyte score per sample is the average expression of the pericytes-specific genes from (He et al., 2016). The normalized counts were used to compute this

average. Cell-cycle was assessed using the CellCycleScoring function and the cc.genes list provided in Seurat.

4.3 *In Vivo* imaging of pericytes, microvasculature and cerebral blood flow after fMCAo/sham surgery

4.3.1 Chronic cranial window implantation

All tools required for surgery were sterilized prior to operation. Mice were injected with 0.1 mg/kg buprenorphine s.c 30 minutes prior to surgery for intraoperative anesthesia. Animals were injected with (Medetomidine 0.5 mg/kg, Midazolam 5 mg/kg and Fentanyl 0.05 mg/kg, MMF). Paw reflex was tested to ensure that anesthesia was taking effect before mice were placed onto a heating pad at 37°C and fixed by ear bars and nose clamp into a stereotactic frame. Once the head was fixed, the surface was cleaned by ethanol before making a ~ 1.5 cm incision on the surface of the head from left to right. Lidocaine (2%) was then topically applied as local anesthesia before using a fresh cotton swap to clear the skull area of fascia and skin. A 4 mm biopsy punch was lightly applied to the skull and rotated to indent landmarks for drilling over the somatosensory cortex of the left hemisphere before applying iBond® self-etching curing agent to the surrounding skull bone. This curing agent was treated with UV light for ~ 30 seconds to harden and cover the exposed skull surface.

With the guide ring created by the biopsy punch in place and the exposed skull protected by the agent, a dental drill was used to gently trace around the biopsy punch to thin the skull until it became lightly transparent; during this process skull fragments created by the drilling were cleared using compressed air. Once drilling was near complete, the tip of the dental drill was rested against the resulting bone island to assess whether more drilling was necessary. Once the bone island was pliable, the skull flap was lifted with forceps and pulled carefully away from the skull; exposing the cortex underneath. Immediately after removal of the bone island, saline-coated gelfoam was placed on the exposed cortex to avoid drying of the brain surface. Any bleeding of the dura mater and vessels within the skull was absorbed through the gel foam without touching the cortex by resting a dry cotton swab against the gel foam, drawing up any blood by capillary action.

The gel foam was removed and saline was applied to the exposed cortex allowing the dura mater to be slowly peeled from the brain surface in a clockwise motion with a blunted, abrasive forcep tip that captures the dura mater. Gel foam soaked in saline was applied again to the brain surface and resultant blood absorbed using the cotton swab to clean the exposed cortex. A 4 mm round customized cover glass cleaned with ethanol and air-dried was applied to the brain surface and the surrounding saline was absorbed using sugi-swabs leaving the window placed within the boundaries of the skull resting on a small drop of saline. Vetbond® adhesive was applied to the boundary of cover glass and skull creating a bond between the two that was left for several minutes to dry. After sealing the cortex with the round cover glass, tetric evoflow® UV hardening dental cement was injected over the exposed skull surface creating an insulated layer on which to place a titanium ring holder. This dental cement was hardened for ~ 30 seconds with UV light, fixing the titanium ring in place. To further attach the ring, dental cement was carefully placed around the inner circumference of the titanium ring and dried by UV light to finish the surgery.

Mice were then injected with antagonist (Atipamezol 0.5 mg/ml, Flumazenil 5 mg/ml, Naloxon 3 mg/ml) and allowed to wake before being placed in a heating chamber at 32°C for observation for 2 hours.

4.3.2 Customized cover glass preparation for cranial window implantation

Briefly, a 4 mm round coverslip was placed onto a microscope slide coated with Kwik-Sil™ silicone sealant (wpiinc, Sarasota, Florida, USA) and held in place with forceps by applying light directed pressure to the coverslip. A softened drill bit on low speed was used to make two circular indentions ~ 1mm apart at the top of the coverslip for use as coordinate markers in later experiments. The drill indentations were then filled in with black permanent, water resistant marker after the chronic cranial window procedure was complete to create vessel independent, fixed landmarks for use in 2-photon microscopy.

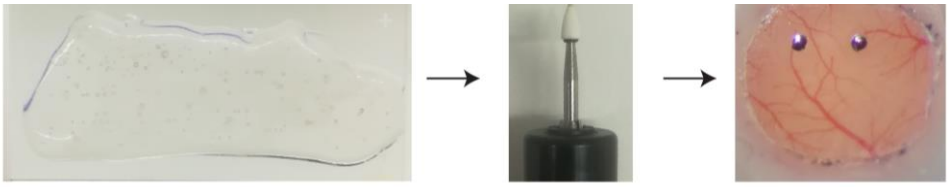

Fig. 14. Components and creation of customized cover glass for chronic cranial window experimentation.

Left, dried Kwik-Sil™ on a microscope slide forms a stable gripping bed on which to place the 4mm round cranial windows. Middle, the soft tipped drill bit is pressed into the cranial window until circular depressions are made. Right, permanent marker is drawn into the depressions and set to dry, creating coordinate markers for subsequent use.

4.3.3 *In vivo* imaging of pericyte cell fate and blood-flow post stroke

NG2DsRed$^{+/-}$PDGFRbEGFP^{+} mice between 14-20 weeks old were implanted with customized cranial windows as previously described and subjected to either sham or stroke surgery in an attempt to fate map pericytes and their response to stroke, cerebral blood flow alterations and response to stroke induced damage in the ischemic brain over the course of a week. Specifically, mice with cranial windows were left for a minimum of one month to recover from the initial surgery induced injury during cranial window surgery. 15 mins prior to laser speckle/2-photon imaging, to provide subtle anaesthesia and label the vasculature, mice were injected with two small subcutaneous injections of 100 mg/kg of medetomidine and 50 µl of 25 mg/ml (3000 MW) TexasRed® neutral anionic dextrans. Low levels (0.5% - 0.75%) of isoflurane were used in combination with medetomidine injection to maintain mice in a shallow level of anesthesia.

Mice were subjected to one round of baseline imaging (1hour) 3 - 4 days prior to either sham or fMCAo surgery, where a 3 minute baseline of laser speckle imaging recorded cortical CBF within the cranial window. Immediately after, mice were transferred to the 2-photon imaging platform and 4, 425 µm x 425 µm x 300 µm (x, y, z dimensions, z step=1 µm) ROI's were imaged from the brain surface down to cover the pial surface and capillary beds in cortical layers 1-3. In detail, the 2-photon imaging was comprised of first navigating to two custom-made window drilled dots using the binoculars at the 2-photon microscope. Once the left dot was in the center of the field of view (FOV) the stage coordinates of the microscope were set to 0, then the FOV was navigated to the right dot and the stage position was recorded (this served to set scale for comparison of laser speckle and 2-photon imaging sets). After, the stage position was returned home to the left dot at

coordinate X=0, Y=0, the brain surface was scanned at the oculars from left to right, recording stage positions that represented FOVs that had minimal pial vessel coverage and highlighted capillary beds within the MCA and ACA territories. Each of the 4 ROIs were then imaged subsequently, with each ROI taking approximately 11-12 minutes to complete.

After 3-4 days, mice were subjected to either stroke or sham surgery as previously described without the attachment of the LDF probe. After 30 mins of either sham or stroke surgery animals were imaged for 3 minutes using the laser speckle device to record CBF alterations following stroke or sham. This step allowed validation of stroke induction as well as the selection of two of the most appropriate ROIs; image areas of extremely low blood flow that correspond to the area perfused by the MCA. After 3 minutes of baseline imaging at the laser speckle, mice were immediately transferred to the 2-photon imaging platform, the left drill dot was located and the stage set to 0. Finally, the selected coordinates of the ROIs to be imaged were typed into the stage system and adjusted using a line-grid comparison to the same area at baseline. Here, special care was taken to line up cortical pericytes with the voxels occupied by that of the same cortical pericytes at baseline using a 1024x1024 line grid. This ensured the same regions could be followed up longitudinally over time with minimal post-processing. This process was repeated for all subsequent follow up time-points: +90 mins post reperfusion, +24 hours, +3 Days, +7 Days. A schematic of how pericytes were voxel matched over time as well as the experimental outline is shown on the two pages below.

At the end of the experiment, mice were injected with MMF (as described in section 4.1.4) and subjected to ice-cold 1XPBS perfusion for 5 minutes followed by 4% PFA perfusion for 5 minutes to fix the brain tissue, the brain was extracted and placed in 4% PFA at 4°C overnight and exchanged to 1XPBS the next day for further processing.

4.3.4 Experimental plan for acute-chronic multimodal imaging (2-photon microscopy and laser speckle imaging) after transient ischemic stroke

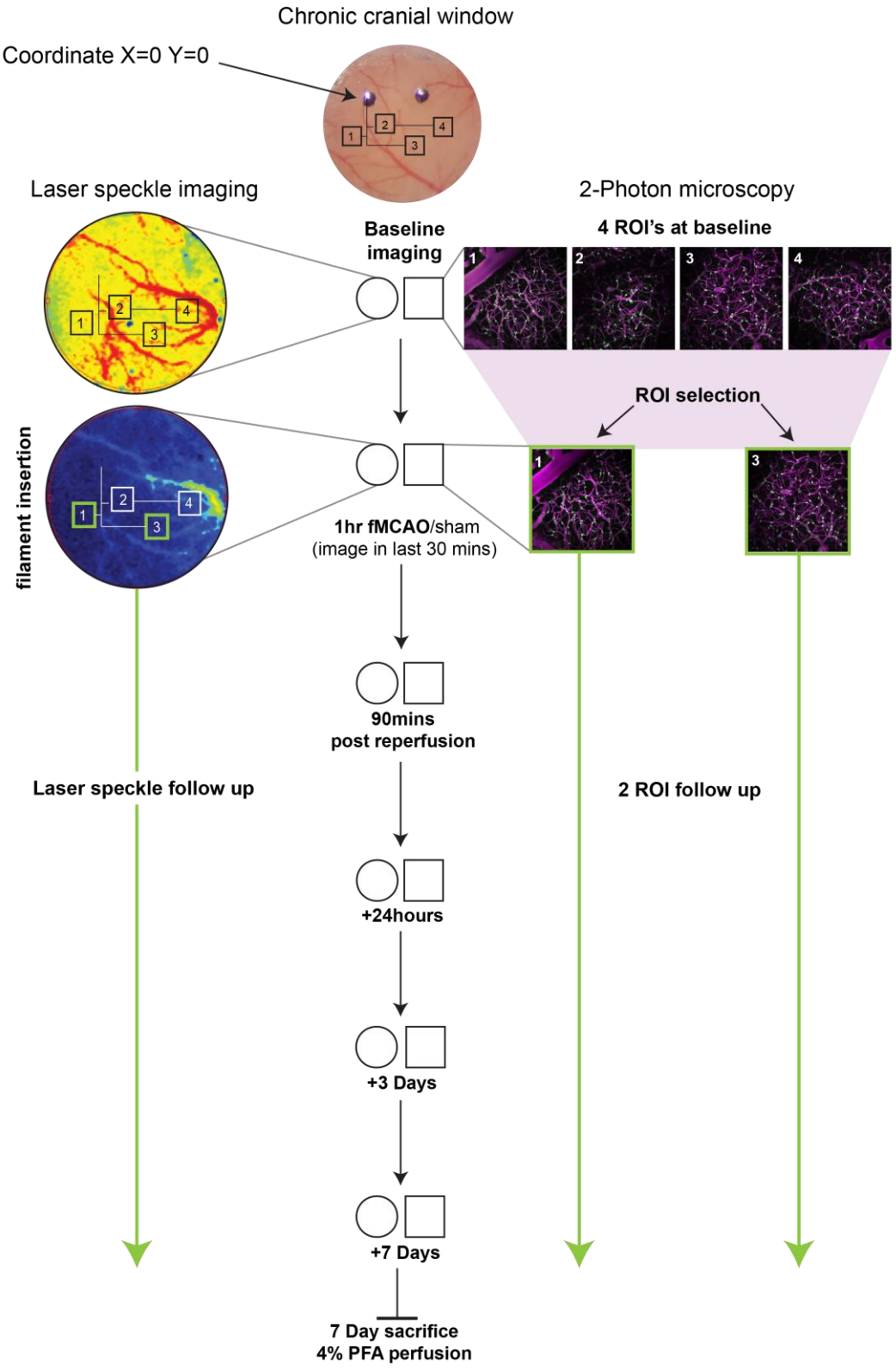

Fig. 15. Experimental protocol for pericyte *in vivo* imaging after stroke.

4.3.5 Voxel matching of capillary pericytes across multiple time-points in the context of stroke/sham surgery with 2 photon microscopy

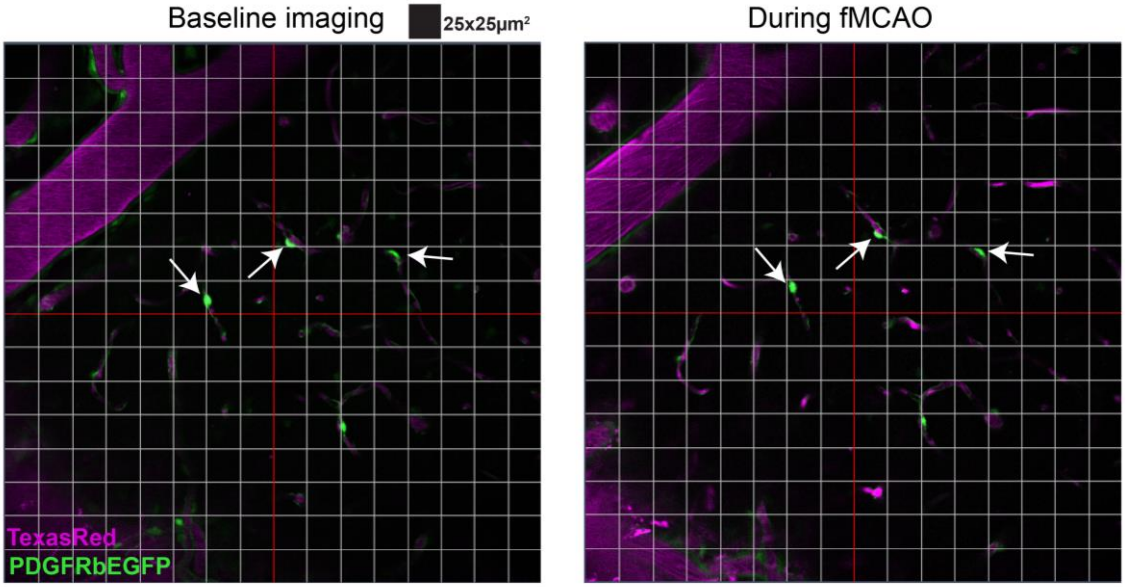

Fig. 16. Voxel matching of capillary pericytes across time-points using placement grids.

In the above image, evenly spaced grid lines 25 µm apart are used to line up cortical pericytes within the ischemic tissue with the same pericytes imaged 3 – 4 days prior at the baseline imaging time-point. White arrows indicate the EGFP+ pericytes that are lined up. This process of cellular alignment to the same grid positions at subsequent time-points was necessary to image the same cortical pericytes in the capillary bed over time and while not perfect, it allowed for direct longitudinal measurement of cortical pericyte characteristics in the context of edema, vessel loss and pericyte loss. Overall, this process took between 2-5 mins prior to the 11 minute imaging process per ROI allowing each time-point measurement at the 2-photon in less than 30 mins - which reduces the chances that the experiment will be compromised by prolonged exposure to mild (0.5% - 0.75% isoflurane, 100 mg/kg medetomidine) anesthesia. In the context of edema, cellular alignment is notably more difficult due to pial vessel rearrangement on the cortical surface, for that reason, priority was given to capillary beds and not the pial vasculature, because the study of pericytes during stroke pathology is the primary aim of this research project.

4.3.6 Longitudinal vessel lumen diameter analysis at pericyte cell soma

To analyze pericytes and the microvasculature in each mouse after stroke or sham surgery the cortical brain surface was removed from each image by cropping because the TexasRed® dye leaks from sinusoidal-like porous vessels on the brain surface. After cropping was complete, image sets were separated into 4 ~ 50 µm - 60 µm stacks of increasing depth (eg. 180 - 240 µm, 120 - 180 µm, 60 - 120 µm, 1 - 60 µm) to allow a maximum projection in z to be created which highlighted mural cells at the capillary level. The pericytes in these maximum z projections were then divided into sub-types from baseline images into: thin-strand pericytes, junctional pericytes, mesh pericytes and ensheathing pericytes based on previously published criteria (Grant et al., 2019). Each pericyte sub-type definition was then individually labelled to generate a pre-defined 'pericyte annotation map' which could be used as a reference point for analysis. Once pericyte annotation maps were generated for all mice across all depths, tables were created in Excel and measurement of lumen diameter proximal to the cell soma of each pericyte was measured by drawing a line across the lumen in FIJI software at 3 points (left, middle, right) of the cell soma in individual z-sections. These measurements were then averaged to give an average lumen diameter for each pericyte at each location and the measurement lines were added to the pericyte annotation map to serve as landmark measurement points for the same pericytes across either sham or stroke surgery. The measurement of these points was repeated across all time-points to assess the diameter change of the lumen across the course of stroke/sham disease pathology. Care was taken at each time-point to measure exactly the same location (left, middle, right) at the cell soma. These measurement points were then averaged to give lumen diameter changes at the pericyte cell body over time. A schematic detailing this work flow is shown below. If a pericyte disappeared at future time-points or if the vessel edges could not easily be defined, this was noted and the possible reason for no measurement taking place was added to the table. This occurred for several reasons such as: edema pushing the pericyte out of the FOV, a decrease in signal-noise ratio, a loss of the vessel itself or pial surface rearrangement creating a vessel shadow over the pericyte which limited 2-photon excitation of the vessel in that location. Once the dataset was completed for all mice, a duplicate check was performed to check whether any cells from the boundaries between two adjacent stacks (eg. 120 - 180, 180 - 240 µm) had been measured twice and if they were, the cell was removed from the final analysis. To analyze normalized diameter changes over time, the time point normalized was divided over the baseline value to give a change in percentage representing the relative change in lumen diameter in relation to baseline.

4.3.7 Definition of pericyte annotation maps & lumen diameter analysis

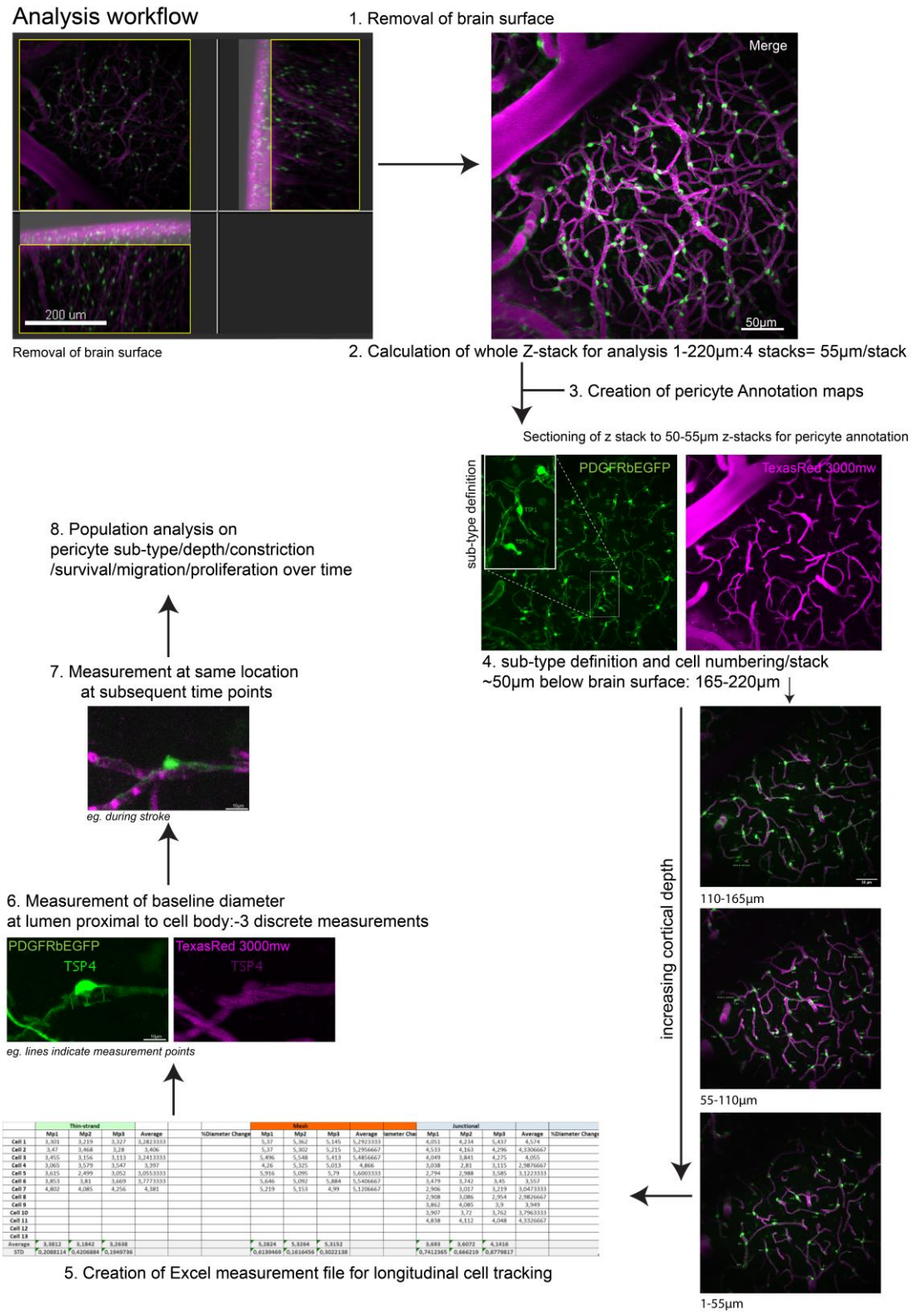

Fig. 17. Workflow of pericyte sub-type analysis after stroke.

4.3.8 Analysis of capillary stalls and their association with pericytes in the 2-photon data set

Capillary stalls were analyzed in stroke/sham animals in each of the four cortical z-columns that were created to define the pericyte annotation maps, giving a value of number of capillary stalls/~50 µm per ROI during stroke. To do this, z-stacks were assessed for red blood cells (which appear as a shadow in the vessel lumen not stained by TexasRed®) according to the following pre-defined criteria. The scan time of 1 frame at the 2-photon microscope was 1.6 seconds, therefore, If the RBC shadow in the capillary was present for 3 or more consecutive frames of scanning (4.8 seconds) the capillary was deemed 'stalled' by an RBC. This is because the average flux of 50 RBC/s is reported in pia 0-100 µm below the surface, and the number of capillary stalls was quantified in this way using the cell counter in FIJI software (Schmid et al., 2017). This process was repeated over additional time-points during stroke/sham, 90 minutes post-reperfusion and 24 hours post-stroke/sham with the additional criteria for assessing whether pericytes were associated with the stalls in question. Pericytes were termed stall associated if the stall appeared less than 5 µm from the pericyte soma, or excluded from the analysis if the stall was greater than 5 µm from the cell soma. This process was repeated across all cortical depths.

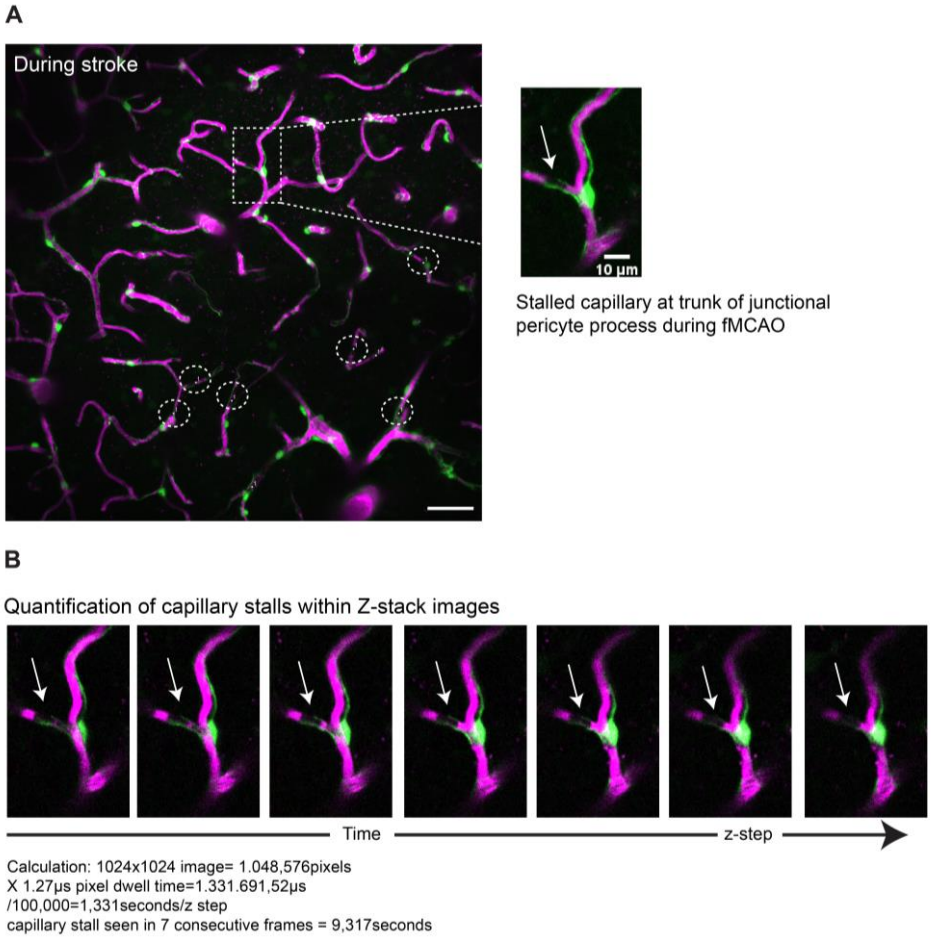

Fig. 18. Capillary stall analysis within the 2-photon dataset

A) Left, Example of a stalled capillary bed during stroke, stalled segments are highlighted by white dotted circles. Right, zoomed in view of a junctional pericyte associated capillary stall during stroke. **B)** Quantification and depiction of traversing subsequent z-sections over-time to create a pseudo-time analysis of the non-flowing vascular element highlighted in A (Right). The stall within this image did not move for almost 10 seconds of 2-photon scanning.

4.3.9 Laser speckle imaging

Three minutes prior to 2-photon imaging after either stroke or sham surgery; mice were anesthetized as previously mentioned (100 mg/kg, medetomidine subcutaneous and 0.5% - 0.75% isoflurane) and fixed in a head holder with a titanium ring, the laser speckle imaging device was placed over the cranial window and positioned 10 cm distal to the surface of the superficial cortex. Focus over the cortical surface was determined automatically by pimsoft® software and images were acquired at a frame rate of 44 images/second and averaged 10 times to produce an average of 4.4 images a second. Three mins of cortical blood flow was imaged for each time-point: Baseline, During fMCAo/Sham, 90 mins post reperfusion, + 24 hours, + 3 Days, + 7 Days.

4.3.10 Statistical analyses and figure creation

To begin ***ex vivo*** experimental work, an experiment was performed to determine the extent of pericyte loss/death after experimental stroke. Five male 6-12 week old C57BL6/J mice were randomly assigned to either Naïve, Sham, Day 1 or Day 3 post-stroke groups. After tissue processing and immunofluorescence staining, microscope slides were blinded and equal numbers of images were stereotactically taken in each brain region across all groups, pericyte density was compared using an unpaired, two-tailed Student's t-test after passing a Shapiro-Wilk test for normality. This process was repeated for vessel coverage, but normality tests failed for pericyte coverage (Infarct core – $p<0.03$), therefore a non-parametric Mann-Whitney rank sum test was used to determine significant differences between groups and data was displayed as median with interquartile range. Shapiro-Wilk tests for normality also failed for the number of proliferation bodies observed (peri-infarct day 1 – $p<0.04$, infarct core day 1 – $p<0.0001$), therefore, a Mann-whitney rank sum test was performed to assess significant differences between groups. (Fig.20, 21).

Once no death or alteration in pericyte density was observed in either sham or naïve groups, the decision was made to ask whether pericytes are visibly damaged within stroked animals hyper acutely post-reperfusion, because pericyte death was observed in stroked animals in the prior experiment. Here, 4 PDGFRbEGFP mice were sacrificed 90 minutes post reperfusion of the occluded artery and high-resolution images were taken of individual pericytes in either infarct core or contralateral areas in an unbiased, stereotactic manner. Individual selection of the pericytes to be analyzed was performed by a colleague in a randomized manner and this was used to determine the percentage of damaged/intact pericytes in the infarct core. Then, analysis was performed using an equivalent pipeline across all groups for nuclear volume, nuclear sphericity and nuclear EGFP intensity. Damaged pericytes were subsequently separated from intact pericytes in the infarct core and contralateral pericytes, and differences between the groups were assessed using an unpaired Student's t-test for junctional and mesh pericytes after passing a Shapiro-Wilk normality test in Junctional and Mesh pericyte nuclear EGFP intensity in intact, damaged and contralateral groups. Nuclear EGFP intensity in the damaged population of the thin-strand pericytes however, failed a Shapiro-Wilk normality test ($p<0.01$). Therefore, a Kruskall-Wallis test was used to determine significant differences and data was displayed as median and 95% confidence intervals. For assessment of nuclear volume, all intact, damaged or contralateral pericytes were compared using an unpaired two-tailed Student's t-test and no significant differences were found (Fig.22).

Subsequently, variances in pericyte density throughout the brain were assessed on day 3 post-stroke along a caudal-rostral axis in four 6 - 12 week old male PDGFRbEGFP mice. Here, complete brain sections were stained with NeuN to label neurons and scanned at high resolution using

confocal microscopy. A pipeline within Imaris® was created to identify EGFP spots greater than 8 µm in size, which corresponded to EGFP soma within the tissue. Subsequently, the pipeline highlighted EGFP soma and soma on large vessels (arterioles, venuoles, arteries or veins) were excluded from the analysis by deselecting the dots. Then, masks were applied to each region of the brain depending on whether the cells were in either ipsilateral, infarct core or contralateral brain regions. Number of spots per region was normalized to mm^2 by using the masks to determine the size of the region each population of spots were located within. Then, the number of spots/mm^2 was divided over the contralateral number of spots/mm^2 to generate the pericyte density reduction/mm^2 within infarct core and ipsilateral regions. Differences along a caudal-rostral axis were compared against each other using an unpaired, two-tailed Student's t-test after passing a Shapiro-Wilk test for normality.

To investigate pericyte EdU uptake and Ki67 reactivity with a view to determine whether pericytes were entering the cell cycle post-stroke, equal numbers of images were taken stereotactically in each PDGFRbEGFP mouse on day 3 post-stroke in infarct core, peri-infarct and contralateral regions of the striatum and cortex respectively. Differences between groups in each region for EdU^+ and $Ki67^+$ pericytes were compared using an unpaired, two-tailed Student's t-test after passing a Shapiro-Wilk test for normality. These experiments also served to assess differences in pericyte density between cortex and striatum in ipsilateral, infarct core and contralateral tissue respectively and were subject to the same statistical tests after confirming normality of the data using a Shapiro-Wilk test (Fig.24).

After discovering that a portion of pericytes were indeed surviving stroke and entering the cell cycle. FACS isolation and transcriptomic sequencing was performed to investigate the pericyte transcriptomic profile alterations within ipsilateral, contralateral, infarct core or sham animals on day 3 post-stroke. Care was taken to ensure that one stroked animal and one sham animal was used per FACS isolation, to ensure pericytes were isolated under exactly the same conditions for downstream analyses. This was repeated three times, during which point the quality was assessed by BGI (a transcriptomic sequencing company, (https://www.bgi.com/global/sequencing-services/rna-sequencing-solutions/transcriptome-sequencing/) which determined that one of the sham samples contained poor quality RNA and was thus excluded. This left an n=3 stroke animals and n=2 sham animals. For downstream analysis, raw transcript counts were normalized using the NormalizeData function of Seurat with a scale factor of 100,000. Dataset were scaled and percentage of ERCCs and plate batches were regressed using ScaleData function. This enabled effective discrimination and comparison of the stroke-isolated pericytes, ipsilateral pericytes and contralateral pericytes within stroked animals together with sham isolated pericytes, using downstream analytical methods such as principal component and gene ontology analyses. To determine the percentage of each transcriptomic pool entering the cell cycle within each brain region (sham, ipsilateral, contralateral and stroke) normalized counts were processed through the Seurat cell cycle scoring function (Fig.26, 27, 28).

***In vivo* experimentation**: To assess differences of laser speckle blood flow post either stroke or sham surgery, a two-way ANOVA with greenhouse-geisser correction method was used because one stroke mouse which died before the end-point of the experiment, creating empty values which cannot be assessed using a standard two-way ANOVA. This makes the data unspherical and the greenhouse-geisser method is used to compensate for such scenarios. To compare individual time points, a Shapiro-Wilk test was performed to confirm normality and differences between stroke and sham animals were compared using multiple unpaired Welch's t-tests, one per row, to

account for the uneven group size (n=7 in stroke group, n=4 in sham group) in order to assess significant differences at individual time-points (Fig.29).

To test for differences between the lumen diameter associated within a pre-determined (at baseline) population of pericytes during either sham or stroke surgery, a Shapiro-Wilk test was performed to confirm normality within pericyte sub-type populations across all time-points. This was followed by a two-way ANOVA with greenhouse geisser correction and was repeated for stroke/sham pericytes 90 mins post-reperfusion of the occluded artery or 90 mins post-sham surgery at all subsequent time-points. Next, investigations on whether variance existed between pericyte sub-types that constricted during ischemia were performed. Here, the normalized extent of constriction of stroked pericytes within each sub-type was compared using an unpaired Student's t-test after a Shapiro-Wilk test was performed to confirm normality of the dataset (Fig.31, 33).

After establishing that pericytes constricted during stroke, the average number of capillary stalls during either stroke or sham surgery were assessed as a function of cortical depth after confirming normality of the data using a Shapiro-Wilk test. Here, within groups a one-way ANOVA was performed across cortical depths, and to test between groups an unpaired Welch's t-test was used at each cortical depth to control for uneven group size (n=7 stroke group, n=4 sham group). To test for differences in stalls associated with pericytes over time between stroke and sham, a Shapiro-Wilk normality test was performed. Once data normality was confirmed, each pericyte sub-type during either stroke/sham, 90 mins post reperfusion or sham surgery and 24 hours after sham/stroke surgery was assessed with a two-way ANOVA with greenhouse-geisser analyses was performed with Sidak's multiple comparison to assess difference between groups over time. Finally, to test for differences in the association of capillary stalls with each pericyte sub-type during stroke, an unpaired Welch's t-test was used following confirmation of normality using a Shapiro-Wilk test (Fig.32).

To test for variances in pericyte constriction as a function of cortical depth, an unpaired Student's t-test was performed after confirming normality of the data with a Shapiro-Wilk test within the stroke group at the during stroke time-point. Then, to find out how lumen diameter changes associated with pericytes differed between stroke and sham across subsequent time-points (since prior data normality was confirmed during analysis of figure 30), a two-way ANOVA with greenhouse-geisser correction was used and individual time-points were compared between groups using an unpaired Welch's t-test. Once a bi-phasic constriction profile in pericytes was elucidated, 659x659 pericytes from the six surviving stroke mice were arranged on a heatmap from least constricted to most constricted and the relationship between each pericyte was assessed by looking at how each pericyte behaved across all 5 time-points after baseline using a Pearson's correlation co-efficient. This correlation co-efficient was then normalized using a z-fisher transform to spread the data and normalize the correlation scores across the population (Fig.34).

Finally, to assess whether laser speckle variations in blood flow are correlated with pericyte vessel constriction during stroke, we first performed a Shapiro-Wilk test to confirm normality of the data, then a Pearson's correlation test between the six surviving stroke mice. To assess the coefficient of determination and thus give an R^2 value for the dataset, we performed a linear regression analysis of the data (Fig.35). These statistical analyses were performed in Graphpad (Prism®) 9.1.0 and the resulting figures were then made using Adobe Illustrator ®.

5. Results

5.1 Standardization of a transient 60-minute transient middle cerebral artery occlusion model

Before assessing the pericyte response to stroke, it was necessary to develop the technical skills to produce a large cortico-striatal infarct, which produces ischemic cell death and simulates reperfusion injury after stroke in a clinically relevant manner. To that end, we performed a standardization aptitude test to confirm the consistency of filament middle cerebral artery occlusion across 10, 6-week-old C57BL/6 mice. We confirmed the induction of stroke using a laser doppler fluxmetry probe attached to the temporal bone of the skull, which can be used to measure blood flow in the distal MCA and noted a significant reduction in blood flow of less than 20% of baseline in all animals ($p<0.0001$) (Fig.19.A). We then sacrificed the animals after 24 hours and performed a sectional analysis evaluating the size of the infarct in sections serially cut across the whole brain every 750 µm using Nissl staining (Fig.19.B).

Nissl staining is an immunohistochemical method commonly used for the study of pathology in neural tissue (Kádár et al., 2009). Once fresh-frozen brain sections are stained with the cresyl violet dye, Nissl staining reveals the cytoplasm of neurons through binding interactions with DNA in the cell nuclei and RNA which is highly concentrated in the rough endoplasmic reticulum of neurons, where the amount of active protein synthesis is very high (Knowles et al., 1996, Kosik and Krichevsky, 2002). Nissl staining can be used to discriminate neurons that are structurally intact from those which have died and can be used without recognizing the cytoplasm of other cells within the brain, in this way we tested the severity of our stroke model. We found that the infarct spread from the anterior cortex to the posterior cortex and produced an average cortico-striatal infarct volume of 80 mm^3 after measuring all mice. All mice showed a large region of Nissl$^-$ area after 24 hours consistent with the loss of neurons within the ischemic territory perfused by the occluded MCA (Fig.19.C, D). Therefore, we conclude that stroke can be effectively induced to produce a large infarct that eradicates neurons from the post-stroke brain after 24 hours, serving as a test bed to study the pericyte response to stroke under the same conditions.

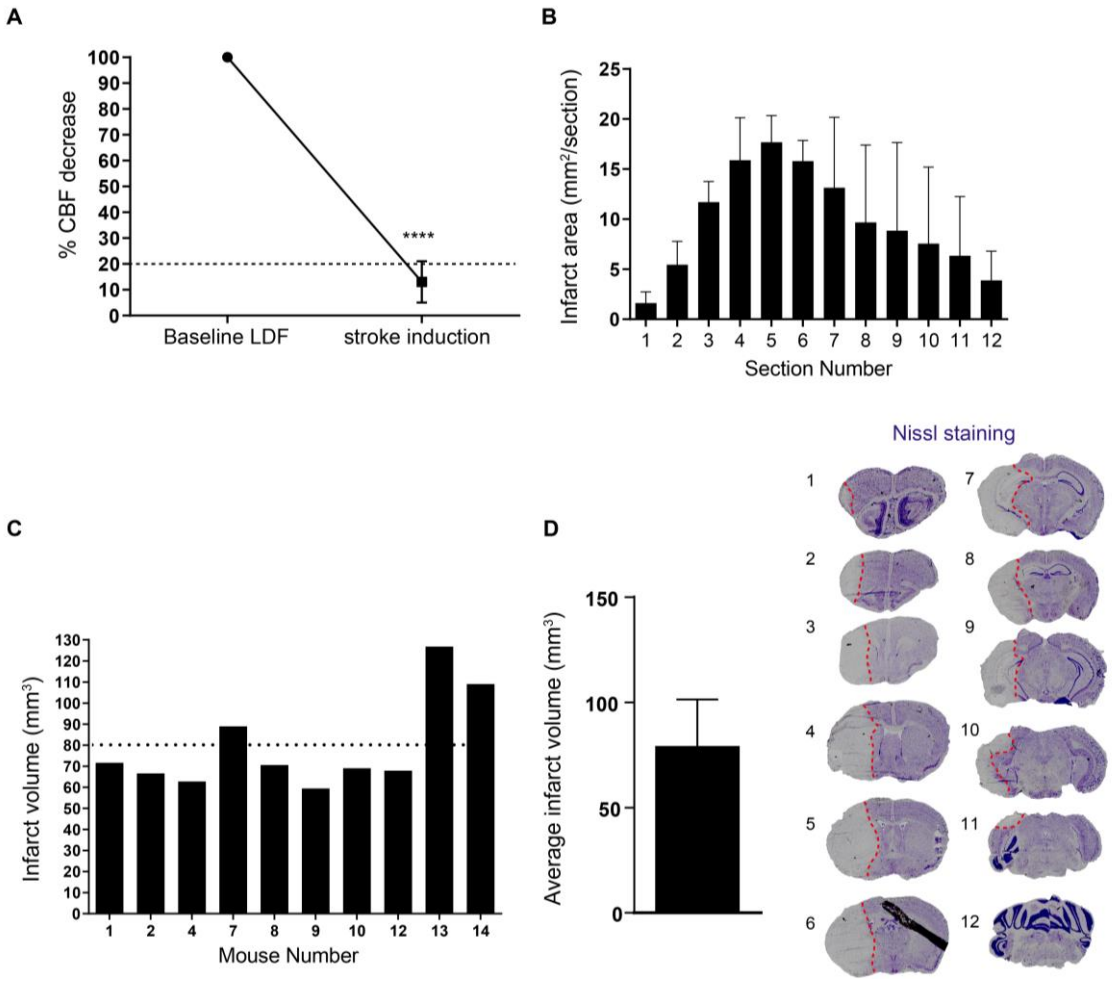

Fig. 19. Standardization of the filament middle cerebral artery occlusion model of transient ischemia

A) Normalized LDF fluxmetry of stroke induction and blood flow reduction during fMCAo. **B)** Average section-by-section analysis of infarct area in 6-week-old C56BL/6J mice. **C)** Average non-corrected infarct volume ($Nissl^-$ area) per mouse. **D)** Left, average corrected infarct volume of all mice stroked. Right, Section-by-section view of Nissl staining depicting the $Nissl^+$ and $Nissl^-$ area (red dotted line delineates the border between the two). *Statistics, unpaired two-tailed Student's t-test. Data is shown as mean +/- SD.*

5.2 *Ex vivo* characterization of pericyte cell fate

As a starting point, we aimed to determine the extent of pericyte death following transient cerebral ischemia. Previous reports suggest that the majority of the pericyte population is lost in the acute phase. To investigate this, we first attempted to use PDGFRbEGFP mice in combination with Terminal deoxynucleotidyl transferase (Tdt) dUTP nick end labeling (TUNEL); an enzymatic reaction that transfers nucleotides to the 3' hydroxyl termini of DNA double strand breaks for visualization. These double strand breaks in DNA are a prominent feature of apoptotic cells; allowing dead cells to be separated from living populations through $TUNEL^+$ vs $TUNEL^-$ cell counts. Together with EGFP this would have enabled assessment of dying pericytes present in the infarct core acutely after stroke, however despite repeated efforts (data not shown), PFA fixed vibratome tissue appears incompatible with Tdt enzyme function. Therefore, the experiment was approached from a different angle.

5.2.1 Characterization of pericyte density after stroke

We subjected five 6-12 week old C57BL6/J male mice to either immediate sacrifice, sham or stroke surgery (Day 1 and Day 3). Using LDF fluxmetry, we confirmed stroke induction (Fig.20.B, upper) in all stroke mice and utilized serial fresh-frozen brain sections to confirm cortical-striatal infarction leaving a large region of neuronal cell death at the MCA territory using Nissl staining (Fig.20.B). We then treated the fresh-frozen tissue with a combination of antibodies to label pericytes (PDGFRb), the basement membrane (Collagen IV), dying cells (TUNEL) and nuclei (DAPI), to assess pericyte density and death in the acute phase of stroke (Fig.20.A).

$PDGFRb^+$ cells encased within a Collagen IV^+ matching pericyte morphology were counted across each group: Naïve, Sham, Day1 and Day3 fMCAo groups. Groups were assessed in a randomized, blinded manner based on cell counting in three regions: Contralateral, peri-infarct and infarct core areas (Fig.20.B). 350/363/346 pericytes per mm^2 were observed in each region corresponding to the contralateral, peri-infarct and infarct core areas (under conditions of stroke) respectively under naïve conditions (Fig.20.D). The difference in pericyte density between regions selected for analysis within the naïve group was not significant, suggesting pericyte density was broadly uniform in the regions selected. In addition, sham surgery did not significantly alter pericyte density in any region when compared against naïve mice. These data indicate that sham surgery does not significantly affect pericyte density after 24 hours. After stroke, pericyte density in the infarct core and peri-infarct regions was reduced by ~ 25% compared to contralateral regions after 24 hours (infarct core: 292 cells/mm^2, peri-infarct region 300 cells/mm^2 - contralateral: 399 cells/mm^2), however, this reduction in pericyte density did not reach significance, but instead implied a trend toward mild pericyte loss after 24 hours. 3 days post stroke, pericyte density in the infarct core was reduced by ~ 16% and 15% in the peri-infarct regions compared to the contralateral region (infarct core: 328 cells/mm^2, peri-infarct region 333 cells/mm^2 - contralateral: 388 cells/mm^2). This density reduction did not reach significance (Fig.20.D). These results suggest that stroke does not significantly affect visibility of the $PDGFRb^+$ pericyte population between days 1 and 3 and imply a trend toward a transient pericyte density reduction (~ 25% on day 1, 16% on day 3) post stroke in the acute phase, and may indicate a partial reconstitution of the pericyte population on day 3 post stroke.

5.2.2 Characterization of pericyte cell death

In the same experiment, TUNEL$^+$ cells were visualized under 3 out of 4 conditions tested (Naïve, days 1 and 3 post stroke) and appeared as red cells which allowed separation of the contralateral, peri-infarct and infarct core regions after stroke respectively (Fig.20.A, upper to lower image panel). Under Naïve and sham conditions, little to no evidence of TUNEL$^+$ cells/pericytes could be visualized across putative contralateral, peri-infarct and infarct core regions with the exception of one TUNEL$^+$ pericyte in the naïve group and these differences did not reach significance (Fig.19.A, E). On day 1 and 3 after stroke however, both TUNEL$^+$, PDGFRb$^+$ and TUNEL$^-$ PDGFRb$^+$ cells matching pericyte morphology could be visualized in both the infarct core and peri-infarct regions (Fig.20.C). These cells were quantified as a percentage of the total pericyte population counted within each region (Fig.20.E).

We found that stroke induced the appearance of significantly more TUNEL$^+$ pericytes in the infarct core compared to the number of TUNEL$^+$ pericytes in the contralateral hemisphere on day 1 post-stroke (Infarct core 30% TUNEL+ pericytes - 0.2% TUNEL$^+$ pericytes in contralateral hemisphere, $p<0.000002$). In addition, we found significantly more TUNEL$^+$ pericytes within peri-infarct regions, than in the contralateral hemisphere (17% - 0.2%, $p<0.001$). At a population level, 88/291 pericytes of pericytes were TUNEL$^+$ in the infarct core and 49/300 pericytes were TUNEL$^+$ in the peri-infarct region compared with just 1/399 TUNEL$^+$ pericytes in the contralateral hemisphere of stroked mice after 24 hours. On day 3 post stroke however, just 3% of pericytes within the infarct core and peri-infarct regions were TUNEL$^+$ (infarct core: 9/328 pericytes, peri-infarct region: 11/333 pericytes) with no TUNEL$^+$ pericytes observed in the contralateral hemisphere (Fig.20.E). These differences indicate significantly more pericyte loss in the infarct core and peri-infarct region than in contralateral regions on day 3 post-stroke (infarct core – contralateral, $p<0.004$, peri-infarct region – contralateral, $p<0.009$). Furthermore, we found significantly more TUNEL$^+$ pericytes were present on day 1 post-stroke than on day 3 post-stroke within infarct and peri-infarct regions (infarct core day 1 – day 3, $p<0.000005$, peri-infarct regions day 1 - day 3, $p<0.004$).

Taken together, these results (Fig.20.D, E) suggest that transient cerebral ischemia (60mins) results in incomplete, but acute pericyte cell death within the infarct core, peaking after 24 hours and continuing at low levels on day 3 post-stroke. This is accompanied by a 25% reduction in the pericyte density before 24 hours, and a milder 15 - 16% reduction in pericyte density on day 3 post-stroke in infarct core and peri-infarct regions respectively. Cumulatively, these data indicate that pericyte cell death is an acute response to stroke, which ultimately leaves a large portion (approximately ~ 50%) of the pericyte population intact in the sub-acute phase, where low levels of pericyte cell death continue.

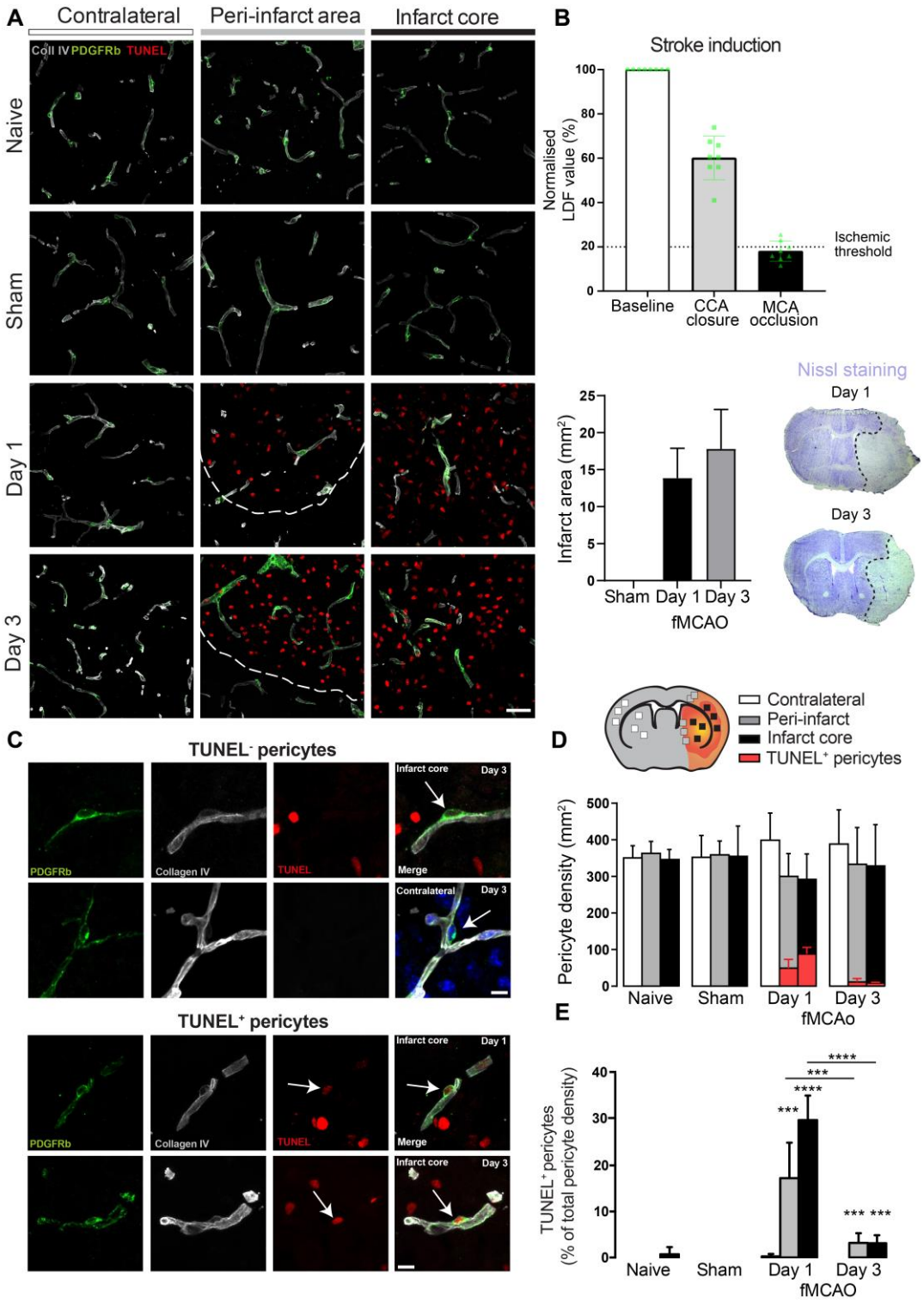

Fig. 20. A population of pericytes die in the acute phase of stroke.

A) Confocal micrographs of Collagen IV (gray), PDGFRb (green) TUNEL (red) immunofluorescence staining in C57BL/6J mice after no surgery, sham, day 1 or day 3 post stroke. **B)** Upper, validation of stroke induction using LDF fluxmetry at the distal MCA territory. Lower, average infarct area at the MCA territory calculated using Nissl staining (day 1 and day 3 post-stroke), infarct core is highlighted with red dotted line (right). **C)** TUNEL- pericytes in the infarct core surrounded by TUNEL+ cells on day 3 in the infarct core and contralateral hemisphere (upper). TUNEL+ pericytes in the infarct core on day 1 and day 3 post-stroke. **D)** Pericyte density per mm^2 in each region, number of $TUNEL^+$ pericytes are highlighted in red. **E)** $TUNEL^+$ pericytes expressed as a percentage of the total pericyte density recorded. *n=5 mice per group, Statistics, unpaired two-tailed Student's t-test, Scale bars 50 µm and 10 µm respectively. Data is shown as mean +/- SD.*

5.2.3 Analysis of pericyte coverage, vessel density and pericyte clustering

Since, decreased pericyte coverage and pericyte migration is reported after a number of neurological pathologies (Dore-Duffy et al., 2000, Ghosh et al., 2015, Kisler et al., 2017b), we next sought to assess whether pericyte coverage and location were affected by stroke. To that end, the images generated by the experiments described in Fig.20 were assessed for variances in vessel density, pericyte coverage and pericyte clustering.

Across all brain regions and all mouse groups (Naïve, Sham, Day 1 post stroke, Day 3 post stroke) no significant differences in vessel density were observed in any region post stroke (Fig.21.A, B). Pericyte coverage was assessed by dividing the PDGFRb$^+$ pixel area per image by the collagen IV$^+$ pixel area. Under naïve conditions, pericytes covered approximately 30 - 35% of the vessel area (Fig.21.C) No significant differences between pericyte coverage per area were observed in naïve, sham or day 1 post stroke time points between regions, however, a significant increase in pericyte coverage was measured on day 3 post stroke in both peri-infarct and infarct core regions when compared against the contralateral pericyte coverage at the same time-point (Infarct core/contralateral, $p<0.008$, peri-infarct/contralateral, $p<0.008$). These data indicate that collagen IV$^+$ vessel structures remain present after acute infarction and that PDGFRb$^+$ cells are expanding vessel coverage in the sub-acute phase of stroke.

Furthermore, we noticed stroke induced the appearance of ‘proliferation bodies’ which we termed as a result of their appearance (Fig.21.D, left panel images). These ‘proliferation bodies’ were accumulations of PDGFRb$^+$ cells present with the collagen IV$^+$ basement membrane comprising at least two or more cells in close physical contact. We found this intriguing, as pericytes are normally territorial in their distribution along the cerebral vasculature. Therefore, we quantified the phenomenon. We found proliferation bodies on both days 1 and 3 after stroke in both infarct core and peri-infarct areas (0.6 proliferation bodies/mm^2/ group, day 1, Fig.21.E) and their frequency was significantly more prevalent on day 3 in the peri-infarct region compared to day 1 ($p<0.02$), while an increase between day 1 and day 3 in the infarct core was also detected, there was no significant difference at the statistical level. In summary, initial observations of pericyte death following transient cerebral ischemia suggested that pericyte death was incomplete and the population of pericytes that remained within the stroked tissue may still be viable and actively responding to ischemic sequelae.

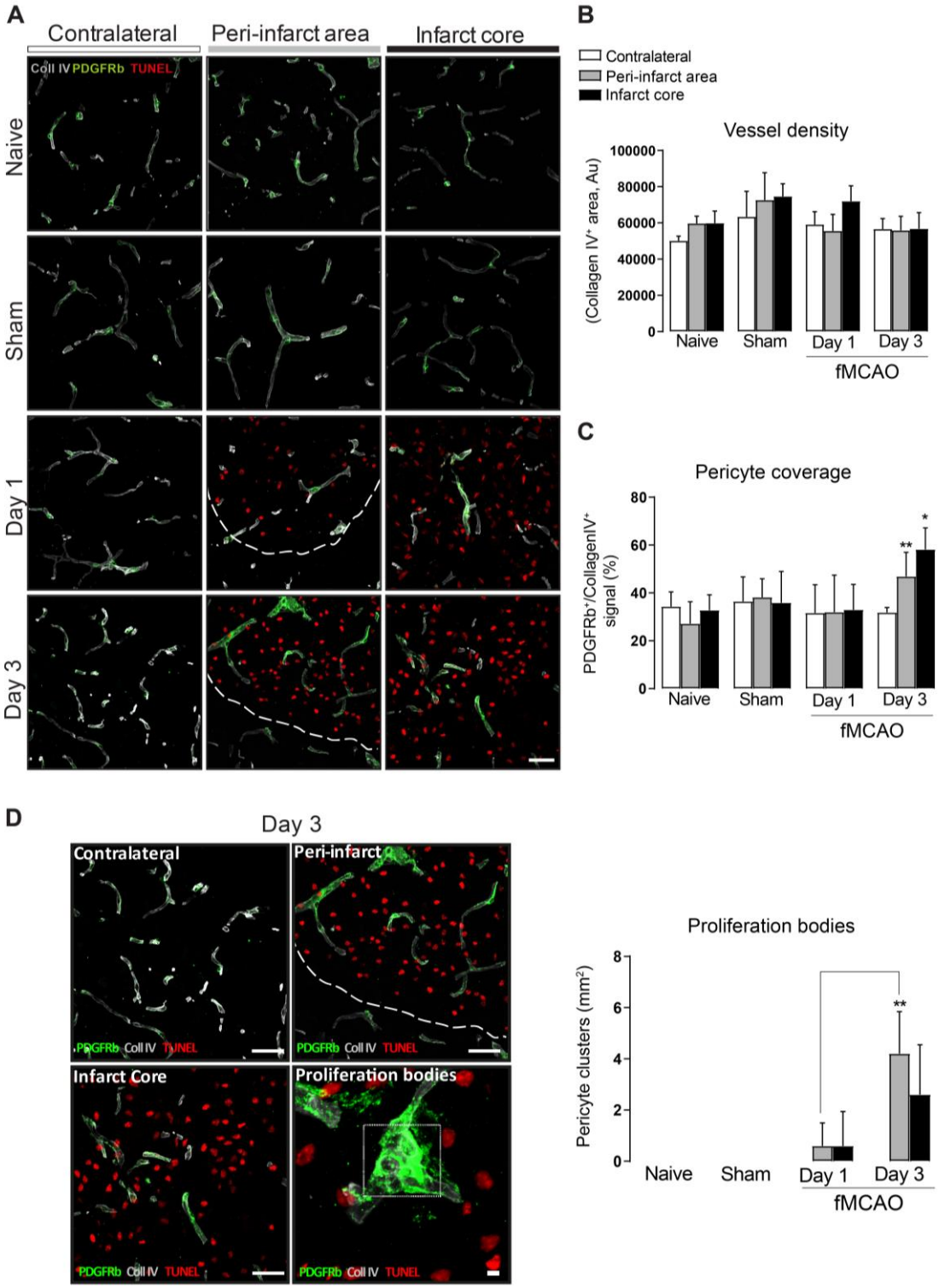

Fig. 21. Surviving pericytes expand vessel coverage and form clusters suggestive of proliferation on day 3 post stroke.

A) Confocal micrographs of Collagen IV (gray), PDGFRb (green) TUNEL (red) immunofluorescence staining in C57BL/6J mice after no surgery, sham, day 1 or day 3 post stroke. **B)** Vessel density expressed as the amount of total pixels covered by Collagen IV$^+$ pixels in each experimental group. **C)** Quantification of pericyte coverage expression as a ratio of PDGFRb$^+$/Collagen IV$^+$ pixel area. **D)** Confocal micrographs of the contralateral hemisphere and infarct core on day 3 post stroke respectively (left). Border zone of the infarct with the presence of PDGFRb$^+$ and Collagen IV$^+$ cell clusters within the infarct border zone (Right). Quantification of the appearance of proliferation bodies per mm2 induced by stroke. *n=5 mice per group, Statistics, unpaired two-tailed Student's t-test, Scale bars 50 µm and 10 µm respectively. Data is shown as mean +/- SD.*

5.2.4 Pericytes incur membrane damage during ischemia and diverge into intact and damaged phenotypes acutely post-reperfusion

To further refine our understanding of pericyte damage/death, we sought to return to experimentation with PDGFRbEGFP mice, as they provide a more robust assessment of pericytes under experimental conditions and allow morphological distinction of pericyte subtypes. Although we observed almost no signs of pericyte loss in fixed tissue from PDGFRbEGFP animals 24 hours post-stroke (data not shown), we speculated that this may be dependent on the relatively long half-life of the EGFP protein and therefore hypothesized that signs of ischemic pericyte damage may be still be visible acutely after the reperfusion of the occluded artery (Danhier et al., 2015). Fortuitously, at the same time, during the establishment of pericyte *in vivo* imaging after stroke, we noted the sparse formation and appearance of blebs in pericytes under ischemic conditions (Fig.22.A). We hypothesized that these small blebs may be indicative of pericyte damage, which may be easier to visualize *ex vivo* (given that confocal imaging provides up to 2.5x the resolution of the 2-photon microscope). We then quantified the prevalence of this newly appearing phenotype acutely; 90 minutes post reperfusion of the occluded artery in fixed tissue sections from PDGFRbEGFP mice using high-resolution confocal imaging. We observed the loss of $Iba1^+$ microglia and $GFAP^+$ astrocytes when scanning across toward the infarct from the extra-lesional tissue to the infarct core, but pericytes remained visible (Fig.22.B).

Upon closer examination, using Collagen IV staining to label the basement membrane (in which pericytes are normally encased), we found that pericytes split into two distinct categories (Fig.22.B, lower panel), those with an intact cytoplasm in which EGFP was contained within the basement membrane, and pericytes which appeared to have pathological protrusions of EGFP beyond the basement membrane. Using line profile measurement, we confirmed that EGFP particles had escaped the basement membrane (Fig.22.C) which in turn suggested that molecules of EGFP had leaked from the pericyte into the surrounding parenchyma. When quantifying the prevalence of these two distinct phenotypes (Intact, damaged pericytes), we found that 59% of thin-strand pericytes appeared damaged with leakage of EGFP from beyond the cytoplasm of the pericyte, while 41% appeared to have retained an intact cytoplasm. 47.5% of junctional pericytes appeared to be damaged, leaving 52.5% of the junctional pericyte population intact (Fig.22.D, E). We then quantified the prevalence of damage within the mesh pericyte population, we observed that 57.1% of the mesh pericyte population appeared damaged, leaving 42.9% of the population with an intact cytoplasmic appearance (Data not shown due to low n number).

To further investigate the divergence of pericyte phenotypes 90 minutes after reperfusion following one hour of transient ischemia, we used nuclear staining (DAPI) within pericytes to gate and compare the amount of EGFP fluorescence intensity within pericytes that appeared damaged with those that had an intact cytoplasm. We performed analysis of EGFP intensity in the nucleus and not the cytoplasm for three reasons. Firstly, pericytes possess a wide array of morphologies and extend processes over large regions of the vasculature making quantitative immunofluorescence of the entire cytoplasm impractical at high-resolution. Secondly, EGFP can freely translocate in and out of the nucleus and therefore we postulate that this should be consistent among the entire pericyte population. Thirdly, nuclear volume and sphericity were not statistically significantly different when comparing pericytes which appeared damaged and those which appeared intact. We observed that pericytes which were split prior into a damaged phenotype had significantly less EGFP intensity in their nuclei compared to those pericytes with an intact cytoplasm (damaged - intact, $p<0.0003$, damaged - contralateral, $p<0.0001$) while EGFP intensity in pericyte nuclei with an intact cytoplasm did not differ significantly with EGFP intensity within the nuclei of

the same pericyte sub-type in the contralateral hemisphere (Fig.22.F). These differences remained consistently significant within the junctional pericyte population (damaged - intact, $p<0.0005$, damaged - contralateral, $p<0.0001$). However, we observed no difference in EGFP intensity in the nuclei of damaged mesh pericytes compared to intact mesh pericytes, but differences between damaged mesh pericyte nuclear EGFP intensity and contralateral mesh pericyte nuclear EGFP intensity were still significant (damaged - contra, $p<0.03$, data not shown). These data strongly suggest that pericyte membrane integrity is compromised during stroke, which persists up to 90 mins post reperfusion - allowing separation and quantification of damaged/intact pericytes in fixed tissue.

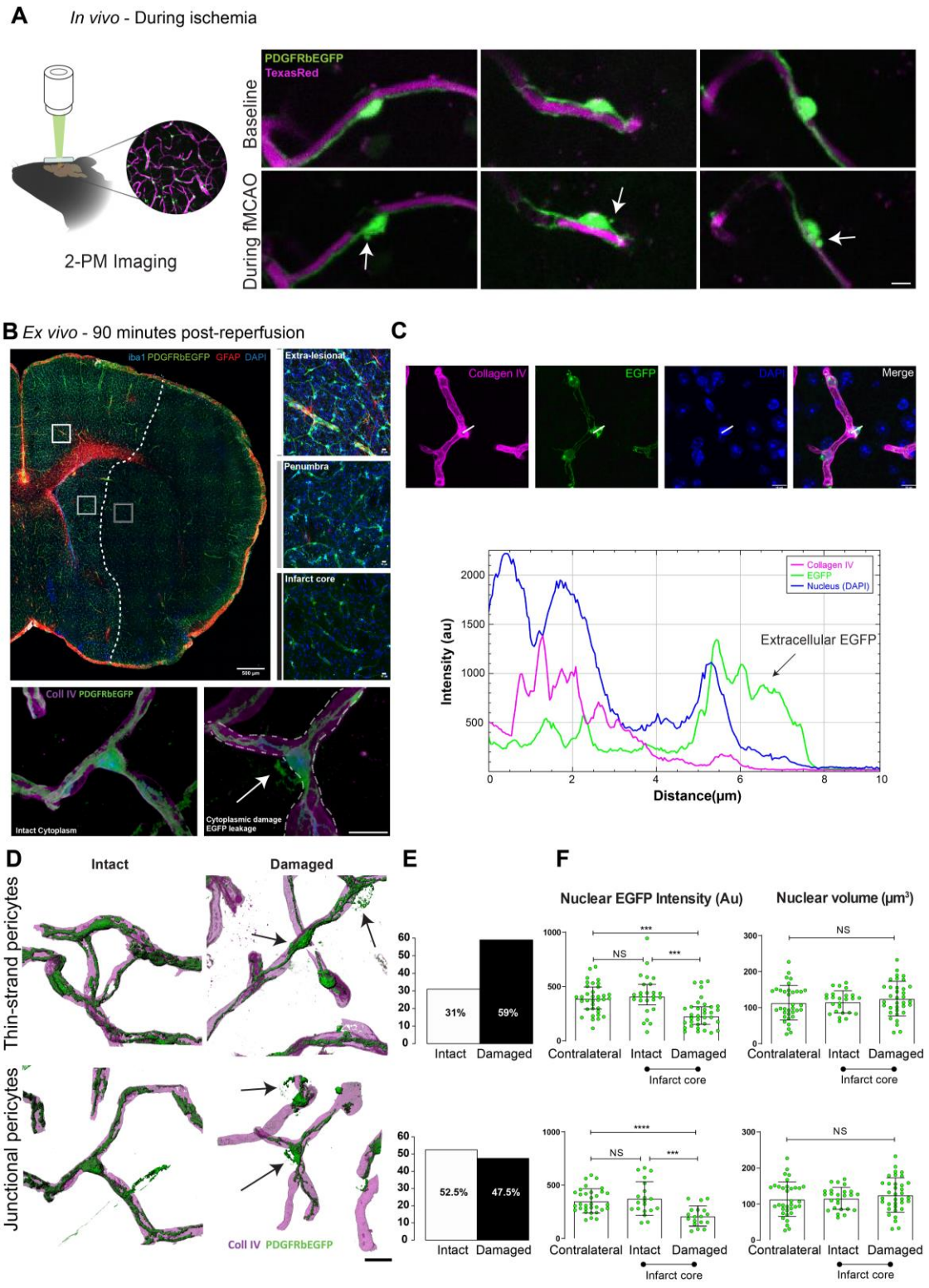

Fig. 22. Pericytes are damaged during ischemia and damage persists post reperfusion.

A) *In vivo* evidence of membrane blebs associated with membrane damage during ischemia. **B)** Upper, *Ex vivo* brain slice overview in PDGFRbEGFP mouse brain day 90 mins post reperfusion. Right, extra-lesional tissue staining with Iba1 (microglia) GFAP (astrocytes). Lower, divergence of intact and membrane damaged pericyte phenotype. **C)** Line profile measurement of EGFP leakage beyond the collagen IV^{+} basement membrane. **D)** 3D Imaris reconstruction of Intact and damaged pericytes. **E)** Percentage of intact vs damaged pericytes. **F)** Quantification of nuclear EGFP intensity in intact, damaged and contralateral pericytes 90 mins post reperfusion. *n=4 stroked PDGFRbEGFP mice, Statistics, after assessing normality of the data with Shapiro-Wilk test, Kruskall-Wallis test (F, Nuclear EGFP intensity) and unpaired two-tailed Student's t-test (F, lower) Scale bars, 10 µm, 500 µm, 10 µm. Data is shown as mean +/- SD, for F (Nuclear EGFP intensity) - Median with interquartile range.*

5.2.5 Pericyte survival after stroke is region dependent (Day 3 post stroke)

To interrogate the validity of previous findings (Fig.20, Fig.21, Fig.22) and develop an anatomical understanding of where pericyte survival was most prominent, four adult PDGFRbEGFP mice were stroked and sacrificed on day 3 and stained for markers for neurons, astrocytes and microglia (NeuN, GFAP/Aqp4/Iba1,Fig23.A). This experiment allowed comparison of how pericyte survival compared to other crucial cell types within the NVU. A qualitative assessment of neurons and astrocytes indicated that both cell types were eliminated from the infarct core, while pericytes and a small population of microglia remained visible (Fig.23.A).

Using a caudal-rostral analysis of PDGFRbEGFP mice stained with NeuN to label neurons, surviving pericytes could be visualised within the $NeuN^-$ infarct core (Fig.23.B left, right). Quantification of caudal-rostral sections from posterior MCA territory (Bregma -0.9/-1.2 mm), MCA territory (Bregma 0/1 mm) - anterior cortex (Bregma +2.5/2.71 mm) revealed a caudal-rostral axis dependency of pericyte survival within the $NeuN^-$ infarct core region. Pericyte loss was highest within the posterior stroked MCA territory, with a highly significant reduction in pericyte cell density of 56% ($p<0.008$, 63 pericytes/mm^2) relative to the contralateral pericyte density (152 pericytes/mm^2). Proximal to the stroked MCA territory, pericyte density was significantly reduced by 45% ($p<0.03$, 82 pericytes/mm^2) compared to the MCA territory of the contralateral hemisphere (150 pericytes/mm^2). Surprisingly, pericyte density in the anterior cortex infarct core was reduced by only 15% (102 pericytes/mm^2), leaving 85% of pericytes visible when compared against the contralateral hemisphere, this difference, was not significant (122 pericytes/mm^2) (Fig.23.B, lower panel quantification).

When comparing regional differences in pericyte loss between each stroked territory, it is crucial to take into account the relative pericyte densities in each section of brain tissue. Therefore, the pericyte density in the stroked hemisphere was calculated relative to the pericyte density in the same region in the contralateral hemisphere to generate a pericyte density reduction for the anterior cortex, MCA territory and posterior MCA territory respectively. We observed that pericyte survival in the anterior cortex was significantly higher than in the posterior MCA territory ($p<0.002$) and MCA territory ($p<0.02$). These results suggested that pericyte loss is highest in caudal sections of the brain where the main branch of the middle cerebral artery directly enters the brain and that pericyte survival increases as one examines the infarct along a caudal-rostral axis. Moreover, these data also suggested increased survival as the cortex becomes a larger proportion of the infarct relative to the striatum. To test this notion, we examined coronal sections taken from the MCA territory of PDGFRbEGFP mice on day 3 post stroke (Fig.23.D). Within the infarct core, the difference in remaining pericyte density was not significantly different in the striatum compared to the cortex (58% in the striatum compared with 69% in the cortex), while differences in pericyte density trended toward significance in the peri-infarct striatum and cortex respectively (60%, 80%) (Fig.23.D). Cumulatively, these data suggested that pericytes survive after ischemic stroke in a region dependent manner, and that pericyte death occurs most where the main branch of the middle cerebral artery directly enters the brain. Importantly, these data also hinted towards increased pericyte survival in the cortex of stroked animals.

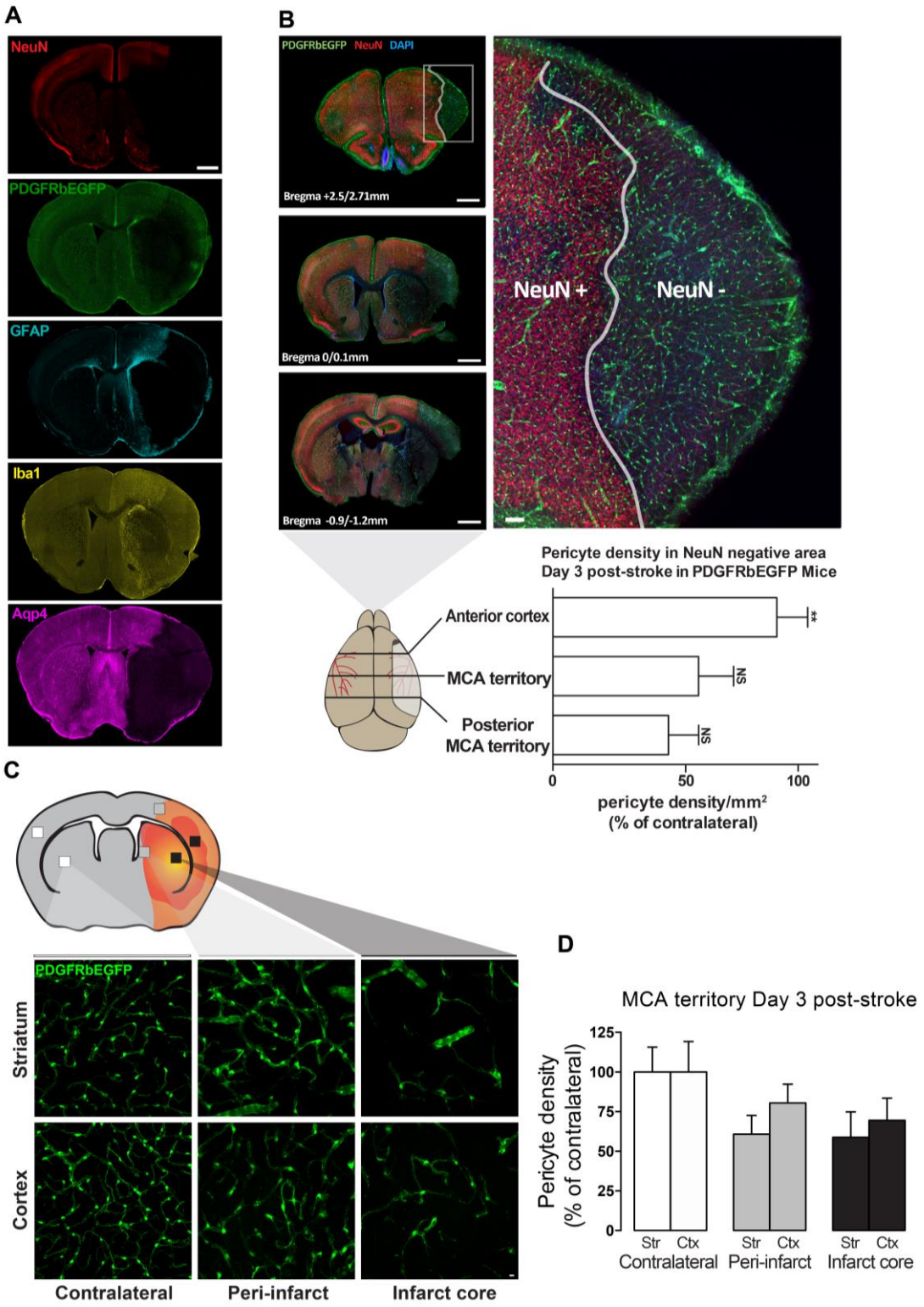

Fig. 23. Pericytes survive ischemic stroke in a region-dependent manner.

A) Confocal overviews of NeuN (Neurons) EGFP, Iba1 (Microglia) Aqp4 (Astrocyte end-feet) and GFAP (astrocytes) on day 3 post stroke. **B)** Caudal-rostral brain slice overviews of PDGFRbEGFP, NeuN and DAPI on day 3 post-stroke (left). Brain slice overview of the NeuN- infarct core (right). Quantification of pericyte density within the NeuN- area as a percentage of the contralateral hemisphere per mm2 (lower). **C)** Coronal view of PDGFRbEGFP pericyte survival from contralateral, peri-infarct and infarct core from left to right. **D)** Quantification of pericyte density in the MCA territory in striatum and cortex respectively compared as a percentage of contralateral pericyte density. *n=4 PDGFRbEGFP mice per quantification, Statistics, after confirming normality with Shapiro-Wilk test, unpaired two-tailed Student's t-test, scale bars, 1 mm, 50 µm, 1 mm, 10 µm from upper to lower. Data is shown as mean +/- SD.*

5.2.6 Surviving pericytes enter the cell cycle where pericyte density is reduced in the sub-acute phase (Day 3 post-stroke)

The experiments performed previously indicated that pericytes were not eliminated from the ischemic brain. In addition, the appearance of proliferation bodies between days 1 and 3 post stroke (Fig.21.D) implied that a population of pericytes may be responding to stroke in a compensatory capacity. To investigate this further, we injected four PDGFRbEGFP mice intraperitoneally with EdU 24 hours after stroke every 8 hours until sacrifice on day 3, to explore whether pericytes may incorporate this traceable nucleotide base into their DNA during DNA synthesis (Fig.24.A).

We observed that many cells in the ischemic brain incorporated EdU into their nuclei (Fig.24.B). Overall, 15% of all cells in the infarct core striatum and 8% of cells in the infarcted cortex were EdU^+, significantly more than in each region in the contralateral hemisphere (infarct core striatum-contralateral striatum $p<0.001$, infarct core cortex-contralateral cortex, $p<0.004$). In the peri-infarct striatum, 21% of all cells were EdU^+ in the striatum and 9.5% of all cells were EdU^+ in the cortex (peri-infarct striatum-contralateral striatum $p<0.0001$, peri-infarct cortex-contralateral cortex $p<0.02$). In the contralateral striatum and cortex, just 0.5% of all cells were EdU^+; indicating that stroke significantly induces EdU uptake in living cells between day 1 and day 3 post stroke in the ischemic territory.

Upon closer inspection of EdU^+ cell populations, we found that several EdU^+ nuclei were co-localised with $EGFP^+$ cells matching a pericyte morphology (Fig.24.C, D). Specifically, in areas where pericyte density was reduced by stroke, EdU^+ pericytes could be found (Fig.24.D). Pericyte density was significantly reduced in the infarct core striatum compared with contralateral striatum tissue ($p<0.01$) and in this region we found a significant increase in the amount of pericytes that were EdU^+ compared with pericytes in the contralateral striatum (15% of pericytes were EdU^+ in the infarcted striatum, compared with 0% in the contralateral striatum, $p<0.009$, Fig.24.E). In the infarcted cortex we found significantly more (8% of all pericytes) EdU^+ pericytes than when compared against 0% of EdU^+ pericytes found in the contralateral cortex, and in the infarcted cortex, pericyte density was significantly reduced compared against the contralateral pericyte density (pericyte density - $p<0.04$, difference in EdU^+ pericytes, $p<0.008$). In peri-infarct striatum where density was also significantly reduced (by 40% in the striatum, compared to contralateral striatum $p<0.007$) we also noted a 13% increase in the percentage of EdU^+ pericytes compared to the number of EdU^+ pericytes in the contralateral striatum, though this difference was not significant (Fig.24.E). In peri-infarct cortex tissue, where pericyte density was reduced by 20% compared to contralateral cortical pericyte density, we noted a 0.7% increase in the percentage of EdU^+ pericytes compared to the percentage of contralateral EdU^+ pericytes, where both the density reduction in pericytes and difference in EdU^+ pericyte count did not reach significance (Fig.24.E). Taken together, these results suggest that significant reductions in pericyte density caused by stroke, initiate significantly more cell cycle entry in a small population of pericytes within and around the infarcted tissue and that this occurs most prominently within the core of the infarcted tissue.

To validate these findings, we stroked a fresh cohort of PDGFRbEGFP mice and sacrificed them on day 3 post stroke for subsequent Ki67 staining (an established marker for cell cycle entry). Once again, we noted the appearance of $Ki67^+$ cells in the infarct core on day 3 post stroke (Fig.24.F). In detail, some of these $Ki67^+$ cells co-localised with $EGFP^+$ cells matching pericyte morphology (Fig.24.G). Upon quantification, we observed a significant 50% and 43% reduction in pericyte density in the infarct core striatum and cortex respectively ($p<0.00002$, $p<0.001$). Within the remaining population, 12% of pericytes in the infarct striatum were $Ki67^+$ and 15.9% of pericytes were $Ki67^+$ in the infarct cortex (significantly more than in each respective region in the

contralateral hemisphere, $p<0.04$, $p<0.01$). In peri-infarct tissue, striatal pericyte density was 65% of contralateral striatal pericyte density (significantly reduced, $p<0.0001$) and pericyte density was reduced 43% in the peri-infarct cortex (significantly reduced, $p<0.03$). Within these regions, 26% of pericytes were $Ki67^+$ in the striatum and 9.9% of pericytes were $Ki67^+$ in the peri-infarct cortex (significantly more than contralateral $Ki67^+$ pericytes in the striatum, $p<0.007$, but not in the cortex) (Fig.24.H). Taken together, these results provide evidence that pericytes respond to ischemic cell death within the population by entering the cell cycle, incorporating nucleotides for DNA synthesis and responding to pericyte network damage in a compensatory capacity in the sub-acute phase of stroke, particularly in sites where pericyte density is reduced.

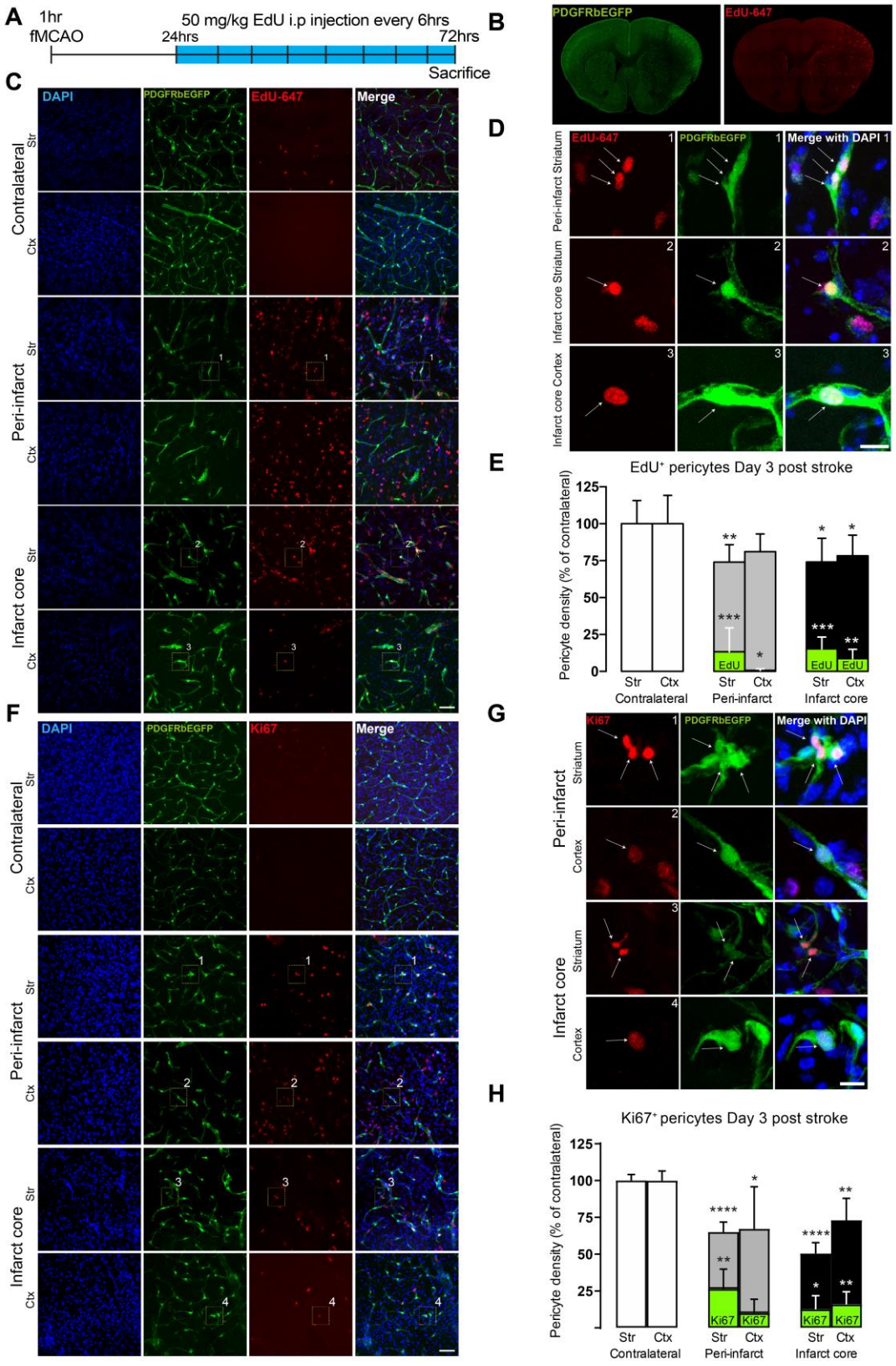

Fig. 24. Surviving pericytes enter the cell cycle on day 3 post stroke.

A) Schematic of EdU injection. **B)** Overviews of EdU$^+$ cells in PDGFRbEGFP mice day 3 post stroke. **C)** Region specific images of EGFP$^+$ cells stained with DAPI (blue) and EdU647 (red). **D)** Zoomed in view of region specific EdU647$^+$ pericytes. **E)** Quantification of pericyte density and percentage of EdU$^+$ pericytes on day 3 post stroke. **F)** Region specific images of EGFP$^+$ cells stained with DAPI (blue) and Ki67 (red). **G)** Zoomed in view of region specific EdU647$^+$ pericytes.**H)** Quantification of pericyte density and percentage of Ki67$^+$ pericytes on day 3 post stroke. *n=4 PDGFRbEGFP mice per quantification, Statistics, unpaired two-tailed Student's t-test, scale bars B= 1 mm, C, F=25 µm, D, G=10 µm. Data is shown as mean +/- SD.*

5.2.7 Establishment of FACS isolation of pericytes in stroked tissue

Cumulatively, these data indicate after an initial wave of pericyte death between day 1 and 3 post stroke, surviving pericytes begin to enter the cell cycle in areas where pericyte density is reduced. These data also suggested that pericytes may be activated by stroke, potentially responding to local reductions in pericyte density by replicating where the pericyte cell network is disrupted. Therefore, we reasoned that surviving pericytes in the infarct core might display a unique transcriptomic profile when compared against pericytes in the contralateral hemisphere - possibly providing further insights about their pathophysiological function. We formed a collaboration with the lab of Ozgun Gokce (group leader of the Gokce lab of Systems Neuroscience - Cell diversity) and worked together to adapt an existing protocol (Crouch and Doetsch, 2018) specifically for the isolation of pericytes from the adult mouse brain using endogenous reporters EGFP (under the control of the PDGFRb promoter) and DsRed (under control of the NG2 promoter). Together with Buket Bulut (from the Gokce lab) we isolated $EGFP^+$ and $DsRed^+$ cells from distinct brain regions in PDGFRbEGFPxNG2DsRed animals on day 3 post-stroke/sham for bulk transcriptomic sequencing. 6 - 12 week old male mice were operated in pairs (1 stroke and 1 sham) per FACS experiment to ensure equal comparison across repeated FACS isolation attempts.

After three days of either stroke or sham surgery mice were sacrificed via cervical dislocation, the brain was extracted and immediately placed on ice cold 2% FBS in 1XPBS solution in a petri-dish. Brains were transported from animal surgery to the laboratory and placed in a Perspex brain mold and kept consistently hydrated with 2% FBS in 1XPBS solution. Once in the brain mold, the cerebellum and olfactory bulbs were removed and the remaining tissue was dissected using a small dissection scalpel into three distinct regions: infarct core, ipsilateral hemisphere and contralateral hemisphere and placed in three separate petri dishes containing 3 ml of tissue collection solution (HBSS/BSA/glucose buffer) and 150 µl of DNAase stock solution at a concentration of 10 mg/ml. Next, brain tissue from each region was carefully dissociated mechanically by gently splitting the tissue up into pieces about 1 mm in size using micro-forceps and placed in a 15 ml falcon containing tissue collection solution. A crucial note at this point is that the density of tissue differs between the stroke core regions (stroke tissue is much less dense) and the other regions, care was taken to ensure that tissue pieces were of a similar size and viscosity when collected in the tissue collection solution (Fig.25.A). Each falcon tube containing the brain homogenate was then centrifuged at 300 g at 4°C for 5 minutes. During this time preparation for the enzymatic dissociation began by warming up collagenase/dispase solution (250 µl of collagenase/dispase 100 mg/ml stock solution in ultrapure dH_20 added to 7.5 ml of 2% FBS in 1XPBS) in at water bath at 37°C. Once centrifugation of tissue homogenate was complete, supernatant was discarded and 7.75 ml of collagenase/dispase solution was added and the homogenate was resuspended and incubated on a rotisserie device in at incubator at 37°C for 30 minutes. This process breaks down extracellular matrix components such as collagen IV and other basement membrane proteins to release mural cells into the tissue homogenate. Once complete, falcon tubes containing the cell homogenate were centrifuged at 300 g at 4°C to generate a pellet of cells from which the supernatant was decanted and the remaining cell pellet was resuspended in 1 ml of trituration solution (2% FBS in 1XPBS). Cell pellet was triturated carefully with p1000 pipettes, then p200 pipettes 100x respectively, to breakdown remaining tissue components into an individual cell solution; care was taken at this point to match the consistency of cell suspensions across the different regions of the stroked brain. The triturated cell solution was then centrifuged at 300 g for 5 minutes at 4°C, the supernatant was discarded and the pellet was resuspended in 1 ml of HBSS/BSA/Glucose buffer containing 40 µM of actinomycin (a chemical compound which inhibits mRNA synthesis) and filtered through a 40 µm cell strainer and split into three tubes. These tubes

were then centrifuged at 300 g for 5 mins at 4°C and the supernatant was discarded, the resultant pellet was resuspended in 1 ml of HBSS/BSA/Glucose buffer containing 40 µM actinomycin, and immediately placed on ice for further processing. Each region: infarct core, ipsilateral hemisphere and contralateral hemisphere cell solutions were split into three tubes respectively each containing 1 ml of cell suspension in HBSS/BSA/Glucose buffer. Here, we confirmed that $EGFP^+$ cells had survived the mechanical and enzymatic digestion procedure by placing the cell suspension on a microscope slide and staining the cells with NucRed647, a vital dye that labels living nuclei (Fig.25.B). Subsequently, the first tube in each sample was left unstained and was used to adjust gating strategies for EGFP and dsRed while the second tube was incubated with DAPI at a concentration of 1:500 on ice for 20 minutes. The final tube was left on ice as it represented the final cell populations to be sorted. After defining the gating strategy for EGFP and DsRed, the $DAPI^+$ sample was washed 3X in HBSS/BSA/Glucose buffer in a sequence of centrifugation and resuspension till no DAPI stain was left in the sample and processed through the cell sorter to define the gating strategy for $DAPI^-$ negative $EGFP^+$ and $DsRed^+$ cell populations. Finally, the third tube of each brain region: infarct core, ipsilateral hemisphere and contralateral hemisphere were used to sort cells for bulk sorting (50 cells in each well of a 96 well plate on a high yield setting) while single cells were sorted using an ultra-high purity setting into single wells of a 96 plate using the Sony SH800 cell sorter (Fig.25.C). This experiment was repeated 3X to generate 3 replicates of $NG2DsRed^+xPDGFRbEGFP^+$ cells from each region 3 days after stroke and 3 replicates of sham treated cells three days after surgery. In this way, the difference ischemia had on the transcriptome of $NG2DsRED^+xPDGFRbEGFP^+$ mural cells could be interrogated without the effect of surgery confounding the data set.

Prior to these experiments, validation experiments determining the signature of $EGFP^+$ cells and $DsRed^+$ cells was carried out in which C57BL/6 mice carrying neither fluorescent reporter were compared to $NG2DsRed^+xPDGFRbEGFP^+$ mice to define boundaries of fluorescence using the same isolation procedure (Fig.25.D).

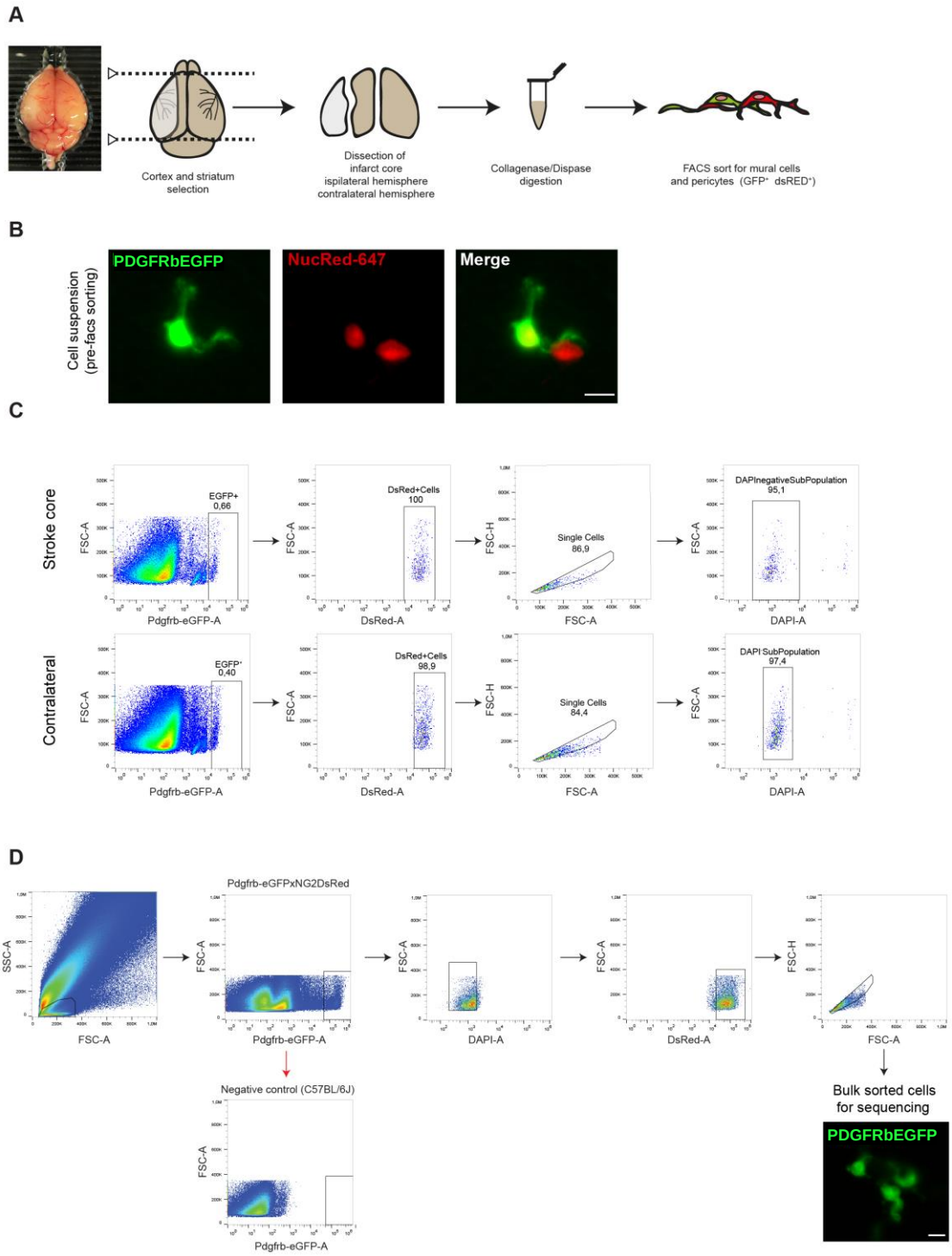

Fig. 25. FACS isolation of pericytes after stroke.

A) Workflow of pericyte isolation from cortical-striatal regions of mouse brain following fMCAo day 3 post stroke. **B)** EGFP positive mural cells (Left) stain positive for the vital dye NucRed-647 (Middle, Right) following enzymatic and mechanical dissociation. **C)** EGFP and DsRed+ cells are DAPI negative in both stroke core and contralateral hemisphere (95.1% and 97.4% respectively). **D)** Gating strategy for isolation of EGFP$^+$/DsRed+ pericytes for BulkSeq. *Scale bars, 10µm*

5.2.8 Pericytes in the ischemic brain show a unique, region dependent transcriptomic profile on day 3 post stroke

Because the promoters used for FACS isolation labels numerous types of mural cells (pericytes, fibroblasts, smooth muscle cells, oligodendrocytes) we first sought to verify the specificity of our isolation procedure by comparing our transcriptomic database against a panel of transcripts typically associated with various cell types within the brain (Fig.26.A, produced by Simon-Besson Girard). To do this, transcript counts were normalized across each sample isolated and arranged in a heat-map corresponding to log fold enrichment. We found little to no expression of transcripts associated with the following cell types: microglia, neurons, neural stem cells (NSCs), oligodendrocytes, oligodendrocyte precursors (OPCs). A small percentage of transcripts overlapped with astrocytes and vascular associated transcripts; however, the majority of the significantly enriched transcripts were associated with pericytes (Fig.26.A). Transcripts used to identify the pericyte signature were taken from a study performed in 2016 which analyzed the mural transcriptome for the first time (He et al., 2016). In this study, the authors validated their results using single cell fluorescent in-situ hybridization techniques ultimately finding the following combination of gene expression unique to pericytes: Acta2, Kcnj8, pdgfrb, cd248, Anpep, Des, Dlk1, Zic1, Abcc9, Rgs5, and Cspg4.

Our transcriptomic pericyte signature (Fig.26.B, produced by Simon-Besson Girard) shows high expression of 7 out of 11 transcripts listed by the previous study: Acta2, Kcnj8, pdgfrb, Cd248, Abcc9, Rgs5 and Cspg4. Interestingly, we found low expression of a typically specific reporter of pericytes CD13 (Anpep), in addition, we saw little to no expression of Dlk1, Zic1 and Desmin (Des). Importantly however, Cspg4 (NG2) and pdgfrb were controlling expression of DsRed and EGFP respectively, validating our gating strategy specificity. These data strongly suggest that the pericyte component of mural cells is enriched within our dataset. Therefore, we attempted to grade the quality of each sample using a ‘periscore’, which relates each sample isolated to the relative expression of the pericyte specific gene list (Fig.26.C). We found that each sample isolated was highly enriched (Log fold enrichment > 3 or greater) for pericyte associated transcripts and using dimensionality reduction, we showed that many of the samples remain transcriptomically distinct, while retaining the presence of a common pericyte signature (Fig.26.C).

Using principal component analysis on 2000 of the most variable genes, we found that each set of samples isolated from each brain region: infarct core, ipsilateral hemisphere and contralateral hemisphere was transcriptomically distinct in the brain 3 days after stroke. Samples from the infarct core, clustered with samples from the ipsilateral hemisphere, whereas samples from the contralateral hemisphere clustered with samples isolated from the ipsilateral hemisphere of sham operated animals (Fig.26.D).

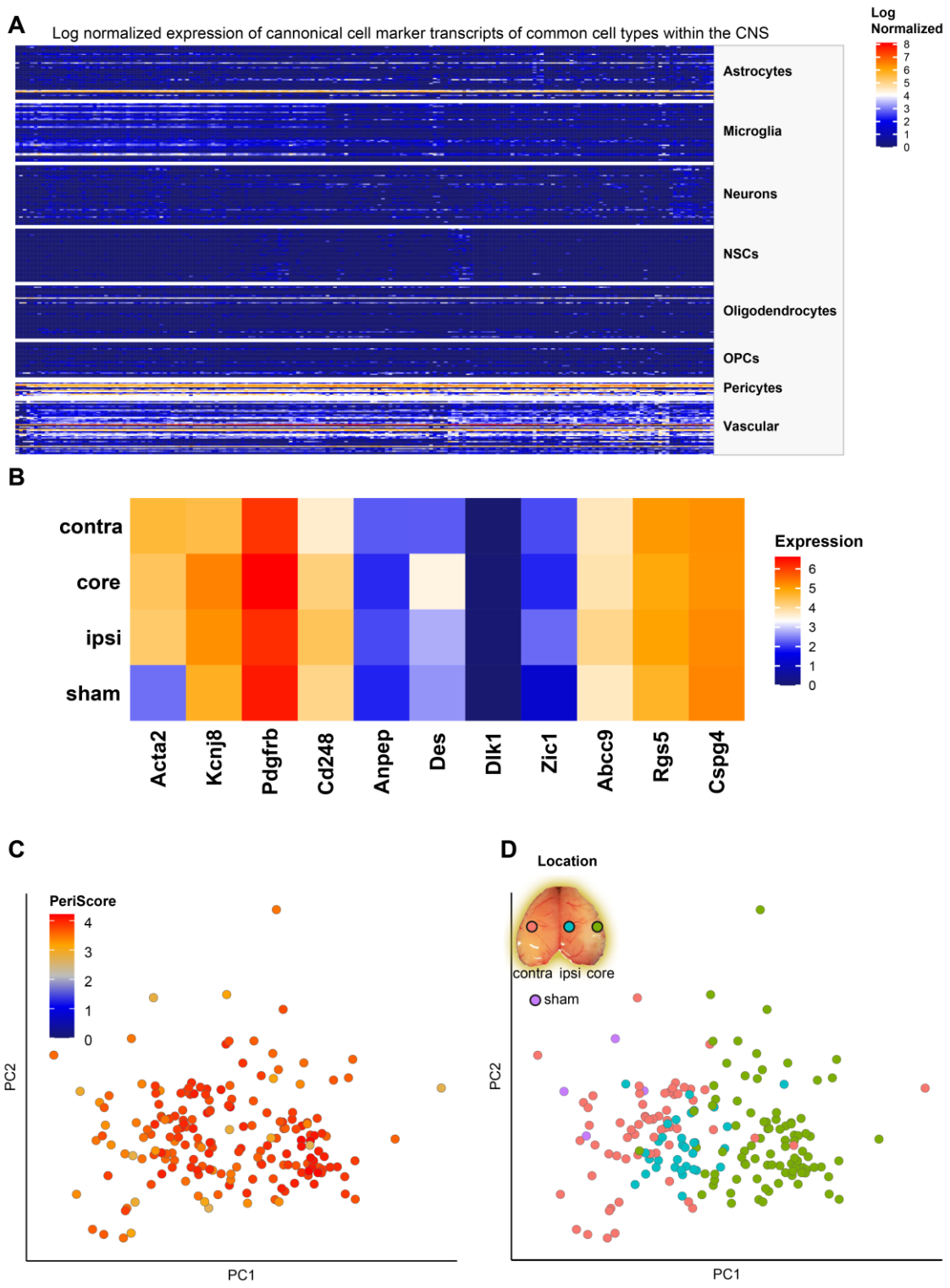

Fig. 26. Pericytes upregulate distinct transcriptomic profiles in response to stroke.

A) Transcriptomic heat-map of genes associated with each cell type within the NVU. **B)** Specific regional expression variances in genes associated with the pericyte signature. **C)** Principal component analysis of all samples sequenced within the brain and their relative expression of pericyte associated genes listen in B. **D)** Principal component analysis of samples from each section of the brain, contra (red), ipsi (blue) core (green) sham (purple). Samples from each brain region cluster together, meaning samples from each isolated brain region are transcriptomically distinct. *n = 3 PDGFRbEGFP mice day 3 post stroke, 2 PDGFRbEGFP sham mice, PCA based on 2000 genes per sample.*

We detected enrichment of 259 genes in samples isolated from the infarct core, while 75 genes were found depleted. 50 genes were found to be enriched in the contra, while 179 were found to be depleted. 1 gene was found enriched in the ipsilateral samples and 1 gene was found to be depleted. Together, this transcript variance explains each samples position along the principal component analysis.

5.2.9 Protein level qualitative validation of the bulk transcriptomic gene enrichment in the infarct core pericyte gene set

To validate bulk RNA sequencing of the pericyte population at the protein level and confirm our sequencing has intrinsic value in deciphering pathophysiological function of pericytes, we first sought to visualise the largest contributors to each principal component analyses (Fig.27.A). Briefly, these genes are significantly differentially regulated between infarct core samples and ipsilateral, contralateral and sham samples ($p<0.05$) – meaning they are either significantly enriched or depleted in the infarct core relative to other genes.

These differentially enriched genes were loaded into string database (Jensen et al., 2009) (Fig.27.B) where initial gene ontology analysis suggested many pathways were altered in pericytes in the infarct core compared to pericytes in other isolated brain regions. Among these altered pathways, we focused in on proteins involved in cell-cell interaction and identified galectin 1 (Lgals1), a gene with a log 2 fold enrichment of 893 within in the infarct core compared to other regions (adjusted p value <9.44E-19) and performed immunofluorescence staining with an anti-galectin1 antibody. We found galectin1 (a protein involved in apoptosis regulation and a regulator of cell proliferation) to be highly expressed within the infarct core on day 3 post stroke and specifically localised its expression to cells in the infarct core, including pericytes (Fig.27.C). These qualitative data suggest that transcriptomic changes within our bulk sequencing may indeed reflect important changes within the ischemic pericyte population at the protein level.

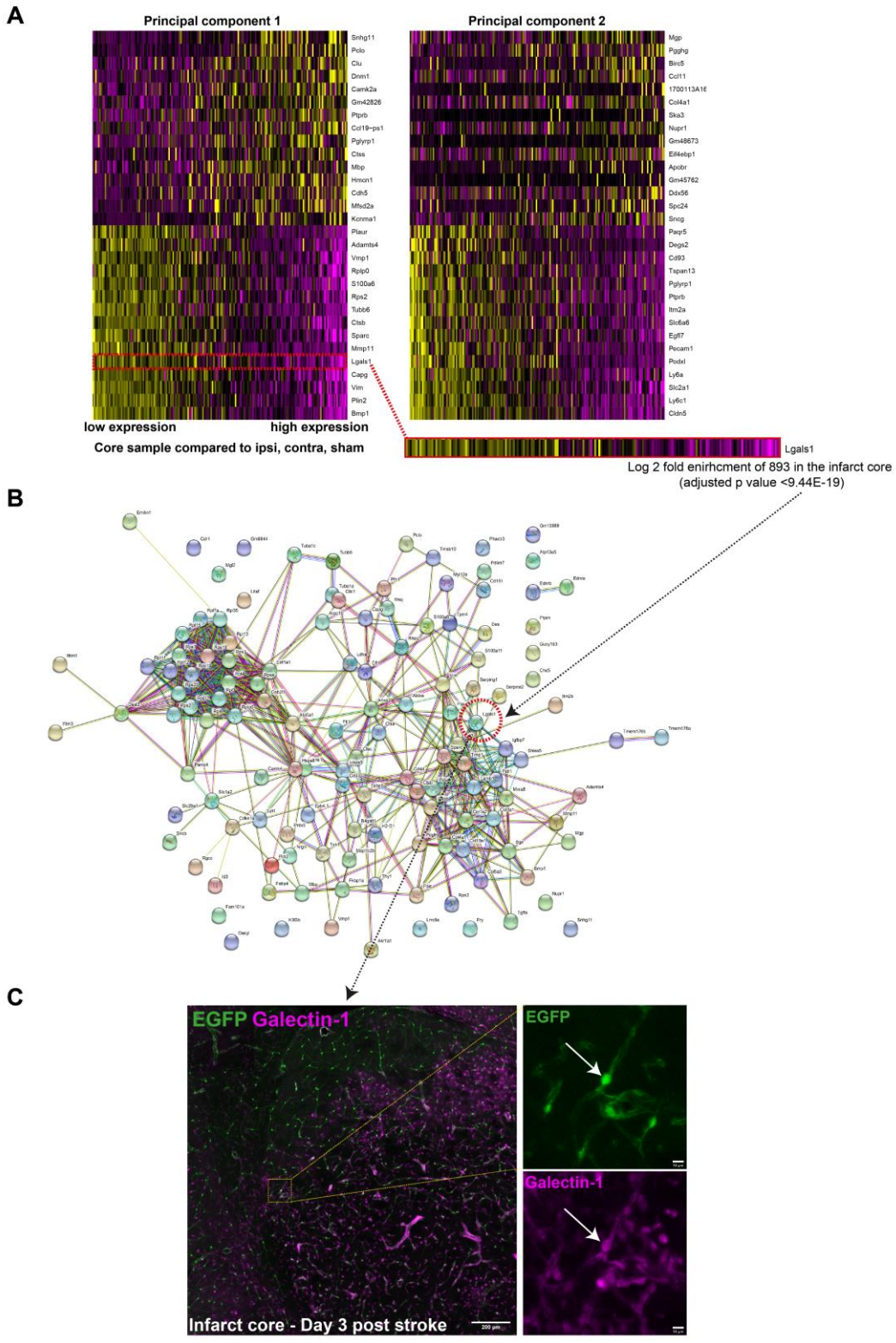

Fig. 27. Transcriptomic sequencing of pericytes provides identification of novel transcripts upregulated after stroke expressed at the protein level.

A) PC1 loadings, these genes contribute most to the variance between core samples and other samples (ipsi, contra, sham) PC2 loadings explain the resulting variance not explained by PC1. Galectin-1 is upregulated in core samples 893 fold. **B)** String database analysis of upregulated transcripts in the core relative to other samples. The top left cluster is associated with ribosomal synthesis, the bottom left cluster is associated with extracellular matrix reorganization. **C)** Immunofluorescence staining of galectin-1 (magenta) in the infarct core of a PDGFRbEGFP mouse on day 3 post stroke (left). Galectin-1 expression co-localizes with a PDGFRbEGFP^{+} pericyte (right). *Scale bars, 200 µm, 10 µm respectively.*

5.2.10 Gene ontology enrichment analysis suggests an active, remodelling and proliferative state of surviving pericytes within stroked tissue

Knowing our transcriptomic sequencing can at least partially reflect changes at the protein level, we returned to the principal component analysis on the top 2000 most variable genes. Using this form of dimensionality reduction, each gene is weighted based on how much they contribute to the variability of the dataset. In our case, PC1 explained 4.4% of the variability in our dataset, PC2 explained 1.8% and PC3 explained 1.4% of the variation. This indicates that relatively few genes from our initial analysis of 2000 contribute to the major differences between samples (core, ipsi, sham and contra). Therefore, we selected the top 100 genes and bottom 100 genes from PC 1 and 2 (Fig.27.A) and ran a gene ontology analysis to better understand pathways which are significantly altered within the transcriptome of pericytes in each brain region (Fig.28A). We found that PC1 negative loadings (lower left quadrant Fig.28.A) were primarily associated with a group of transcripts encoding for an alteration towards an endothelial cell differentiated transcriptome (-log10p6.247) while PC1 positive loadings appeared to show that samples in the core (Fig.28.A lower right quadrant) were upregulating transcripts associated with extracellular matrix reorganisation (-log10p16.74). PC2 positive loadings showed primarily contralateral and sham samples heavily skewed toward transcriptional pathways encoding for transcripts associated with blood vessel morphogenesis (-log10p-15). Interestingly, PC2 negative loadings showed contra, ipsi and core samples primarily associated with cell division (-log10p-6.5). While these altered transcriptomic pathways require further investigation, this last gene ontology analysis particularly piqued our interest because of previous findings related to cell cycle entry and proliferation (Fig.21, 24).

Therefore, Simon-Besson Girard (from the Systems Neuroscience - Cell diversity group) ran our sequencing data through the Seurat cell cycle vignette script (an R package for transcriptomic analysis). This script searches for genes associated with two distinct phases with the cell cycle, G2/M phase and S phase. Those samples with a low relative expression of both of these cell cycle phases remain associated with G1 phase (Interphase).

G2/M genes	S genes
Hmgb2,Cdk1,Nusap1,Ube2c,Birc5,Tpx2,Top2a,Ndc80,Cks2,Nuf2,Cks1b,Mki67,Tmpo,Cenpf,Tacc3,Fam64a,Smc4,Ccnb2,Ckap2l,Ckap2,Aurkb,Bub1,Kif11,Anp32e,Tubb4b,Gtse1,Kif20b,Hjurp,Cdca3,Hn1,Cdc20,Ttk,Cdc25c,Kif2c,Rangap1,Ncapd2,Dlgap5,Cdca2,Cdca8,Ect2,Kif23,Hmmr,Aurka,Psrc1,Anln,Lbr,Ckap5,Cenpe,Ctcf,Nek2,G2e3,Gas2l3,Cbx5,Cenpa	Mcm5,Pcna,Tyms,Fen1,Mcm2,Mcm4,Rrm1,Ung,Gins2,Mcm6,Cdca7,Dtl,Prim1,Uhrf1,Mlf1ip,Hells,Rfc2,Rpa2,Nasp,Rad51ap1,Gmnn,Wdr76,Slbp,Ccne2,Ubr7,Pold3,Msh2,Atad2,Rad51,Rrm2,Cdc45,Cdc6,Exo1,Tipin,Dscc1,Blm,Casp8ap2,Usp1,Clspn,Pola1,Chaf1b,Brip1,E2f8

Table 13: Genes of interest.

Surprisingly, we found that a large number of our transcriptomic samples were associated with cell cycle entry in the ischemic brain on day 3 post stroke. 100% of sham samples had little to no expression of the cell cycle genes listed in the table above and as a result, all pericytes were scored into G1 (interphase). In the ischemic brain, 20% of contralateral samples showed an upregulation of transcripts associated with S-phase of the cell cycle (upregulation of genes in the right box of table 13) while the rest of the samples remained associated with interphase. In the ipsilateral hemisphere 20% of samples showed an upregulation of transcripts associated with S-phase, 10% of samples showed an association to G2/M phase (left box of table 13) and 70% remained associated with interphase. Within the ischemic core however, 70% of samples appeared to be upregulating genes associated with the cell cycle. 40% of samples were upregulating transcripts associated with S-phase of the cell cycle and a further 30% of samples were found to be upregulating transcripts associated with G2/M phase of the cell cycle (Fig.28.C). Cumulatively, this suggests a gradient of cell cycle activation in the brains of stroked animals, which curiously, also occurs in the contralateral hemisphere. Samples moving toward the infarct show an upregulation of transcripts associated with cell division (G2/M phase) suggesting that pericytes in the infarct core may be pushed toward entering the cell cycle and thus upregulate transcripts associated with proteins associated with mitosis. Crucially, these results provide transcriptional evidence for the protein level evidence displayed in figure 24, and may explain many of the core upregulated pathways making the ischemic pericyte transcriptome distinct from sham samples. Together, these results suggest pericytes are responding to stroke with the purpose of reconstituting the pericyte population lost, and remodeling the extracellular matrix and associated vasculature early after stroke.

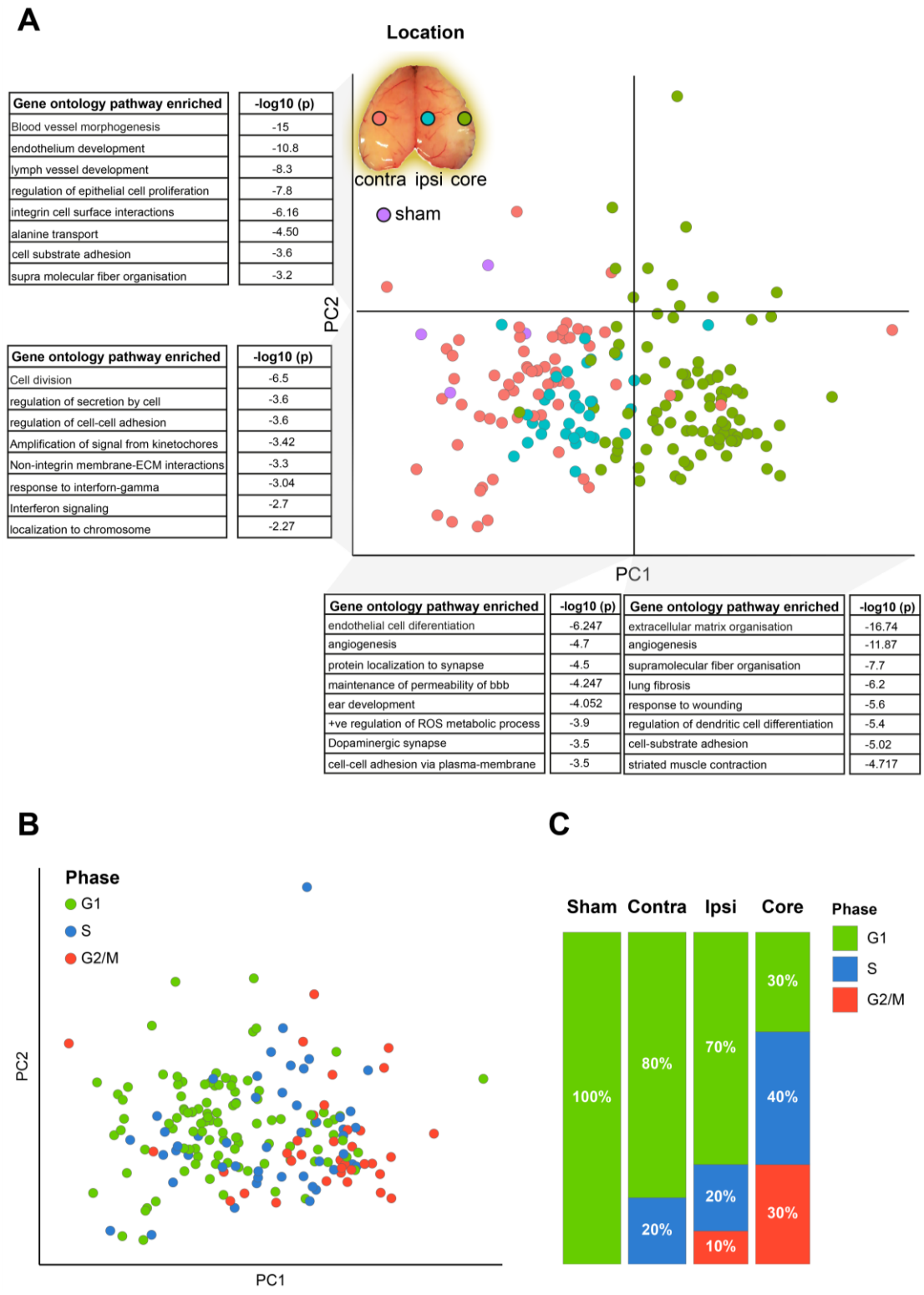

Fig. 28. Pericytes activated by stroke engage in extracellular matrix reorganization and enter the cell cycle.

A) PC analysis broken down through gene ontology. Each quadrant displays specific gene ontological pathways that discriminate samples from each other. PC1+ve is associated with ECM organization while PC1-ve is associated with endothelial cell differentiation, PC2+ve is associated with blood vessel morphogenesis while PC2-ve is associated with cell division. **B)** Seurat's cell cycle vignette applied to the PCA, which determines transcriptional uniqueness among samples isolated from each region of the stroked brain. Core samples are preferentially associated with cell cycle entry, while sham is preferentially associated with interphase pericytes. Contra and ipsi samples show a mild level of cell cycle entry compared to core. **C)** Bar graph of percentage cell cycle associated genes per brain region. *n=3 NG2dsRedxPDGFRbEGFP stroke mice, 2 NG2dsRedxPDGFRbEGFP sham mice.*

5.3 *In vivo* characterisation of pericyte cell fate and blood flow regulation

The previous *ex vivo* findings indicate that a population of pericytes can survive the initial phase of ischemic stroke in a region dependent manner. Put simply, these findings informed us that imaging pericytes in the living brain under conditions of stroke might be possible. Therefore, we aimed to decipher how pericytes regulate blood flow under conditions of ischemia by designing a chronic multi-modal *in vivo* imaging experiment (detailed in methods section 4.3) to address at both mesoscale level (laser speckle) and single cell level (longitudinal 2-photon microscopy imaging), *if* pericytes possess the capacity to constrict the microvasculature during and after stroke.

5.3.1 Laser speckle can detect fMCAo induction and reveals a biphasic blood flow variation post-stroke/sham surgery

Confirmation of stroke induction for this experiment would normally be achieved by attaching a laser Doppler probe (LDF) to the skull proximal to the distal branch of the MCA. However, placement of a chronic cranial window to image pericytes in the somatosensory cortex of the left hemisphere takes prohibits measurement of blood flow reduction using conventional methods; therefore, we validated stroke induction and blood flow alterations for one week post stroke/sham using a laser speckle device placed above the cranial window.

At baseline, pial blood flow appears red (Fig.29.A) while parenchymal flow is typically yellow. During stroke surgery as the filament was inserted, both pial flow and parenchymal flow appear heavily reduced (Fig.29.A,C) while mild reductions in flow are seen during sham surgery. We grouped each MCA territory measurement and separated regions by stroke or sham and noted a highly significant decrease in blood flow in the MCA territory during fMCAo compared with sham surgery induction (sham - stroke, $p<0.000001$). 90 minutes after reperfusion of the occluded artery we observed a highly significant reduction in blood flow within the stroke group compared to 90 mins after sham surgery (sham - stroke, $p<0.000001$). 24 hours post sham/stroke a significant difference in blood flow between groups was not observed. In the sub-acute phase, differences in blood flow between stroke and sham animals showed a strong trend toward significant reductions in blood flow in the stroke group, but did not reach significance while on day 7, stroke animals had a significant reduction in upper cortical bloodflow compared to sham animals ($p<0.002$). To further confirm infarction of the cortex and striatum had taken place in a manner resembling typical fMCAo, we stained fixed brain tissue from animals sacrificed after the last imaging time-point on day 7 with NeuN, a marker labelling neurons. We observed the loss of neurons along a caudal-rostral axis within the infarct core of the ipsilateral hemisphere in all 6 stroke animals which survived till day 7 (Fig.29.D). To further validate stroke induction produced infarction in the *in vivo* imaging cohort, we performed MR imaging on the fixed brain tissue prior to serial sectioning at the vibratome (performed by Antonia When). We observed no infarction in all four sham animals, while all six surviving stroke animals produced an average lesion volume of 36 mm^3 (Fig.29.E). Taken together, these qualitative data of infarction and quantitative data of stroke size and blood flow alterations indicated that transient ischemic stroke was correctly induced in these animals and that as a result, blood flow was persistently altered within the ischemic cortex in a biphasic manner. This suggested that the 2-photon imaging data set would provide valuable insight about how ischemic pericytes respond to stroke in the ischemic brain.

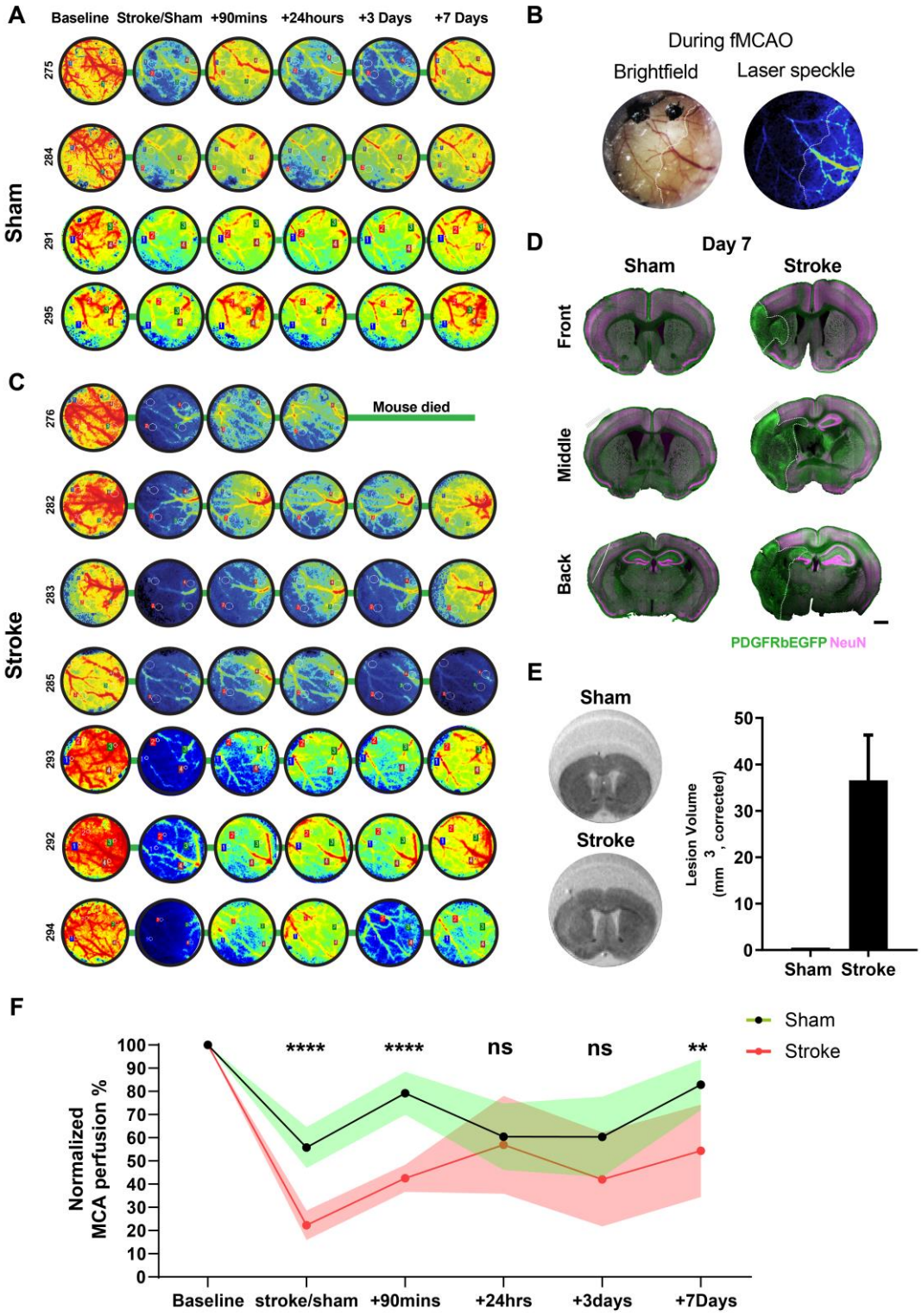

Fig. 29. Laser speckle assessment of blood flow reveals a bi-phasic reduction post stroke.

A) Raw laser speckle fluxmetry of the sham animal cranial windows over the course of the experimental timeline. High and moderate levels of flow are represented as red and yellow respectively, while low flow is represented in green and blue. **B)** Bright-field microscopy view of the cranial window of an animal experiencing stroke, perfused areas are a pink red color, while non-perfused tissue is white (upper). **C)** Laser speckle flow during fMCAo, white line indicates the MCA territory occluded by the filament (left) while to the right of the white line, flow is partially maintained within the ACA territory. **D)** Caudal-Rostral axis qualitative immunostaining of neurons (NeuN, magenta) and PDGFRbEGFP (green) in sham and stroke animals respectively, gray bars indicate approximate location of cranial window. **E)** Lesion volume on day 7 post-stroke/sham measured in fixed brains using MR imaging. **F)** Quantification of normalized laser speckle values in stroke and sham groups over the experimental time course. *n=7 stroke mice, 4 sham mice. Statistics, after confirming normality (Shapiro-Wilk test), two-way ANOVA with greenhouse-geisser correction, individual time points, unpaired Welch's t-test. Scale bar, 1mm. Data is shown as mean +/- SD.*

5.3.2 Identification of pericyte sub-types and their baseline vessel characteristics

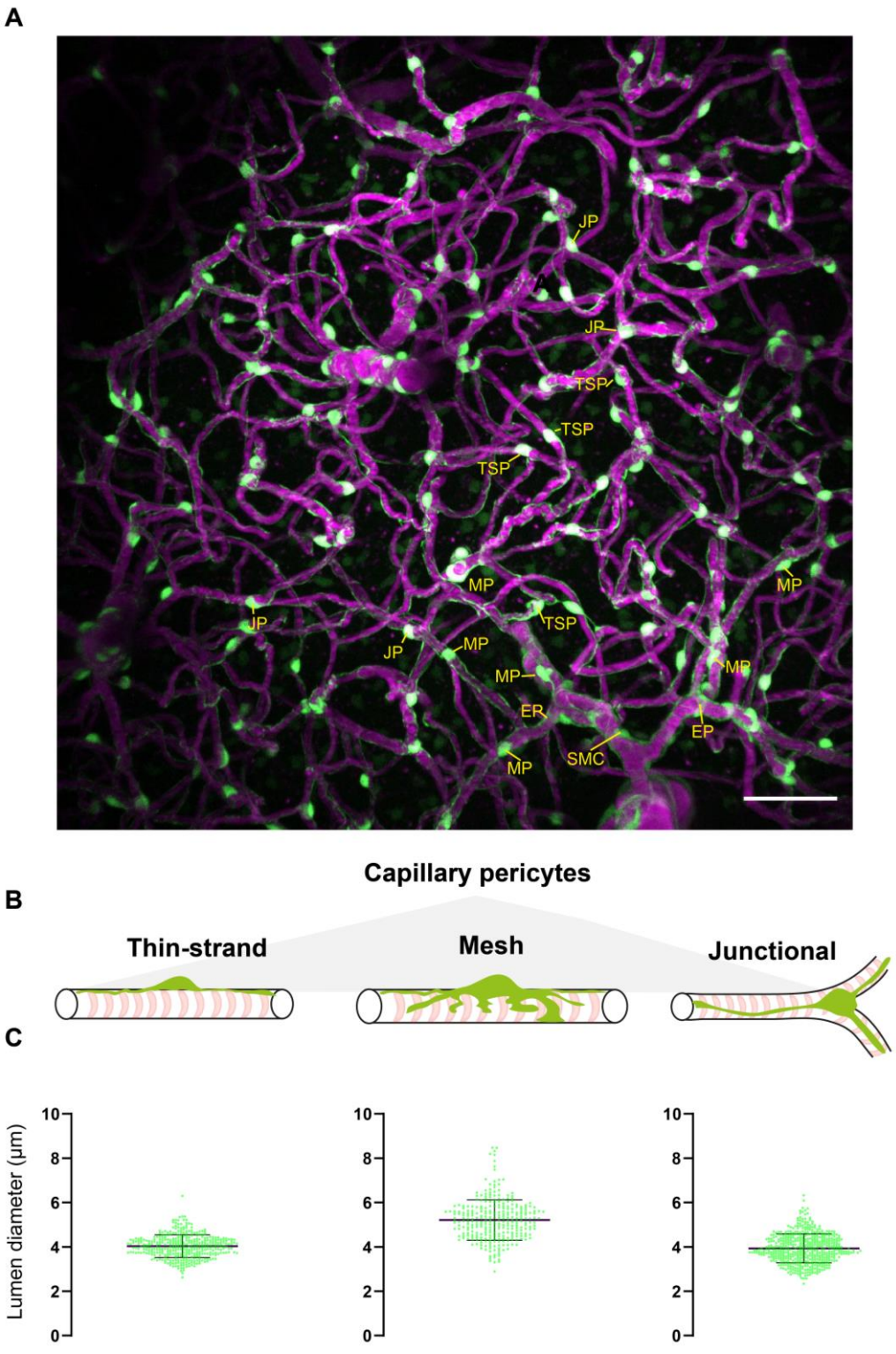

Fig. 30. Identification of pericyte sub-types and associated baseline diameters.

A) A typical capillary bed splayed out covering a region of interest perfused by a penetrating arteriole used for *in vivo* analysis. Yellow text identifies pericyte sub-types emanating from the penetrating arteriole, MP-mesh, JP-Junctional, TSP-Thin-strand pericytes; SMC and EP represent smooth muscle cells and ensheathing pericytes. **B)** Schematic of morphological features of pericyte sub-types analyzed. **C)** Mean average vessel lumen diameter measured at each pericyte sub-type soma. *n=11 PDGFRbEGFP mice. Scale bars, 50 µm. Data is shown as mean +/- SD.*

5.3.3 Ischemia constricts all cortical pericyte sub-types *in vivo* and pericytes remain constricted acutely after reperfusion

By selecting capillary beds emanating from penetrating arterioles (Fig.30.A) unobstructed by large pial vessels, we imaged pericytes up to 250 µm deep in the somatosensory cortex to record a baseline diameter of the vessel lumen at the pericyte soma and further classify and number pericytes into their respective sub-types (Fig.30.A, B, C). Using the vascular territory affected during stroke to select two ischemic regions of interest out of four regions of interest previously imaged at baseline, we then quantified variances in vessel lumen diameter at pericyte soma during and after stroke/sham surgery (Fig.31.B).

We found that during stroke, 87% of all vessel lumen diameters at pericyte soma (thin-strand, mesh, junctional) constricted heavily relative to baseline compared to vessel lumen diameters at pericyte soma sub-types during sham surgery (Fig.31.C).

When comparing the mean of constriction amongst vessel lumen diameters associated with each pericyte sub-type, we found that the lumen diameters associated with thin-strand pericyte soma constricted significantly more than vessel lumen diameters proximal to mesh or junctional pericytes (Fig.31.D). Vessel lumen diameters associated with thin-strand pericytes constricted by an average of 25% after stroke compared to an average constriction at vessel lumen diameters associated with mesh and junctional pericytes of 20% and 21% respectively (thin-strand-junctional, $p<0.0001$, thin-strand-mesh, $p<0.0005$).

When comparing stroke and sham, vessel lumen diameters associated thin-strand pericytes constricted by an average of 25% during stroke compared to an average of 2.5% during sham surgery ($p<0.000001$) and remained constricted by an average of 10% 90 mins post reperfusion of the occluded artery compared to an average dilation of 3% 90 mins post-sham ($p<0.000001$). These findings in vessel lumen diameters associated with thin-strand pericytes mimic those of the junctional pericyte population, where vessel lumen diameters constricted by an average of 20% during stroke compared to sham, where vessel lumen diameters associated with junctional pericytes constricted by 5% on average ($p<0.000001$). 90 mins after reperfusion of the occluded artery in the stroke group, vessel lumen diameters associated with junctional pericytes were constricted by an average of 9% in the stroke group whereas 90 mins post sham surgery, vessel lumen diameters associated with junctional pericytes were constricted by less than 1% ($p<0.000001$). Moreover, vessel lumen diameters associated with mesh pericytes constricted significantly during stroke by an average of 21.3% compared to an average during sham surgery of 2.7% ($p<0.000001$). 90 mins after reperfusion of the artery, vessel lumen diameters associated with mesh pericytes were constricted by an average of 11.2% which reached significance compared to vessel lumen diameters associated with mesh pericytes in the sham group which were constricted by less than 1% ($p<0.000001$)(Fig.31.E).

These findings are likely a reflection of the how the whole pericyte subtype population responds. To that end, we separated vessel lumen diameters associated with each pericyte sub-type into constricting (>5% constriction relative to baseline) dilating (>5% dilated relative to baseline) or baseline diameter (within 95% - 105% of baseline diameter) (Fig.31.F). We found that during stroke 92% of lumen diameters associated with thin-strand pericytes were constricted, while 48.5% of lumen diameters associated with thin-strand pericytes during sham surgery were constricted.

Less than 1% of vessel lumen diameters at thin-strand pericyte soma were dilating during stroke while 7% remained at baseline. During sham surgery however, 21% of vessel lumen diameters associated with thin-strand pericytes were dilated relative to baseline and 29% remained within a baseline threshold. 90 mins post reperfusion of the occluded artery 69% of vessel lumen diameters associated with thin-strand pericyte soma remained constricted, while 11.9% dilated; leaving 19% of vessel lumen diameters associated with thin-strand pericyte soma remaining within baseline levels. Conversely, 90 mins after sham surgery, 24% of vessel lumen diameters associated with thin-strand pericytes remained constricted while 38% of vessel lumen diameters dilated, 36% of vessel diameters associated with thin-strand pericyte soma 90 mins after sham surgery remained within baseline levels.

In line with results concerning thin-strand pericytes, 86% of vessel lumen diameters associated with mesh pericytes constricted during stroke, while 43% of vessel lumen diameters associated with mesh pericytes constricted during sham surgery. Only 3% of vessel lumen diameters associated with mesh pericytes dilated during stroke, while 10% remained within baseline diameter measurement levels. Furthermore, 16% of vessel lumen diameters proximal to mesh pericytes were dilated during sham surgery while 39% remained at baseline levels. 90 mins after reperfusion in the stroke group 71% of vessel diameters associated with mesh pericytes remained constricted, leaving 5.6% dilated and a further 23.4% returning to baseline levels. 90 mins after sham surgery, 33% of vessel lumen diameters associated with mesh pericytes constricted, while 17.5% dilated and 49.5% were found at baseline levels.

Vessel lumen diameters associated with junctional pericytes showed the same pattern, 85% of vessel lumen diameters associated with junctional pericytes were constricted during stroke while 3.7% were dilated leaving 11.3% unchanged from baseline. During sham surgery, 52.8% of vessel diameters associated with junctional pericytes constricted while 16.4% were dilated leaving 30.82% unchanged from baseline levels. 90 mins after reperfusion of the occluded artery, 66% of vessel lumen diameters associated with mesh pericytes remained constricted, while 11% were dilated and 22.6% returned to baseline levels. 90 mins after sham surgery, 36.7% of vessels associated with mesh pericytes were constricted, while 29.1% were dilated, 34.2% of vessels associated with mesh pericytes remained at baseline diameter levels.

Taken together, these results demonstrate that the majority of the pericyte population constricts in response to ischemia *in vivo*, that thin-strand pericytes are particularly affected by ischemia and that constriction persists for at least 90 minutes post reperfusion of the occluded artery in the majority of the pericyte population – *strongly* implicating pericyte constriction as a contributor to ‘no-reflow’ phenomenon.

From this point on, having established that pericytes convey a strong influence on vessel diameter, we collapse the phrase ‘vessel lumen diameters associated with mesh, junctional or thin-strand pericytes’ to simply mesh, junctional or thin-strand pericyte constriction/dilation to describe the effects they exert on vessel lumen diameter.

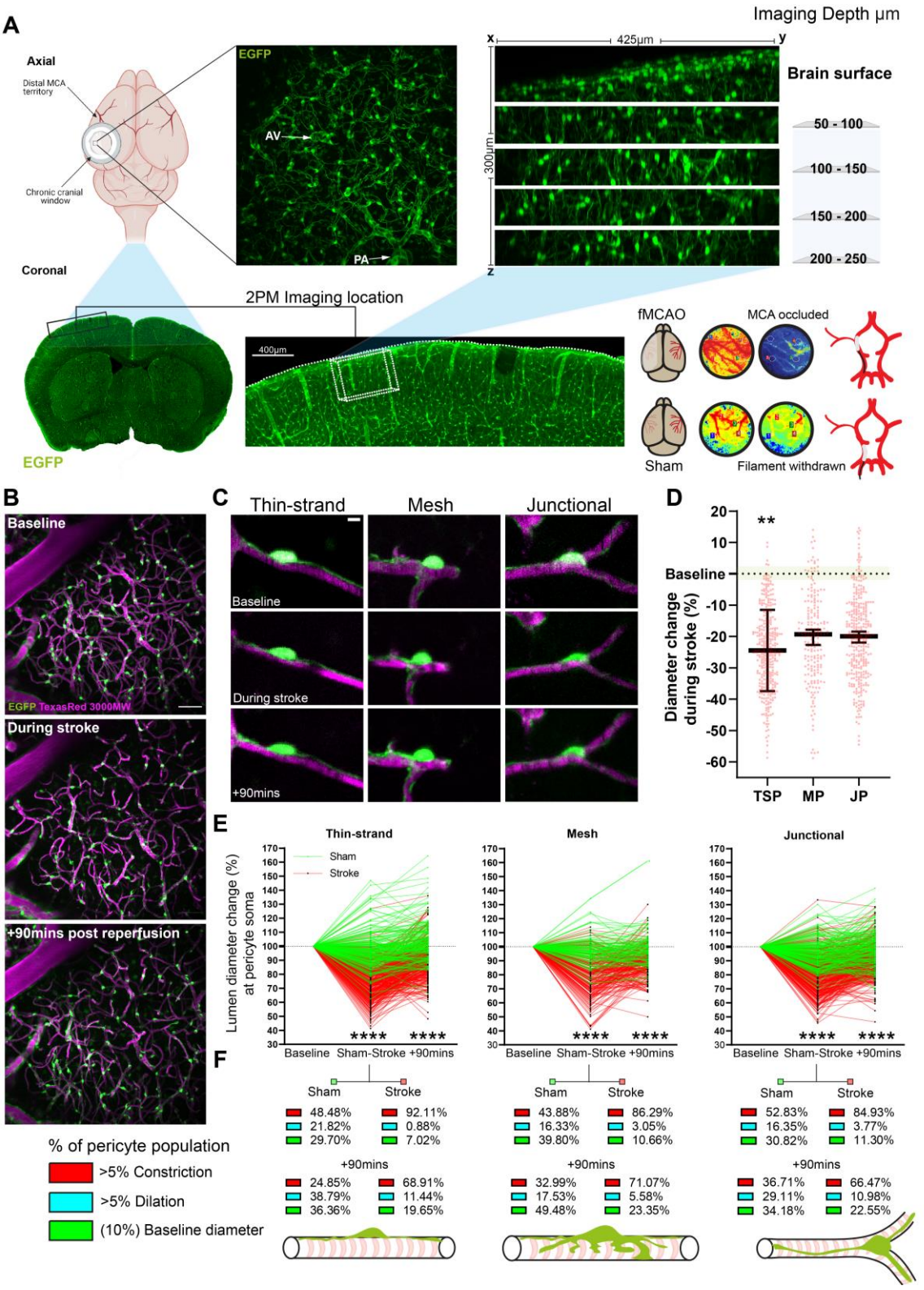

Fig. 31. Ischemia constricts all pericyte sub-types and constriction persists post reperfusion.

A) Schematic of the imaging plane covered (upper) and cortical area covered by 2-photon imaging (lower left) experimental groups (lower right). **B)** Capillary beds imaged, EGFP+ pericytes shown in green, blood vessels, TexasRed3000MW (magenta). **C)** 2 photon images of each pericyte sub-type at baseline, during stroke and 90 mins post reperfusion. **D)** Quantification of the mean constriction of each pericyte sub-type during stroke, individual pericytes shown in pink. **E)** Upper, XY graphs of normalized individual pericyte sub-types during stroke/sham surgery, 90 mins post reperfusion. **F)** Percentage of each sub-type population either constricting by more than 5% (red) dilating by more than 5% (blue) or within 10% of baseline diameter (green). *n=7 stroke, 4 sham PDGFRbEGFP mice. Statistics, after confirming normality (Shapiro-Wilk test), D, unpaired two-tailed Students t-test, E, two-way ANOVA corrected using the greenhouse-geisser correction. Scale bars 50 µm, 5 µm. Data is shown as mean +/- SD.*

5.3.4 Capillary stall frequency is increased by stroke and the frequency of capillary stalls associated with pericytes increases under ischemic conditions

After establishing that ischemia constricts pericytes, we next sought to address whether these constrictions would increase the likelihood of capillary stalls. We term TexasRed negative locations that are present across multiple z-steps of our imaging modality capillary stalls and not erythrocyte entrapment because we cannot discriminate between RBC's and leukocytes with our current experimental design. Essentially, these regions of the vasculature are non-flowing, and could to contribute to on-going ischemia downstream of the stalled vessel segment. We noted capillary stalls form under both stroke and sham conditions in all mice (Fig.32.A, B), however mice undergoing fMCAo surgery had significantly more capillary stalls across all cortical depths per region of interest imaged (Fig.32.B). Stroked mice had on average 15.8 capillary stalls 50 - 100 µm below the cortical surface compared to 1.9 capillary stalls in the sham group. 100 - 150 µm below the cortical surface, stroked mice showed an average of 8.14 capillary stalls per region of interest, while sham only displayed one on average. 150 - 200 µm below the cortical surface, stroked mice had 7.8 capillary stalls on average, compared to 1.4 capillary stalls in the sham group, 200 - 250 µm below the cortical surface, stroked mice showed 7.4 capillary stalls compared with 1.1 capillary stalls in the sham group; overall, the differences between each group reached statistical significance. ($p<0.02$). Taken together, these results indicate that ischemia increases the frequency of capillary stalls in mice undergoing fMCAo surgery.

Interestingly, when examining differences within cortical depth within groups, significant differences in number of capillary stalls were only found within the stroke group (sham, all cortical depth comparisons, n.s). Within the stroke group, we observed significantly more capillary stalls 50 - 100 µm below the cortical surface compared to deeper cortical depths (100 - 150 µm, $p<0.001$, 150 - 200 µm, $p<0.0006$, 200 - 250 µm, $p<0.0003$) but not within deeper, adjacent cortical layers (Fig.32.B). These data imply that during stroke, significantly more entrapped, 'non-flowing' vascular elements are sequestered close to the cortical surface.

Next, we sought to indirectly establish whether pericytes played a role in this capillary stall formation during stroke, 90 mins post-reperfusion and 24 hours post-reperfusion (in collaboration with Fabio Loredo, a GSN masters student). To achieve this, we used pre-defined criteria to assess whether a capillary stall was pericyte associated. Pericytes are widely reported to present 'nodal-like' constrictions preferentially at the cell soma; and during our analysis of pericyte constriction, we noted capillary stalls at pericyte soma which appeared to be persistent over time (Fig.32.D, Upper) (Yemisci et al., 2009, Hall et al., 2014). Therefore, we analyzed our images to locate capillary stalls and termed them 'pericyte associated' if they were within 5 µm distance from the cell soma, if capillary stalls were found further than 5 µm from the cell soma, they were excluded from this analysis (Fig.32.C). We subsequently found that there were significantly more pericyte associated capillary stalls during stroke than during sham surgery, with 30% of pericytes associated with capillary stalls compared to 4% of pericytes associated with capillary stalls in sham-treated mice ($p<0.0002$) (Fig.32.D). 90 minutes reperfusion of the occluded artery in the stroke group, we found 9% of pericytes were associated with capillary stalls, compared to 1.8% of pericytes in the sham group. This difference was statistically significant ($p<0.04$). Crucially, this suggested that a small population of pericytes might entrap elements within the vasculature acutely after ischemia (Fig.32.D). 24 hours after stroke or sham surgery, we found little evidence of pericyte associated capillary stalls, with only 3.5% of pericytes associated with capillary stalls in the stroke group, and 0.3% of pericytes associated with capillary stalls in the sham group, the

difference between the two groups was not significant. These data indicate that pericytes are more likely to be associated with capillary stalls under conditions of ischemia than after sham surgery and demonstrate that capillary stalls remain associated with pericytes acutely after reperfusion following transient ischemia.

To understand variances within each pericyte sub-type population, we compared the average percentage of each pericyte sub-type population associated with capillary stalls during stroke (Fig. 32.E). We found that during stroke, significantly more of the thin-strand and junctional pericyte populations were associated with capillary stalls than mesh pericytes, but that the differences between associations in junctional and thin-strand populations during stroke were not significant (TSP-MP, $p<0.02$, JP-MP, $p<0.02$). These data imply that different pericyte sub-types are associated with capillary stalls to differing degrees during ischemia.

In addition, we compared capillary stalls associated with each sub-type against each other after either stroke or sham. We found that during stroke, significantly more thin-strand pericytes were associated with capillary stalls compared to thin-strand pericytes during sham surgery (stroke 35.3%, sham, 2.7%, $p<0.00007$). 90 minutes post-reperfusion of the occluded artery, 9.5% of thin-strand pericytes were associated with capillary stalls compared to 1.3% of sham thin-strand pericytes, but the differences between the two groups were no longer significant. 24 hours after stroke, we observed that 5.4% of thin-strand pericytes were associated with capillary stalls compared to just 0.6% of sham thin-strand pericytes 24 hours after surgery, but again these differences did not reach statistical significance (Fig.32.F, left).

During stroke we observed significantly more mesh pericytes were associated with capillary stalls compared to than mesh pericytes during sham surgery (stroke, 17.4%, sham, 1.5%, $p<0.013$). 90 minutes after reperfusion we observed 3.4% of mesh pericytes were associated with capillary stalls compared with 0.7% of mesh pericyte associated capillary stalls in the sham group, however this difference was not significant. 24 hours after stroke, we found 1% of mesh pericytes were associated with capillary stalls, while we found no mesh pericytes associated with capillary stalls in the sham group, which again did not reach statistical significance (Fig.32.F, Middle).

Concerning junctional pericytes, we found significantly more junctional pericytes were associated with capillary stalls under conditions of stroke than in the sham group (Stroke, 33.9%, sham, 6.9%, $p<0.0002$). 90 minutes after reperfusion of the occluded artery in the stroke group, we found 7% of junctional pericytes were associated with capillary stalls, while 3.1% of sham junctional pericytes were associated with capillary stalls, this difference did not reach statistical significance. 24 hours after stroke we observed 4.6% of junctional pericytes were associated with capillary stalls and found no junctional pericyte associated capillary stalls 24 hours after sham surgery, which again did not achieve statistical significance (Fig.32.F, Right). Taken together, these results indicate that ischemic pericytes are more likely to be associated with capillary stalls than pericytes during sham surgery, and that this continues at a pericyte population level post-reperfusion, causally implicating pericytes in the ‘no-reflow’ phenomenon.

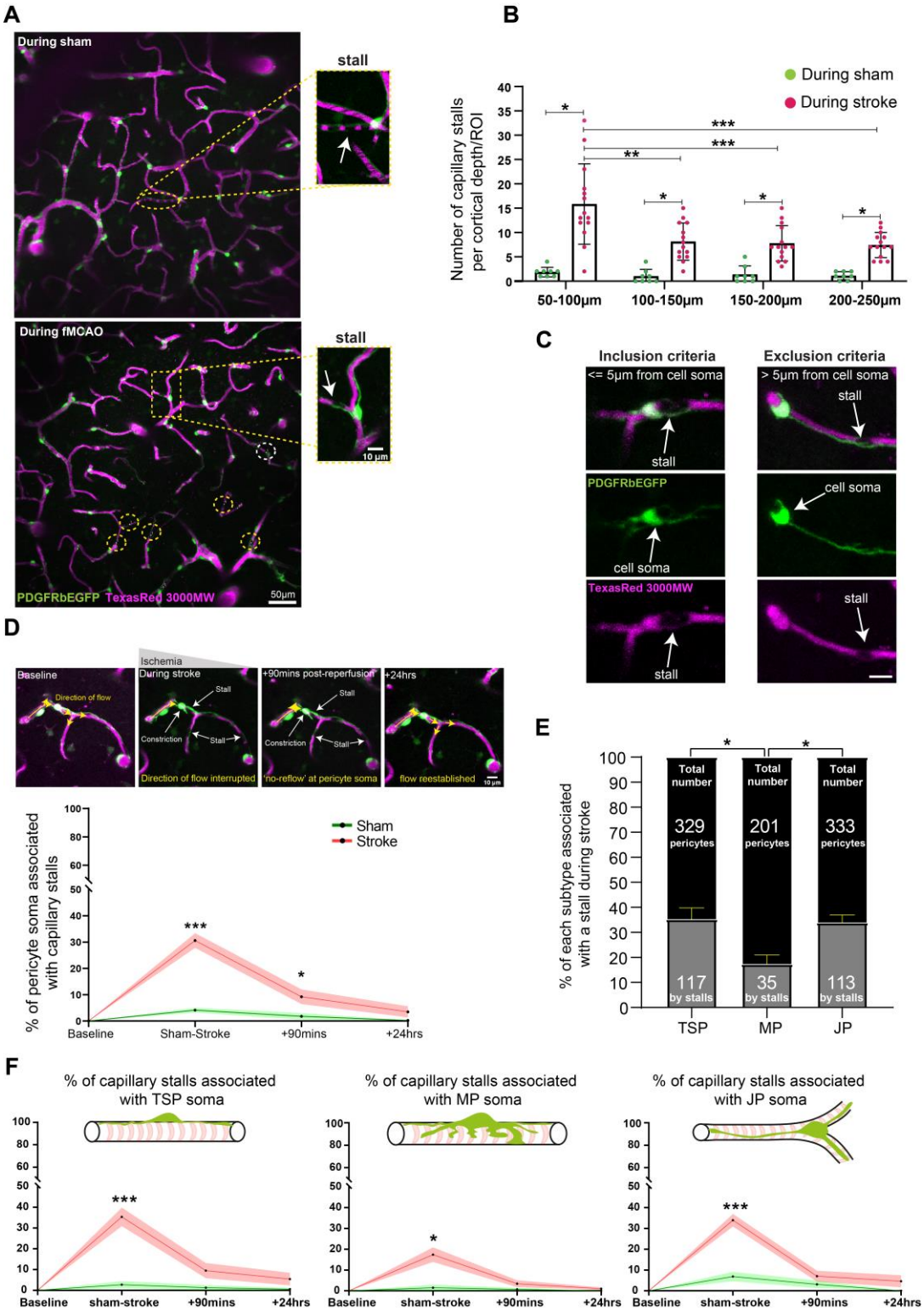

Fig. 32. Ischemia increases capillary stall occurrence near the cortical surface and promotes association of capillary stalls with pericytes.

A) Left, capillary stalls during either stroke or sham surgery, yellow bands indicate sites of capillary stalls highlighted in zoomed in images, Right. **B)** Quantification of total capillary stalls per cortical depth/ROI during either stroke or sham surgery. **C)** Inclusion and exclusion criteria for capillary stalls associated with pericytes. **D)** Upper, *in vivo* evidence of 'no-reflow' at a pericyte soma. Lower, Percentage of capillary stalls associated with either stroke or sham pericytes over time. **E)** Percentage of each pericyte subtype associated with capillary stalls during stroke. **F)** Percentage of capillary stalls associated with either stroke or sham pericyte sub-types over time. *n=7 stroke and 4 PDGFRbEGFP Sham mice. Statistics, after confirming normality (Shapiro-Wilk test), between groups B, unpaired Welch's t-test, within groups one-way ANOVA D, F - Two-way anova with Sidak's multiple comparisons test E, unpaired Welch's t-test. Scale bars, 50 µm and 10 µm respectively. Data is shown as mean +/- SD for B, for D, E, F – mean +/- S.E.M.*

5.3.5 Surviving pericytes constrict vessels in a biphasic manner post stroke while pericyte visibility declines after 24 hours

After confirming that pericytes constrict acutely during stroke and remain constricted 90 mins post reperfusion (Fig.31) we followed up pericyte influence on vessel lumen diameter and tracked the same individual pericytes at 24 hours post stroke, 3 days post stoke and 7 days post stroke (Fig.33.A, D, G upper panels).

While thin-strand pericytes constricted significantly during stroke and 90 mins post reperfusion when compared to sham thin-strand pericytes (Fig.31.E, left), we found that thin-strand pericytes had dilated by 10% (101% of baseline) at 24 hours post stroke relative to 90 mins post reperfusion and that the difference between thin-strand pericyte diameter in stroke and sham groups was no longer significant (sham were mildly dilated with a mean average of 105% of baseline diameter) (Fig.33.B). 3 days post-stroke, thin-strand pericytes constricted on average by 6% compared to baseline levels, while sham thin-strand pericytes had dilated by 5% relative to baseline diameter, indicating thin-strand pericytes had significantly re-constricted on day 3 post stroke ($p<0.0001$). By day 7, thin-strand pericytes had constricted 7% compared to baseline levels while sham thin-strand pericytes had dilated 2% relative to baseline levels, the difference between stroke and sham thin-strand pericyte constriction was again significant ($p<0.0001$).

Concomitantly with these vessel alterations, within the stroke group the number of visible thin-strand pericytes started to decline while the number of thin-strand pericytes in the sham group remained consistent (165 measured at baseline, 164 measured on day 7). We were able to track 345 thin-strand pericytes at baseline in the stroke group, during stroke however, the number of visible thin-strand pericytes dropped by 1% (342), 90 mins post-reperfusion by 1.2% (341), 24 hours post reperfusion by 10% (313) by 20% 3 days post stroke and on day 7 post stroke by 44% (194) (Fig.33.C). The reasons for this decline within the stroke group are many fold (edema pushing cells out of the imaging frame, loss of signal-noise ratio and importantly, pericyte loss) and will be discussed in further detail in the discussion section.

As referred to previously (Fig.31.E, middle panel) mesh pericytes constricted significantly (by 21%) during stroke and 90 mins post reperfusion (11%) compared to sham mesh pericytes (2.7%, 1% respectively) ($p<0.000001$). At 24 hours post-stroke, mesh pericytes had returned to baseline levels (100.4% of baseline) while sham mesh pericytes 24 hours post surgery were found dilated by 1% (Fig.33.E). The difference between or within groups at 24 hours did not reach significance. On day 3 post stroke, mesh pericytes were significantly constricted by 4.2% compared to baseline levels ($p<0.007$) while mesh pericytes in the sham group had constricted by 3.1% relative to baseline levels, this difference between groups was not significant. By day 7 post stroke, mesh pericytes were constricted by 3.3% relative to baseline levels though this difference was not significant, while sham mesh pericytes were constricted by 1.1% relative to baseline levels. Interestingly, no significant difference could be observed between groups on day 7 either (Fig.33.E).

As with thin-strand pericytes, mesh pericyte visibility declined in the stroke group while the sham group was unaffected (Fig.33.F) (sham number of mesh pericytes at baseline-96, on day 7, 96). During stroke, 2% of mesh pericytes were no longer visible (197/201), 90 mins post reperfusion this remained unchanged until 24 hours post stroke where a further decline of 9% in mesh pericyte visibility could be observed (179/201). On day 3 post stroke, mesh pericyte visibility declined by a further 15% (149/201) and again by 7% on day 7 (136/201).

As previously described, junctional pericytes constricted significantly during stroke (by 20%) and 90 mins post reperfusion (by 9%, Fig.31.E right panel) when compared to junctional pericytes in the sham group ($p<0.000001$, $p<0.000001$ respectively). Interestingly, at 24 hours post stroke, junctional pericytes had dilated to baseline levels with less than a 1% change relative to baseline diameter (1%) while 24 hours post sham junctional pericytes were significantly dilated by 4% relative to baseline diameter ($p<0.02$) (Fig.33.H). Differences in junctional pericyte diameter at 24 hours relative to baseline in the stroke group were not significant, but remained significant between groups ($p<0.01$). On day 3 post stroke, we observed that junctional pericytes were constricted by 5.5% in the stroke group relative to baseline diameter and were significantly more constricted than junctional pericytes in the sham group on day 3 (2% dilated, $p<0.000001$). Within the stroke group, this 5.5% constriction was significant compared to baseline ($p<0.0001$) however sham junctional pericytes were not significantly altered relative to baseline on day 3. On day 7, junctional pericytes in the stroke group were significantly constricted by 5.4% relative to baseline levels ($p<0.0001$) and the difference between junctional pericyte constriction on day 7 and junctional pericyte dilation (1% dilated relative to baseline) in the sham group was significant ($p<0.000001$). On day 7, the 1% dilation of junctional pericytes within the sham population was not significant compared to baseline levels.

As reported for the mesh pericyte population, the number of junctional pericytes imaged within the sham group remained remarkably consistent over time (159 at baseline, 157 on day 7) however; stroke induced a reduction in the number of visible junctional pericytes (Fig.33.I). 345 junctional pericytes were imaged at baseline within the stroke group, this number dropped by 2.4% during stroke (337) by 1.5% relative to baseline 90 mins post reperfusion (340), by 7% 24 hours post stroke (321), by 16% (290) 3 days post stroke and by 21% (273) on day 7 post stroke.

Taken together, these results demonstrate a bi-phasic profile of pericyte constriction occurs during the first week of stroke in the thin-strand pericyte and junctional pericyte population during which time, visibility in the population decreases within a period consistent with our previous findings concerning pericyte death (Fig.20). Curiously, mesh pericytes appear to constrict akin to thin-strand and junctional pericytes during stroke and 90 minutes post reperfusion of the occluded artery, but appear to sustain a baseline level of influence over vessel tone in the sub-acute phase similar to that of sham. These results suggest heterogeneity of response between pericytes. To dive deeper into what determines surviving pericyte constriction profiles after stroke, we gathered the data generated such that individual pericyte traces could be visualized against each other and the relationships between them could be teased apart. We envisaged this would allow a greater dissection of the variances in pericyte response to stroke and provide additional insight into the factors driving pericyte influence over vessel diameter.

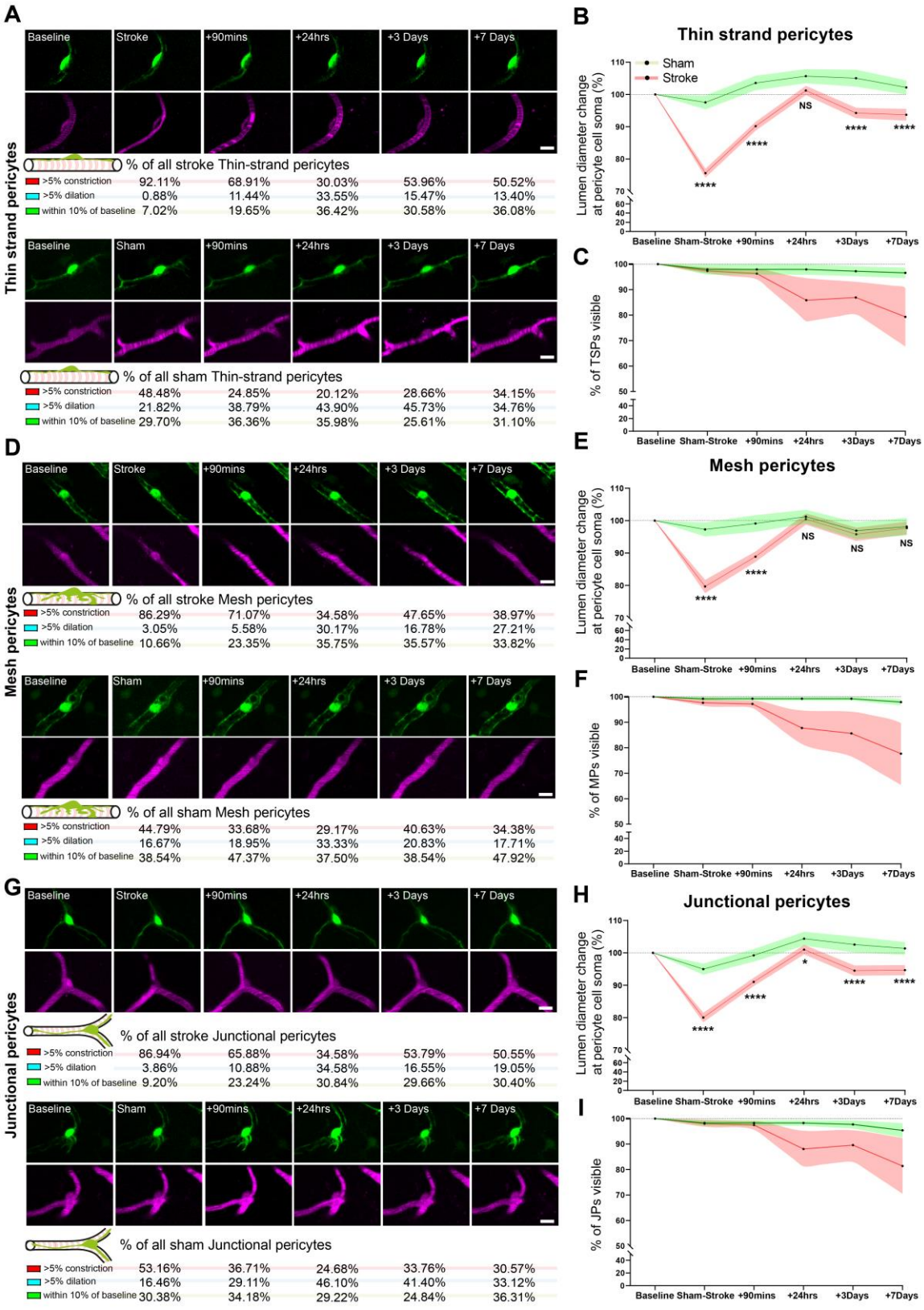

Fig. 33. Pericytes constrict the microvasculature in a bi-phasic manner post-stroke.

A,D,G) Upper**,** *In vivo* image time-course of pericyte subtype response to stroke and sham, Lower, percentage of pericyte sub-type population constricting, dilating or remaining at baseline. **B, F, H)** Quantification of vessel diameter changes over time associated with each pericyte sub-type. **C, F, I)** Percentage of each pericyte sub-type visible over experimental series in sham and stroke group. *n=7 (up to 24 hours), 6 (after 24 hours) stroked mice, 4 sham PDGFRbEGFP mice. Statistics, after confirming normality (Shapiro-Wilk test), two-way ANOVA with greenhouse-geisser correction, comparison of individual time points, unpaired Student's t-test, Scale bars, 10 µm. Data is shown as mean +/- 95% CI for B, E, H. For C, F, I, data is shown as mean +/- SEM.*

5.3.6 Pericyte constriction is cortical depth dependent and future pericyte influence on vessel diameter is determined by severity of constriction during stroke

As previously shown (Fig.31.A), we imaged pericytes in a z-stack over time. This allowed us to segregate pericyte responses to stroke at a variety of depths, 50 - 100 µm below the cortical surface, 100 - 150 µm below, 150 - 200 µm and 200 - 250 µm below the brain surface. Such a step-wise depth dependent imaging modality should cover both neuronal cortical layer 1 and layers 2/3. We hypothesized that a depth dependent constriction effect may be present within our dataset. To test this, we grouped pericyte sub-types by the cortical depths previously mentioned.

We found that thin-strand pericytes between 50 - 100 µm below the brain surface constricted on average by 21.3%, while thin-strand pericytes 100 – 150 µm constricted by 23.6%, the difference between the two layers did not reach significance (Fig.34.A, left). However, when comparing thin-strand pericytes 50 - 100 µm below the surface to those 150 - 200 µm below the surface, which constricted by 26.4% on average, a significant difference was observed ($p<0.003$). Thin-strand pericytes 200 - 250 µm constricted by 25.1% on average, however when compared against those 50 - 100 µm below the surface, only a trend was observed. Significant differences between constriction levels in thin-strand pericytes within adjacent cortical layers was not found.

No significant difference in mesh pericytes 50 - 100 µm (19.4% constriction) below the brain surface was observed when compared against those 100 - 150 µm below the cortical surface (19.3%) (Fig.34.A, middle). Mesh pericytes 150 - 200 µm below the surface constricted by 20.7% on average, but not significantly more than mesh pericytes 50 - 100 µm or 100 - 150 µm below the surface. Mesh pericytes 200 - 250 µm below the brain surface constricted on average by 23.1% but did not constrict significantly more than mesh pericytes at any other cortical depths measured.

When examining the differences in the junctional pericyte population, we observed that junctional pericytes 50 - 100 µm below the brain surface constricted by 18.8% but this constriction was not significantly different from junctional pericytes 100 - 150µm below the brain surface (Fig34.A, right). Junctional pericytes 150 - 200 µm below the surface constricted by 18.2% on average but did not constrict significantly more than junctional pericytes above. Junctional pericytes at a depth of 200 - 250 µm constricted on average by 23.1% which reached statistical significance when compared to those 50 - 100 µm below the surface ($p<0.008$) but not when compared to junctional pericytes between 100 - 200 µm below the brain surface.

Taken together, these differences indicate a depth dependent pericyte sub-type specific constriction effect. These data imply that thin-strand and junctional pericytes within different cortical layers constrict to different degrees during stroke.

To elucidate commonalities and differences in surviving stroked pericytes as a population throughout our time series (during stroke, 90 mins post reperfusion, 24 hours, 3 days and 7 days); we calculated the relationship between every pericyte with every other pericyte by computing the Pearson's linear correlation coefficient. We then arranged all surviving pericytes (659x659 in six stroke mice) based on the severity of constriction into a 'right-tailed' Pearson's linear correlation coefficient heat-map. To spread out the data generated by the Pearson's r correlation and transform the sample distribution to match normally distributed data, we used a z-fisher transformation and visualised the result in the heat-map (Fig.34.C).

We found that pericytes that did not constrict strongly during stroke (Fig.34.C, Q1) have a low level of correlation with each other at subsequent time-points post-stroke, with a correlation score

of Q1:0.199, and a standard deviation of +/-0.585. As the extent of pericyte constriction during stroke grew (Q2, Q3, and Q4), so did the correlation between pericyte diameter at subsequent time-points (Q2, 0.509+/-0.508, Q3: 0.866+/-0.469, Q4: 1.229+/-0.466).

	Mean diameter % Q1 (SD)	**Mean diameter % Q2 (SD)**	**Mean diameter % Q3 (SD)**	**Mean diameter % Q4 (SD)**
Baseline	100 (0)	100 (0)	100 (0)	100 (0)
During stroke	95.8 (6.7)	82.8 (2.5)	73.8969 (2.8)	61.8 (5.9)
+ 90 mins post reperfusion	93.8 (10.9)	92.7 (11.7)	89.59 (12.2)	87.6 (10.2)
+ 24 hours	103.5 (13.3)	99.4 (11.5)	100.6 (12.4)	98 (11.5)
+ 3 days	95.8 (12.6)	94.3 (12.3)	94.771 (14.1)	91.3 (10.8)
+ 7 days	97.19 (14.8)	94.9 (13.7)	94.627 (10.6)	92.87 (11.5)

Table 14: Mean of quadrant-by-quadrant analysis on pericyte behaviour post-stroke.

These data strongly suggest that pericyte constriction during stroke drives pericyte influence over vessel diameter at later time-points. Specifically, pericytes that constrict strongly during stroke are more correlated at subsequent time-points than those pericytes that did not constrict strongly during stroke, with the latter showing almost no correlation at later time-points (Q1:0.199 – Q4 1.229).

Taken together, these data indicate that pericytes at deeper cortical layers constrict more, and that those which constrict heavily maintain a basal level of constriction in the sub-acute phase below that of what would be considered ‘basal tone’ after transiently dilating at 24 hours. Moreover, these data imply that beyond a certain amplitude of constriction during stroke, reconstriction of those same pericytes in the sub-acute phase is almost a certainty.

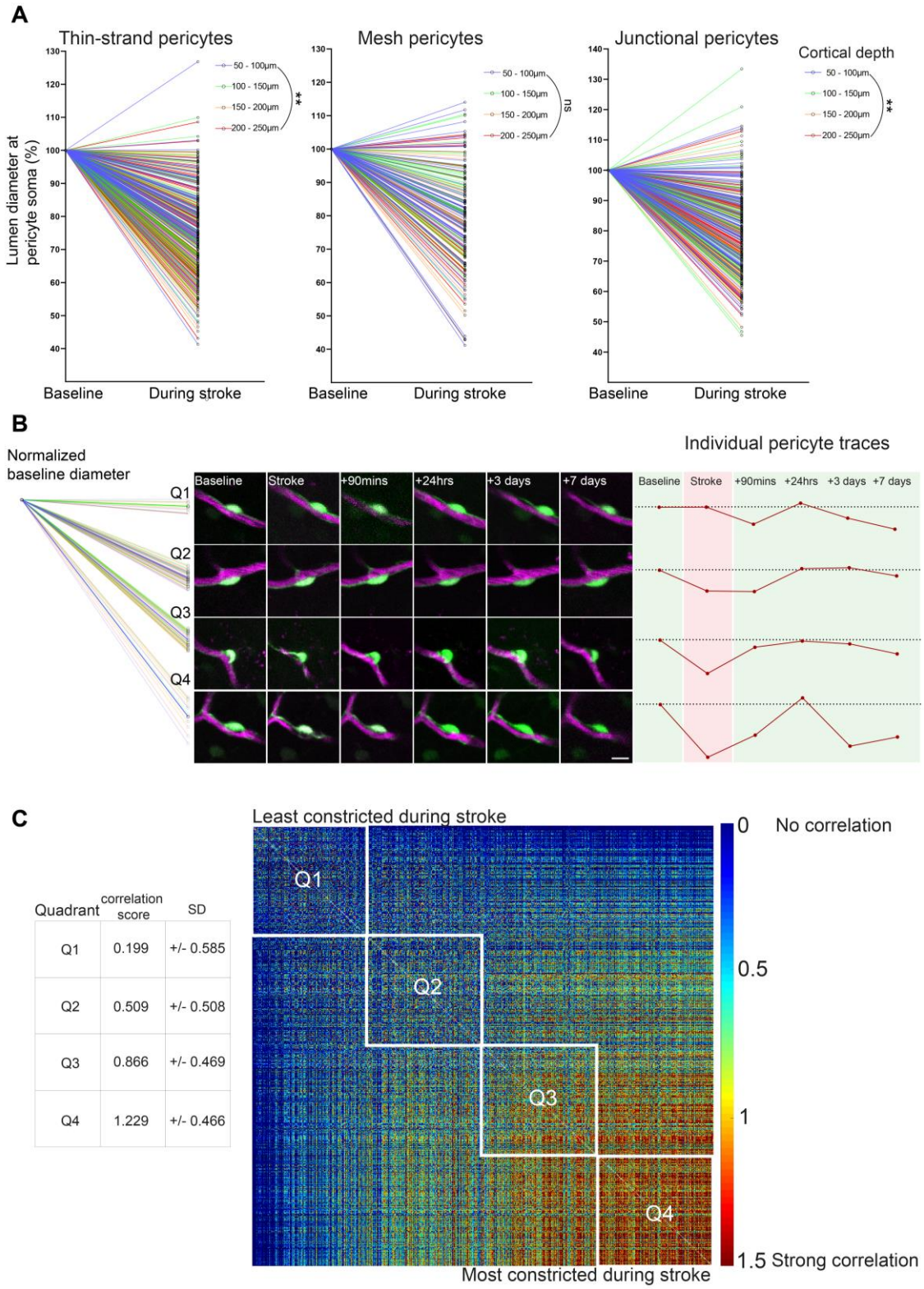

Quadrant	correlation score	SD
Q1	0.199	+/- 0.585
Q2	0.509	+/- 0.508
Q3	0.866	+/- 0.469
Q4	1.229	+/- 0.466

Fig. 34. Pericyte constriction during stroke determines future pericyte influence over vessel diameter.

A) Individual pericyte constriction during stroke per cortical depth analyzed 50-100 µm (blue), 100-150 µm (green), 150-200 µm (orange) 200-250 µm (red). **B)** Individual stroke pericyte traces from quadrants 1 - 4 as they respond to stroke over the experimental time course. Right, constriction or dilation from baseline. **C)** Left, correlation score in each quadrant. Right, heat-map of 659x659 pericytes arranged by amplitude of constriction correlated against each other. A deep red indicates a strong correlation at subsequent time-points, while a blue colour indicates no correlation. *n=6 PDGFRbEGFP stroked mice. Statistics, A) unpaired two-tailed Student's t-test after passing Shapiro-wilk normality test C) Pearson's rank correlation corrected using z fisher correction. Scale bars, 10 µm.*

5.3.7 Pericyte influence over vessel diameter correlates with mesoscale blood flow changes after stroke

After ascertaining that severity of pericyte constriction drives predictability of future pericyte influence over capillary diameter, we next sought to assess whether this influence was reflected at large, in a broader context within our dataset. We noted that over the course of our experimental series, percentage changes in lumen diameter at pericyte soma at a population level after stroke, mimic our observations of blood flow reduction post-stroke using the laser speckle device (Fig.35.A, B). To that end, given that the capillary bed and capillaries proximal to feeding arterioles represent the largest resistance to cortical blood supply, we hypothesized that blood flow reduction within the somatosensory cortex affected by stroke may well be partly determined by changes in pericyte diameter and attempted to interrogate the cross talk between the two datasets (Gould et al., 2017). We grouped stroke animals to display the average change in MCA laser speckle perfusion over time, and in the same animals, grouped the pericyte response in terms of lumen diameter change at all pericyte sub-type soma together, to assess whether the two experimental variables were correlated. We found a significant correlation between the two datasets (Pearson's correlation, $p<0.04$) and tested whether the correlation relationship can be explained using a linear regression model. We subsequently found that these data display an R^2 value of 0.79, indicating that pericyte induced changes in capillary diameter are reflected in broad, mesoscale alterations in blood flow observed using laser speckle measurement (Fig.35.C). Specifically, the relationship between these data imply that approximately 79% of the measured blood flow alterations within the cranial window can be explained by stroke induced alteration of pericyte contractility following stroke. Taken together, these data explain that pericyte contraction of the lumen alters the resistance to flow within the capillary network over broad scales that are large enough to be detected using mesoscale imaging systems.

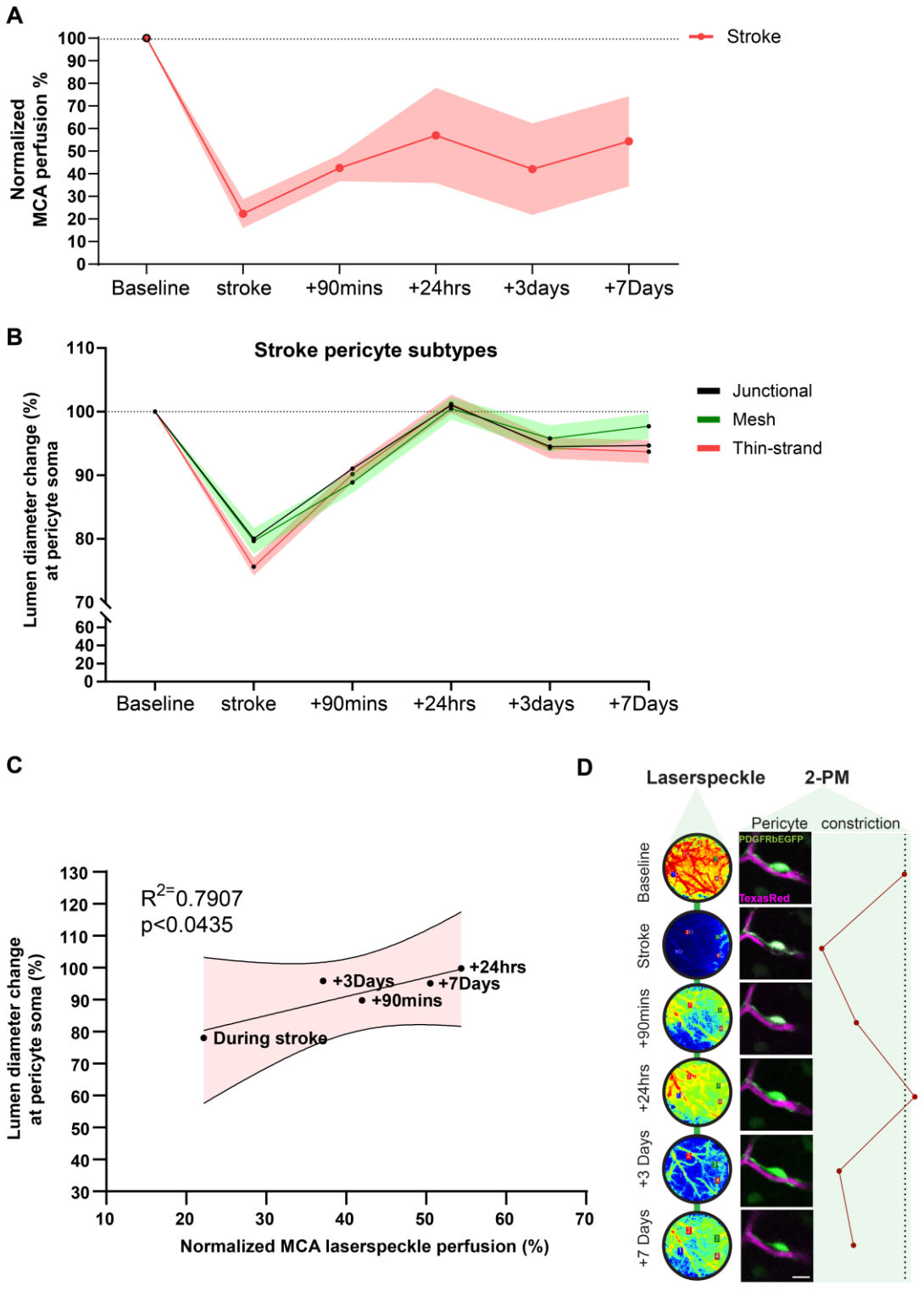

Fig. 35. Pericyte influence over vessel diameter informs laser speckle blood flow.

A) Normalized laser speckle blood flow over the MCA territory perfused by the distal MCA within the stroke group. **B)** Normalized lumen diameter change at pericyte soma sub-types within the stroke group. **C)** Pearson correlation and simple linear regression between normalized changes in lumen diameter at pericyte soma during stroke -7 days post stroke and associated laser speckle perfusion changes. **D)** Left, Representative raw laser speckle images of stroked animal 294. Right, alterations in individual pericyte influence over capillary lumen diameter over time. *n=6 PDGFRbEGFP stroked mice. Statistics, Pearson's rank correlation corrected using z fisher correction. Scale bars, 10 µm. Data is shown as mean +/- SD. For B, mean +/- 95%CI, C, Mean and error.*

5.3.8 Regarding pericyte death *in vivo* (a qualitative assessment)

During the course of *in vivo* experimentation, we noticed a divergence in stroke response based on the development or absence of malignant edema formation. While the data presented on pericyte constriction groups these differential outcomes into one stroke group, we noticed that pericyte visibility declines predominantly in animals that develop edema. Because only two out of 7 stroked animals developed significant edema, we do not at present have enough data to quantitatively assess pericyte loss *in vivo* and so term it 'pericyte visibility' in prior figures (Fig.33). Despite this, we qualitatively assessed one such animal with malignant edema, animal 294 (Fig.36.C, bottom panel) in which blood flow was consistently reduced on days 3 and 7 post stroke.

We found that the vascular bed looks drastically different in these animals over-time (Fig.36.A). At 24 hours post-stroke edema formation appears to enlarge the field of view imaged and the total visible vasculature appears to be reduced, while pericytes remain visible on the upper brain surface, (Fig.36.B) pericytes in deeper cortical layers start to disappear (Fig.34.C). Curiously, these findings become more apparent on day 3 post-stroke where pericyte visibility further declines considerably. These findings *in vivo* are in line with a pericyte density reduction on day 3 post-stroke in PDGFRbEGFP animals reported earlier (Fig.23.A); leading us to believe we are observing pericyte decline.

By looking closer at how these pericytes affect vessel diameter, we can appreciate that pericytes gradually disappear from view, appearing to degenerate on the vessel and importantly, at this time, the vessel continues expanding in diameter (dotted lines indicate that we can't accurately measure vessel diameter further) (Fig.36.C, D). This appeared to be the case in almost all pericytes that disappeared from view (Fig.36.D); suggesting pericyte degeneration leads to a loss of constrictive basal tone, which is normally promoted by functional pericytes and is required for efficient neurovascular coupling.

Concomitantly with the loss of pericyte visibility in these regions of animal 294, TexasRed 3000 MW, which was used to visualize blood vessels, appears to spread in a diffuse pattern around the vessel; gradually decreasing the signal-noise ratio in deeper cortical layers until day 7 where lower layers can no longer be visualized. These findings may hint at BBB damage at sights of pericyte degeneration, or could imply that the vessel itself is beginning to degenerate.

While pericytes which survive in the upper cortical layers of the same field of view are still visible, many appear to be constricted on days 3 and 7 which we find suggestive of on-going damage within the area. Together, these data strongly support that we have managed to image the infarct core in stroke animals and that in the context of edema, pericyte survival may be particularly compromised. To that end, imaging more mice which go on to develop malignant edema after stroke will be important in the future - though it is sadly beyond the scope of this PhD thesis.

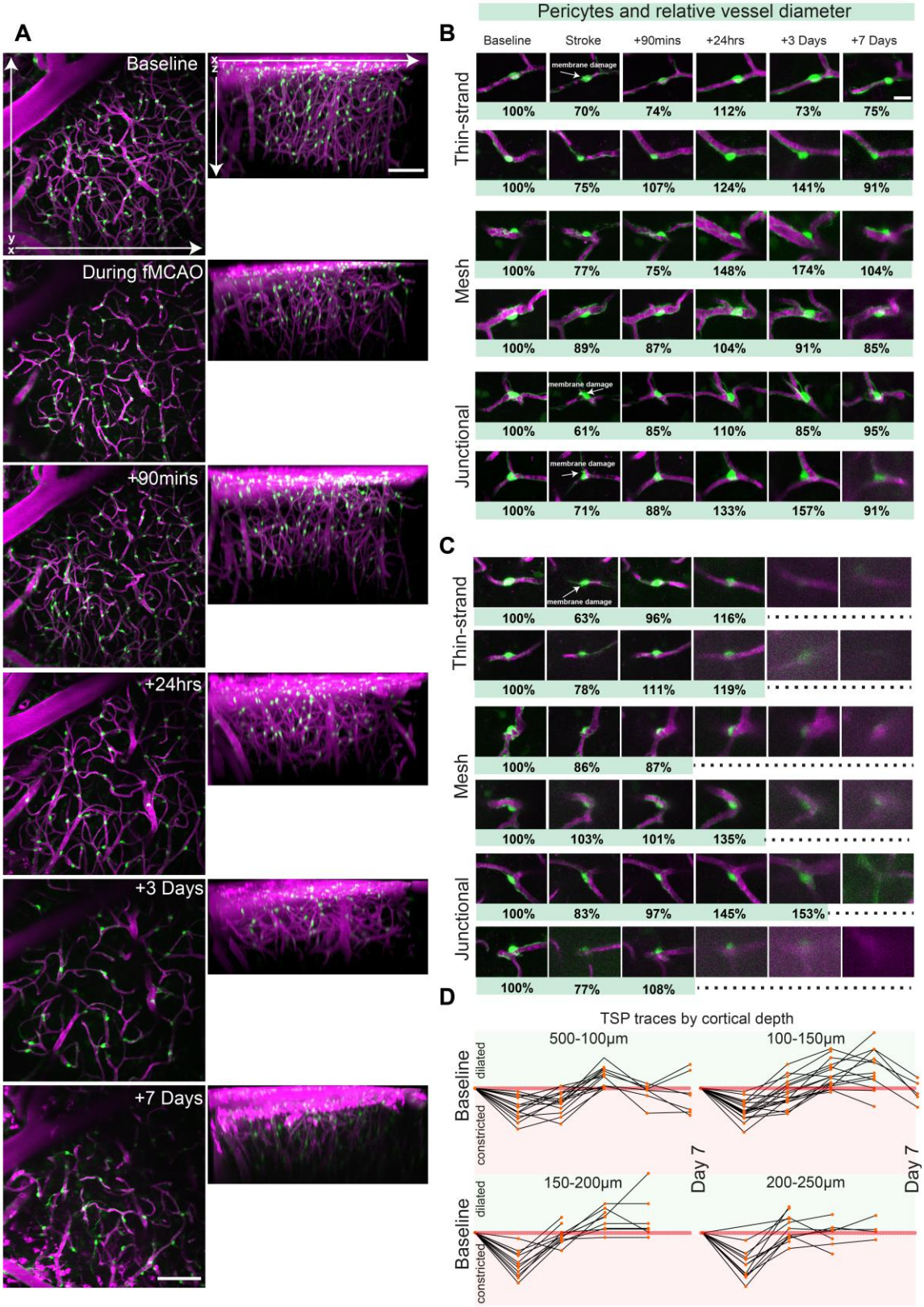

Fig. 36. Pericyte loss appears to be depth dependent.

A) XY and XZ maximum intensity projections of the capillary bed imaged in animal 294 over the stroke experimental time-line. **B)** Surviving pericytes and their relative diameters over-time within the capillary bed imaged. **C)** Degenerating pericytes within the capillary bed imaged. **D)** Thin-strand pericyte diameter traces across different cortical depths in the capillary bed imaged, note that many pericytes disappear before day 7, each orange dot represents one time-point. *n= Animal 294, PDGFRbEGFP stroked mouse. Scale bars, 50 µm, 10 µm.*

6. Discussion

6.1 Reconciliation of *ex vivo* and *in vivo* experimentation

Only recently, pericytes have been reported as an integral cell type of the neurovascular unit, conveying stability to the endothelium, enabling the formation and maintenance of the BBB (Armulik et al., 2010), regulating blood flow under physiological conditions (Hartmann et al., 2018, Peppiatt et al., 2006) and crucially, potentially contributing to the 'no-reflow phenomenon' in the context of ischemia in many organs (Hall et al., 2014, O'Farrell and Attwell, 2014). While the lack of a specific pericyte marker had previously made identification of pericytes challenging (Armulik et al., 2011), leading to controversy about their role in NVC (Hill et al., 2015), recent advancements in characterization make the study of pericyte dysfunction in cerebral ischemia possible through a more focused, accurate lens (Grant et al., 2019). In the current thesis, we attempt to specifically address the fate of the pericyte cell population in the context of stroke by using complementary imaging modalities and techniques to answer questions posed by previous research (Hall et al., 2014, Yemisci et al., 2009) and uncover several novel properties of pericyte dysfunction and cell fate during the first week of stroke.

6.1.1 Hyper-acute phase pericyte response to stroke

In our dataset we find that during stroke, the majority of all pericyte sub-types in the ischemic brain constrict the vasculature heterogeneously in a sub-type and depth dependent manner (Fig.22, 31, 34). Concomitantly, ischemia induces an increase in the frequency of entrapped non-flowing vascular elements associated with pericytes and the total number of capillary stalls near the cortical surface, which crucially, continues acutely post reperfusion of the occluded artery because the majority of pericytes remain constricted (Fig.32). Within this period, we demonstrate that 50-60% of pericytes sustain visible membrane damage during ischemia itself, and this damage persists at least 90 minutes after reperfusion of the occluded artery; in the form of visible extrusions of cytoplasmic EGFP beyond the basement membrane in which pericytes are encased (Fig.22). Importantly, our data confirm pericyte constriction during stroke and their persistent constriction in relation to the 'no-reflow' phenomenon acutely after reperfusion, using established morphological criteria consistent with existing reports on the appearance of distinct pericyte sub-types (Grant et al., 2019).

6.1.2 Acute pericyte response to stroke

24 hours after ischemic stroke, we report that pericyte loss occurs in a region dependent fashion, with preferential survival along a caudal-rostral axis in regions where the cortex represents the majority of infarcted tissue; importantly this happens in the same region neurons are eradicated from the brain (Fig.23). We further show that PDGFRb^{+} pericyte density is reduced by 25% (Fig.20, Fig.23) and 30% of remaining pericytes appear TUNEL^{+} proximal to the MCA territory, suggesting a small amount of hyper-acute necrotic pericyte death and a slower mechanism of cell death involving DNA fragmentation that peaks after 24 hours, compromising approximately half of all pericytes in the ischemic brain. Crucially, this leaves half of the pericytes intact where they are able to transiently restore vessels to a baseline diameter, but without neuronal input, as the severity of our transient ischemia model causes neuronal loss within 24 hours (Fig.19, 20). These

findings strongly complement our analysis of pericyte membrane damage and suggest such damage may indeed prove fatal to pericytes irreversibly compromised by ischemia (Fig.22). Nevertheless, such data highlight pericytes as more resistant to ischemia than previously appreciated and demonstrate that pericytes can outlive neurons after transient ischemia - raising questions about how pericytes regulate blood flow amidst the loss of neuroglial cells within the NVU (Fig.23) (Fernández-Klett et al., 2013, Hall et al., 2014).

Qualitatively, we note that this pericyte death appears to occur on the vessel, in deeper cortical layers *in vivo*, and as pericytes degenerate between days 1 and 3, the associated vessels appear to expand (Fig.36).

6.1.3 Surviving pericyte response to stroke

Day 3 post-stroke marks a divergent point in which the majority of pericytes heavily damaged by stroke have died in a region dependent manner, leaving the surviving population in an activated state, expanding their process coverage over the remaining vasculature and clustering within the basement membrane (Fig.21). Concomitantly, in the upper ischemic cortex, surviving pericyte sub-types perfused by the distal MCA transiently reestablish basal vascular tone, before re-constricting in a manner in on days 3 and 7 to an extent governed by how strongly each pericyte constricted initially during ischemia (Fig.33, 34). These data implicate severity of constriction during stroke as one of the primary determinant factors in future pericyte influence over vessel diameter. Importantly these pericyte population changes in vessel diameter regulation are reflected and correlated with blood flow alterations at the mesoscale level, suggesting pericytes play an important role in mediating vascular resistance to flow (Fig.35). Moreover, we demonstrate that within this population of surviving pericytes, 70% begin to express mRNA transcripts associated with cell cycle entry, along with 30% of pericytes in the ipsilateral hemisphere and 20% of cells in the contralateral hemisphere (Fig.27) suggesting brain wide alteration in the pericyte transcriptome by day 3 post-stroke.

Importantly, pericyte cell cycle entry appears to occur most prominently in areas where pericyte density is reduced by stroke, and is accompanied by striking changes in infarct core pericyte morphology (Fig.24). Small amounts (10 - 20%) of this population of surviving pericytes incorporate EdU into their DNA in the infarct core and peri-infarct edge and express Ki67, providing proof of pericyte viability and protein level evidence that pericytes are entering the cell cycle and responding to the changes in their local microenvironment caused by ischemic stroke (Fig.24). These findings are supported by gene ontology analyses, which demonstrate a shift toward extracellular matrix reorganization in the infarct core, blood vessel morphogenesis and cell division. Interestingly, pericytes in the ipsilateral and contralateral stroke regions show a transcriptional shift toward endothelial cell differentiation. Taken together, transcriptomic sequencing data provides crucial hints for further study and mirrors much of the published data which suggest pericytes shift toward a developmental, wound healing state after experiencing an acute on-set ischemic injury.

In summary, the results presented here demonstrate that despite acutely incurring membrane damage in approximately half of the population during ischemia, pericytes are more resilient than previously believed. Surprisingly, pericytes survive in the infarct core where they contribute to no-reflow in a bi-phasic manner potentially harmful for other cells within the NVU. Despite this, a population of PDGFRb^{+} pericytes appear to recover from the damage sustained and engage in a proliferative response at both the transcriptomic and protein level, maintaining their location within

the basement membrane and entering a blood vessel remodeling transcriptomic pathway in the sub-acute phase.

In the following discussion, we attempt to assimilate our data into the existing scientific literature concerning pericytes in the context of stroke, by comparing and contrasting our dataset with those already published to gain a greater understanding of how the research presented here clarifies questions posed by previous research. Ultimately, with a view to suggest when and how a therapeutic stratagem to modulate pericyte function could be developed to ameliorate stroke outcome.

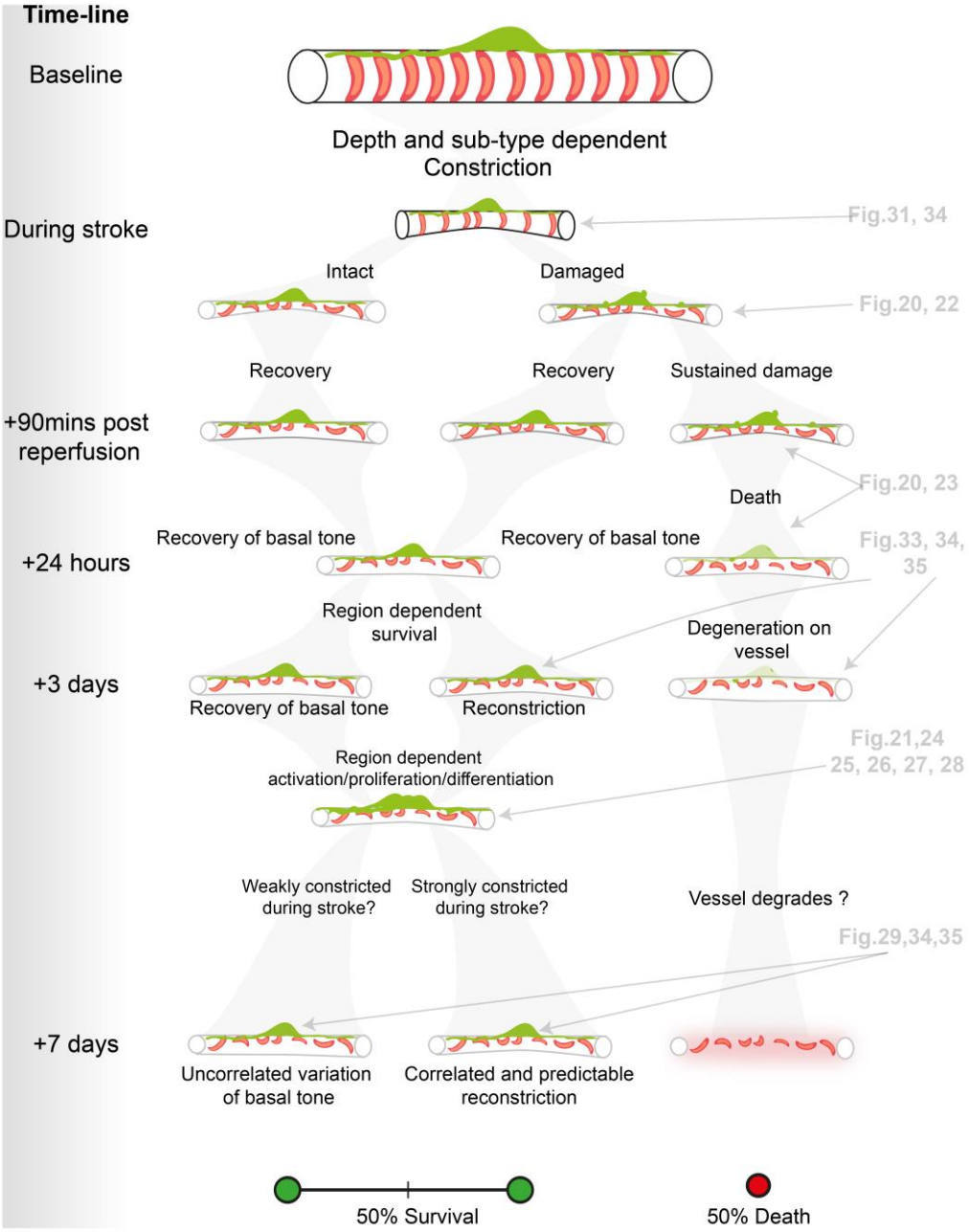

Fig. 37. Divergent fate of cortical pericyte response to transient cerebral ischemia.

Conceptual view of the pericyte response to ischemia according to experiments performed within this thesis. Gray bands indicate possible fate of an observed pericyte according to our experimental series.

6.2 Pericyte response during ischemia

Under ischemic conditions, pericytes have been reported to contract and impede the microcirculation in response to oxidative-nitrative stress even after the reopening of an occluded artery (Yemisci et al., 2009). Here, the researchers implicate the prominent increase in free-radical generation within the microvasculature under ischemic conditions as an important mechanism of pericyte contraction by demonstrating that pericytes contract in response to peroxynitrate application (Chan, 1996, Chong et al., 2005, Heo et al., 2005). Furthermore, they show that suppression of oxidative-nitrative stress relieves pericyte contraction, reducing erythrocyte stalls and recovering microvascular patency after the reopening of the occluded artery. These data, while implying pericytes may be involved in 'no-reflow' in the context of ischemia, leave considerable room for discussion. Many of the findings presented lacked definitive histological proof of pericyte involvement, extrapolation from *ex vivo* data regarding vessel diameter from fixed tissue and a lack of convincing *in vivo* demonstration of erythrocyte trapping by pericytes. In subsequent years, research stimulated by publications like these have further refined our understanding of pericytes in ischemic contexts.

In 2014, we learned that glutamate release from neurons evokes the release of messengers to dilate capillaries by actively relaxing pericytes, which requires the use of ATP. This process is understood to be mediated by prostaglandin E2 and is dependent on the suppression of 20-HETE synthesis by nitric oxide to provide a sustained increase in capillary diameter (Hall et al., 2014). In the same study, the authors show that this may increase blood flow by as much as 84% and is impaired in the context of ischemia where pericytes are reported to constrict. This constriction, studied in *ex vivo* slices under conditions of simulated ischemia, reduces capillary diameter by 60% at pericyte soma locations in a nodal-like fashion as previously reported (Yemisci et al., 2009) (Hall et al., 2014). Subsequently, they demonstrate this constriction is followed by death 'in rigor' (in this context, meaning permanent constriction of the vessel) with pericytes appearing propidium iodide positive after one hour. In detail, the authors postulate that pericyte constriction and death occur because of an intra-cellular $Ca2^{+}$ increase following ATP depletion and failure of the Na^{+}/K^{+} exchange pump, in turn causing a permanent failure in membrane potential.

While these data are convincing, and the use of propidium iodide as a marker for cell death is appropriate and has been long recognized by the literature as a marker for cell death, these pericytes are not responding to a clinically translatable model of ischemia *in vivo*. Counter-intuitively, in the context of TBI (in which regions around the contusion suffer from ischemic damage due to reduced blood flow), many cells can recover membrane integrity by 24 hours and even after labelling propidium iodide positive, can be $TUNEL^{-}$ *living* cells in the injured brain (Whalen et al., 2007). Moreover, to date, pericyte 'death in rigor' *has never been observed* in the living brain. Understanding whether pericyte constriction is terminal, or represents a functional impairment of pericytes that can recover, is pivotal in deciphering whether they represent a therapeutic strategy to ameliorate stroke outcome. The research presented in this thesis, attempts to address these questions and sheds light on aspects of all three previous publications mentioned, which we now attempt to discuss in detail.

6.2.1 Pericyte influence over vessel diameter during stroke

Specifically, we imaged pericytes in the somatosensory cortex during the last 30 minutes of a one-hour fMCAo surgery, which is in line with observing maximally constricted pericytes from previous publications in models of retinal and simulated ischemia (Hall et al., 2014, Alarcon-Martinez et al., 2020). We find that *all* pericyte sub-types constrict during ischemia *in vivo*, however to a lesser extent than reported in previous research (Hall et al., 2014). Specifically, while pericytes in our dataset can constrict during stroke by 60% (Fig.31.E) we find that to be the extreme end of a spectrum of constriction, with a typical average constriction across the whole pericyte population of between 20 - 25%. Nevertheless, in our dataset, 87% of all pericytes constricted during stroke (average of all pericyte sub-type constricting populations Fig.31.F), which can be expected to impart a vast increase in resistance to remaining flow within the ischemic cortex and exacerbate ischemic sequelae when already dwindling cellular energy stores are depleted.

Importantly, this constriction appears to be depth dependent, with pericytes in deeper cortical depths constricting significantly more than pericytes proximal to the cortical surface (Fig.35). This may occur for several reasons as our model of transient ischemia is severe and results in complete neuronal loss within 24 hours (Fig.19, 20). Consequently, it is possible that the higher neuronal density in cortical layer 2/3, which represents the lower cortical depths in our data set (Fig.34), provides a more intense source of local glutamate release during ischemia, which induces constriction via excitotoxic damage and can kill pericytes (Hall et al., 2014). In contrast, pericytes in cortical layer 1 sit amid the apical dendritic arbors of pyramidal neurons, which may reflect a less damaging environment.

Alternatively, this difference in constriction may reflect changes in O_2 availability following RBC trapping in capillaries in upper cortical layers, which we also provide indirect evidence for in our experimentation (Fig.32 A, B). Specifically, we find that trapped vascular elements representing capillary stalls are significantly more common proximal to the cortical surface, which could conceivably starve vascular elements downstream of crucial energy supplies required to maintain membrane potential, with eventual constriction following in sequence. This hypothesis is supported by recent research, showing that the largest pressure drop in RBC flow occurs in capillaries at cortical depths of <400 µm from the cortical surface. This may make RBC flux particularly sensitive to ischemic insult in upper cortical layers, in which capillaries account for 37% of the pressure drop. This is not the case in depths greater than 400 µm, where arterioles account for 61% of the pressure drop (Schmid et al., 2017). In our experimental paradigm, we focused on imaging up to 250 µm deep into the ischemic cortex, and so we would expect these effects to be at play. Consequently, a superficial energy gradient could exist from the cortical surface downward, with the rate of energy loss a function of depth; this may cause differential rates of glycogen depletion in astrocyte end-feet following ischemia and therefore compromise pericyte energy metabolism and membrane potential differentially (Alarcon-Martinez et al., 2019). It is also possible that the CSF influx reported early during stroke (Mestre et al., 2020) washes away harmful glutamate release from neurons as it travels deeper into the cortex from above and that this extracellular glutamate builds up in more dense cortical layers causing differential constrictive effects.

Our data support the notion that pericyte constriction occurs in a ‘nodal-like’ like fashion by demonstrating longitudinal images of $EGFP^+$ pericyte soma directly above the sites of most severe vascular diameter decrease (Fig.31, 32, 33). Therefore, in our data set, we assume that contractile elements within the pericyte proximal to the pericyte soma mediate the constrictive

effects observed on the vascular lumen at this point. This is completely in line with previous literature and consequently we address the decreases in lumen diameter at the pericyte soma as 'pericyte constriction' thereafter (Peppiatt et al., 2006, Yemisci et al., 2009).

Despite this, we cannot exclude that pericytes also convey a broader constrictive range than the one we describe here, and recent reports suggest γ-actin, which is expressed in pericyte processes, could also potentially mediate a constrictive effect (Alarcon-Martinez et al., 2018). We did not quantify the vascular diameter over the entirety of the pericyte cytoplasm, or at non-pericyte locations. This is because measurement of entire vascular networks vessel diameters is extremely time intensive when analysis is performed manually without the use of machine learning (which fails to measure accurately vessel diameters in the context of ischemia), therefore, we made the decision to focus exclusively on the lumen diameter at pericyte soma and here, the constrictive effect is most apparent.

6.2.2 Differential constriction between pericyte sub-types during stroke

We note that the aforementioned nodal constriction occurs most prominently in junctional and thin-strand pericytes, whereas mesh pericytes appear to constrict in a broader bi-concave fashion (Fig.31, 33). This may reflect cellular alterations in cytoskeletal arrangement, differential expression of αSMA along the arterio-venous axis or individual pericyte contractile force, or simply relate to changes in the way outward pressure of RBC velocity imparts on contractile morphology and capability.

Interestingly, we find that on average, thin-strand pericytes constrict significantly more than junctional or mesh pericytes (Fig.31.D). There are many potential reasons for such differential constrictive effects between pericyte sub-populations. On average, pericytes sit between 8 - 23 µm away from neurons and so are well positioned to receive chemical messengers from the neuropil. It is plausible that the differences in constriction we observe may relate to the proximity of each pericyte to constrictive cellular messengers released by neuroglial cells under conditions of ischemia. In such a scenario, thin-strand pericytes may be particularly prone as they convey the broadest single cell coverage distance along the endothelium, whereas mesh and junctional pericytes for example are typically located on slightly larger capillaries and sit closer to neighboring pericytes (Fig.30.B) (Grant, 2019). Furthermore, differential constriction may be related to topological gradients of ischemia within the tissue or an epiphenomenon of differential flow within the microvasculature. If plasma flow under conditions of ischemia is partially maintained, and the outward radial force this provides is higher in lower order capillaries than in higher order capillaries (where thin-strand pericytes reside), this may impart a greater resistance to constriction on the endothelial tube acted upon by the pericyte (Dalkara, 2019).

Alternatively, these constrictive differences may reflect fundamental differences in the internal components and response rates of pericyte sub-types. Unlike ensheathing (which we did not find numerous enough to quantify) or mesh pericytes, thin-strand pericytes present on >4th order capillaries are typically reported to respond up to 25 times slower to optogenetic stimulation and produce a very small pool of αSMA - which is expressed in pericytes in an inverse fashion along the arterio-venuous axis (Grant, 2019, Hartmann et al., 2018, Alarcon-Martinez et al., 2018, Hartmann et al., 2021). Though this topic remains contentious, a small pool of αSMA has recently been found to exist in pericytes on higher order capillaries of the retinal plexus, and it is entirely possible that its rapid degradation under ischemic conditions is sufficient to produce a more severe long-lasting constriction as a result. One could also speculate that the location of thin-strand pericytes on higher order capillaries, when compared against ensheathing or mesh pericytes,

predisposes them to more intense bouts of ischemia, as they tend to reside further along the arterio-venous axis and may take longer to resynthesize or rearrange cytoskeletal elements (Fig.38).

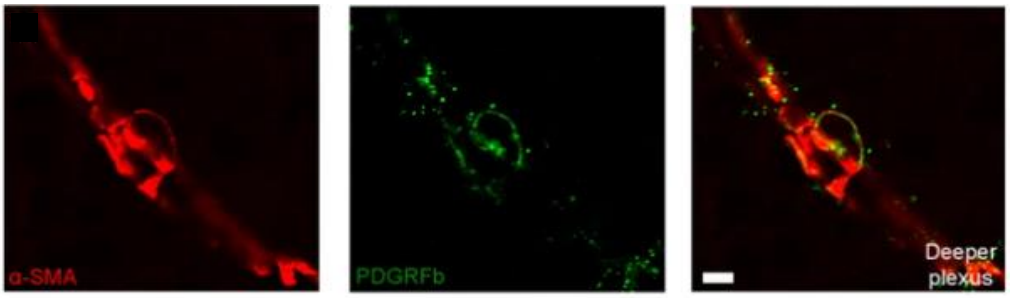

Fig. 38. Thin-strand pericytes in the retinal plexus express α-SMA only detectable through rapid methanol fixation.

Adapted with permission from (Alarcon-Martinez et al., 2018)

In contrast to this notion, under physiological conditions, reports indicate that thin-strand pericytes do not require αSMA to alter their associated vessel diameter and constrict at the same rate as thin-strand pericytes which express αSMA; producing a decrease in capillary diameter of 20% over 10s of seconds when optogenetically stimulated *in vivo* (Hartmann et al., 2018). These data imply that the rate of pericyte contraction is independent of αSMA expression, but do not address constriction severity in relation to other pericyte sub-types.

Moreover, these findings use light-sensitive channel rhodopsin gated calcium channels to permit calcium influx, which likely reflects a different, less severe route of constriction than under conditions of ischemia found in our model, but interestingly produce a very similar average extent of constriction (our data report 25%, their data show 20%). Consequently, a 20% reduction in capillary diameter produces a 20% reduction in red blood cell velocity at the thin-strand pericyte soma. While the average constriction of thin-strand pericytes within our dataset is 25%, we also find pericyte constriction is a spectrum, with some that constrict up to 60% in our *in vivo* experimentation during ischemia (Fig.31.D). These findings imply that optogenetic stimulation of pericyte constriction, which causes Ca^{2+} influx, does not reach the constriction maxima of pericytes, and suggests that additional contractile stimulants present under ischemic conditions may mediate these effects. Here, many pathways could exacerbate pericyte contraction such as higher levels of intracellular Ca^{2+}, unsuppressed 20-HETE production, elevations in ROS production, loss of prostaglandin E2 binding to associated receptors on pericytes, or high levels of extracellular glutamate, all of which will constrict pericytes (Hall et al., 2014). Deciphering what compounds mediate this spectrum of pericyte contraction, and through which downstream cellular components under conditions of ischemia *in vivo*, will be an important challenge for the future. So far, we understand that the actin cytoskeleton plays an important role in pericyte contraction. Researchers have recently shown that the clinically approved Rho-kinase inhibitor Fasudil, prevented optogenetic induced Ca^{2+} mediated pericyte contraction and even prohibited erythrocyte arrest at pericyte soma locations, suggesting reorganization of actin filaments may be enough to modulate basal vascular tone at higher order capillary levels.

We do not find this surprising, as circumferential arrangement of actin filaments (which could exert such a nodal constrictive effect) in pericytes has been previously reported (Wallow and Burnside, 1980), and we think it likely that a pericyte produces exactly as much constrictive elements as is

required to actively regulate basal capillary tone and respond to stimulation at each section along the arterio-venuous axis. Logically, at sites upstream, where blood pressure is higher, the amount of contractile elements required to maintain flow at a steady, controlled state would also increase. Ultimately, while this remains to be thoroughly investigated, we expect the extent of contractile elements in pericytes to be inversely proportional to the blood pressure at each stage of the vasculature.

Taken together, these data provide to our knowledge, the first detailed evidence of pericyte constriction in the context of a clinically relevant model of cerebral ischemia that simulates reperfusion injury *in vivo,* and identifies pericyte constriction as a ubiquitously occurring, depth and sub-type dependent heterogeneous phenomenon during stroke. Crucially, pericyte constriction appears to be transient in the ischemic cortex, as lumen diameters at pericyte soma increase upon reperfusion and strongly suggests that pericyte constriction during stroke occurs because of functional impairment, and temporally precedes permanent constriction and 'death in rigor' in the cortex by a significant margin (Fig.33, 36) (Hall et al., 2014). One limitation of our approach is that we cannot confirm whether this post-reperfusion lumen diameter increase occurs locally within the ischemic capillary bed imaged and is initiated by the pericyte, or by the flow increase generated by removal of the filament upstream. Here, we find that blood flow is increased by 20% in the ischemic cortex 90 minutes following filament removal using laser speckle imaging and therefore cannot definitively state that pericytes themselves recover vessel diameter acutely post-reperfusion (Fig.29.F). However, we note that the majority of ischemic pericytes remain visible in subsequent imaging time-points after stroke and it follows that both options are equally plausible. In the future, optogenetic stimulation of pericytes to induce vasodilatation through pericyte relaxation after stroke would be of benefit here; this will definitively answer whether the vasoconstriction we observe is an intrinsic property of pericyte dysfunction or involves mechanisms upstream, though these experiments were beyond the scope of this thesis.

6.2.3 Pericyte sub-type damage during ischemia

During conditions of oxygen-glucose deprivation or situations of intense optogenetic stimulation, pericytes are reported to form membrane blebs which may be associated with damage. In recent publications (Hartmann et al., 2021) 30% of pericytes opto-genetically stimulated to permit Ca^{2+} influx through light sensitive channel rhodopsins formed localized protrusions of the fluorescent reporter YFP in a 'bleb' like manner (Fig.39.C). The authors speculate that these blebs, which form as protrusions from the membrane a few microns in circumference, may occur due to cytoskeletal rearrangement proximal to the pericyte cell membrane. Interestingly, blebs of a similar appearance, but more variable in size and appearance, also formed when researchers exposed retinal capillary pericytes to ischemia; suggesting a conserved pericyte response to cellular stress within the pericyte population (Alarcon-Martinez et al., 2020) (Fig.39.A).

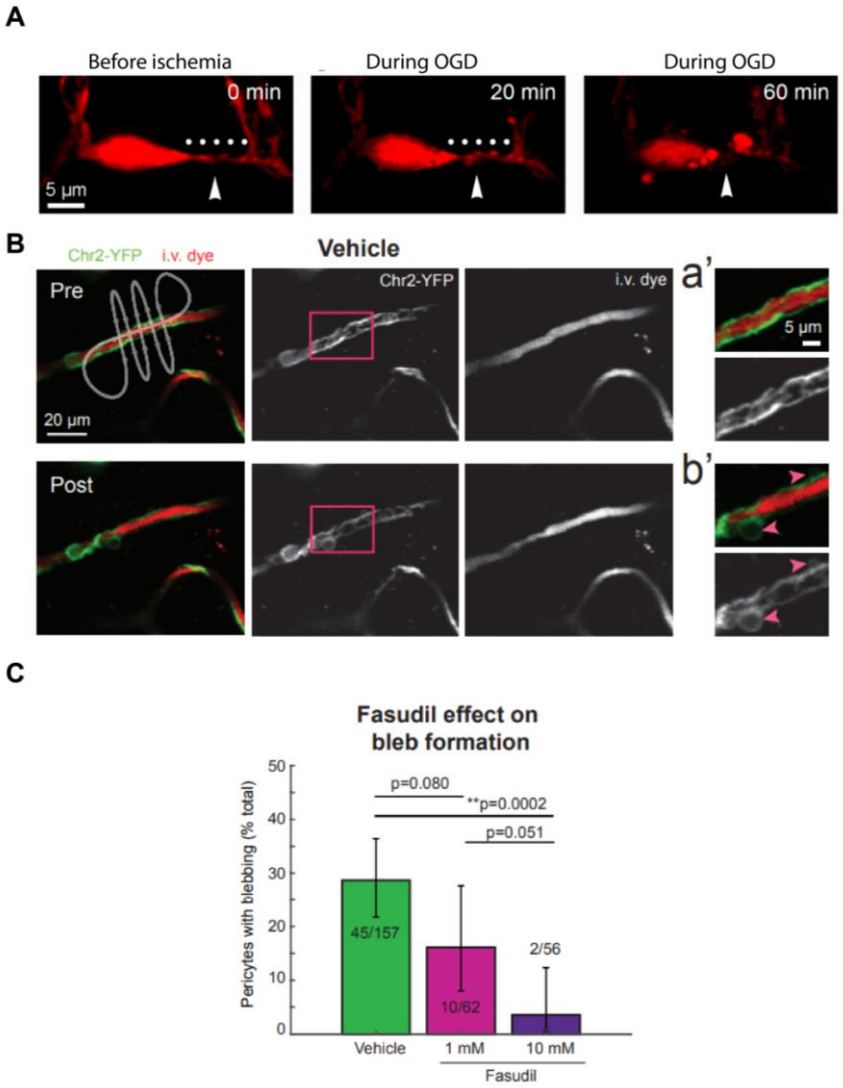

Fig. 39. Membrane blebs reported to form after Ca2+ influx are Rho-kinase dependent.

A) An NG2DsRed expressing pericyte forming membrane blebs after oxygen-glucose deprivation. (Adapted with permission from Alarcon-Martinez et al., 2020) **B)** Upper, Chr2-YFP expression in pericytes before light induced stimulation together with I.V dye to label blood vessel. Lower, an optically stimulated pericyte forming a membrane bleb along primary pericyte processes, a' before stimulation, b' after stimulation. **C)** Rho-kinase inhibitor Fasudil decreases bleb formation in a dose dependent manner. (Adapted with permission from Hartmann et al., 2021). *Scale bars 5 µm and 20 µm respectively. Data is shown as mean +/- SD.*

Intriguingly, our data are in line with these findings, and confirm that membrane blebs form *in vivo* under conditions of ischemia in the cerebral cortex (Fig.22.A). These membrane blebs appear similar in nature to that of recent research (Alarcon-Martinez et al., 2020) and do not form in sham treated animals or in the contralateral hemisphere, suggesting they form primarily under hypoxic/stress conditions. One limitation of our approach to quantify this damaged phenotype is that we could only detect evidence of membrane damage in three out of seven stroke animals within our *in vivo* imaging experiment. This is likely because of the limiting spatial resolution in X/Y of the 2-photon microscope (0.415 µm) and imaging artifacts associated with vasomotion. Unfortunately, this does not allow an effective sample size to determine whether membrane blebs are especially associated with more severely constricting pericytes *in vivo*, or whether there are significant differences in contractile forces between 'blebbing' and 'non-blebbing' pericytes, though

one might assume in response to cellular stress that pericytes constrict more, or are more prone to dying at later time-points. Nevertheless, it is curious that many pericytes imaged in the upper cortex had no obvious membrane protrusions *in vivo*, those that did often only displayed them transiently and pericytes that did not at all still constricted (Fig.36). This suggests ischemia causes a spectrum of pericyte damage, resulting in different levels of membrane damage and possibly different levels of Ca^{2+} influx, which trigger a non-uniform pericyte stress response within the pericyte population.

Although our transient ischemia model is severe and causes neuronal loss within 24 hours, this cannot be extrapolated to the survival of pericytes after ischemia, and our data would instead imply that pericytes are on the edge of a viability threshold within ischemic tissue, which produces two distinct phenotypes; pericytes with membrane damage and pericytes with an intact membrane. Our data show at least half of the pericyte population appear to have an intact membrane within the ischemic territory, indicating that a proportion of pericytes can withstand our 60-minute fMCAo model of transient ischemia and display no membrane deformations acutely after the reperfusion of the occluded artery (Fig.22).

Importantly however, using high-resolution confocal microscopy, we demonstrate that membrane blebs are found in pericytes that show *extracellular* extrusions of EGFP beyond the basement membrane in fixed tissue *ex vivo* 90 minutes post-reperfusion of the occluded artery, in all mice (Fig.22.B, C, D). This is important, because the entirety of a pericyte cytoplasm is encased within the basement membrane under physiological conditions, and the nature of extracellular EGFP found beyond the pericyte cytoplasm does not match that which we would expect of programmed exocytosis (Kuo et al., 2008). Therefore, we believe we are observing pericyte membrane damage and catch pericytes in fixed tissue that are actively leaking intracellular contents into the extracellular space 90 minutes following reperfusion of the occluded artery. This could be expected after ischemia as consistent anoxic depolarization triggers membrane potential failure and has previously been reported in pericytes in *ex vivo* brain slices modeling ischemia, where pericytes stain propidium iodide positive (Hall et al., 2014). When examining the extracellular accumulations of EGFP found in infarct core pericytes, we found that 59% of thin-strand pericytes showed signs of extracellular EGFP. In addition, 47.5% of junctional pericytes and 57% of mesh pericytes showed extracellular accumulations of EGFP, implying that at least half of the pericyte population suffer membrane damage as an immediate consequence of ischemia in the hyper acute phase (Fig.21).

We believe extracellular accumulations of EGFP emanating from pericytes to be a morphologically distinct phenomenon to blebbing, and therefore quantified it as such. We find it probable that what we observe is temporally distinct phases of necrotic cell death, and blebbing may represent the precursor to irreversible pericyte membrane damage or possibly the initiation of apoptotic processes; thus, they both fall under the same rubric (Fig.22.E, F). It will be necessary to investigate this in detail in the near future to determine what exact factors trigger these dramatic morphological alterations.

Taken together, these data lead us to identify a novel damaged phenotype occurring during stroke *in vivo* and persisting hours after reperfusion where it could be quantified *ex vivo* (Fig.22). We speculate that these morphological criteria identify a population of pericytes critically damaged by ischemia. Though an exact mechanism of pericyte cell death in the hyper-acute phase remains elusive (though we have tested for inflammasome and pyroptotic cell death markers), it is highly likely that a portion of pericytes succumb to ischemia in a manner that resembles necrosis, and

we believe this could may well be the downstream cellular consequences underlying our current observations.

Cumulatively, our data imply that at least half of the pericyte population experience high levels of membrane damage, resulting in acute changes in cytoskeletal arrangement in the form of blebs, which may be in part mediated by Rho kinase (Hartmann et al., 2021). This would be consistent with literature on cellular responses to ischemia, which demonstrate that cellular membrane blebs form after ischemia mediated Ca^{2+} influx in a variety of cell types (Armstrong et al., 2001, Yi et al., 2012, Jansen et al., 2019). Ultimately, we speculate this could damage pericyte function, as an astrocytic end-foot sheath, covering approximately 98% of the vasculature, envelops pericytes. It is conceivable that these plasma membrane deformations affect signaling between astrocytes and pericytes, and affect micro-domains within the pericyte cytoplasm, potentially negatively affecting propagation of intercellular Ca^{2+} waves between pericytes and disrupting the retrograde signaling cascade reported to be at play within the pericyte connectome (Kovacs-Oller et al., 2019, Peppiatt et al., 2006). Further work dissecting the exact cytoskeletal deformation caused by this damage is planned and currently being performed and will provide useful information on this issue.

6.3 Pericyte death post-stroke

To date, pericyte loss after stroke has been investigated in two key publications. Francisco Fernandez-Klett and colleagues investigated pericyte loss after stroke using CD13 as a marker for pericytes responding to fMCAo (Fernández-Klett et al., 2013). They found a 40% loss in $CD13^+$ pericytes after 24 hours, with a progressive loss of 80% of the population occurring over the course of one week. Later, Catherine Hall and colleagues investigated pericyte response to chemical ischemia in rat cerebellar slices and found 70% of pericytes were dead after one hour of oxygen-glucose deprivation. Furthermore, experiments performed in a rat model of 90-minute fMCAo assessed 22.5 hours later indicated a similar amount of pericyte loss (75%) (Hall et al., 2014). Taken together, these results would appear to suggest that the majority of the population is lost acutely after stroke.

Our results are semi-compatible with prior publications, we report 25% of pericyte loss prior to 24 hours, with 30% of the remaining 75% of pericytes appearing $TUNEL^+$ in the infarct core; but crucially, this leaves half of the pericyte population intact after 24 hours. Subsequently, low levels of pericyte death continue to occur on day 3 (3%) but as a whole, our data suggest that pericytes are more resilient than previous publications would indicate and that when pericytes die, they die acutely after stroke. The discrepancy in results may occur for several reasons such as the experimenter performing the model of stroke, age of the mice used and criteria used for pericyte measurement. Nevertheless, our transient fMCAo model produces a severe stroke in adult mice, reducing cerebral blood flow by more than 80% and results in the complete loss of neurons within the infarct core in 24 hours (Fig.19, 20, 23).

Of particular note in relation to previous publications is the use of CD13 as a marker for pericytes (Fernández-Klett et al., 2013). While CD13 is reported to be a specific marker for pericytes, our data would imply that CD13 is not transcribed at particularly high levels in relation to other transcripts that are commonly used for labelling pericytes (PDGFRb, NG2, RGS5, Kcnj8, Fig.25.B). It is therefore possible that the early loss of pericytes after 24 hours simply reflects protein degradation that may occur following stroke and that transcription of a new pool of CD13 is initially inhibited by hypoxic conditions, but the pericytes may still be viable. This calls the use of CD13

as a marker acutely post-stroke to measure pericytes into question, as do reports of endothelial upregulation of CD13 under hypoxic conditions (Bhagwat et al., 2001).

When comparing our dataset with pericyte death under conditions of oxygen glucose deprivation in brain slices extracted from the rat cerebellum, clear differences can be observed. These are likely due to pericyte damage during tissue processing, differential O_2 diffusion and placing pericytes in an environment lacking endothelial tone and a steady state of blood/plasma flux. Therefore, we take observations of pericyte death *ex vivo* into consideration, but would not attempt to state that they reflect the truth *in vivo,* particularly because of the large amounts of pericyte death reported in sham preparations in *ex vivo* models (Hall et al., 2014). Subsequently, in the same paper, the authors report 75% pericyte loss after 22.5 hours of a 90-minute fMCAo surgery. We find these data convincing, as our model show approximately 50% pericyte loss after 24 hours following 60 minutes of fMCAo and we would expect the number of dying pericytes to scale with the duration of ischemia as damage within ischemic tissue scales with the severity of the occlusion and the duration (Dirnagl and Macleod, 2009). We find the observation that a small population of remaining pericytes become cleaved caspase 3^+ on day 3 post stroke in the infarct core to be highly likely, as we also report low levels of on-going pericyte death on day 3 post-stroke which could be mediated through this mechanism (Fernández-Klett et al., 2013).

Moreover, our investigation into pericyte density in PDGFRbEGFP mice on day 3 post-stroke reveals an approximate 60% reduction in pericyte density proximal to the MCA territory when examining $EGFP^+$ pericytes. These data synergize nicely with $TUNEL^+$ pericyte data presented previously (Fig.20) and the aforementioned publications and we therefore believe a combination of all datasets to triangulate on the true nature of pericyte decline (Fernández-Klett et al., 2013).

Taken together, the datasets would appear to present pericyte death as an acute phase phenomenon, with a small number of pericytes dying in the hyper-acute phase through unregulated necrosis followed by a wave of pericyte death claiming a larger population due to terminal membrane failure in which pericytes stain propidium $iodide^+$ and then become $TUNEL^+$ thereafter. This results in approximately 50% pericyte loss in the infarct core, with a further 10% reduction in pericyte density occurring in the sub-acute phase, likely through a mechanism involving apoptosis inducing factor (AIF) or cleaved caspase 3 mediated apoptosis. Interestingly, our qualitative observations of pericyte visibility decline in *in vivo* experiments would support this viewpoint (Fig.36). Here, we observe pericyte loss peaking on day 3 post-stroke, not 24 hours post-stroke. This likely reflects the time-taken for EGFP to degrade (15 hours, (Danhier et al., 2015)) and so naturally pericyte death at 24 hours would still leave the pericyte visible for up to 39 hours post-death if pericytes degenerate on the vessel and are not removed by local activated microglia, which is speculated by prior investigations (Hall et al., 2014).

In conclusion, pericyte death is a region dependent acute response to stroke and regions in which pericytes survive within the infarct core are likely to be perfused by the distal branch of the MCA, possibly in specific sections of particularly hypoxic tissue reminiscent of previously reported mini-cores and mini-penumbras after stroke (del Zoppo et al., 2011). Ultimately, this appears to leave many cortical pericytes intact in a hypoxic environment, where they no longer receive input from neurons or astrocytes (Fig.23). While the reasons for pericyte death were not fully explored within the focus of this thesis (because it is surviving pericytes that represent an opportunity for pericyte directed therapy), we speculate that loss of membrane potential due to highly ischemic conditions for one hour will ravage the pericyte population. Curiously, we note that membrane damage apparent in the form of blebs *in vivo* does disappear in some cases (Fig.36.B) but we speculate many of the pericytes visibly affected during stroke will die between day 1 and day 3 post-stroke.

One more point of inquiry relates to ‘pericyte death in rigor’. While we note that the majority of membrane-damaged pericytes appear constricted (Fig.22, 36) our qualitative data would suggest that at least in the cortex, pericytes degenerate between days 1 and 3 and that in this time, their constrictive capacity declines in accordance with their degeneration. Consequently, we would expect a modification of this theory in relation to cortical pericytes, which appear to die slower. We find it more plausible that a pericyte must be alive to constrict, as prolonged degeneration appears to be associated with vessel expansion (Fig.36.D). Moreover, when comparing our results to those of laser ablation studies of pericytes, in which pericytes also degenerate after one to three days, the vessel also expands (Hartmann et al., 2021, Berthiaume et al., 2018a).

Taken together, we speculate that complexity of the cytoskeleton is required to produce a constrictive effect, a complexity that one would expect to be compromised once apoptotic processes are initiated. As apoptotic vesicles containing the cytoskeleton are formed during pericyte degeneration, this constrictive effect should no loosen a pericytes grasp on its associated vessel, with a loss of basal tone and vessel expansion following in sequence. Such a scenario would mimic those pericytes which appear to recover basal tone 24 hours post-stroke in our dataset, but vessel expansion would continue further after the pericyte degrades between day 1 and day 3 (Fig.36.D).

Conversely, if pericytes die via unregulated necrosis (an unregulated form of cell death), we would expect the effect to be congruent with the idea of ‘pericyte death in rigor’. In such a scenario, one would indeed expect a long-lasting resistance to flow at these former pericyte locations; however, from 890 pericytes imaged in the ischemic brain, we did not see any evidence of this in the upper layers of the ischemic cortex. Put simply, we saw no pinched vessels at locations pericytes used to be - throughout our dataset. Importantly, in future work, 3-photon imaging, which will allow us to penetrate deeper into the brain may provide evidence for the existence of both hyper-acute and prolonged pericyte degeneration *in vivo*, and provide an understanding of the threshold of ischemia required for each possible pathway of pericyte death. This will be important in future to develop a therapeutic strategy targeting pericytes for the improvement of stroke outcome.

6.3.1 Understanding regional differences in pericyte death within the ischemic brain

One confounding limitation of the data presented within this thesis relates to the use of the transient fMCAo model to assess pericyte death. Though this model is well established, and accurately simulates both ischemia and reperfusion injury, it is susceptible to variation like other precisely controlled permanent stroke models such as distal coagulation of the MCA or photothrombotic stroke induction because of the unique anatomical nature of each mouse stroked, and the presence of collaterals (Fluri et al., 2015). Though this variation itself mimics the unique aspects of human response to stroke, it can lead to difficulties when observing the phenomenon of cell death described in this thesis.

We observe the highest reductions of pericyte density posterior to, and directly where the main branch of the MCA enters the brain. Specifically we observe a 60% reduction within the posterior MCA territory and a 40% reduction in pericyte density within regions perfused by the main branch of the MCA (Fig.23.D). The high level of pericyte loss at this location within the mouse brain is not surprising, as lenticulostriate arteries which perfuse the striatum, basal ganglia and regions of the thalamus are reported to be ‘end’ arteries which have little access to collaterals or proximal anastomoses (Bozzao et al., 1989). Though variable interferences in flow after insertion of the filament during fMCAo occur, we validated the reliability of the experimentation performed and so the level

of ischemia caused at 'end' arteries that perfuse the striatum should be severe (Fig.19) (Zhang and Faber, 2019). Contrastingly, we observe a pericyte density reduction of just 20% in the anterior cortex (Fig.23.D). We speculate that though the level of ischemia was sufficient to eradicate neurons within this region, pericytes may outlive neurons and subsequently be able to make use of the energy supplied by neighboring collaterals or retrograde flow from vasculature proximal to the infarcted region during and after stroke. Pial collaterals are well known to connect the outermost branches of the MCA, anterior communicating artery and posterior communicating artery trees (Faber et al., 2014, Nishijima et al., 2015, Bang et al., 2015). When one of these arterial tree systems becomes blocked or receives insufficient blood supply, in this case the MCA, it has been shown that leptomeningeal collaterals (LMCs) emanating from the ACA can provide a retrograde source of blood flow, which may indeed sustain anterior cortical pericytes, but not terminally damaged neurons (Ma et al., 2020). Though it is not known when LMCs are recruited after stroke in humans, the recruitment of blood flow from LMCs to an ischemic zone has been shown to occur immediately in mice (Akamatsu et al., 2015). LMCs in humans are found in varying magnitude in 80% of stroke patients with an MCA occlusion, and if this mechanism provides an extended period of survival to pericytes, differential caudal rostral survival of pericytes may therefore translate to human stroke as well (Tariq and Khatri, 2008). Overall, the selection of the filament middle cerebral artery occlusion model allowed the investigation of how pericytes respond to severe ischemia, like other models such as coagulation of the distal MCA and photothrombotic stroke, but it also permitted the study of how ischemic pericytes respond once blood flow is restored.

6.4 'No-reflow'

One of the key novel aspects of this thesis is the attempt to longitudinally follow pericytes in the post-stroke brain with a view to determining their fate and the duration of their influence over the vessel in the context of 'no-reflow'. This has important clinical implications as alluded to in the introduction section because 'time is brain' and the transition of penumbra to infarct is inevitable in the context of sustained oligemia. Therefore, it is imperative to ascertain whether pericytes permanently constrict vessels in the aftermath of ischemia to identify a therapeutic window for treatment of these cells, which govern how blood flow and resistance to blood flow will be distributed throughout the brain.

6.4.1 Pericytes entrap non-flowing vascular elements during and acutely after reperfusion of the occluded artery

To ascertain whether the pericyte constriction observed within our *in vivo* experiment was causally responsible for 'no-reflow' after stroke, we analyzed the frequency of capillary stalls within stroke and sham groups. This is important because previous reports suggest that pericytes may be responsible for inducing erythrocyte arrest despite the reopening of the occluded artery following ischemia, but provide little convincing evidence of this at the single cell level (Yemisci et al., 2009). Though we lack dynamic RBC flux measurements of erythrocyte stalling in action due to the nature of our experimental setup, which is something we can address in future. We can confidently assess whether a vascular segment is flowing or non-flowing because of the time it takes for each singular z-step of 2-photon scanning across a capillary to complete (see methods section 4.3.7). Strikingly, our data fully confirm existing findings which indicate blood flow is interrupted at nodal sections within the vasculature and indicate that during stroke, 1 in 3 pericytes are associated

with capillary stalls (which themselves are found more frequently during and after stroke, than after sham surgery) (Fig.32.A, B, D) (Yemisci et al., 2009). This can be expected to exacerbate on-going ischemia within the capillary bed associated with the stall, precisely at the pericyte soma location.

Furthermore, 90 minutes post reperfusion of the occluded artery; we find a persistently higher amount of capillary stalls at pericyte locations after ischemia when compared against sham pericytes. In this scenario, 1 in 10 pericytes are associated with capillary stalls and this data provides indirect evidence that pericytes play a causal role in 'no-reflow' by functionally impairing the flow of vascular elements acutely after reopening of the occluded artery (Fig.32.D, upper). This is expected, as our data demonstrate that the majority of the pericyte population remain constricted acutely after reperfusion of the occluded artery and is consistent with previous literature (Fig.33) (Yemisci et al., 2009). Importantly, unlike other models of ischemia that assess pericyte contraction, this effect in our experiment appears to be transient, because ischemic pericytes are no longer associated with capillary stalls 24 hours after stroke when compared to sham pericytes (Yemisci et al., 2009, Hall et al., 2014). In future, scaling the length of ischemia to define upper and lower limits on the time required to produce long-lasting pericyte constriction after reperfusion must be performed to delineate and better understand how pericytes contribute to 'no-reflow'. Cumulatively, these data clearly indicate that during the acute phase, 'no-reflow' is *transiently* promoted by functional impairment of pericytes acutely after the reopening of the occluded artery after one hour of ischemia. Given that the majority of capillary stalls were found near the upper cortical surface within our dataset, we speculate this may jeopardize the function and health of the microvasculature in deeper cortical layers, and may underlie the loss of signal we observe in lower cortical layers (Fig.36.A).

6.4.2 Bi-phasic constriction of pericytes after stroke

To date, very little research has been performed on the sub-acute phase of ischemic stroke concerning no reflow in pericytes, making comparison to existing data difficult. This is in part, due to previous publications, which suggest pericytes constriction is followed by 'death in rigor' (Hall et al., 2014). Consequently, it is implied that the vasculature can no longer be perfused to sufficient levels because of pericyte constriction, leading to tissue necrosis. In such a scenario, the researchers state 'death of pericytes in rigor, after they have been constricted by a loss of energy supply, should produce a long-lasting increase in the resistance of the capillary bed. '. While we find this theory entirely plausible in regions proximal to the main branch of the MCA territory (striatum), the data generated by our *in vivo* experiment in the upper layers of the somatosensory cortex, which is perfused by the distal MCA, are not entirely compatible with this conclusion. Our data indicate that pericytes ubiquitously constrict during ischemia (87% of pericytes, Fig.31) and the majority of the population remain constricted 90 minutes post-reperfusion of the occluded artery (68% of pericytes). However, when the capillary diameter at pericyte soma at 24 hours post-stroke is measured, each pericyte sub-type population has relatively equal proportions of constricting, dilating and baseline diameter associated pericytes (Fig.33, Fig.40).

Consequently, pericytes display an average vessel diameter that is no longer significantly different compared to their pre-stroke baseline levels. These temporal differences strongly suggest a transient recovery phase of pericytes at 24 hours, in which the proportion of constricting pericytes dramatically decreases concomitant with an increase of the dilating pericyte population and a gradual increase in pericytes reaching baseline diameter one day post stroke. The reasons for this global shift toward baseline diameter may lie upstream and if not, could be many fold in

relation to pericytes. Pericytes damaged and thus constricted initially by stroke may have recovered, pericytes originally at baseline diameter may have dilated to compensate for those still constricting and pericytes that are irreparably damaged may begin to degenerate (Fig.22), releasing their control of basal tone in a manner that appears dilatory when, truly, it is a loss of basal constrictive tone due to pericyte death. It is unfortunate we were unable to decipher this within the time period required for the thesis, although many of the pericytes shown in Figure 36C/D appear to dilate before disappearing from view and may represent a significant proportion of those pericytes dilating at 24 hours. Nevertheless, this apparent convergence in the relative populations of pericytes constricting, dilating and at baseline diameter will result in an increased perfusion relative to prior time-points, which is reflected at the mesoscale level (Fig.29.D) in which blood flow alterations post-stroke are no longer significantly different to those of sham animals at the 24 hour time point. It is important to note we cannot exclude the contribution of collateral flow as a contributor to mesoscale measurements of blood flow. We would not consider this an artifact however; as it is entirely possible that pericyte survival is dependent on the opening of lepto-meningeal collaterals (Bozzao et al., 1989, Tariq and Khatri, 2008, Akamatsu et al., 2015, Bang et al., 2015, Nishijima et al., 2015, Zhang and Faber, 2019, Ma et al., 2020). Measurements of blood flow direction and diversion following stroke could be performed in future to address this and will provide useful information on the issue. Ultimately, our data indicate that blood flow transiently increases 24 hours post-stroke and in that time, the mean relative diameters of pericyte sub-types recover to baseline levels. These findings impart critical new information regarding ‘no-reflow’ in relation to pericytes, and suggest that initial constriction induced by ischemia is transiently compensated at 24 hours post-stroke by an increase in the dilating pericyte population and the amount of pericytes which expand vessel diameter back toward baseline levels.

By tracking the same pericytes into the sub-acute phase, intriguingly, our data show a second phase of pericyte constriction. We find that after 24 hours, thin-strand and junctional pericytes constrict the vasculature again by an average of 6% on days 3 and 7 (Fig.33). Although, we see no such significant difference in the mesh pericyte population, suggesting a pericyte sub-type dependent effect on bi-phasic constriction. This secondary constriction represents a divergence of constricting, dilating and baseline associated pericyte populations in which constricted pericytes again dominate the control of blood flow - accounting for control of approximately half of all pericyte controlled vessel diameters (Fig.33, Fig.40). Consequently, this would be expected to reduce blood flow across the cortex and our mesoscale data obtained from the laser speckle

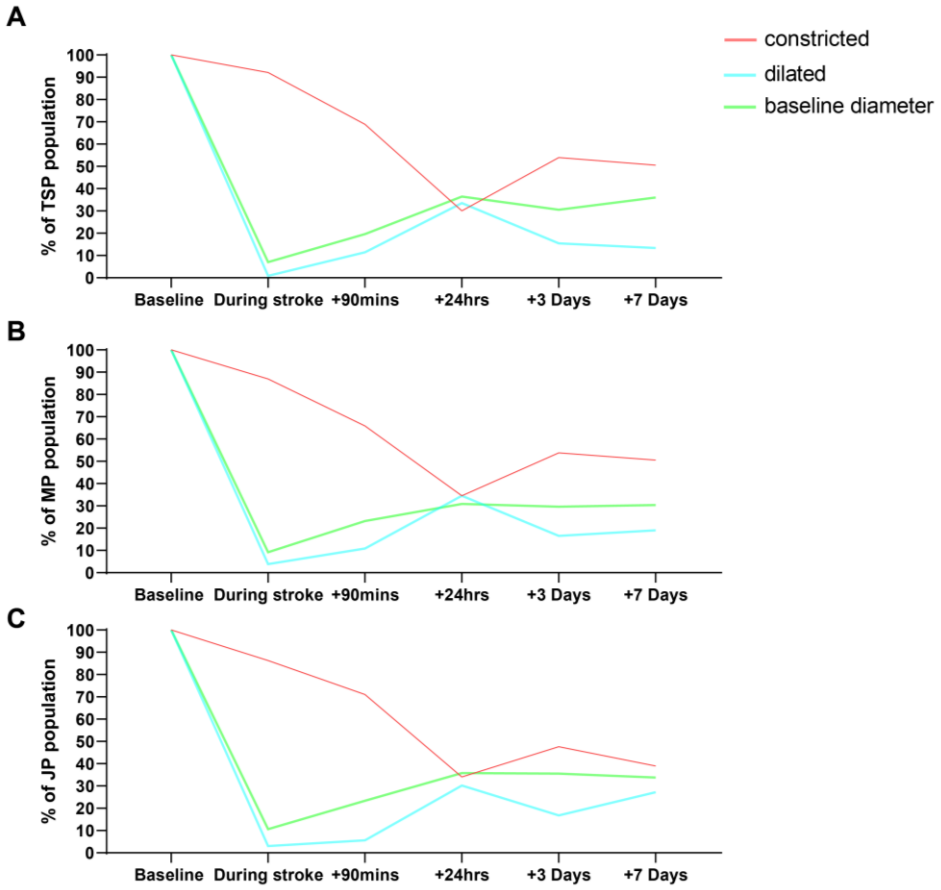

Fig. 40. Pericyte population behavior post-stroke.

A,B,C) Percentage of each stroke pericyte sub-type either constricting, dilating or maintaining baseline diameter over the course of experimental series.

support this view (Fig.29.D); with a drop of 15% in blood flow in the stroke group from 55% of baseline to 40% of baseline pre-stroke levels. Though not significant on day 3 when compared against the sham group, blood flow at the mesoscale is significantly reduced in the stroke group compared to the sham group on day 7, suggesting a delayed hypoperfusion of the upper cortex because of a second phase of milder pericyte constriction. We do not believe this has been reported before, however we speculate that this reduction in blood flow may mimic the sequelae of pericyte degeneration reported elsewhere (Kisler et al., 2017b). In recent publications, researchers used pdgfrb$^{+/-}$ mice, which display a 25% loss of pericytes at 1-2 months of age and found a gradual reduction in oxygen supply to the brain as a result of neurovascular uncoupling, put simply, neurons could no longer efficiently communicate with pericytes to confer a basal tone or effectively dilate pericytes during functional hyperemia. This may indeed lead to a deleterious feedback process in which neurons further degenerate due to limited oxygen supply.

Our experimental series likely functions to display the reverse of these results. We show that living neurons are completely eradicated from the infarct core within 24 hours and are not found in stroked PDGFRbEGFP mice on day 3, while pericytes can survive in a region dependent manner in the infarct core, particularly in the cortex (Fig.19, 20, 23.A). These findings allude to the possibility that pericytes no longer receive crucial feedback from neuron firing, such as potassium release after neuronal activity, which is reported to initiate a decrease in intracellular Ca^{2+} in pericytes, which one would expect to cause pericyte dilation. Recent research performed in the lab

of Bruno Weber by Chaim Glück gives credence to this idea (Glück et al., 2020). The researchers propose that activity induced extracellular elevations in potassium act to suppress intracellular Ca^{2+} increase in pericytes through Kir2.2 and K_{ATP} activation. Inwardly rectifying potassium channels such as these are found extensively within the pericyte transcriptome and are present in our data (Fig.26.B, Kcnj8) and could also mediate these effects (Longden and Nelson, 2015). If potassium release from neurons is necessary to maintain a certain level of dilatory basal tone in pericytes, it would logically follow that on days 3 and 7 post stroke, when capillary pericytes (which sit on average 8 ~ 23 µm away from neurons, (Hall et al., 2014)) no longer receive this external messenger from neuronal activity, that constriction follows. This may explain the second phase of constriction we observe post-stroke, but it is one of many possibilities which further investigation will help to elucidate.

Nevertheless, here we identify a previously unknown bi-phasic constriction in pericytes after stroke, which is reflected in mesoscale blood flow (Fig.29.D, Fig.35.A, B, C), the second wave of which occurs after the initial phase of pericyte cell death (>24 hours). Indeed by looking deeper at the relationship between pericyte constriction and laser speckle blood flow alterations within the stroke group, we observe a significant Pearson correlation ($p<0.04$) between changes in lumen diameter at pericyte soma and laser speckle blood flow changes over time. Furthermore, when assessing the relationship between laser speckle blood flow alterations and pericyte-associated vessel diameters, we observe an R^2 value of 0.79, suggesting pericyte influence over vessel diameter is indeed contributing causally to mesoscale alterations in blood flow post-stroke (Fig.35.C). We do not find this surprising, as the capillary bed and capillaries proximal to feeding arterioles offer the largest hydraulic resistance to cortical blood supply and may explain the current observations (Gould et al., 2017). In turn, we speculate that this could cause further ischemic damage and impart a greater vaso-modulatory burden on the remaining pericytes associated with the vasculature, where they fail to maintain adequate blood flow to the injured cortex - with blood flow only reaching 50% of pre-stroke baseline levels.

6.4.3 Interrogating pericyte sub-type behavior post-stroke

Curiously, during our investigation into pericyte sub-types and their differential constrictive effects, we realized that thin-strand pericytes constricted significantly more than mesh or junctional pericytes (Fig.31). We have previously mentioned why we find this counter-intuitive (6.2.2) when viewed from a classical standpoint of the mechanical machinery involved in conferring constriction, but viewed from other angles, it makes logical sense. Thin-strand pericytes may not be dependent on αSMA for contraction and according to beautiful work carried out by Roger Grant and David Hartmann and others, have a total cell length of 159 µm on average within the mouse cortex (Grant, 2019, Hartmann et al., 2021). While this may be an efficient way to maintain adequate coverage over the endothelium, under pathological conditions it may confer a disadvantage. Conceivably, the large surface area covered by these cells may make them particularly susceptible to ROS species generation, which occurs at high-rates within the microvasculature during stroke (Yemisci et al., 2009). In contrast, mesh and junctional pericytes have average vessel lengths of 100 µm, which may make these sub-types less exposed to constrictive, damaging extracellular compounds.

Therefore, we find it conceivable that thin-strand pericytes may be the weakest link in the pericyte connectome chain, as they reside typically on solitary lengths of capillaries, distal to bifurcations and further away from other neighboring pericytes on higher branch orders than mesh or junctional pericytes (Kovacs-Oller et al., 2019). This may expose thin-strand pericytes to complete

ischemia, where junctional pericytes may receive low levels of oxygen due to their location over capillary bifurcations. Furthermore, mesh pericytes, which typically reside on larger capillaries and at lower branch orders within the capillary network, contain a larger pool of αSMA, which may take longer to degrade under ischemic conditions. While these constrictive effets may stymie blood flow, and in 17% of the stroked mesh pericyte population be associated with capillary stalls, as a population, they may not bring blood flow to a complete standstill.

Contrastingly, thin-strand pericytes and junctional pericytes were found trapping non-flowing vascular elements significantly more frequently than mesh pericytes and both significantly reconstricted in the sub-acute phase when compared against sham pericytes within our dataset. Indeed one in three thin-strand and junctional pericytes were associated with capillary stalls in our dataset during stroke, suggesting that in combination with their contractile capacity, they induce flow arrest much more often. Importantly, damage was non-uniformly disturbed across pericyte sub-type populations as well, with thin-strand pericytes showing the highest percentage of damaged membranes (59% TSP vs 57.5% MP & 47.5% JP, Fig.21). Furthermore, of all pericyte sub-types that disappeared from view during *in vivo* experimentation, we observed the loss of thin-strand pericytes most frequently (40% loss in TSP, 30% loss of MP and 20% loss of JP, Fig.33, 36.D).

Taken together, multiple lines of enquiry from our experimentation converge on the notion that thin-strand pericytes may be a particularly sensitive sub-type during ischemic conditions and that mesh pericytes appear to be more resilient. We speculate this could reflect a combination of their location within the capillary network and non-flowing elements within it, contractile apparatus, and susceptibility to damage and exposure to O_2. Unfortunately, one limitation of our study was that our investigation into pericyte death was performed prior to characterization of pericyte sub-types reported in the aforementioned work (Grant, 2019), therefore, we are sadly unable to discern at the current time, differences in death within distinct pericyte sub-type populations.

6.4.4 Limitations of *in vivo* experimentation on the pericyte response to stroke

Within the *in vivo* experiments described here, we reveal how pericyte sub-types constrict the microvasculature during ischemia, post-reperfusion and negatively contribute to the 'no-reflow' phenomenon in a bi-phasic manner post-stroke to a degree which is observable in mesoscale alterations in blood flow in the somato-sensory cortex (Fig.29 - 36). However, the results described here necessitated many rounds of iterative improvement in experimental design. Though we have achieved our primary aim of imaging ischemic pericytes *in vivo* through careful selection of many criteria*,* many caveats associated with *in vivo* imaging must be addressed, as they may impose an impact on the phenomena we observed.

Firstly, we imaged pericytes through the implantation of a 4 mm round chronic cranial window after removing the skull and dura from the somatosensory cortex of our mice. We chose not to thin the skull but remove it due to its opacity and negative effects on imaging quality (Xu et al., 2007). Although all mice were imaged one month after implantation of the cranial window, many acute inflammatory processes (reported to peak at 3 - 10 days post drilling of the cranial window) may not be entirely resolved. Reports of chronic astroglial and microglial reactivity post-cranial window implantation show that most glial reactivity is resolved after 3 - 4 weeks, but despite this, we cannot exclude low levels of on-going inflammation (which are undetectable through histological methods) affecting our observations of the NVU in a fully nascent, naïve state (Goldey et al., 2014, Holtmaat et al., 2009).

A more serious consideration is that we removed the dura mater before the chronic cranial window was implanted, while this conveys several imaging advantages because the dura is not fully transparent and can regrow; it also compromises several physiological functions of the brain. Removing the dura can compromise cortical layer 1 in mice, promote tissue swelling and alter intracranial pressure if not performed carefully. Therefore, a colleague (Severin Filser) with extensive experience in this area performed the chronic cranial window procedure (Dorostkar et al., 2014, Luckner et al., 2018). Nevertheless, this may stimulate vascular growth on the surface of the brain and rearrangement of pericytes as even minor manipulations of the dura can elicit cortical spreading depolarizations (Ayata et al., 2004). Despite this, we imaged both sham and stroke mice with the dura removed and any alterations caused by dura removal we therefore expect to be the same in both groups.

One further cause for caution is the use of medetomidine in our experimental paradigm. Though the amount of medetomidine used was low (100 mg/kg) and retains mouse consciousness at a level high enough to enable modelling of cortical networks using transgenic neuronal Thy1GCaMP6 mice, it is possible that this interfered with stroke outcome (Cramer et al., 2019). Medetomidine is an adrenergic α2- agonist that was used in our experimental paradigm to sedate animals prior to *in vivo* imaging at the 2-photon microscope and laser speckle imaging platforms. In addition to its sedative effects, additional effects include peripheral hypertension, hyperglycaemia, diuresis, muscle relaxation and analgesia. Specifically, medetomidine causes sedation through activation of α2-adrenoreceptors in the locus coeruleus, which prevents excitatory neurotransmitter release in the CNS, and therefore depresses cortical arousal. It is therefore possible that administration of medetomidine in our stroke animals suppresses excitatory neurons during on-going ischemia; and that this leads to reduced amounts of excitotoxic cell death in our experimental paradigm. Though we note that this does not prevent neuronal cell death in our model (Fig.28), it may alter the rate at which excitotoxic compounds are released into the brain parenchyma. This may differentially affect the pericyte response and their tolerance to ischemic damage. Nevertheless, we also see pronounced pericyte survival in the absence of medetomidine administration from our *ex vivo* experimentation (Fig.19, 20, 22, 23).

Another caveat in our *in vivo* experimental paradigm relates to the glass covering the cranial window itself. Under normal conditions, the temperature at the cortical surface of the brain is similar to the core temperature of mice (38-39°C). However, under the glass of a chronic cranial window, temperatures are reported to be 2-3°C lower than normal physiological parameters, which may influence cerebral blood flow (Roche et al., 2019). Furthermore, we imaged the cortex through a 20x water immersion objective at the 2-photon for approximately 30 minutes during a one hour transient filament middle cerebral artery occlusion. During this time, research shows that the brain would have dropped by 2-3°C close to the cortical surface, which may have caused a drop in resting capillary flow, capillary pO2, haemoglobin saturation and tissue pO2 (Roche et al., 2019). While this undoubtedly altered the rates of the phenomena we observed, this difference was consistent across both sham and stroke mice groups.

Taken together, several caveats must be applied to the *in vivo* results generated within this thesis, but all applied caveats were consistent across both sham and stroke treated animals, and we expect all caveats mentioned to alter the brain in a less severe way that the induction of ischemia itself. As a whole, our dataset represents a window on the true phenomena occurring during and after stroke, though it cannot claim to reflect the true nature of the pericyte response in an entirely unaltered physiological brain. To address this in the future, 3-photon microscopy can and will be

used through the intact skull and dura, enabling a more realistic picture on how pericytes respond to stroke, though it will also be subject to its own experimental limitations.

6.5 Pericyte activation in the sub-acute phase of stroke

Pericytes are generally considered to respond differentially with respect to their location in the infarcted hemisphere of the brain. Pericytes within the infarct core are widely reported to be deleterious for neuronal survival because of interruptions in microvascular flow and the negative impacts pericyte death imparts on BBB integrity, ultimately, promoting the transfer of penumbra to infarcted tissue as a consequence of 'no-reflow'. Conversely, pericytes in peri-infarct tissue are widely reported to be favorable for stroke outcome (Ozerdem and Stallcup, 2003, Gerhardt and Betsholtz, 2003, Zhang et al., 2012). Within peri-infarct tissue, a range of reports indicate that pericytes detach from vessels and engage in an activation state which promotes neurogenic and angiogenic properties within at risk tissue. This is in part, due to the plastic nature of pericytes, which have been found to dynamically remodel the vasculature in laser ablation studies and mouse models of epilepsy (Berthiaume et al., 2018a, Arango-Lievano et al., 2018).

Our *ex vivo* findings fully support the existing data in this regard. We find significant upregulation of pericyte coverage in infarct core and peri-infarct tissue on day 3 post-stroke, maintenance of vessel density and the appearance of pericyte clusters that we term 'proliferation bodies' within the infarct core and peri-infarct borders (Fig.21). We hypothesize that this occurs as a result of PDGFb upregulation in regions proximal to hypoxia and ultimately serves to confine tissues suffering from ischemic damage from those regions of the vasculature still salvageable after stroke (Schito et al., 2012). Endothelial cells, which survive stroke preferentially compared to pericytes (Hall et al., 2014) start to proliferate and produce angiogenic sprouts as early as 12 - 24 hours post ischemia resulting in new vessel formation in peri-infarct regions on day 3 post-stroke (Hayashi et al., 2003, Beck and Plate, 2009). In tandem, upregulation of PDGFb by endothelial cells within the core of the infarct should benefit pericyte recovery as the reciprocal interaction between PDGFb and PDGFRb promotes pericyte survival (Olson and Soriano, 2011).

The appearance of proliferation bodies (Fig.21) within our dataset also fits well with previous research as concomitantly with endothelial cell proliferation, pericyte proliferation is also reported in peri-infarct tissue where they attach to newly formed vessel sprouts and ensure their maturation (Dore-Duffy et al., 2000, Dulmovits and Herman, 2012). Interestingly, while some of this research implies that pericytes detach from the vessel wall in order to mediate this angiogenic effect, we see PDGFRb pericyte proliferation bodies appearing within the Collagen IV^{+} basement membrane, which is more in-line with how neuroblasts migrate to sites of injury post-stroke (Thored et al., 2007). A novel aspect we believe to be at play within our dataset, is the difference in number of proliferation bodies in each region affected by stroke. We observe that stroke induces the appearance of these proliferation bodies 24 hours after stroke in both infarct and peri-infarct regions, however a significant increase in the number of proliferation bodies from day 1 to day 3 post-stroke is only observed in peri-infarct tissue and not in the infarct core. This may suggest that a population of pericytes are inhibited from progressing through the cell cycle within the infarct core, and would be in-line with previous publications which imply that OGD inhibits cell cycle progression in pericytes through down regulation of several cell cycle proteins that act to arrest pericytes at the G2/M phase checkpoint (Wei et al., 2017).

Despite this, our data strongly imply that a population of pericytes (5 - 20%) affected by stroke in the ipsilateral hemisphere are committed to engage in cell cycle entry (Fig.24) with around 10-

20% of pericytes up-taking and incorporating the nucleotide EdU into their DNA and staining positive for the cell cycle entry marker Ki67. These findings are strengthened by FACS isolation and transcriptomic analyses of pericytes within the infarct core, of which 70% are associated with cell cycle entry. Congruent with the previous histological data (Fig.24), 30% of pericytes in the ipsilateral hemisphere also show transcriptional commitment to cell cycle entry (Fig.26.C). These findings are entirely consistent with existing literature where the number of $CD13^{+}$ $Ki67^{+}$ pericytes significantly increases after stroke on day 3 (Fernández-Klett et al., 2013) and under conditions of ischemia in skeletal muscle, where pericyte proliferation is also reported at the transcriptomic level (Teng et al., 2021). It remains to be determined whether this proliferation is truly beneficial for stroke outcome or whether it contributes to the beginning of aberrant angiogenesis(Yao et al., 2014).

Concomitant with the proliferation and expansion of the pericyte population observed within our dataset and those within the literature, a strong upregulation of PDGFRb is reported, which is replicated within our transcriptomic dataset and is accompanied by the upregulation of a myriad of genes associated with extracellular matrix deposition such as: Col18a1, Col3a1,Col4a1, Bmp1, Dcn, Mmp11 and sparc (Fig.28, gene ontology analyses). These data are entirely consistent with reports of pericytes contributing to extracellular matrix deposition post-stroke (Fernández-Klett et al., 2013) and encompassed by a broadly conserved transcriptional program of wound-repair exerted by pericytes in response to acute injury. Though this dramatic extent of extracellular matrix deposition appears to perform a beneficial role in stroke recovery (Kamouchi et al., 2012), it is not favorable in all disease contexts and appears to inhibit the growth of axonal projections following spinal cord injury (Dias et al., 2018). Specifically here it is crucial to mention the contributions of scientists like Christian Göritz and Alexander Birbrair, who describe the existence of two pericyte sub-types that contribute differentially to tissue repair. Type 1 pericytes are $nestin^{-}$ and have remarkable regenerative capacities in the context of adipogenesis, whereas type 2 pericytes are $nestin^{+}$ and contribute to angiogenesis and neurogenesis within the CNS. Christian Göritz, who describes pericytes as Type A or type B pericytes based on the presence or absence of the Glutamate aspartate transporter (GLAST) further highlights the differences between pericyte subtype populations in the context of injury. In a recent paper, his team describe that type A pericytes (GLAST expressing, representing 10% of all $PDGFRb^{+}$ pericytes) as the scar forming pericyte sub-type after ischemic stroke. Currently, due to the bulk sequencing nature of our transcriptomic analyses, it is not possible to dissect these two distinct populations from one another, but it is likely that the pericytes that enter the cell cycle in the infarct core and peri-infarct regions on day 3 after stroke in our dataset represent type A pericytes.

In conclusion, our transcriptomic analyses and histological data on pericyte activation after stroke mimic recent work by others and suggest that pericytes proliferate in response to stroke in order to form a fibrotic scar around the lesion and that this process is on-going on day 3 (Birbrair et al., 2014). This may serve to limit the exfiltration of harmful damage associated molecular patterns (DAMPs) into functional parts of the ipsilateral hemisphere, cordoning the damaged brain from regions of the intact brain and stimulating angiogenesis that ultimately benefit stroke recovery. Conversely, one could also argue that it secures the fate of the ischemic tissue over-time, inhibiting neurogenesis once neurons have died following ischemia. This may prevent previously ischemic tissue from any chance of repopulation with a newborn set of neurons derived from the sub-ventricular zone, which ultimately are forced to settle on peri-infarct tissue proximal to the lesion (Liang et al., 2019, Cheng et al., 2018). While it may be possible to modulate pericyte activation in the sub-acute phase in a manner beneficial to stroke recovery, those engaged in pericyte research would target pericytes earlier in an attempt to ameliorate stroke outcome.

7. Targeting pericyte dysfunction to ameliorate stroke outcome

Our results confirm *in vivo*, embellish and specify how pericytes contribute to the 'no-reflow' phenomenon in the upper cortical layers in the context of transient cerebral ischemia and support the notion that pericytes jeopardize reperfusion following stroke. To that end, given that 'time is brain' during ischemia, we echo the thoughts of pericyte researchers (such as David Attwell, Turgay Dalkara and Catherine Hall) who believe targeting pericytes immediately upon reperfusion may be the best therapeutic approach to promote tissue and by extension, neuronal survival. Incomplete reperfusion is a consistent feature of patients suffering from stroke who have undergone intra-arterial or intra-venous recanalization therapies, of which only 20% are eligible to begin with (Albers et al., 2018, Horsch et al., 2015). Furthermore, throughout several clinical studies, reperfusion has been shown to be best predictor of outcome following stroke in patients (del Zoppo et al., 2011). Despite the view that reformation of micro-thrombi downstream of the primary clot may be involved, and recent reports that leukocyte plugging plays a previously underappreciated role (El Amki et al., 2020), it is overwhelmingly clear due to evidence from the basic science to clinical level that microcirculatory impairment plays a leading role in 'no-reflow'. Our data show that pericytes play a significant role in mediating that impairment.

These findings are likely translatable to humans, and are made particularly clear in primarily angiograms of contrast material injected distally from the thrombus in patients suffering from stroke. Here, clinical evidence suggests that if the capillary network distal to the thrombus can be visualized, a favorable outcome is more likely, but in approximately 1/5th of patients, this is not the case (Al-Ali et al., 2013). Such findings highlight that the microcirculation downstream of the clot is already severely compromised, and push the need for a drug ameliorating pericyte dysfunction into the spotlight of ischemic stroke research. Critically, our research suggests that these pericytes may still be viable, but functionally impaired.

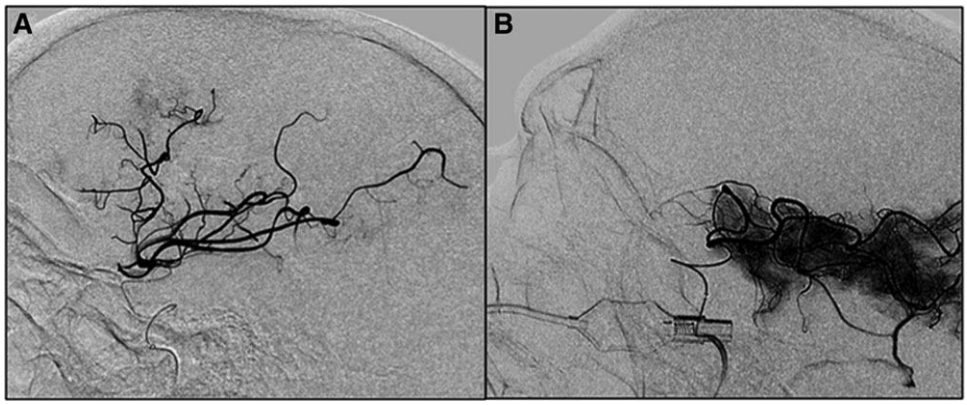

Fig. 41. Significant microcirculatory injury during ischemia negatively impacts postrecanalization reperfusion.

Adapted from (Dalkara, 2019)(Wolters Kluwer Health, Inc.) who reprinted it from (Arsava et al., 2018) with permission. **A)** microcirculation can't be visualized distal to the thrombus in 7 out of 34 patients, all of whom had an unfavorable prognosis (modified Rankin Scale [mRS] score of >2) at 90-d, in contrast 48% of patients exhibiting post-thrombus capillary filling before recanalization as shown in **B)**, had a good prognosis (mRS score =0–2) at 90-d.

7.1 Uncovering a therapeutic strategy

Given that our data and the data of others suggest that pericytes remain contracted following the reperfusion of the occluded artery, but most do not immediately die before 24 hours, it seems apparent that treating pericytes acutely after reperfusion would be a sound strategy to bridge the gap between restoration of baseline diameter and further potentiate neuronal survival. Indeed, by using adenosine (a powerful relaxant of pericyte contraction) nanoparticles injected after reperfusion researchers could restore capillary flow in mice (Gaudin et al., 2014). This data was also replicated in the context of myocardial infarction and appears to show potential (O'Farrell and Attwell, 2014). Alternative approaches also confirmed to be effective were the use of inhaled nitric oxide, which strongly relaxes pericytes and the use of free radical scavengers such as N-tert-butyl-α-phenylnitrone, which both improved 'no-reflow' after stroke in mice (Yemisci et al., 2009). While these therapies attempt to target pericyte contraction following stroke, curiously others have had equal success ameliorating plugging of the microvasculature with the use of BBB impermeable molecules such as Sodium 2-sulfophenyl-N-tert-butyl nitrone (S-PBN) to confer neuroprotection, suggesting pericyte contraction is not the only deleterious factor at play (Gursoy-Ozdemir et al., 2012).

The aforementioned therapeutic options, while attractive, are not without drawbacks. Given that our data identify a bi-phasic, long lasting contraction of pericytes interrupted by a transient recovery to baseline at 24 hours, they may need to be administered consistently for several hours after the recanalization of the occluded artery. Furthermore, while the use of adenosine nano-particles and inhaled nitric oxide acutely may not be deleterious to blood pressure short-term (Terpolilli et al., 2012, Gaudin et al., 2014), not enough is known about their long-term effects to support their clinical use to date. Moreover, none of the proposed therapies so far can claim to restore pericyte health, and therefore may promote increased blood flow into a damaged brain in which pericytes return to a damage state as soon as the therapy is ceased. We have described in this thesis how pericyte membranes are damaged during stroke and that this persists for at least 90 mins post reperfusion of the occluded artery. By taking advantage of the passive targeting that pericyte contraction provides to the sight of ischemic injury by nature of utilizing the vasculature to deliver compounds, we believe that a polypharmacy approach would be of most benefit to a stroke patient. Such a polypharmacy approach would benefit from the addition of Fasudil, which has recently been shown to ameliorate RBC trapping by pericytes *in vivo* following optogenetically mediated pericyte contraction (Hartmann et al., 2021).

Fundamentally, a drug cocktail aimed at ameliorating microcirculatory dysfunction in pericytes after recanalization should avoid risk of hemorrhagic transformation (Powers et al., 2018), recover pericyte membrane potential, restore basal tone and dilatory capacity, reduce the production of free radicals and avoid lowering blood-pressure for as long as it is administered. To date, no single drug provides such effects, though certain therapies such as 3K3A-APC (A Recombinant Variant of Human Activated Protein C) are approaching this level of effectiveness (Lyden et al., 2019).

In the coming years, a flurry of technological advances in diagnoses will enable differentiation of hemmorhagic from ischemic stroke within the ambulance, by making use of the inherent difference in absorption spectra of oxy/deoxhemoglobin, regardless of depth within the brain using holography. Concomitantly, at the basic science level, new technological imaging methods such as 3-photon imaging and mesoscale imaging modalities will help us understand the true nature of this complex multiphasic disease, and provide better definition of exactly when and how to develop better therapeutic strategies targeting at risk brain cells within ischemic tissue.

References

ABBOTT, N. J., PATABENDIGE, A. A., DOLMAN, D. E., YUSOF, S. R. & BEGLEY, D. J. 2010. Structure and function of the blood-brain barrier. *Neurobiol Dis,* 37**,** 13-25.

ABRAMSSON, A., LINDBLOM, P. & BETSHOLTZ, C. 2003. Endothelial and nonendothelial sources of PDGF-B regulate pericyte recruitment and influence vascular pattern formation in tumors. *J Clin Invest,* 112**,** 1142-51.

AKAMATSU, Y., NISHIJIMA, Y., LEE, C. C., YANG, S. Y., SHI, L., AN, L., WANG, R. K., TOMINAGA, T. & LIU, J. 2015. Impaired Leptomeningeal Collateral Flow Contributes to the Poor Outcome following Experimental Stroke in the Type 2 Diabetic Mice. *The Journal of Neuroscience,* 35**,** 3851-3864.

AL-ALI, F., JEFFERSON, A., BARROW, T., CREE, T., LOUIS, S., LUKE, K., MAJOR, K., NEMETH, D., SMOKER, S. & WALKER, S. 2013. The capillary index score: rethinking the acute ischemic stroke treatment algorithm. Results from the Borgess Medical Center Acute Ischemic Stroke Registry. *J Neurointerv Surg,* 5**,** 139-43.

AL AHMAD, A., GASSMANN, M. & OGUNSHOLA, O. O. 2009. Maintaining blood-brain barrier integrity: pericytes perform better than astrocytes during prolonged oxygen deprivation. *J Cell Physiol,* 218**,** 612-22.

ALARCON-MARTINEZ, L., VILLAFRANCA-BAUGHMAN, D., QUINTERO, H., KACEROVSKY, J. B., DOTIGNY, F., MURAI, K. K., PRAT, A., DRAPEAU, P. & DI POLO, A. 2020. Interpericyte tunnelling nanotubes regulate neurovascular coupling. *Nature,* 585**,** 91-95.

ALARCON-MARTINEZ, L., YILMAZ-OZCAN, S., YEMISCI, M., SCHALLEK, J., KILIÇ, K., CAN, A., DI POLO, A. & DALKARA, T. 2018. Capillary pericytes express α-smooth muscle actin, which requires prevention of filamentous-actin depolymerization for detection. *eLife,* 7**,** e34861.

ALARCON-MARTINEZ, L., YILMAZ-OZCAN, S., YEMISCI, M., SCHALLEK, J., KILIÇ, K., VILLAFRANCA-BAUGHMAN, D., CAN, A., DI POLO, A. & DALKARA, T. 2019. Retinal ischemia induces α-SMA-mediated capillary pericyte contraction coincident with perivascular glycogen depletion. *Acta neuropathologica communications,* 7**,** 134-134.

ALBERS, G. W., MARKS, M. P., KEMP, S., CHRISTENSEN, S., TSAI, J. P., ORTEGA-GUTIERREZ, S., MCTAGGART, R. A., TORBEY, M. T., KIM-TENSER, M., LESLIE-MAZWI, T., SARRAJ, A., KASNER, S. E., ANSARI, S. A., YEATTS, S. D., HAMILTON, S., MLYNASH, M., HEIT, J. J., ZAHARCHUK, G., KIM, S., CARROZZELLA, J., PALESCH, Y. Y., DEMCHUK, A. M., BAMMER, R., LAVORI, P. W., BRODERICK, J. P. & LANSBERG, M. G. 2018. Thrombectomy for Stroke at 6 to 16 Hours with Selection by Perfusion Imaging. *N Engl J Med,* 378**,** 708-718.

ALLEN, D. M., CHEN, L. E., SEABER, A. V. & URBANIAK, J. R. 1995. Pathophysiology and related studies of the no reflow phenomenon in skeletal muscle. *Clinical orthopaedics and related research***,** 122-133.

AMBROSIO, G., WEISMAN, H. F., MANNISI, J. A. & BECKER, L. C. 1989. Progressive impairment of regional myocardial perfusion after initial restoration of postischemic blood flow. *Circulation,* 80**,** 1846-61.

AMES, A., 3RD, WRIGHT, R. L., KOWADA, M., THURSTON, J. M. & MAJNO, G. 1968. Cerebral ischemia. II. The no-reflow phenomenon. *Am J Pathol,* 52**,** 437-53.

ANDRAE, J., GALLINI, R. & BETSHOLTZ, C. 2008. Role of platelet-derived growth factors in physiology and medicine. *Genes Dev,* 22**,** 1276-312.

ARANGO-LIEVANO, M., BOUSSADIA, B., DE TERDONCK, L. D. T., GAULT, C., FONTANAUD, P., LAFONT, C., MOLLARD, P., MARCHI, N. & JEANNETEAU, F. 2018. Topographic Reorganization of Cerebrovascular Mural Cells under Seizure Conditions. *Cell Reports,* 23**,** 1045-1059.

ARMSTRONG, S. C., SHIVELL, L. C. & GANOTE, C. E. 2001. Sarcolemmal blebs and osmotic fragility as correlates of irreversible ischemic injury in preconditioned isolated rabbit cardiomyocytes. *J Mol Cell Cardiol,* 33**,** 149-60.

ARMULIK, A., GENOVÉ, G. & BETSHOLTZ, C. 2011. Pericytes: Developmental, Physiological, and Pathological Perspectives, Problems, and Promises. *Developmental Cell,* 21**,** 193-215.

ARMULIK, A., GENOVÉ, G., MÄE, M., NISANCIOGLU, M. H., WALLGARD, E., NIAUDET, C., HE, L., NORLIN, J., LINDBLOM, P., STRITTMATTER, K., JOHANSSON, B. R. & BETSHOLTZ, C. 2010. Pericytes regulate the blood-brain barrier. *Nature,* 468**,** 557-61.

ARSAVA, E. M., ARAT, A., TOPCUOGLU, M. A., PEKER, A., YEMISCI, M. & DALKARA, T. 2018. Angiographic Microcirculatory Obstructions Distal to Occlusion Signify Poor Outcome after Endovascular Treatment for Acute Ischemic Stroke. *Translational Stroke Research,* 9**,** 44-50.

ASAHINA, K., ZHOU, B., PU, W. T. & TSUKAMOTO, H. 2011. Septum transversum-derived mesothelium gives rise to hepatic stellate cells and perivascular mesenchymal cells in developing mouse liver. *Hepatology,* 53**,** 983-95.

ASTRUP, J., SIESJÖ, B. K. & SYMON, L. 1981. Thresholds in cerebral ischemia - the ischemic penumbra. *Stroke,* 12**,** 723-5.

AYATA, C., SHIN, H. K., SALOMONE, S., OZDEMIR-GURSOY, Y., BOAS, D. A., DUNN, A. K. & MOSKOWITZ, M. A. 2004. Pronounced hypoperfusion during spreading depression in mouse cortex. *J Cereb Blood Flow Metab,* 24**,** 1172-82.

BANG, O. Y., GOYAL, M. & LIEBESKIND, D. S. 2015. Collateral Circulation in Ischemic Stroke: Assessment Tools and Therapeutic Strategies. *Stroke,* 46**,** 3302-9.

BARON, J. C. 1999. Mapping the ischaemic penumbra with PET: implications for acute stroke treatment. *Cerebrovasc Dis,* 9**,** 193-201.

BECK, H. & PLATE, K. H. 2009. Angiogenesis after cerebral ischemia. *Acta Neuropathologica,* 117**,** 481-496.

BELL, R. D., WINKLER, E. A., SAGARE, A. P., SINGH, I., LARUE, B., DEANE, R. & ZLOKOVIC, B. V. 2010. Pericytes control key neurovascular functions and neuronal phenotype in the adult brain and during brain aging. *Neuron,* 68**,** 409-27.

BERGWERFF, M., VERBERNE, M. E., DERUITER, M. C., POELMANN, R. E. & GITTENBERGER-DE GROOT, A. C. 1998. Neural crest cell contribution to the developing circulatory system: implications for vascular morphology? *Circ Res,* 82**,** 221-31.

BERTHIAUME, A.-A., GRANT, R. I., MCDOWELL, K. P., UNDERLY, R. G., HARTMANN, D. A., LEVY, M., BHAT, N. R. & SHIH, A. Y. 2018a. Dynamic Remodeling of Pericytes Maintains Capillary Coverage in the Adult Mouse Brain. *Cell Reports,* 22**,** 8-16.

BERTHIAUME, A. A., HARTMANN, D. A., MAJESKY, M. W., BHAT, N. R. & SHIH, A. Y. 2018b. Pericyte Structural Remodeling in Cerebrovascular Health and Homeostasis. *Front Aging Neurosci,* 10**,** 210.

BEVAN, S., TRAYLOR, M., ADIB-SAMII, P., MALIK, R., PAUL, N. L., JACKSON, C., FARRALL, M., ROTHWELL, P. M., SUDLOW, C., DICHGANS, M. & MARKUS, H. S. 2012. Genetic heritability of ischemic stroke and the contribution of previously reported candidate gene and genomewide associations. *Stroke,* 43**,** 3161-7.

BHAGWAT, S. V., LAHDENRANTA, J., GIORDANO, R., ARAP, W., PASQUALINI, R. & SHAPIRO, L. H. 2001. CD13/APN is activated by angiogenic signals and is essential for capillary tube formation. *Blood,* 97**,** 652-9.

BIRBRAIR, A., ZHANG, T., FILES, D. C., MANNAVA, S., SMITH, T., WANG, Z. M., MESSI, M. L., MINTZ, A. & DELBONO, O. 2014. Type-1 pericytes accumulate after tissue injury and produce collagen in an organ-dependent manner. *Stem Cell Res Ther,* 5**,** 122.

BJARNEGÅRD, M., ENGE, M., NORLIN, J., GUSTAFSDOTTIR, S., FREDRIKSSON, S., ABRAMSSON, A., TAKEMOTO, M., GUSTAFSSON, E., FÄSSLER, R. & BETSHOLTZ, C. 2004. Endothelium-specific ablation of PDGFB leads to pericyte loss and glomerular, cardiac and placental abnormalities. *Development,* 131**,** 1847-57.

BORDONE, M. P., SALMAN, M. M., TITUS, H. E., AMINI, E., ANDERSEN, J. V., CHAKRABORTI, B., DIUBA, A. V., DUBOUSKAYA, T. G., EHRKE, E., ESPINDOLA DE FREITAS, A.,

BRAGA DE FREITAS, G., GONÇALVES, R. A., GUPTA, D., GUPTA, R., HA, S. R., HEMMING, I. A., JAGGAR, M., JAKOBSEN, E., KUMARI, P., LAKKAPPA, N., MARSH, A. P. L., MITLÖHNER, J., OGAWA, Y., PAIDI, R. K., RIBEIRO, F. C., SALAMIAN, A., SALEEM, S., SHARMA, S., SILVA, J. M., SINGH, S., SULAKHIYA, K., TEFERA, T. W., VAFADARI, B., YADAV, A., YAMAZAKI, R. & SEIDENBECHER, C. I. 2019. The energetic brain - A review from students to students. *J Neurochem,* 151**,** 139-165.

BOZZAO, L., FANTOZZI, L. M., BASTIANELLO, S., BOZZAO, A. & FIESCHI, C. 1989. Early collateral blood supply and late parenchymal brain damage in patients with middle cerebral artery occlusion. *Stroke,* 20**,** 735-40.

BROUNS, R., WAUTERS, A., DE SURGELOOSE, D., MARIËN, P. & DE DEYN, P. P. 2011. Biochemical markers for blood-brain barrier dysfunction in acute ischemic stroke correlate with evolution and outcome. *Eur Neurol,* 65**,** 23-31.

CAMPBELL, B. C. V., DE SILVA, D. A., MACLEOD, M. R., COUTTS, S. B., SCHWAMM, L. H., DAVIS, S. M. & DONNAN, G. A. 2019. Ischaemic stroke. *Nature Reviews Disease Primers,* 5**,** 70.

CHABRIAT, H., BOUSSER, M. G. & PAPPATA, S. 1995. Cerebral autosomal dominant arteriopathy with subcortical infarcts and leukoencephalopathy: a positron emission tomography study in two affected family members. *Stroke,* 26**,** 1729-30.

CHABRIAT, H., JOUTEL, A., DICHGANS, M., TOURNIER-LASSERVE, E. & BOUSSER, M. G. 2009. Cadasil. *Lancet Neurol,* 8**,** 643-53.

CHAIT, L. A., MAY, J. W. J., O'BRIEN, B. M. & HURLEY, J. V. 1978. THE EFFECTS OF THE PERFUSION OF VARIOUS SOLUTIONS ON THE NO-REFLOW PHENOMENON IN EXPERIMENTAL FREE FLAPS. *Plastic and Reconstructive Surgery,* 61.

CHAN, P. H. 1996. Role of oxidants in ischemic brain damage. *Stroke,* 27**,** 1124-9.

CHENG, J., KORTE, N., NORTLEY, R., SETHI, H., TANG, Y. & ATTWELL, D. 2018. Targeting pericytes for therapeutic approaches to neurological disorders. *Acta Neuropathologica,* 136**,** 507-523.

CHIANG, J., KOWADA, M., AMES, A., 3RD, WRIGHT, R. L. & MAJNO, G. 1968. Cerebral ischemia. III. Vascular changes. *Am J Pathol,* 52**,** 455-76.

CHOI, D. W. & ROTHMAN, S. M. 1990. The role of glutamate neurotoxicity in hypoxic-ischemic neuronal death. *Annu Rev Neurosci,* 13**,** 171-82.

CHONG, Z. Z., LI, F. & MAIESE, K. 2005. Oxidative stress in the brain: novel cellular targets that govern survival during neurodegenerative disease. *Prog Neurobiol,* 75**,** 207-46.

CLARK, E. A. & BRUGGE, J. S. 1995. Integrins and signal transduction pathways: the road taken. *Science,* 268**,** 233-9.

CRAMER, J. V., GESIERICH, B., ROTH, S., DICHGANS, M., DÜRING, M. & LIESZ, A. 2019. In vivo widefield calcium imaging of the mouse cortex for analysis of network connectivity in health and brain disease. *Neuroimage,* 199**,** 570-584.

CROUCH, E. E. & DOETSCH, F. 2018. FACS isolation of endothelial cells and pericytes from mouse brain microregions. *Nature Protocols,* 13**,** 738-751.

CUDMORE, R. H., DOUGHERTY, S. E. & LINDEN, D. J. 2017. Cerebral vascular structure in the motor cortex of adult mice is stable and is not altered by voluntary exercise. *J Cereb Blood Flow Metab,* 37**,** 3725-3743.

DALKARA, T. 2019. Pericytes. *Stroke,* 50**,** 2985-2991.

DANEMAN, R., ZHOU, L., KEBEDE, A. A. & BARRES, B. A. 2010. Pericytes are required for blood-brain barrier integrity during embryogenesis. *Nature,* 468**,** 562-6.

DANHIER, P., KRISHNAMACHARY, B., BHARTI, S., KAKKAD, S., MIRONCHIK, Y. & BHUJWALLA, Z. M. 2015. Combining Optical Reporter Proteins with Different Half-lives to Detect Temporal Evolution of Hypoxia and Reoxygenation in Tumors. *Neoplasia (New York, N.Y.),* 17**,** 871-881.

DARBY, D. G., BARBER, P. A., GERRATY, R. P., DESMOND, P. M., YANG, Q., PARSONS, M., LI, T., TRESS, B. M. & DAVIS, S. M. 1999. Pathophysiological topography of acute ischemia by combined diffusion-weighted and perfusion MRI. *Stroke,* 30**,** 2043-52.

DE LA TORRE, J. C., FORTIN, T., SAUNDERS, J. K., BUTLER, K. & RICHARD, M. T. 1992. The no-reflow phenomenon is a post-mortem artifact. *Acta Neurochir (Wien),* 115**,** 37-42.

DE LA TORRE, J. C. & MUSSIVAND, T. 1993. Can disturbed brain microcirculation cause Alzheimer's disease? *Neurol Res,* 15**,** 146-53.

DEGUCHI, K., LIU, N., LIU, W., OMOTE, Y., KONO, S., YUNOKI, T., DEGUCHI, S., YAMASHITA, T., IKEDA, Y. & ABE, K. 2014. Pericyte protection by edaravone after tissue plasminogen activator treatment in rat cerebral ischemia. *J Neurosci Res,* 92**,** 1509-19.

DEL ZOPPO, G. J. & MABUCHI, T. 2003. Cerebral microvessel responses to focal ischemia. *J Cereb Blood Flow Metab,* 23**,** 879-94.

DEL ZOPPO, G. J., SHARP, F. R., HEISS, W. D. & ALBERS, G. W. 2011. Heterogeneity in the penumbra. *J Cereb Blood Flow Metab,* 31**,** 1836-51.

DIAS, D. O., KALKITSAS, J., KELAHMETOGLU, Y., ESTRADA, C. P., TATARISHVILI, J., ERNST, A., HUTTNER, H. B., KOKAIA, Z., LINDVALL, O., BRUNDIN, L., FRISÉN, J. & GÖRITZ, C. 2020. Pericyte-derived fibrotic scarring is conserved across diverse central nervous system lesions. *bioRxiv***,** 2020.04.30.068965.

DIAS, D. O., KIM, H., HOLL, D., WERNE SOLNESTAM, B., LUNDEBERG, J., CARLÉN, M., GÖRITZ, C. & FRISÉN, J. 2018. Reducing Pericyte-Derived Scarring Promotes Recovery after Spinal Cord Injury. *Cell,* 173**,** 153-165.e22.

DÍAZ-FLORES, L., GUTIÉRREZ, R., MADRID, J. F., VARELA, H., VALLADARES, F., ACOSTA, E., MARTÍN-VASALLO, P. & DÍAZ-FLORES, L., JR. 2009. Pericytes. Morphofunction, interactions and pathology in a quiescent and activated mesenchymal cell niche. *Histol Histopathol,* 24**,** 909-69.

DICHGANS, M., MAYER, M., UTTNER, I., BRÜNING, R., MÜLLER-HÖCKER, J., RUNGGER, G., EBKE, M., KLOCKGETHER, T. & GASSER, T. 1998. The phenotypic spectrum of CADASIL: clinical findings in 102 cases. *Ann Neurol,* 44**,** 731-9.

DIJKHUIZEN, R. M., BEEKWILDER, J. P., VAN DER WORP, H. B., BERKELBACH VAN DER SPRENKEL, J. W., TULLEKEN, K. A. & NICOLAY, K. 1999. Correlation between tissue depolarizations and damage in focal ischemic rat brain. *Brain Res,* 840**,** 194-205.

DIRNAGL, U. & MACLEOD, M. R. 2009. Stroke research at a road block: the streets from adversity should be paved with meta-analysis and good laboratory practice. *British Journal of Pharmacology,* 157**,** 1154-1156.

DOBIN, A., DAVIS, C. A., SCHLESINGER, F., DRENKOW, J., ZALESKI, C., JHA, S., BATUT, P., CHAISSON, M. & GINGERAS, T. R. 2013. STAR: ultrafast universal RNA-seq aligner. *Bioinformatics,* 29**,** 15-21.

DORE-DUFFY, P., OWEN, C., BALABANOV, R., MURPHY, S., BEAUMONT, T. & RAFOLS, J. A. 2000. Pericyte migration from the vascular wall in response to traumatic brain injury. *Microvasc Res,* 60**,** 55-69.

DOROSTKAR, M. M., BURGOLD, S., FILSER, S., BARGHORN, S., SCHMIDT, B., ANUMALA, U. R., HILLEN, H., KLEIN, C. & HERMS, J. 2014. Immunotherapy alleviates amyloid-associated synaptic pathology in an Alzheimer's disease mouse model. *Brain,* 137**,** 3319-26.

DULMOVITS, B. M. & HERMAN, I. M. 2012. Microvascular remodeling and wound healing: A role for pericytes. *The International Journal of Biochemistry & Cell Biology,* 44**,** 1800-1812.

EBERTH, C. J. 1871. Handbuch der Lehre von der Gewegen des Menschen und der Tiere. Vol 1 (Leipzig).

EL AMKI, M., GLÜCK, C., BINDER, N., MIDDLEHAM, W., WYSS, M. T., WEISS, T., MEISTER, H., LUFT, A., WELLER, M., WEBER, B. & WEGENER, S. 2020. Neutrophils Obstructing Brain Capillaries Are a Major Cause of No-Reflow in Ischemic Stroke. *Cell Reports,* 33**,** 108260.

ESCHENFELDER, C. C., KRUG, R., YUSOFI, A. F., MEYNE, J. K., HERDEGEN, T., KOCH, A., ZHAO, Y., CARL, U. M. & DEUSCHL, G. 2008. Neuroprotection by oxygen in acute transient focal cerebral ischemia is dose dependent and shows superiority of hyperbaric oxygenation. *Cerebrovasc Dis,* 25**,** 193-201.

EVROVA, O. & BUSCHMANN, J. 2017. In vitro and in vivo effects of PDGF-BB delivery strategies on tendon healing: a review. *Eur Cell Mater,* 34**,** 15-39.

FABER, J. E., CHILIAN, W. M., DEINDL, E., VAN ROYEN, N. & SIMONS, M. 2014. A brief etymology of the collateral circulation. *Arterioscler Thromb Vasc Biol,* 34**,** 1854-9.

FABRIS, L. & STRAZZABOSCO, M. 2011. Epithelial-mesenchymal interactions in biliary diseases. *Semin Liver Dis,* 31**,** 11-32.

FEIGIN, V. L., KRISHNAMURTHI, R. V., PARMAR, P., NORRVING, B., MENSAH, G. A., BENNETT, D. A., BARKER-COLLO, S., MORAN, A. E., SACCO, R. L., TRUELSEN, T., DAVIS, S., PANDIAN, J. D., NAGHAVI, M., FOROUZANFAR, M. H., NGUYEN, G., JOHNSON, C. O., VOS, T., MERETOJA, A., MURRAY, C. J. & ROTH, G. A. 2015. Update on the Global Burden of Ischemic and Hemorrhagic Stroke in 1990-2013: The GBD 2013 Study. *Neuroepidemiology,* 45**,** 161-76.

FERNÁNDEZ-KLETT, F., OFFENHAUSER, N., DIRNAGL, U., PRILLER, J. & LINDAUER, U. 2010. Pericytes in capillaries are contractile in vivo, but arterioles mediate functional hyperemia in the mouse brain. *Proceedings of the National Academy of Sciences,* 107**,** 22290.

FERNÁNDEZ-KLETT, F., POTAS, J. R., HILPERT, D., BLAZEJ, K., RADKE, J., HUCK, J., ENGEL, O., STENZEL, W., GENOVÉ, G. & PRILLER, J. 2013. Early loss of pericytes and perivascular stromal cell-induced scar formation after stroke. *J Cereb Blood Flow Metab,* 33**,** 428-39.

FLURI, F., SCHUHMANN, M. K. & KLEINSCHNITZ, C. 2015. Animal models of ischemic stroke and their application in clinical research. *Drug design, development and therapy,* 9**,** 3445-3454.

FOO, S. S., TURNER, C. J., ADAMS, S., COMPAGNI, A., AUBYN, D., KOGATA, N., LINDBLOM, P., SHANI, M., ZICHA, D. & ADAMS, R. H. 2006. Ephrin-B2 Controls Cell Motility and Adhesion during Blood-Vessel-Wall Assembly. *Cell,* 124**,** 161-173.

GARCIA, J. H., LIU, K. F., YOSHIDA, Y., CHEN, S. & LIAN, J. 1994. Brain microvessels: factors altering their patency after the occlusion of a middle cerebral artery (Wistar rat). *Am J Pathol,* 145**,** 728-40.

GAUDIN, A., YEMISCI, M., EROGLU, H., LEPETRE-MOUELHI, S., TURKOGLU, O. F., DÖNMEZ-DEMIR, B., CABAN, S., SARGON, M. F., GARCIA-ARGOTE, S., PIETERS, G., LOREAU, O., ROUSSEAU, B., TAGIT, O., HILDEBRANDT, N., LE DANTEC, Y., MOUGIN, J., VALETTI, S., CHACUN, H., NICOLAS, V., DESMAËLE, D., ANDRIEUX, K., CAPAN, Y., DALKARA, T. & COUVREUR, P. 2014. Squalenoyl adenosine nanoparticles provide neuroprotection after stroke and spinal cord injury. *Nat Nanotechnol,* 9**,** 1054-1062.

GERHARDT, H. & BETSHOLTZ, C. 2003. Endothelial-pericyte interactions in angiogenesis. *Cell and Tissue Research,* 314**,** 15-23.

GHOSH, M., BALBI, M., HELLAL, F., DICHGANS, M., LINDAUER, U. & PLESNILA, N. 2015. Pericytes are involved in the pathogenesis of cerebral autosomal dominant arteriopathy with subcortical infarcts and leukoencephalopathy. *Annals of Neurology,* 78**,** 887-900.

GLÜCK, C., FERRARI, K. D., KELLER, A., SAAB, A. S., STOBART, J. L. & WEBER, B. 2020. Distinct signatures of calcium activity in brain pericytes. *bioRxiv***,** 2020.07.16.207076.

GOLDEY, G. J., ROUMIS, D. K., GLICKFELD, L. L., KERLIN, A. M., REID, R. C., BONIN, V., SCHAFER, D. P. & ANDERMANN, M. L. 2014. Removable cranial windows for long-term imaging in awake mice. *Nature protocols,* 9**,** 2515-2538.

GONZALES, A. L., KLUG, N. R., MOSHKFOROUSH, A., LEE, J. C., LEE, F. K., SHUI, B., TSOUKIAS, N. M., KOTLIKOFF, M. I., HILL-EUBANKS, D. & NELSON, M. T. 2020. Contractile pericytes determine the direction of blood flow at capillary junctions. *Proc Natl Acad Sci U S A,* 117**,** 27022-27033.

GOULD, I. G., TSAI, P., KLEINFELD, D. & LINNINGER, A. 2017. The capillary bed offers the largest hemodynamic resistance to the cortical blood supply. *Journal of Cerebral Blood Flow & Metabolism,* 37**,** 52-68.

GOUMANS, M. J., VALDIMARSDOTTIR, G., ITOH, S., ROSENDAHL, A., SIDERAS, P. & TEN DIJKE, P. 2002. Balancing the activation state of the endothelium via two distinct TGF-beta type I receptors. *Embo j,* 21**,** 1743-53.

GRANT, R. I. 2019. Organizational hierarchy and structural diversity of microvascular pericytes in adult cortex. *J cereb Blood Flow Metab.,* 39**,** 411-425.

GRANT, R. I., HARTMANN, D. A., UNDERLY, R. G., BERTHIAUME, A. A., BHAT, N. R. & SHIH, A. Y. 2019. Organizational hierarchy and structural diversity of microvascular pericytes in adult mouse cortex. *J Cereb Blood Flow Metab,* 39**,** 411-425.

GUIMARÃES-CAMBOA, N., CATTANEO, P., SUN, Y., MOORE-MORRIS, T., GU, Y., DALTON, N. D., ROCKENSTEIN, E., MASLIAH, E., PETERSON, K. L., STALLCUP, W. B., CHEN, J. & EVANS, S. M. 2017. Pericytes of Multiple Organs Do Not Behave as Mesenchymal Stem Cells In Vivo. *Cell Stem Cell,* 20**,** 345-359.e5.

GURSOY-OZDEMIR, Y., QIU, J., MATSUOKA, N., BOLAY, H., BERMPOHL, D., JIN, H., WANG, X., ROSENBERG, G. A., LO, E. H. & MOSKOWITZ, M. A. 2004. Cortical spreading depression activates and upregulates MMP-9. *J Clin Invest,* 113**,** 1447-55.

GURSOY-OZDEMIR, Y., YEMISCI, M. & DALKARA, T. 2012. Microvascular protection is essential for successful neuroprotection in stroke. *J Neurochem,* 123 Suppl 2**,** 2-11.

HALEY, M. J. & LAWRENCE, C. B. 2017. The blood-brain barrier after stroke: Structural studies and the role of transcytotic vesicles. *J Cereb Blood Flow Metab,* 37**,** 456-470.

HALL, C. N., REYNELL, C., GESSLEIN, B., HAMILTON, N. B., MISHRA, A., SUTHERLAND, B. A., O'FARRELL, F. M., BUCHAN, A. M., LAURITZEN, M. & ATTWELL, D. 2014. Capillary pericytes regulate cerebral blood flow in health and disease. *Nature,* 508**,** 55-60.

HALLENBECK, J. M., DUTKA, A. J., TANISHIMA, T., KOCHANEK, P. M., KUMAROO, K. K., THOMPSON, C. B., OBRENOVITCH, T. P. & CONTRERAS, T. J. 1986. Polymorphonuclear leukocyte accumulation in brain regions with low blood flow during the early postischemic period. *Stroke,* 17**,** 246-53.

HAMILTON, N. B., ATTWELL, D. & HALL, C. N. 2010. Pericyte-mediated regulation of capillary diameter: a component of neurovascular coupling in health and disease. *Front Neuroenergetics,* 2.

HAMMES, H. P., LIN, J., WAGNER, P., FENG, Y., VOM HAGEN, F., KRZIZOK, T., RENNER, O., BREIER, G., BROWNLEE, M. & DEUTSCH, U. 2004. Angiopoietin-2 causes pericyte dropout in the normal retina: evidence for involvement in diabetic retinopathy. *Diabetes,* 53**,** 1104-10.

HARTMANN, D., GRANT, R. I., HARRILL, S. A., NOONAN, T., LAUER, A. & SHIH, A. Y. 2018. Optogenetic stimulation of pericytes lacking alpha smooth muscle actin produces a decrease in capillary blood flow in the living mouse brain. *The FASEB Journal,* 32**,** 708.1-708.1.

HARTMANN, D. A., BERTHIAUME, A.-A., GRANT, R. I., HARRILL, S. A., KOSKI, T., TIEU, T., MCDOWELL, K. P., FAINO, A. V., KELLY, A. L. & SHIH, A. Y. 2021. Brain capillary pericytes exert a substantial but slow influence on blood flow. *Nature Neuroscience*.

HAYASHI, K., NAKAO, S., NAKAOKE, R., NAKAGAWA, S., KITAGAWA, N. & NIWA, M. 2004. Effects of hypoxia on endothelial/pericytic co-culture model of the blood-brain barrier. *Regul Pept,* 123**,** 77-83.

HAYASHI, T., NOSHITA, N., SUGAWARA, T. & CHAN, P. H. 2003. Temporal profile of angiogenesis and expression of related genes in the brain after ischemia. *J Cereb Blood Flow Metab,* 23**,** 166-80.

HE, L., VANLANDEWIJCK, M., RASCHPERGER, E., ANDALOUSSI MÄE, M., JUNG, B., LEBOUVIER, T., ANDO, K., HOFMANN, J., KELLER, A. & BETSHOLTZ, C. 2016. Analysis of the brain mural cell transcriptome. *Scientific Reports,* 6**,** 35108.

HEGLIND, M., CEDERBERG, A., AQUINO, J., LUCAS, G., ERNFORS, P. & ENERBÄCK, S. 2005. Lack of the central nervous system- and neural crest-expressed forkhead gene Foxs1 affects motor function and body weight. *Mol Cell Biol,* 25**,** 5616-25.

HELLSTRÖM, M., GERHARDT, H., KALÉN, M., LI, X., ERIKSSON, U., WOLBURG, H. & BETSHOLTZ, C. 2001. Lack of pericytes leads to endothelial hyperplasia and abnormal vascular morphogenesis. *J Cell Biol,* 153**,** 543-53.

HEO, J. H., HAN, S. W. & LEE, S. K. 2005. Free radicals as triggers of brain edema formation after stroke. *Free Radic Biol Med,* 39**,** 51-70.

HILL, ROBERT A., TONG, L., YUAN, P., MURIKINATI, S., GUPTA, S. & GRUTZENDLER, J. 2015. Regional Blood Flow in the Normal and Ischemic Brain Is Controlled by Arteriolar Smooth Muscle Cell Contractility and Not by Capillary Pericytes. *Neuron,* 87**,** 95-110.

HIRSCHI, K. K., ROHOVSKY, S. A., BECK, L. H., SMITH, S. R. & D'AMORE, P. A. 1999. Endothelial cells modulate the proliferation of mural cell precursors via platelet-derived growth factor-BB and heterotypic cell contact. *Circ Res,* 84**,** 298-305.

HOLTMAAT, A., BONHOEFFER, T., CHOW, D. K., CHUCKOWREE, J., DE PAOLA, V., HOFER, S. B., HÜBENER, M., KECK, T., KNOTT, G., LEE, W.-C. A., MOSTANY, R., MRSIC-FLOGEL, T. D., NEDIVI, E., PORTERA-CAILLIAU, C., SVOBODA, K., TRACHTENBERG, J. T. & WILBRECHT, L. 2009. Long-term, high-resolution imaging in the mouse neocortex through a chronic cranial window. *Nature protocols,* 4**,** 1128-1144.

HORSCH, A. D., DANKBAAR, J. W., NIESTEN, J. M., VAN SEETERS, T., VAN DER SCHAAF, I. C., VAN DER GRAAF, Y., MALI, W. P. & VELTHUIS, B. K. 2015. Predictors of reperfusion in patients with acute ischemic stroke. *AJNR Am J Neuroradiol,* 36**,** 1056-62.

HOSSMANN, K. A. 1994. Viability thresholds and the penumbra of focal ischemia. *Ann Neurol,* 36**,** 557-65.

HOSSMANN, K. A. 2006. Pathophysiology and therapy of experimental stroke. *Cell Mol Neurobiol,* 26**,** 1057-83.

ILIFF, J. J., WANG, M., LIAO, Y., PLOGG, B. A., PENG, W., GUNDERSEN, G. A., BENVENISTE, H., VATES, G. E., DEANE, R., GOLDMAN, S. A., NAGELHUS, E. A. & NEDERGAARD, M. 2012. A Paravascular Pathway Facilitates CSF Flow Through the Brain Parenchyma and the Clearance of Interstitial Solutes, Including Amyloid β. *Science Translational Medicine,* 4**,** 147ra111-147ra111.

ITURRIA-MEDINA, Y., SOTERO, R. C., TOUSSAINT, P. J., MATEOS-PÉREZ, J. M. & EVANS, A. C. 2016. Early role of vascular dysregulation on late-onset Alzheimer's disease based on multifactorial data-driven analysis. *Nat Commun,* 7**,** 11934.

JANSEN, C., TOBITA, C., UMEMOTO, E. U., STARKUS, J., RYSAVY, N. M., SHIMODA, L. M. N., SUNG, C., STOKES, A. J. & TURNER, H. 2019. Calcium-dependent, non-apoptotic, large plasma membrane bleb formation in physiologically stimulated mast cells and basophils. *J Extracell Vesicles,* 8**,** 1578589.

JEANSSON, M., GAWLIK, A., ANDERSON, G., LI, C., KERJASCHKI, D., HENKELMAN, M. & QUAGGIN, S. E. 2011. Angiopoietin-1 is essential in mouse vasculature during development and in response to injury. *J Clin Invest,* 121**,** 2278-89.

JENSEN, L. J., KUHN, M., STARK, M., CHAFFRON, S., CREEVEY, C., MULLER, J., DOERKS, T., JULIEN, P., ROTH, A., SIMONOVIC, M., BORK, P. & VON MERING, C. 2009. STRING 8--a global view on proteins and their functional interactions in 630 organisms. *Nucleic Acids Res,* 37**,** D412-6.

JONES, N., VOSKAS, D., MASTER, Z., SARAO, R., JONES, J. & DUMONT, D. J. 2001. Rescue of the early vascular defects in Tek/Tie2 null mice reveals an essential survival function. *EMBO Rep,* 2**,** 438-45.

JOUTEL, A., CORPECHOT, C., DUCROS, A., VAHEDI, K., CHABRIAT, H., MOUTON, P., ALAMOWITCH, S., DOMENGA, V., CÉCILLION, M., MARECHAL, E., MACIAZEK, J., VAYSSIERE, C., CRUAUD, C., CABANIS, E. A., RUCHOUX, M. M., WEISSENBACH, J., BACH, J. F., BOUSSER, M. G. & TOURNIER-LASSERVE, E. 1996. Notch3 mutations in CADASIL, a hereditary adult-onset condition causing stroke and dementia. *Nature,* 383**,** 707-10.

JOUTEL, A., MONET-LEPRÊTRE, M., GOSELE, C., BARON-MENGUY, C., HAMMES, A., SCHMIDT, S., LEMAIRE-CARRETTE, B., DOMENGA, V., SCHEDL, A., LACOMBE, P. & HUBNER, N. 2010. Cerebrovascular dysfunction and microcirculation rarefaction precede white matter lesions in a mouse genetic model of cerebral ischemic small vessel disease. *J Clin Invest,* 120**,** 433-45.

KÁDÁR, A., WITTMANN, G., LIPOSITS, Z. & FEKETE, C. 2009. Improved method for combination of immunocytochemistry and Nissl staining. *J Neurosci Methods,* 184**,** 115-8.

KAMOUCHI, M., AGO, T., KURODA, J. & KITAZONO, T. 2012. The possible roles of brain pericytes in brain ischemia and stroke. *Cell Mol Neurobiol,* 32**,** 159-65.

KARIBE, H., ZAROW, G. J. & WEINSTEIN, P. R. 1995. Use of mild intraischemic hypothermia versus mannitol to reduce infarct size after temporary middle cerebral artery occlusion in rats. *J Neurosurg,* 83**,** 93-8.

KISLER, K., NELSON, A. R., MONTAGNE, A. & ZLOKOVIC, B. V. 2017a. Cerebral blood flow regulation and neurovascular dysfunction in Alzheimer disease. *Nat Rev Neurosci,* 18**,** 419-434.

KISLER, K., NELSON, A. R., REGE, S. V., RAMANATHAN, A., WANG, Y., AHUJA, A., LAZIC, D., TSAI, P. S., ZHAO, Z., ZHOU, Y., BOAS, D. A., SAKADŽIĆ, S. & ZLOKOVIC, B. V. 2017b. Pericyte degeneration leads to neurovascular uncoupling and limits oxygen supply to brain. *Nature Neuroscience,* 20**,** 406-416.

KNOWLES, R. B., SABRY, J. H., MARTONE, M. E., DEERINCK, T. J., ELLISMAN, M. H., BASSELL, G. J. & KOSIK, K. S. 1996. Translocation of RNA granules in living neurons. *J Neurosci,* 16**,** 7812-20.

KORN, J., CHRIST, B. & KURZ, H. 2002. Neuroectodermal origin of brain pericytes and vascular smooth muscle cells. *J Comp Neurol,* 442**,** 78-88.

KOSIK, K. S. & KRICHEVSKY, A. M. 2002. The message and the messenger: delivering RNA in neurons. *Sci STKE,* 2002**,** pe16.

KOVACS-OLLER, T., IVANOVA, E., BIANCHIMANO, P. & SAGDULLAEV, B. T. 2019. Dynamic connectivity maps of pericytes and endothelial cells mediate neurovascular coupling in health and disease. *bioRxiv***,** 830398.

KRAUS, A. B. R. 1898. Über eine bisher unbekannte toxische Wirkung der Gallensäuren auf das Zentralnervensystem. *Centralblatt. Inn. Med,* .

KRISHNAMURTHI, R. V., MORAN, A. E., FEIGIN, V. L., BARKER-COLLO, S., NORRVING, B., MENSAH, G. A., TAYLOR, S., NAGHAVI, M., FOROUZANFAR, M. H., NGUYEN, G., JOHNSON, C. O., VOS, T., MURRAY, C. J. & ROTH, G. A. 2015. Stroke Prevalence, Mortality and Disability-Adjusted Life Years in Adults Aged 20-64 Years in 1990-2013: Data from the Global Burden of Disease 2013 Study. *Neuroepidemiology,* 45**,** 190-202.

KUO, M.-C., PATSCHAN, D., PATSCHAN, S., COHEN-GOULD, L., PARK, H.-C., NI, J., ADDABBO, F. & GOLIGORSKY, M. S. 2008. Ischemia-Induced Exocytosis of Weibel-Palade Bodies Mobilizes Stem Cells. *Journal of the American Society of Nephrology,* 19**,** 2321-2330.

LAURITZEN, M., DREIER, J. P., FABRICIUS, M., HARTINGS, J. A., GRAF, R. & STRONG, A. J. 2011. Clinical relevance of cortical spreading depression in neurological disorders: migraine, malignant stroke, subarachnoid and intracranial hemorrhage, and traumatic brain injury. *Journal of cerebral blood flow and metabolism : official journal of the International Society of Cerebral Blood Flow and Metabolism,* 31**,** 17-35.

LEE, D. H., KANG, D. W., AHN, J. S., CHOI, C. G., KIM, S. J. & SUH, D. C. 2005. Imaging of the ischemic penumbra in acute stroke. *Korean J Radiol,* 6**,** 64-74.

LEVÉEN, P., PEKNY, M., GEBRE-MEDHIN, S., SWOLIN, B., LARSSON, E. & BETSHOLTZ, C. 1994. Mice deficient for PDGF B show renal, cardiovascular, and hematological abnormalities. *Genes Dev,* 8**,** 1875-87.

LEWANDOWSKY, M. 1900. Zur Lehre der Zerebrospinalflussigkeit. *Z Klin Med,* 40**,** 480–484.

LI, P. A., GISSELSSON, L., KEUKER, J., VOGEL, J., SMITH, M. L., KUSCHINSKY, W. & SIESJÖ, B. K. 1998. Hyperglycemia-exaggerated ischemic brain damage following 30 min of middle cerebral artery occlusion is not due to capillary obstruction. *Brain Res,* 804**,** 36-44.

LIANG, H., ZHAO, H., GLEICHMAN, A., MACHNICKI, M., TELANG, S., TANG, S., RSHTOUNI, M., RUDDELL, J. & CARMICHAEL, S. T. 2019. Region-specific and activity-dependent regulation of SVZ neurogenesis and recovery after stroke. *Proceedings of the National Academy of Sciences,* 116**,** 13621-13630.

LINDBLOM, P., GERHARDT, H., LIEBNER, S., ABRAMSSON, A., ENGE, M., HELLSTROM, M., BACKSTROM, G., FREDRIKSSON, S., LANDEGREN, U., NYSTROM, H. C., BERGSTROM, G., DEJANA, E., OSTMAN, A., LINDAHL, P. & BETSHOLTZ, C. 2003. Endothelial PDGF-B retention is required for proper investment of pericytes in the microvessel wall. *Genes & development,* 17**,** 1835-1840.

LIU, S., CONNOR, J., PETERSON, S., SHUTTLEWORTH, C. W. & LIU, K. J. 2002. Direct visualization of trapped erythrocytes in rat brain after focal ischemia and reperfusion. *J Cereb Blood Flow Metab,* 22**,** 1222-30.

LIU, S., LEVINE, S. R. & WINN, H. R. 2010. Targeting ischemic penumbra: part I - from pathophysiology to therapeutic strategy. *J Exp Stroke Transl Med,* 3**,** 47-55.

LLOYD-JONES, D., ADAMS, R. J., BROWN, T. M., CARNETHON, M., DAI, S., DE SIMONE, G., FERGUSON, T. B., FORD, E., FURIE, K., GILLESPIE, C., GO, A., GREENLUND, K., HAASE, N., HAILPERN, S., HO, P. M., HOWARD, V., KISSELA, B., KITTNER, S., LACKLAND, D., LISABETH, L., MARELLI, A., MCDERMOTT, M. M., MEIGS, J., MOZAFFARIAN, D., MUSSOLINO, M., NICHOL, G., ROGER, V. L., ROSAMOND, W., SACCO, R., SORLIE, P., ROGER, V. L., THOM, T., WASSERTHIEL-SMOLLER, S., WONG, N. D. & WYLIE-ROSETT, J. 2010. Heart disease and stroke statistics--2010 update: a report from the American Heart Association. *Circulation,* 121**,** e46-e215.

LONGDEN, T. A. & NELSON, M. T. 2015. Vascular inward rectifier K+ channels as external K+ sensors in the control of cerebral blood flow. *Microcirculation,* 22**,** 183-96.

LOURBOPOULOS, A., MAMRAK, U., ROTH, S., BALBI, M., SHROUDER, J., LIESZ, A., HELLAL, F. & PLESNILA, N. 2017. Inadequate food and water intake determine mortality following stroke in mice. *Journal of cerebral blood flow and metabolism : official journal of the International Society of Cerebral Blood Flow and Metabolism,* 37**,** 2084-2097.

LOUVI, A., ARBOLEDA-VELASQUEZ, J. F. & ARTAVANIS-TSAKONAS, S. 2006. CADASIL: a critical look at a Notch disease. *Dev Neurosci,* 28**,** 5-12.

LOVE, S. 1999. Oxidative stress in brain ischemia. *Brain Pathol,* 9**,** 119-31.

LUCKNER, M., BURGOLD, S., FILSER, S., SCHEUNGRAB, M., NIYAZ, Y., HUMMEL, E., WANNER, G. & HERMS, J. 2018. Label-free 3D-CLEM Using Endogenous Tissue Landmarks. *iScience,* 6**,** 92-101.

LYDEN, P., PRYOR, K. E., COFFEY, C. S., CUDKOWICZ, M., CONWIT, R., JADHAV, A., SAWYER, R. N., JR., CLAASSEN, J., ADEOYE, O., SONG, S., HANNON, P., ROST, N. S., HINDUJA, A., TORBEY, M., LEE, J. M., BENESCH, C., RIPPEE, M., RYMER, M., FROEHLER, M. T., CLARKE HALEY, E., JOHNSON, M., YANKEY, J., MAGEE, K., QIDWAI, J., LEVY, H., MARK HAACKE, E., FAWAZ, M., DAVIS, T. P., TOGA, A. W., GRIFFIN, J. H. & ZLOKOVIC, B. V. 2019. Final Results of the RHAPSODY Trial: A Multi-Center, Phase 2 Trial Using a Continual Reassessment Method to Determine the Safety and Tolerability of 3K3A-APC, A Recombinant Variant of Human Activated Protein C, in Combination with Tissue Plasminogen Activator, Mechanical Thrombectomy or both in Moderate to Severe Acute Ischemic Stroke. *Ann Neurol,* 85**,** 125-136.

MA, J., MA, Y., SHUAIB, A. & WINSHIP, I. R. 2020. Improved collateral flow and reduced damage after remote ischemic perconditioning during distal middle cerebral artery occlusion in aged rats. *Sci Rep,* 10**,** 12392.

MAJESKY, M. W., DONG, X. R., REGAN, J. N. & HOGLUND, V. J. 2011. Vascular smooth muscle progenitor cells: building and repairing blood vessels. *Circ Res,* 108**,** 365-77.

MAJNO, G., AMES, A., III, CHIANG, J. & WRIGHT, R. L. 1967. NO REFLOW AFTER CEREBRAL ISCHEMIA. *The Lancet,* 290**,** 569-570.

MARKUS, R., REUTENS, D. C., KAZUI, S., READ, S., WRIGHT, P., PEARCE, D. C., TOCHON-DANGUY, H. J., SACHINIDIS, J. I. & DONNAN, G. A. 2004. Hypoxic tissue in ischaemic stroke: persistence and clinical consequences of spontaneous survival. *Brain,* 127**,** 1427-36.

MATHIISEN, T. M., LEHRE, K. P., DANBOLT, N. C. & OTTERSEN, O. P. 2010. The perivascular astroglial sheath provides a complete covering of the brain microvessels: an electron microscopic 3D reconstruction. *Glia,* 58**,** 1094-103.

MAYER, M. L. & MILLER, R. J. 1990. Excitatory amino acid receptors, second messengers and regulation of intracellular Ca²⁺ in mammalian neurons. *Trends in Pharmacological Sciences,* 11**,** 254-260.

MESTRE, H., DU, T., SWEENEY, A. M., LIU, G., SAMSON, A. J., PENG, W., MORTENSEN, K. N., STÆGER, F. F., BORK, P. A. R., BASHFORD, L., TORO, E. R., TITHOF, J., KELLEY, D. H., THOMAS, J. H., HJORTH, P. G., MARTENS, E. A., MEHTA, R. I., SOLIS, O., BLINDER, P., KLEINFELD, D., HIRASE, H., MORI, Y. & NEDERGAARD, M. 2020. Cerebrospinal fluid influx drives acute ischemic tissue swelling. *Science,* 367**,** eaax7171.

MIES, G., IIJIMA, T. & HOSSMANN, K. A. 1993. Correlation between peri-infarct DC shifts and ischaemic neuronal damage in rat. *Neuroreport,* 4**,** 709-11.

MINERS, J. S., SCHULZ, I. & LOVE, S. 2018. Differing associations between Aβ accumulation, hypoperfusion, blood-brain barrier dysfunction and loss of PDGFRB pericyte marker in the precuneus and parietal white matter in Alzheimer's disease. *J Cereb Blood Flow Metab,* 38**,** 103-115.

MOHAMED MOKHTARUDIN, M. J. & PAYNE, S. J. 2015. Mathematical model of the effect of ischemia-reperfusion on brain capillary collapse and tissue swelling. *Math Biosci,* 263**,** 111-20.

MONTAGNE, A., NATION, D. A., SAGARE, A. P., BARISANO, G., SWEENEY, M. D., CHAKHOYAN, A., PACHICANO, M., JOE, E., NELSON, A. R., D'ORAZIO, L. M., BUENNAGEL, D. P., HARRINGTON, M. G., BENZINGER, T. L. S., FAGAN, A. M., RINGMAN, J. M., SCHNEIDER, L. S., MORRIS, J. C., REIMAN, E. M., CASELLI, R. J., CHUI, H. C., TCW, J., CHEN, Y., PA, J., CONTI, P. S., LAW, M., TOGA, A. W. & ZLOKOVIC, B. V. 2020. APOE4 leads to blood-brain barrier dysfunction predicting cognitive decline. *Nature,* 581**,** 71-76.

MURPHY, B. D., FOX, A. J., LEE, D. H., SAHLAS, D. J., BLACK, S. E., HOGAN, M. J., COUTTS, S. B., DEMCHUK, A. M., GOYAL, M., AVIV, R. I., SYMONS, S., GULKA, I. B., BELETSKY, V., PELZ, D., HACHINSKI, V., CHAN, R. & LEE, T. Y. 2006. Identification of penumbra and infarct in acute ischemic stroke using computed tomography perfusion-derived blood flow and blood volume measurements. *Stroke,* 37**,** 1771-7.

NAGHAVI, M., ABAJOBIR, A. A., ABBAFATI, C., ABBAS, K. M., ABD-ALLAH, F., ABERA, S. F., ABOYANS, V., ADETOKUNBOH, O., AFSHIN, A., AGRAWAL, A., AHMADI, A., AHMED, M. B., AICHOUR, A. N., AICHOUR, M. T. E., AICHOUR, I., AIYAR, S., ALAHDAB, F., AL-ALY, Z., ALAM, K., ALAM, N., ALAM, T., ALENE, K. A., AL-EYADHY, A., ALI, S. D., ALIZADEH-NAVAEI, R., ALKAABI, J. M., ALKERWI, A. A., ALLA, F., ALLEBECK, P., ALLEN, C., AL-RADDADI, R., ALSHARIF, U., ALTIRKAWI, K. A., ALVIS-GUZMAN, N., AMARE, A. T., AMINI, E., AMMAR, W., AMOAKO, Y. A., ANBER, N., ANDERSEN, H. H., ANDREI, C. L., ANDROUDI, S., ANSARI, H., ANTONIO, C. A. T., ANWARI, P., ÄRNLÖV, J., ARORA, M., ARTAMAN, A., ARYAL, K. K., ASAYESH, H., ASGEDOM, S. W., ATEY, T. M., AVILA-BURGOS, L., AVOKPAHO, E. F. G., AWASTHI, A., BABALOLA, T. K., BACHA, U., BALAKRISHNAN, K., BARAC, A., BARBOZA, M. A., BARKER-COLLO, S. L., BARQUERA, S., BARREGARD, L., BARRERO, L. H., BAUNE, B. T., BEDI, N., BEGHI, E., BÉJOT, Y., BEKELE, B. B., BELL, M. L., BENNETT, J. R., BENSENOR, I. M., BERHANE, A., BERNABÉ, E., BETSU, B. D., BEURAN, M., BHATT, S., BIADGILIGN, S., BIENHOFF, K., BIKBOV, B., BISANZIO, D., BOURNE, R. R. A., BREITBORDE, N. J. K., BULTO, L. N. B., BUMGARNER, B. R., BUTT, Z. A., CAHUANA-HURTADO, L., CAMERON, E., CAMPUZANO, J. C., CAR, J., CÁRDENAS, R., CARRERO, J. J., CARTER, A., CASEY, D. C., CASTAÑEDA-ORJUELA, C. A., CATALÁ-

LÓPEZ, F., CHARLSON, F. J., CHIBUEZE, C. E., CHIMED-OCHIR, O., CHISUMPA, V. H., et al. 2017. Global, regional, and national age-sex specific mortality for 264 causes of death, 1980–2016: a systematic analysis for the Global Burden of Disease Study 2016. *The Lancet,* 390**,** 1151-1210.

NELSON, A. R., SAGARE, M. A., WANG, Y., KISLER, K., ZHAO, Z. & ZLOKOVIC, B. V. 2020. Channelrhodopsin Excitation Contracts Brain Pericytes and Reduces Blood Flow in the Aging Mouse Brain in vivo. *Front Aging Neurosci,* 12**,** 108.

NICCOLI, G., BURZOTTA, F., GALIUTO, L. & CREA, F. 2009. Myocardial no-reflow in humans. *J Am Coll Cardiol,* 54**,** 281-92.

NISHIJIMA, Y., AKAMATSU, Y., WEINSTEIN, P. R. & LIU, J. 2015. Collaterals: Implications in cerebral ischemic diseases and therapeutic interventions. *Brain Res,* 1623**,** 18-29.

NISHIMURA, A., AGO, T., KURODA, J., ARIMURA, K., TACHIBANA, M., NAKAMURA, K., WAKISAKA, Y., SADOSHIMA, J., IIHARA, K. & KITAZONO, T. 2016. Detrimental role of pericyte Nox4 in the acute phase of brain ischemia. *J Cereb Blood Flow Metab,* 36**,** 1143-54.

NORTLEY, R., KORTE, N., IZQUIERDO, P., HIRUNPATTARASILP, C., MISHRA, A., JAUNMUKTANE, Z., KYRARGYRI, V., PFEIFFER, T., KHENNOUF, L., MADRY, C., GONG, H., RICHARD-LOENDT, A., HUANG, W., SAITO, T., SAIDO, T. C., BRANDNER, S., SETHI, H. & ATTWELL, D. 2019. Amyloid β oligomers constrict human capillaries in Alzheimer's disease via signaling to pericytes. *Science,* 365**,** eaav9518.

NOWAK, L., BREGESTOVSKI, P., ASCHER, P., HERBET, A. & PROCHIANTZ, A. 1984. Magnesium gates glutamate-activated channels in mouse central neurones. *Nature,* 307**,** 462-5.

O'DONNELL, M. J., XAVIER, D., LIU, L., ZHANG, H., CHIN, S. L., RAO-MELACINI, P., RANGARAJAN, S., ISLAM, S., PAIS, P., MCQUEEN, M. J., MONDO, C., DAMASCENO, A., LOPEZ-JARAMILLO, P., HANKEY, G. J., DANS, A. L., YUSOFF, K., TRUELSEN, T., DIENER, H. C., SACCO, R. L., RYGLEWICZ, D., CZLONKOWSKA, A., WEIMAR, C., WANG, X. & YUSUF, S. 2010. Risk factors for ischaemic and intracerebral haemorrhagic stroke in 22 countries (the INTERSTROKE study): a case-control study. *Lancet,* 376**,** 112-23.

O'FARRELL, F. M. & ATTWELL, D. 2014. A role for pericytes in coronary no-reflow. *Nat Rev Cardiol,* 11**,** 427-32.

OBRENOVITCH, T. P., URENJAK, J., RICHARDS, D. A., UEDA, Y., CURZON, G. & SYMON, L. 1993. Extracellular neuroactive amino acids in the rat striatum during ischaemia: comparison between penumbral conditions and ischaemia with sustained anoxic depolarisation. *J Neurochem,* 61**,** 178-86.

OLSON, L. E. & SORIANO, P. 2011. PDGFRβ signaling regulates mural cell plasticity and inhibits fat development. *Dev Cell,* 20**,** 815-26.

ÖZEN, I., DEIERBORG, T., MIHARADA, K., PADEL, T., ENGLUND, E., GENOVÉ, G. & PAUL, G. 2014. Brain pericytes acquire a microglial phenotype after stroke. *Acta Neuropathol,* 128**,** 381-96.

ÖZEN, I., ROTH, M., BARBARIGA, M., GACEB, A., DEIERBORG, T., GENOVÉ, G. & PAUL, G. 2018. Loss of Regulator of G-Protein Signaling 5 Leads to Neurovascular Protection in Stroke. *Stroke,* 49**,** 2182-2190.

OZERDEM, U. & STALLCUP, W. B. 2003. Early Contribution of Pericytes to Angiogenic Sprouting and Tube Formation. *Angiogenesis,* 6**,** 241-249.

PATAN, S. 1998. TIE1 and TIE2 receptor tyrosine kinases inversely regulate embryonic angiogenesis by the mechanism of intussusceptive microvascular growth. *Microvasc Res,* 56**,** 1-21.

PEPPIATT, C. M., HOWARTH, C., MOBBS, P. & ATTWELL, D. 2006. Bidirectional control of CNS capillary diameter by pericytes. *Nature,* 443**,** 700-4.

POWERS, W. J., RABINSTEIN, A. A., ACKERSON, T., ADEOYE, O. M., BAMBAKIDIS, N. C., BECKER, K., BILLER, J., BROWN, M., DEMAERSCHALK, B. M., HOH, B., JAUCH, E.

C., KIDWELL, C. S., LESLIE-MAZWI, T. M., OVBIAGELE, B., SCOTT, P. A., SHETH, K. N., SOUTHERLAND, A. M., SUMMERS, D. V. & TIRSCHWELL, D. L. 2018. 2018 Guidelines for the Early Management of Patients With Acute Ischemic Stroke: A Guideline for Healthcare Professionals From the American Heart Association/American Stroke Association. *Stroke,* 49**,** e46-e99.

PURO, D. G. 2007. Physiology and pathobiology of the pericyte-containing retinal microvasculature: new developments. *Microcirculation,* 14**,** 1-10.

QUE, J., WILM, B., HASEGAWA, H., WANG, F., BADER, D. & HOGAN, B. L. 2008. Mesothelium contributes to vascular smooth muscle and mesenchyme during lung development. *Proc Natl Acad Sci U S A,* 105**,** 16626-30.

REZKALLA SHEREIF, H. & KLONER ROBERT, A. 2002. No-Reflow Phenomenon. *Circulation,* 105**,** 656-662.

ROCHE, M., CHAIGNEAU, E., RUNGTA, R. L., BOIDO, D., WEBER, B. & CHARPAK, S. 2019. In vivo imaging with a water immersion objective affects brain temperature, blood flow and oxygenation. *Elife,* 8.

ROUGET, C. 1873. Memoire sur le developpement, la structures et les proprietes des capillaires sanguins et lymphatiques.

Archs Physiol Norm Pathol., 5**,** 603-633.

SAFAIYAN, S., BESSON-GIRARD, S., KAYA, T., CANTUTI-CASTELVETRI, L., LIU, L., JI, H., SCHIFFERER, M., GOUNA, G., USIFO, F., KANNAIYAN, N., FITZNER, D., XIANG, X., ROSSNER, M. J., BRENDEL, M., GOKCE, O. & SIMONS, M. 2021. White matter aging drives microglial diversity. *Neuron,* 109**,** 1100-1117.e10.

SAGARE, A. P., BELL, R. D., ZHAO, Z., MA, Q., WINKLER, E. A., RAMANATHAN, A. & ZLOKOVIC, B. V. 2013. Pericyte loss influences Alzheimer-like neurodegeneration in mice. *Nature Communications,* 4**,** 2932.

SAKUMA, R., KAWAHARA, M., NAKANO-DOI, A., TAKAHASHI, A., TANAKA, Y., NARITA, A., KUWAHARA-OTANI, S., HAYAKAWA, T., YAGI, H., MATSUYAMA, T. & NAKAGOMI, T. 2016. Brain pericytes serve as microglia-generating multipotent vascular stem cells following ischemic stroke. *J Neuroinflammation,* 13**,** 57.

SAVER JEFFREY, L. 2006. Time Is Brain—Quantified. *Stroke,* 37**,** 263-266.

SCHITO, L., REY, S., TAFANI, M., ZHANG, H., WONG, C. C.-L., RUSSO, A., RUSSO, M. A. & SEMENZA, G. L. 2012. Hypoxia-inducible factor 1-dependent expression of platelet-derived growth factor B promotes lymphatic metastasis of hypoxic breast cancer cells. *Proceedings of the National Academy of Sciences,* 109**,** E2707-E2716.

SCHMID, F., TSAI, P. S., KLEINFELD, D., JENNY, P. & WEBER, B. 2017. Depth-dependent flow and pressure characteristics in cortical microvascular networks. *PLOS Computational Biology,* 13**,** e1005392.

SCHRIMPF, C. & DUFFIELD, J. S. 2011. Mechanisms of fibrosis: the role of the pericyte. *Curr Opin Nephrol Hypertens,* 20**,** 297-305.

SEGER, R. & KREBS, E. G. 1995. The MAPK signaling cascade. *Faseb j,* 9**,** 726-35.

SHEPRO, D. & MOREL, N. M. 1993. Pericyte physiology. *Faseb j,* 7**,** 1031-8.

SIMS, D. E. 1986. The pericyte--a review. *Tissue Cell,* 18**,** 153-74.

STROKE, F. 2017. *National stroke audit acute services. Inform me*.

STROKEUNITTRIALISTSCOLLABORATION 1997. Collaborative systematic review of the randomised trials of organised inpatient (stroke unit) care after stroke. Stroke Unit Trialists' Collaboration. *Bmj,* 314**,** 1151-9.

STUART, T., BUTLER, A., HOFFMAN, P., HAFEMEISTER, C., PAPALEXI, E., MAUCK, W. M., 3RD, HAO, Y., STOECKIUS, M., SMIBERT, P. & SATIJA, R. 2019. Comprehensive Integration of Single-Cell Data. *Cell,* 177**,** 1888-1902.e21.

SUMMERS, W. K. & JAMISON, R. L. 1971. The no reflow phenomenon in renal ischemia. *Lab Invest,* 25**,** 635-43.

TARIQ, N. & KHATRI, R. 2008. Leptomeningeal collaterals in acute ischemic stroke. *J Vasc Interv Neurol,* 1**,** 91-5.

TENG, Y.-C., PORFÍRIO-SOUSA, A. L., RIBEIRO, G. M., AREND, M. C., DA SILVA MEIRELLES, L., CHEN, E. S., ROSA, D. S. & HAN, S. W. 2021. Analyses of the pericyte transcriptome in ischemic skeletal muscles. *Stem Cell Research & Therapy,* 12**,** 183.

TERPOLILLI, N. A., KIM, S.-W., THAL, S. C., KATAOKA, H., ZEISIG, V., NITZSCHE, B., KLAESNER, B., ZHU, C., SCHWARZMAIER, S., MEISSNER, L., MAMRAK, U., ENGEL, D. C., DRZEZGA, A., PATEL, R. P., BLOMGREN, K., BARTHEL, H., BOLTZE, J., KUEBLER, W. M. & PLESNILA, N. 2012. Inhalation of Nitric Oxide Prevents Ischemic Brain Damage in Experimental Stroke by Selective Dilatation of Collateral Arterioles. *Circulation Research,* 110**,** 727-738.

THENATIONALINSTITUTEOFNEUROLOGICALDISORDERSANDSTROKERT-PASTROKESTUDYGROUP 1995. Tissue Plasminogen Activator for Acute Ischemic Stroke. *New England Journal of Medicine,* 333**,** 1581-1588.

THORED, P., WOOD, J., ARVIDSSON, A., CAMMENGA, J., KOKAIA, Z. & LINDVALL, O. 2007. Long-term neuroblast migration along blood vessels in an area with transient angiogenesis and increased vascularization after stroke. *Stroke,* 38**,** 3032-9.

THURSTON, G., SURI, C., SMITH, K., MCCLAIN, J., SATO, T. N., YANCOPOULOS, G. D. & MCDONALD, D. M. 1999. Leakage-resistant blood vessels in mice transgenically overexpressing angiopoietin-1. *Science,* 286**,** 2511-4.

THURSTON, G., WANG, Q., BAFFERT, F., RUDGE, J., PAPADOPOULOS, N., JEAN-GUILLAUME, D., WIEGAND, S., YANCOPOULOS, G. D. & MCDONALD, D. M. 2005. Angiopoietin 1 causes vessel enlargement, without angiogenic sprouting, during a critical developmental period. *Development,* 132**,** 3317-26.

TSUCHIDATE, R., HE, Q. P., SMITH, M. L. & SIESJÖ, B. K. 1997. Regional cerebral blood flow during and after 2 hours of middle cerebral artery occlusion in the rat. *J Cereb Blood Flow Metab,* 17**,** 1066-73.

UEMURA, A., OGAWA, M., HIRASHIMA, M., FUJIWARA, T., KOYAMA, S., TAKAGI, H., HONDA, Y., WIEGAND, S. J., YANCOPOULOS, G. D. & NISHIKAWA, S. 2002. Recombinant angiopoietin-1 restores higher-order architecture of growing blood vessels in mice in the absence of mural cells. *J Clin Invest,* 110**,** 1619-28.

UNDERLY, R. G., LEVY, M., HARTMANN, D. A., GRANT, R. I., WATSON, A. N. & SHIH, A. Y. 2017. Pericytes as Inducers of Rapid, Matrix Metalloproteinase-9-Dependent Capillary Damage during Ischemia. *J Neurosci,* 37**,** 129-140.

VALLET, P., CHARNAY, Y., STEGER, K., OGIER-DENIS, E., KOVARI, E., HERRMANN, F., MICHEL, J. P. & SZANTO, I. 2005. Neuronal expression of the NADPH oxidase NOX4, and its regulation in mouse experimental brain ischemia. *Neuroscience,* 132**,** 233-8.

VATES, G. E., TAKANO, T., ZLOKOVIC, B. & NEDERGAARD, M. 2010. Pericyte constriction after stroke: the jury is still out. *Nature Medicine,* 16**,** 959-959.

VELLA, J., ZAMMIT, C., DI GIOVANNI, G., MUSCAT, R. & VALENTINO, M. 2015. The central role of aquaporins in the pathophysiology of ischemic stroke. *Front Cell Neurosci,* 9**,** 108.

WADE, J. G., AMTORP, O. & SORENSEN, S. C. 1975. No-flow state following cerebral ischemia. Role of increase in potassium concentration in brain interstitial fluid. *Arch Neurol,* 32**,** 381-4.

WALLOW, I. H. & BURNSIDE, B. 1980. Actin filaments in retinal pericytes and endothelial cells. *Investigative Ophthalmology & Visual Science,* 19**,** 1433-1441.

WARDLAW, J. M., MURRAY, V., BERGE, E., DEL ZOPPO, G., SANDERCOCK, P., LINDLEY, R. L. & COHEN, G. 2012. Recombinant tissue plasminogen activator for acute ischaemic stroke: an updated systematic review and meta-analysis. *Lancet,* 379**,** 2364-72.

WARDLAW, J. M., SANDERCOCK, P. A. & BERGE, E. 2003a. Thrombolytic therapy with recombinant tissue plasminogen activator for acute ischemic stroke: where do we go from here? A cumulative meta-analysis. *Stroke,* 34**,** 1437-42.

WARDLAW, J. M., ZOPPO, G., YAMAGUCHI, T. & BERGE, E. 2003b. Thrombolysis for acute ischaemic stroke. *Cochrane Database Syst Rev***,** Cd000213.

WEI, W., YU, Z., XIE, M., WANG, W. & LUO, X. 2017. Oxygen-Glucose Deprivation Induces G2/M Cell Cycle Arrest in Brain Pericytes Associated with ERK Inactivation. *Journal of Molecular Neuroscience,* 61**,** 105-114.

WHALEN, M. J., DALKARA, T., YOU, Z., QIU, J., BERMPOHL, D., MEHTA, N., SUTER, B., BHIDE, P. G., LO, E. H., ERICSSON, M. & MOSKOWITZ, M. A. 2007. Acute Plasmalemma Permeability and Protracted Clearance of Injured Cells after Controlled Cortical Impact in Mice. *Journal of Cerebral Blood Flow & Metabolism,* 28**,** 490-505.

WILM, B., IPENBERG, A., HASTIE, N. D., BURCH, J. B. & BADER, D. M. 2005. The serosal mesothelium is a major source of smooth muscle cells of the gut vasculature. *Development,* 132**,** 5317-28.

XU, H.-T., PAN, F., YANG, G. & GAN, W.-B. 2007. Choice of cranial window type for in vivo imaging affects dendritic spine turnover in the cortex. *Nature Neuroscience,* 10**,** 549-551.

YAMAMOTO, S., MURAMATSU, M., AZUMA, E., IKUTANI, M., NAGAI, Y., SAGARA, H., KOO, B. N., KITA, S., O'DONNELL, E., OSAWA, T., TAKAHASHI, H., TAKANO, K. I., DOHMOTO, M., SUGIMORI, M., USUI, I., WATANABE, Y., HATAKEYAMA, N., IWAMOTO, T., KOMURO, I., TAKATSU, K., TOBE, K., NIIDA, S., MATSUDA, N., SHIBUYA, M. & SASAHARA, M. 2017. A subset of cerebrovascular pericytes originates from mature macrophages in the very early phase of vascular development in CNS. *Sci Rep,* 7**,** 3855.

YAO, Y., CHEN, Z.-L., NORRIS, E. H. & STRICKLAND, S. 2014. Astrocytic laminin regulates pericyte differentiation and maintains blood brain barrier integrity. *Nature communications,* 5**,** 3413-3413.

YEMISCI, M., GURSOY-OZDEMIR, Y., VURAL, A., CAN, A., TOPALKARA, K. & DALKARA, T. 2009. Pericyte contraction induced by oxidative-nitrative stress impairs capillary reflow despite successful opening of an occluded cerebral artery. *Nat Med,* 15**,** 1031-7.

YI, Y.-H., CHANG, Y.-S., LIN, C.-H., LEW, T.-S., TANG, C.-Y., TSENG, W.-L., TSENG, C.-P. & LO, S. J. 2012. Integrin-mediated Membrane Blebbing Is Dependent on Sodium-Proton Exchanger 1 and Sodium-Calcium Exchanger 1 Activity *. *Journal of Biological Chemistry,* 287**,** 10316-10324.

ZEHENDNER, C. M., SEBASTIANI, A., HUGONNET, A., BISCHOFF, F., LUHMANN, H. J. & THAL, S. C. 2015. Traumatic brain injury results in rapid pericyte loss followed by reactive pericytosis in the cerebral cortex. *Scientific Reports,* 5**,** 13497.

ZHANG, H. & FABER, J. E. 2019. Transient versus Permanent MCA Occlusion in Mice Genetically Modified to Have Good versus Poor Collaterals. *Med One,* 4**,** e190024.

ZHANG, L., ZHANG, Z. G. & CHOPP, M. 2012. The neurovascular unit and combination treatment strategies for stroke. *Trends in Pharmacological Sciences,* 33**,** 415-422.

ZHANG, Z. S., ZHOU, H. N., HE, S. S., XUE, M. Y., LI, T. & LIU, L. M. 2020. Research advances in pericyte function and their roles in diseases. *Chin J Traumatol,* 23**,** 89-95.

ZHAO, L., MULLIGAN, M. K. & NOWAK, T. S., JR. 2019. Substrain- and sex-dependent differences in stroke vulnerability in C57BL/6 mice. *Journal of cerebral blood flow and metabolism : official journal of the International Society of Cerebral Blood Flow and Metabolism,* 39**,** 426-438.

ZOZULYA, A., WEIDENFELLER, C. & GALLA, H. J. 2008. Pericyte-endothelial cell interaction increases MMP-9 secretion at the blood-brain barrier in vitro. *Brain Res,* 1189**,** 1-11.

Appendix A:

Appendix B:

Acknowledgements

I would like to thank Prof. Dr. med Nikolaus Plesnila, for his patience, encouragement, belief, statistical advice and guiding hand throughout the last four years in an attempt to make me a more complete scientist. I would also like to thank Uta Mamrak for teaching me the fMCAo model, performing experiments with me and teaching countless other techniques, for always being there and for being a reliable kind soul who always had time for questions. I also have to extend my gratitude to Dr. Severin Filser, who provided exceptional quality chronic cranial windows through which to achieve my long-term goals of imaging pericytes under ischemic conditions and for being a great friend. Thanks also to Bernhard Groschup for being a wonderful scientist to bounce ideas off and an equally great friend.

Thanks to Dr. Burcu Seker, for her advice on laser speckle imaging and for being such an endlessly warm personality to be around. Thank you to the Systems neuroscience group, in particular to Buket Bulut and Simon Besson-Girard for being excellent colleagues to work with under the supervision of Dr. Ozgun Gokce, who I would also like to thank profusely for taking on the sequencing part of this project. Thank you to Dr. Igor Khalin for collaborating and working together on multiple projects, which are now beginning to finally overlap. Thank you to Malo Gaubert and Dr. Benno Gesierich for persisting with my ideas on automatic vessel analysis tools and advances in programming. Thank you to Patrick Bayer and Fabio Loredo, two wonderful students who helped toward the completion of the project. Thank you to Janina Biller and Becky Sienel, who always provides a fun atmosphere to work in and help keep the lab running and to all other lab members who have been a joy to work around. A huge thank you in addition to Hedwig Pietsch, who could well be the best team secretary out there, aside from being just a good friend.

Thanks to Prof. Dr Leda Dimou, Dr. Christoff Haffner and Dr. Kathrin Nehrkorn for their invaluable advice during my TAC meetings and for keeping me focused on what matters most. Thank you to Dr. rer. nat Stefan Roth, for being an excellent friend and one of the most inspiring role models in science during the whole of my PhD, to Dr. Daniel Varga for his Matlab analysis skills and thanks to Steffi for being a good friend over the course of the PhD along with countless other colleagues that make the ISD a joy to work in. Thank you to Dr. Farida Hellal, Dr. Catherine Hall and Prof. David Attwell for their advice and scientific discussion. Thank you to Dr. Antje Heinrich for guiding me very consistently throughout the last steps of my PhD, setting me on the right track and always being patient with questions. Thank you to all evaluators of the thesis, I hope it has been an enjoyable read, that the science you see here means something to you, and the research field at large. Lastly, thank you to my family for being understanding, for being there whenever I needed them, and for providing consistent encouragement throughout life, I hope and endeavor to make you proud, always.

Affidavit

Affidavit

Shrouder, Joshua James

Surname, first name

Feodor-Lynen Strasse 17

Street

81377, Muenchen, Germany

Zip code, town, country

I hereby declare, that the submitted thesis entitled:

The pericyte response to ischemic stroke

is my own work. I have only used the sources indicated and have not made unauthorised use of services of a third party. Where the work of others has been quoted or reproduced, the source is always given.

I further declare that the submitted thesis or parts thereof have not been presented as part of an examination degree to any other university.

München, 02.07.2021

place, date

Joshua James Shrouder

Signature doctoral candidate

Confirmation of congruency

Confirmation of congruency between printed and electronic version of the doctoral thesis

Shrouder, Joshua James

Surname, first name

Feodor-Lynen Strasse 17

Street

81377, Muenchen, Germany

Zip code, town, country

I hereby declare, that the submitted thesis entitled:

The pericyte response to ischemic stroke

is congruent with the printed version both in content and format.

München, 02.07.2021

place, date

Joshua James Shrouder

Signature doctoral candidate

List of publications

1. Inadequate food and water intake determine mortality following stroke in mice. Lourbopoulos A, Mamrak U, Roth S, Balbi M, **Shrouder J**, Liesz A, Hellal F, Plesnila N. Journal of Cerebral Blood Flow & Metabolism. 2017; 37(6):2084-2097. doi:10.1177/0271678X16660986
2. The pseudoprotease iRhom1 controls ectodomain shedding of membrane proteins in the nervous system. Tüshaus J, Müller S, **Shrouder J**, Arends M, Simons M, Plesnila N, Blobel C.P, and Lichtenthaler S.F. *The FASEB Journal* (In submission)
3. Nanoparticles accumulate in vascular occlusions and extravasate acutely after stroke. Khalin I., Filser S., Nagappanpillai A., Schifferer M, Wehn A., **Shrouder J**., Misgeld T., Klymchenko A., Plesnila N. (In preparation)
4. Cortical pericytes persist in the ischemic cortex to constrict the microvasculature in a biphasic manner after stroke. **Shrouder J,** Mamrak U, Filser S, Besson-Girard S, Bulut B, Seker B, Geseirich B, Loredo F, Khalin I, Wehn A, Gökce O, Plesnila N. (In preparation).

8. Supplementary information

Table 13: Neuroscore

Date/Animal															
Body Weight															
Score															
in relation to previous day: increased (0), reduction by <5% (1) reduction by 5-10% (5) reduction by >10% (20)															
State of Consciousness															
awake and agile (0) low state of consciousness: sleepy, reduced activity, reduced escape reflex (5) K comatose (20)															
Behaviour															
normal: sleeping, curiosity, social interaction (0) minor change of normal behaviour: reduced social interaction/curiosity (1) unusual behaviour: hyperkinetic (10) signs of pain, autoaggression, isolation, lethargy, severe hyperkinetic and stereotypy, loss of righting reflex (20)															
General Condition															
fur even,orifices clean, eyes clean/shiny (0) defects in fur: altered grooming (1) fur dull, orifices dirty, unusual posture, higher muscel tone (10) eyes dull, muscle cramped/parlysed, respiratory noise, animal is cold (20)															
Clinical Condition															
normal: temperatur normal, regular breathing, pulse normal, mucosa pink, limbs warm (0) minor change of normal condition (1) temperature change 1-2°C, pulse +30%, enforced breething, peeping respiratory noise (5) K temperature change >2°C, pulse +/-50%, dyspnoea, gasping, respiratory noise (20)															
Wound															
nonirritated wound (0) mildly inflamed wound (5) not healing/inflamed wound (20)															
Neurologic Condition															
model associated defects: light contralateral paresis, paralysis contralateral forepaw, disturbance in sensitivity and coordination (2) mild neurological defect eg seizure (5) K severe neurological defect eg status epilepticus (20)															
Sum															
0 no burden 1-9 small burden: keep evaluating carefully 10-19: moderate burden: contact vet, check animal twice daily, if the condition does not improve within 24h the animal needs to be sacrificed >20 severe burden: animal has to be sacrificed															
Humane End Point: animal needs to be sacrificed immediately **loss of body weight > 10% in relation to baseline in two consecutive days, animal feels cold, legs/belly are blue, high body temperature (> 39°C), abscess,** **sings of pain despite analgesic treatment (immobile, bristeled fur, closed eyes, kyphose), paralysis which prevents feeding, eyes dull, automutilation**															

Table 14: Experimental stroke scale

Behavioral examination fMCAo (Experiment: Animal code:)

Experiment . Animal code: Day of OP:

Time-point post-MCAo	*Day1*	*Day2*	*Day3*	*Day 4*	*Day 5*	*Day 6*	*Day 7*
date							
Daily B.W. (gr) (morning)							
Temp (°C, surface)							
Feeding support							
s.c. fluids							

Time-point post-MCAo	*Day 8*	*Day 9*	*Day 10*	*Day 11*	*Day 12*	*Day 13*	*Day 14*
date							
Daily B.W. (gr) (morning)							
Temp (°C, surface)							
Feeding support							
s.c. fluids							

Mortality: NO☐ YES☐ (date/time: ...../.....)

Autopsy:

Scheduled Brain extraction (perfused)**:**

Behavioral examination fMCAo (Experiment: Animal code:)

	Time-point of scoring		24h	3d	7d	14d	28d
Exp Stroke Scale (focal)	**Body symmetry** (mouse on OBT. observe the nose-tail line)	0. Normal (Body: normal posture, trunk elevated from the bench, with fore and hindlimbs leaning beneath the body. Tail: straight)					
		1. Slight asymmetry (Body: leans on one side with fore and hindlimbs leaning beneath the body. Tail: slightly bent.)					
		2. Moderate asymmetry (Body: leans on one side with fore and hindlimbs stretched out. Tail: slightly bent).					
		3. Prominent asymmetry (Body: bent, on one side lies on the OBT. Tail: bent)					
		4. Extreme asymmetry (Body: highly bent, on one side constantly lies on the OBT. Tail: highly bent)					
	Gait (mouse on OBT. Observed undisturbed)	0. Normal (gait is flexible, symmetric and quick)					
		1. Stiff, inflexible (humpbacked walk, slower than normal mouse)					
		2. Limping, with asymmetric movements					
		3. Trembling, drifting, falling					
		4. Does not walk spontaneously (when stimulated by gently pushing the mouse walks no longer than 3 steps)					
	Climbing (mouse on a 45° surface. Place the mouse in the center of the gripping surface)	0. Normal (mouse climbs quickly)					
		1. Climbs with strain, limb weakness present.					
		2. Holds onto slope, does not slip or climb					
		3. Slides down slope, unsuccessful effort to prevent fail					
		4. Slides immediately, no effort to prevent fail.					
	Circling behavior (mouse on OBT, free observation)	0. Absent circling behavior					
		1. Predominantly one-side turns.					
		2. Circles to one side, although not constantly.					
		3. Circles constantly to one side.					
		4. Pivoting, swaying, or no movement.					
	Forelimb symmetry (mouse suspended by tail)	0. Normal					
		1. Light asymmetry: mild flexion of contralateral forelimb.					
		2. Marked asymmetry: marked flexion of contralateral limb, the body slightly bends on the ipsilateral side.					
		3. Prominent asymmetry: contralateral forelimb adheres to the trunk.					
		4. Slight asymmetry, no body/limb movement.					
	Hindlimb symmetry	0. Normal					
		1. Presence of asymmetry					
	Compulsory circling (forelimbs on bench, hindlimbs suspended by the tail: it reveals the presence of the contralateral limb palsy)	0. Absent. Normal extension of both forelimbs.					
		1. Tendency to turn to one side (the mouse extends both forelimbs, but starts to turn preferably to one side)					
		2. Circles to one side (the mouse turns towards one side with a slower movement compared to healthy mice)					
		3. Pivots to one side sluggishly (the mouse turns towards one side failing to perform a complete circle)					
		4. Does not advance (the front part of the trunk lies on the bench, slow and brief movements)					
	Whisker response (mouse on the OBT)	0. Normal					
		1. Light asymmetry (the mouse withdraws slowly when stimulated on the contralateral side)					
		2. Prominent asymmetry (no response when stimulated to the contralateral side)					
		3. Absent response contralaterally, slow response when stimulated ipsilaterally.					
		4. Absent response bilaterally					

Behavioral examination fMCAo (Experiment: Animal code:)

	Motor tests (Raising mouse by the tail)	0. No trunk flexion					
		1. Head moved more than 10º to the vertical axis within 30 s					
	Forelimb placing	Placing test (motility): 0 = normal, 1 = asymmetry					
		Placing test (deep sensation: pushing the paw against the table edge to stimulate limb muscles) 0 = normal, 1 = no prompt reaction					
	Posture (place the mouse on the palm and swing gently)	0. The mouse stands in the upright position with the back parallel to the palm. During swing, it stands rapidly.					
		1. The mouse stands humpbacked. During the swing, it flattens the body to gain stability.					
		2. The head or part of the trunk lies on the palm					
		3. The mouse lies on one side, barely able to recover the upright position.					
		4. The mouse lies in a prone position, not able to recover the upright position.					
	Beam balance tests (normal=0; max = 6)	0. Balances with steady posture					
		1. Grasps side of beam					
		2. Hugs the beam and one limb falls down from the beam					
		3. Hugs the beam and two limbs fall down from the beam, or spins on beam (>60 s)					
		4. Attempts to balance on the beam but falls off (>40 s)					
		5. Attempts to balance on the beam but falls off (>20 s)					
		6. Falls off: no attempt to balance or hang on to the beam (<20 s)					
	Total score for focal deficits (normal=0 max=42)						

	Time-point of scoring		*24h*	*3d*	*7d*	*14d*	*28d*
Exp Stroke Scale (general)	**Hair**	0. Hair neat and clean					
		1. Localized piloerection and dirty hair in 2 body parts (nose and eyes)					
		2. Piloerection and dirty hair in >2body parts					
	Ears (mouse on an open bench top)	0. Normal (ears are stretched laterally and behind, they react by straightening up following noise)					
		1. Stretched laterally but not behind (one or both), they react to noise					
		2. Same as 1. NO Reaction to noise.					
	Eyes (mouse on OBT)	0. Open, clean and quickly follow the surrounding environment					
		1. Open and characterized by aqueous mucus. Slowly follow the surrounding environment					
		2. Open and characterized by dark mucus					
		3. Ellipsoidal shaped and characterized by dark mucus					
		4. Closed					
	Spontaneous activity (mouse on OBT, free observation)	0. The mouse is alert and explores actively.					
		1. The mouse seems alert, but it is calm and sluggish					
		2. The mouse explores intermittently and sluggishly					
		3. The mouse is somnolent and numb, few movements on-the-spot.					
		4. No spontaneous movements					
	Anxiety/automatic behavior (mouse on OBT, record worse behavior)	0. None					
		1. The mouse is reluctant to handling, show hyperactivity.					
		2. The mouse is aggressive, stressed and stares.					
		3. The mouse shows hyperexcitability, chaotic movements and presence of convulsion following handling					
		4. Generalized seizures associated with wheezing and unconsciousness.					
	Total score for general scoring (normal=0 max=16)						